HAL
open science

Synthèse et fonctionnalisation de polymères hyper-ramifiés issus d'acides gras

Quentin Passet

▶ **To cite this version:**

Quentin Passet. Synthèse et fonctionnalisation de polymères hyper-ramifiés issus d'acides gras. Polymères. Université de Bordeaux, 2019. Français. NNT : 2019BORD0059 . tel-02558923

HAL Id: tel-02558923

https://theses.hal.science/tel-02558923v1

Submitted on 30 Apr 2020

HAL is a multi-disciplinary open access archive for the deposit and dissemination of scientific research documents, whether they are published or not. The documents may come from teaching and research institutions in France or abroad, or from public or private research centers.

L'archive ouverte pluridisciplinaire **HAL**, est destinée au dépôt et à la diffusion de documents scientifiques de niveau recherche, publiés ou non, émanant des établissements d'enseignement et de recherche français ou étrangers, des laboratoires publics ou privés.

université de BORDEAUX

THÈSE PRÉSENTÉE

POUR OBTENIR LE GRADE DE

DOCTEUR DE L'UNIVERSITÉ DE BORDEAUX

ÉCOLE DOCTORALE DES SCIENCES CHIMIQUES

SPÉCIALITÉ : Polymères

Par Quentin PASSET

SYNTHESIS AND FUNCTIONALIZATION OF FATTY ACID-BASED HYPERBRANCHED POLYMERS

Synthèse et fonctionnalisation de polymères hyper-ramifiés issus d'acides gras

Sous la direction de : Pr. Henri CRAMAIL
Co-directeur : Pr. Daniel TATON / Co-encadrant : Dr. Etienne GRAU

Soutenue le 29 Avril 2019

Membres du jury

Mme N.SINTES-ZYDOWICZ	Maître de conférence, Université Lyon 1	Rapporteur
M. J.-L. SIX	Professeur, Université de Lorraine	Rapporteur
M. G. CHOLLET	Chef de projets Lipochimie, ITERG	Examinateur
M. E. GRAU	Maître de conférences, Université de Bordeaux	Examinateur
Mme L. RAMOS	Directeur de recherche, CNRS	Présidente du jury
Mme. N. VOUILLON	Chef de projets R&D, SAS PIVERT	Examinateur
M. H. CRAMAIL	Professeur, Université de Bordeaux	Directeur de thèse
M. D. TATON	Professeur, Université de Bordeaux	Directeur de thèse

Avertissement

« Ce document est confidentiel, et a été réalisé dans le cadre du programme de recherche GENESYS de la SAS PIVERT. Il ne peut être ni reproduit ni exploité sans l'autorisation expresse de la SAS PIVERT.»

Disclaimer

"This document is confidential and was prepared within the frame of the GENESYS research program of the SAS PIVERT. No copy, no distribution, and no exploitation are allowed without the authorization of the SAS PIVERT."

REMERCIEMENTS

Ce manuscrit est le fruit d'un travail de plus de trois ans. Chaque personne que j'ai été amené à rencontrer, a participé, de près ou de loin, à sa réalisation. Je vous remercie sincèrement.

Je tiens tout d'abord à adresser mes remerciements aux membres du jury pour avoir pris le temps d'examiner ces travaux de thèses. Merci à Mme Nathalie Sintes-Zydowicz et M. Jean-Luc Six d'avoir accepté d'être les rapporteurs de ces travaux, ainsi qu'à M. Guillaume Chollet, Mme Nathalie Vouillon et Mme Laurence Ramos pour les avoir examinés. Merci pour vos différents commentaires et remarques, écrits et oraux.

Je souhaite également remercier mes encadrants : Henri, Daniel et Etienne, pour le soutien qu'ils m'ont apporté durant ces trois années et pour leur bienveillance. Merci Henri, Daniel, pour m'avoir accepté au sein de vos équipes respectives. Merci Etienne (bientôt capitaine ?) pour ta disponibilité (quasi) quotidienne.

Ce projet ayant étant le fruit d'une collaboration entre la S.A.S Pivert, l'ITERG, le L2C et le LCPO, je tiens à remercier toutes les personnes qui ont contribué à la bonne réussite de ce projet, à commencer par la S.A.S Pivert, qui l'a financé. Plus particulièrement, merci à Nathalie Vouillon et Caroline Hillairet, de la S.A.S Pivert, pour votre suivi régulier. Merci à Guillaume Chollet, Didier Pintori, Marine et Ludivine, de l'ITERG, pour votre expertise et votre aide pour la synthèse & la caractérisation des polyesters hyper-ramifiés. Merci à Laurence Ramos et Salvatore Costanzo, du L2C, pour votre aide et l'ensemble du travail réalisé pour la caractérisation physico-chimique des polymères hyper-ramifiés (pas toujours facile).

Je tiens à remercier tous les membres du Laboratoire de Chimie des Polymères Organiques (LCPO), particulièrement son directeur, Sébastien Lecommandoux, pour m'avoir accueilli dans les meilleures conditions possibles. Je souhaiterais évidemment remercier Dominique, Corinne, Claude, Loïc, Aude, Séverine, Bernadette et Catherine pour leur aide quotidienne et leur joie de vivre. Merci à Cédric, Anne-Laure, Amélie, Eric, Mélanie, pour votre expertise et votre patience (il

en a fallu !). Je remercie également (et surtout) Gérard et Manu, c'est en partie ~~à cause~~ grâce à vous que je me suis lancé, merci le palétuvier. Je remercie tous les doctorants, post-doctorants, titulaires et stagiaires que j'ai pu rencontrer. Merci à mes stagiaires, Selim et Clément, pour leur implication dans ces travaux.

Je remercie mes amis avec qui j'ai pu partager d'excellents moments. Merci à Sav', mon binôme de la première heure, et à PL. Je ne me souviens plus de la couleur du camembert, mais je crois que j'étais en tête… Merci à Pierre & Roxanne (pour les très bons moments passés, à Bordeaux et Montpellier), Ariane et Lucas (notamment pour vos accueils chaleureux ces derniers mois), Lélé & Alex (pour votre présence et vos petits messages), Michou et Hélène (pour le squash et nos grandes discussions), à Geoffrey et Hélène (qui ont veillé sur moi dans leurs bureaux respectifs), Romain & Anne-Laure, Jérémy & Margaux, à Camille (Sav) et à Mélina (PL), pour ces superbes soirées et week-ends. Merci à Ghita & Antoine et Cécile & Quentin, pour les petites soirées « escape game », raclette et ligue des champions (avec ou sans électricité). Merci à mes partenaires de longue date, Mehdi & Rémy. Merci à la dream team, Arthur & Quentin S., Bakka & David, Loulou & Amélie, Thomas et Audrey pour de très bon moments padel, squash, foot, bières… Un très (très) grand merci à Martin et Fiona pour votre gentillesse et votre aide durant ces derniers mois. Merci également à Antoine B., Camille G., Nicolas, Gauvin H., Christopher, Boris, Guillaume, Antoine F., Léa et Cindy. Merci à Andy & Alexia, il faudra songer à revenir ! Merci à Franck & Agathe, on vous attend. Merci à Emilio & Isis, «c'est ça la vie ».

Je tiens à remercier ma famille qui a toujours été présente pour moi. Merci à mes parents et mon petit-frère pour m'avoir accompagné toutes ces années. Merci à mes grands-parents, mes oncles, tantes et cousins (tout particulièrement Muriel, Manu, Tom, Charlotte et Jules), Gilles & Sylvie, Jacques & Christine et Juliane & Charles pour votre soutien (sans faille j'espère). La vie est chouette à vos côtés.

Enfin, je remercie tout particulièrement Lucie, qui m'a accompagné ces trois années (et plus) et qui continue de le faire. Merci pour ta patience (et ton impatience).

GENERAL TABLE OF CONTENTS

List of abbreviations.....5
Abstract/Résumé.....7
General introduction.....15

Chapter 1. Synthesis, properties and potential of aromatic and aliphatic hyperbranched polyethers 23

1. Hyperbranched polymers.....25
1.1. Introduction to dendritic polymers.....25
1.2. Hyperbranched polymers.....26
1.3. Introduction on hyperbranched polyethers.....30
2. General outline of synthetic approaches for the preparation of hyperbranched polyethers.....31
2.1. Synthesis of aromatic hyperbranched polyethers by step growth polymerization...31
2.2. Synthesis of hyperbranched polyethers by ring-opening polymerization.....40
3. Ring-opening polymerization of glycidol.....54
3.1. Generalities and challenges.....54
3.2. Thermal and thermo-rheological properties.....61
3.3. Functionalization of hyperbranched polyglycidol: towards original properties.....62
3.4. Towards innovative technologies.....76
4. Conclusion and objectives.....79
5. References.....81

Chapter 2. From 10,11-epoxyundecanol to vegetable oil-based hyperbranched polyethers.....91

1. Introduction.....93

2. Synthesis of 10,11-epoxyundecanol.....96

3. Ring-opening multibranching polymerization of 10,11-epoxyundecanol.....98

3.1. Methodology.....98

3.2. Characterization of *hb*PEUnd by NMR spectroscopy.....102

3.3. Polymerization conditions.....111

3.4. Thermal properties.....125

4. Ring-opening copolymerization of 10,11-epoxyundecanol and glycidol.....127

4.1. Random copolymerization of 10,11-epoxyundecanol and glycidol.....127

4.2. Sequential polymerization of 10,11-epoyxundecanol and glycidol.....134

5. Conclusions.....144

6. References.....146

7. Experimental and supporting information.....150

Chapter 3. Functionalization and properties of hyperbranched polyesters.....165

1. Introduction.....167

2. Derivatization of M2HS-based hyperbranched polyester polyol with succinic anhydride.....170

2.1. Functionalization with succinic anhydride.....171

2.2. Properties of the hyperbranched polyester polysuccinate's.....176

2.3. Conclusion.....185

3. Derivatization of M2HS-based hyperbranched polyester polyol with acryloyl chloride.....187

3.1. Functionalization with acryloyl chloride.....190

3.2. Hyperbranched polyester polyacrylate as curing agent for the production of cross-linked PMMA.....195

3.3. Copolymerization of hyperbranched polyester polyacrylate with styrene.....206

3.4. Conclusion.....210

4. Conclusion & outlooks.....212
5. References.....213
6. Experimental and supporting information.....218

General conclusion and perspectives.....223
Materials and methods.....227

ABBREVIATIONS

ACE: active chain-end

AM: activated monomer

COSY: homonuclear correlation spectroscopy

CROP: cationic ring-opening polymerization

***Đ*:** Dispersity

DB: Degree of branching

DCM: dichloromethane

DEPT-135: distortionless enhanced polarization transfer

DLS: diffusion light scattering

DMF: *N, N*-dimethylformamide

DMSO: dimethylsulfoxide

DP_n: degree of polymerization

DSC: differential scanning calorimetry

EUnd: 10,11-epoxyundecan-1-ol

EWG: electron-withdrawing groups

FA: fatty acid

FAME: fatty acid methyl ester

FT-IR: fourier transformed infrared spectroscopy

***Hb*P(aryl ether):** hyperbranched poly(aryl ether)

***Hb*PEUnd:** hyperbranched poly(epoxyundecanol)

***Hb*PG:** hyperbranched polyglycidol

***Hb*PEther:** hyperbranched polyether

***Hb*PEster:** hyperbranched polyester

***Hb*PEster-A:** hyperbranched polyester polyacrylate

***Hb*PEster-COOH:** hyperbranched polyester polyacid

HSQC: heteronuclear single quantum coherence

HTP: proton-transfer polymerization

M: monomer

mCPBA: *meta*-chloroperbenzoic acid

MeOH: methanol

M2HU: methyl 10,11-dihydroxyundecanoate

M2HS: methyl 9,10-dihydroxystearate

MHS: Mark-Houwink-Sakurada

MMA: methyl methacrylate

M_n: number average molecular weight

M_w: weight average molecular weight

NMP: *N*-methyl-2-pyrrolidone

NMR: nuclear magnetic resonance

PEG: polyethylene glycol

P.I.V.E.R.T.: Picardie innovation végétale enseignements et recherches technologiques

PS: polystyrene

ROMBcP: ring-opening multibranching copolymerization

ROMBP: ring-opening multibranching polymerization

ROP: ring-opening polymerization

SEC: size-exclusion chromatography

T: temperature

T_B: boiling temperature

$T_{d5\%}$: temperature corresponding to 5wt% loss

T_g: glass transition temperature

T_m:: melting temperature

TEA: triethylamine

THF: tetrahydrofuran

TGA: thermogravimetric analysis

TMP: 1,1,1-tris(hydroxymethyl)propane

SAXS: small-angle X-ray scattering

SEC: size exclusion chromatography

SiR_3: trialkyl silyl ether

S_NAr: Aromatic subsitution

WAXS: wide-angle X-ray scattering

RESUME

Cette thèse s'inscrit dans le cadre du projet FunHyBioPol (W3P20) et a été menée en collaboration avec le Laboratoire de Chimie des Polymères Organiques (LCPO), le Laboratoire Charles Coulomb (L2C) et le Centre Technique Industriel Français des Huiles et Corps Gras (ITERG). Ce projet a été financé par la S.A.S PIVERT, dont l'objectif est de contribuer au développement d'une filière économique durable, basée sur la valorisation des ressources oléagineuses par le biais de transferts technologiques entre la recherche académique et des industriels.

Les polymères trouvent leur place dans des secteurs d'activités tels que l'emballage, la construction, l'automobile, l'électronique et la santé, pour ne citer que ces seuls exemples. Le succès des matériaux polymères est principalement dû à leur faible coût, leur mise en œuvre relativement facile et la grande diversité et polyvalence de leurs propriétés. Depuis 1950, environ 8 300 millions de tonnes de plastiques ont ainsi été produits, dont 330 millions en 2015.[1,2] Cette production consomme, de nos jours, environ 6 % de la production mondiale de pétrole, soit aux alentours de 4,9 milliards de tonnes/an.[2–4] La substitution de monomères issus de ressources fossiles par d'autres extraits de ressources renouvelables, ainsi que le développement de nouvelles voies de polymérisation plus respectueuses de l'Homme et de l'Environnement, fait partie des enjeux primordiaux pour limiter, entre autres, les émissions de gaz à effet de serre.[5–7] La recherche actuelle s'oriente principalement sur la valorisation de la biomasse, dont la régénération est bien plus rapide que celle du pétrole (dizaines d'année vs. centaines de millions d'années).[8,9]

Le développement de bio-raffineries efficientes, qui suivent les principes de la chimie verte,[10,11] se révèle être une solution durable, permettant de maximiser le potentiel de valorisation de la biomasse pour produire de l'énergie, de la nourriture et des composés de base (ou synthons) pour la chimie.[13-15] Des polymères biosourcés peuvent aussi être obtenus, selon deux méthodes ; (i) l'extraction de polymères naturels à partir de la biomasse (p. ex. cellulose, lignine, amidon) et (ii) la synthèse de polymères à partir de synthons extraits ou dérivés de cette biomasse.

Parmi ces ressources renouvelables, les produits oléagineux représentent une source durable, dont les sous-produits de raffinage peuvent être utilisés pour de nombreuses applications (carburant (biodiesel), alimentation, synthons pour la chimie).[12–15] La forte demande de protéines végétales ainsi que la stagnation du marché du biodiesel (en Europe particulièrement), contribuent à l'augmentation des stocks d'huiles végétales, qui pourraient être utilisées de façon opportune dans l'industrie chimique.[12–15]

Les esters gras notamment, obtenus par transesterification de triglycérides, possèdent un certain nombre de groupes fonctionnels, tels que des esters, des alcools ou des doubles liaisons, qui peuvent être utilisés en chimie pour des réactions de modification chimique ou de polymérisation.[16–18] Les polymères formés, biosourcés, peuvent entrer dans de nombreuses formulations en tant qu'additifs : plastifiants, enduits, lubrifiants, émulsifiants, tensio-actifs ou comme pré-polymères de matériaux de structure.[15]

Les polymères dendritiques, forment l'une des trois principales classes de polymères non réticulés, à côté des polymères linéaires et ramifiés (**Figure 1**). La structure globulaire en 3 dimensions de ces polymères limite leur capacité d'enchevêtrement, facilitant leur solubilité en milieu solvant et leur confère une faible viscosité, les rendant particulièrement adaptés pour de nombreuses applications, en formulation notamment.[19–21] Parmi ces systèmes, les polymères hyper-ramifiés suscitent un fort intérêt, car leurs voies de synthèse en une étape sont plus simples et moins coûteuses que celles des dendrimères.[22,23] Pour autant, ce type de procédé génère des structures moins régulières, une distribution plus large des masses molaires et une plus faible densité de ramifications mais leurs potentiels en terme d'applications sont multiples.[24]

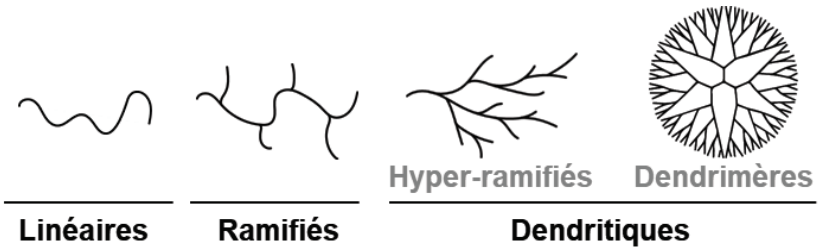

Figure 1. Familles de polymères non-réticulés.

A notre connaissance, l'utilisation de synthons biosourcés pour la synthèse de polymères hyper-ramifiés n'a été décrite que dans quelques publications mais n'a pas encore fait l'objet de développement industriel.[25–29]

Dans un projet réalisé précédemment au LCPO et financé par la S.A.S PIVERT en 2012, un ensemble de polyesters hyper-ramifiés synthétisés à partir de monomères de type AB_n ($n \geq 2$), issus de la fonctionnalisation d'esters gras, a été développé.[22,25,30] Notamment, la polycondensation du 9,10-dihydroxystéarate de méthyle (M2HS), préparé par hydrolyse de l'huile de tournesol époxydée, en polyester hyper-ramifié de type polyol (*hb*PEster-OH), nommé M2HS-*hb*PEster, a été optimisée de façon à produire jusqu'à 1 kg de polymère (ITERG). Dans le cadre du présent travail, il s'est agi d'élargir la gamme de polymères hyper-ramifiés oléosourcés et de modifier leurs propriétés à travers (i) la fonctionnalisation de M2HS-*hb*PEsters et (ii) le développement d'une nouvelle classe de polymères hyper-ramifiés, à savoir les polyéthers.

Après une brève introduction sur les caractéristiques des polymères hyper-ramifiés, le premier chapitre permettra de présenter les différentes voies de synthèses des polyéthers hyper-ramifiés (*hb*PEthers), leurs propriétés et leurs applications. Dans un premier temps, l'attention sera portée sur les modes de synthèse, par substitutions aromatique & nucléophile et par ouverture de cycle (ROP), de polyéthers hyper-ramifiés aromatiques et aliphatiques. La dernière partie de cette étude bibliographique sera dédiée à la synthèse de polyglycidols hyper-ramifiés (*hb*PG), par ouverture de cycle (ROMBP), une classe d'*hb*PEthers ayant fait l'objet de nombreuses recherches. Les différentes méthodes de copolymérisation, impliquant principalement le glycidol comme monomère, et les stratégies de fonctionnalisation d'*hb*PGs seront également présentées, ainsi que les applications de ces composés.

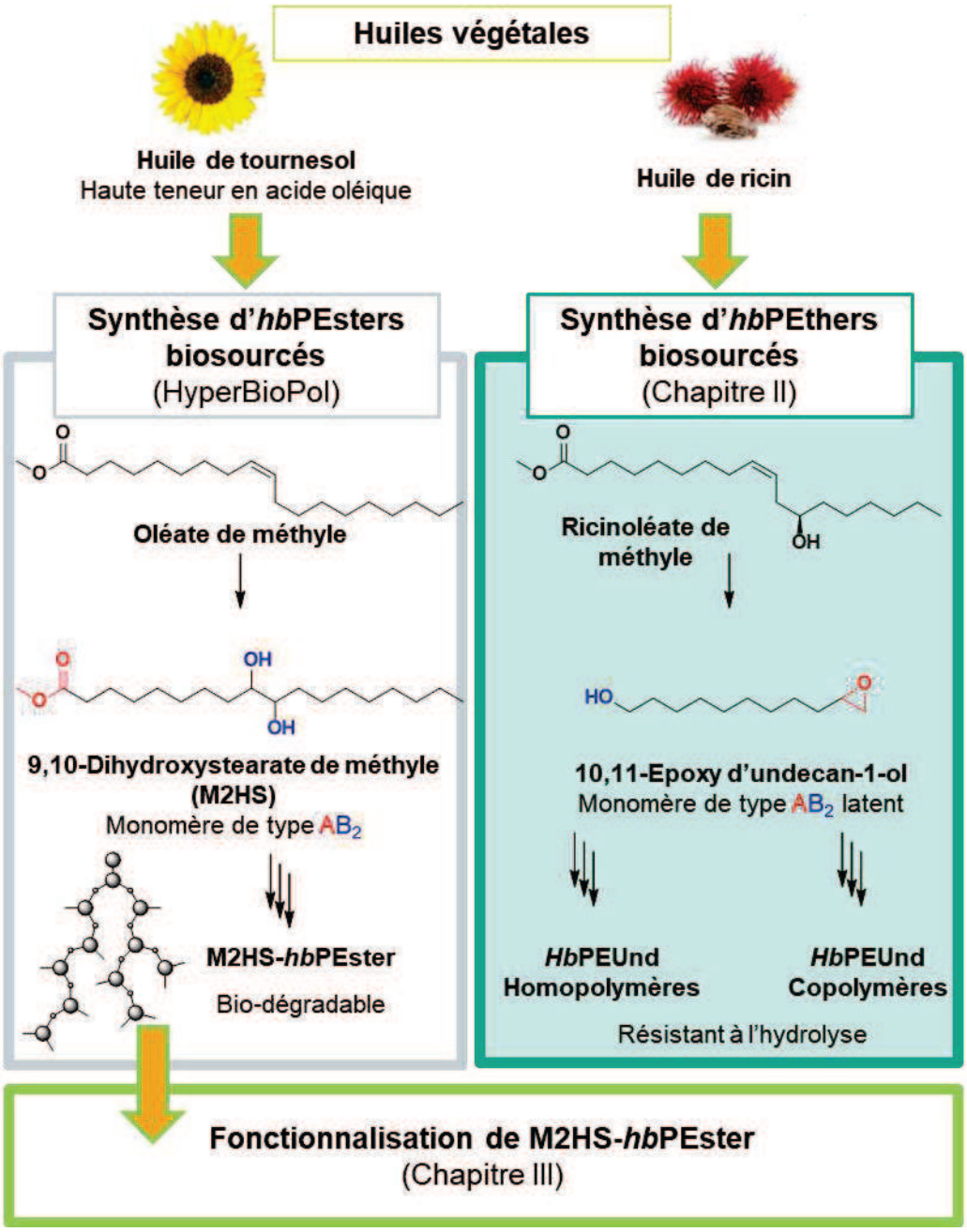

Figure 2. Du projet HyperBioPol vers FunHyBioPol.

Le chapitre II fait état de la synthèse d'un nouveau monomère biosourcé de type α-époxy-ω-alcool, le 10,11-epoxy d'undecan-1-ol (EUnd), issu de l'huile de ricin. Ce monomère a été utilisé pour la synthèse d'un nouveau polyéther hyper-ramifié, nommé *hb*PEUnd. A notre connaissance, l'EUnd est le seul monomère biosourcé, en plus du glycidol et du carbonate de glycérol, à avoir été polymérisé par ouverture de cycle par voie anionique.[31–33] L'accent a été mis sur l'optimisation des conditions opératoires permettant d'obtenir l'homo*hb*PEUnd et sur sa caractérisation. L'élaboration de copolymères, à blocs ou statistiques, entre l'EUnd et le glycidol, sera également détaillée.

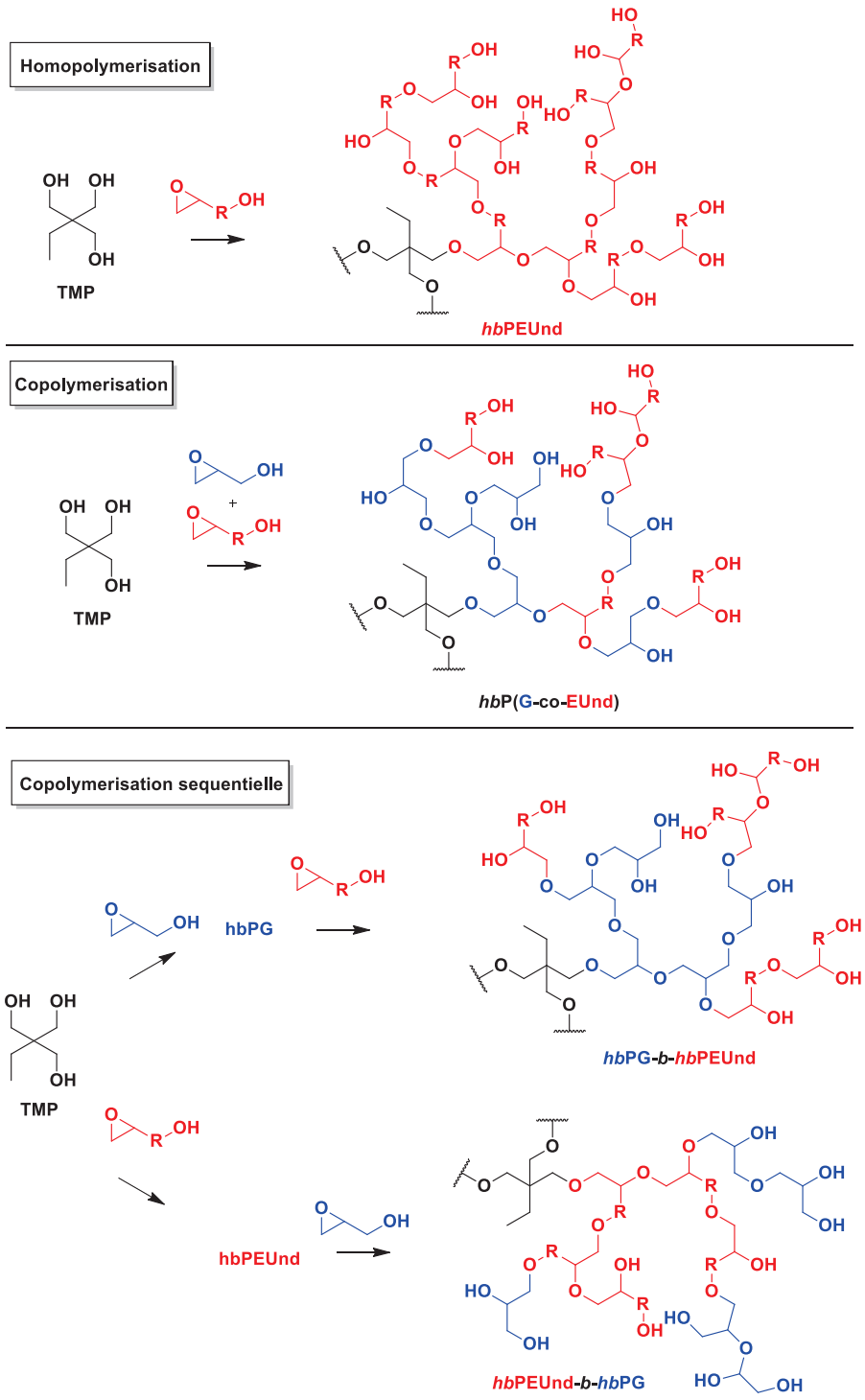

Figure 3. Homopolymérisation d'Eund par ROMBP et copolymérization avec le glycidol par ROMBcP.

Les travaux présentés dans le chapitre III concernent la fonctionnalisation des fonctions OH du M2HS-*hb*PEster, dont l'objectif est d'étendre le champ d'applications de ces substrats biosourcés. La modification des bouts de chaîne de M2HS-*hb*PEsters avec l'anhydride succinique et le chlorure d'acryloyle a permis de générer des polyesters hyper-ramifiés aux terminaisons acide (*hb*PEster-$COOH_x$) solubles dans l'eau ainsi que des *hb*PEsters terminés

avec des fonctions acryloyle réactives (*hb*PEster-A_x). Nous nous sommes intéressés dans un premier temps aux méthodes de fonctionnalisation du M2HS-*hb*PEster et à la caractérisation des polymères formés, puis, à l'étude de leurs propriétés.

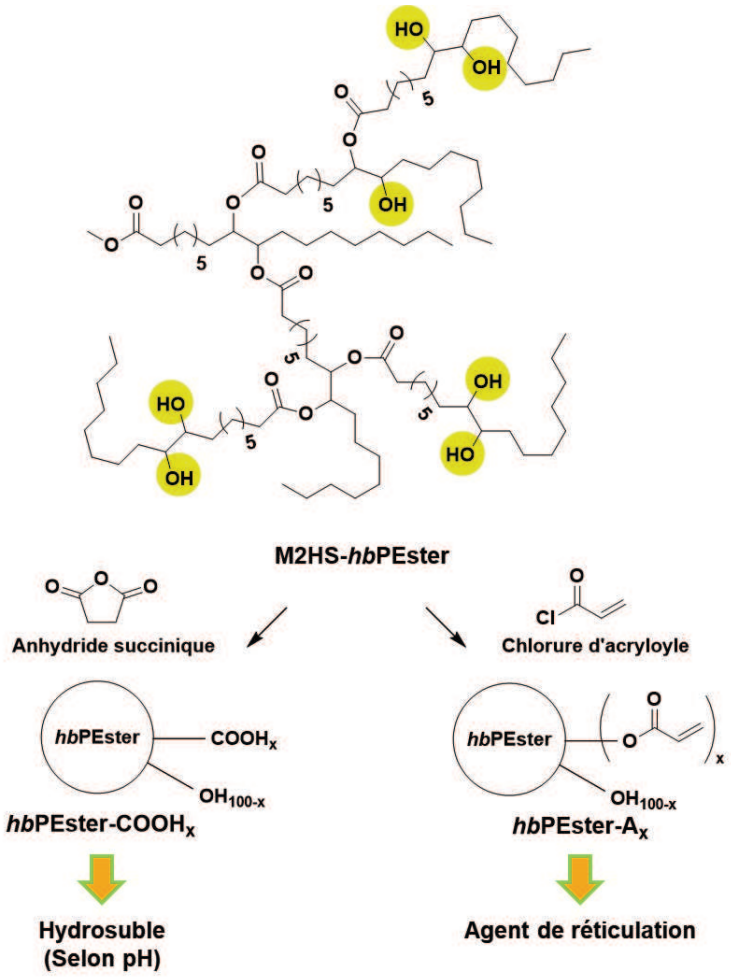

Figure 4. Fonctionnalisation d'*hb*PEster par réaction avec l'anhydride succinique et du chlorure d'acryloyle.

References

(1) Geyer, R.; Jambeck, J. R.; Law, K. L. Production, Use, and Fate of All Plastics Ever Made. *Sci Adv* **2017**, *3*.

(2) PlasticsEurope. Plastics - the Facts 2017: An Analysis of European Plastics Production, Demand and Waste Data. **2017**.

(3) *BP Statistical Review of World Energy 2018*; London, 2018.

(4) *The New Plastics Economy: Rethinking the Future of Plastics & Catalysing Action*; 2017.

(5) Gandini, A. The Irruption of Polymers from Renewable Resources on the Scene of Macromolecular Science and Technology. *Green Chem* **2011**, *13* (5), 1061–1083.

(6) Gandini, A.; Lacerda, T. M.; Carvalho, A. J. F.; Trovatti, E. Progress of Polymers from Renewable Resources: Furans, Vegetable Oils, and Polysaccharides. *Chem Rev* **2016**, *116* (3), 1637–1669.

(7) Brandt-Talbot, A.; Weigand, L. Highlights from the Faraday Discussion: Bio-Resources: Feeding a Sustainable Chemical Industry. *Chem Commun* **2017**, *53*, 12848–12856.

(8) Schneiderman, D. K.; Hillmyer, M. A. 50th Anniversary Perspective : There Is a Great Future in Sustainable Polymers. *Macromolecules* **2017**, *50* (10), 3733–3749.

(9) Okkerse, C.; van Bekkum, H. From Fossil to Green. *Green Chem* **1999**, *1* (2), 107–114.

(10) Anastas, P.; Eghbali, N. Green Chemistry: Principles and Practice. *Chem Soc Rev* **2010**, *39* (1), 301–312.

(11) Sheldon, R. A. Green and Sustainable Manufacture of Chemicals from Biomass: State of the Art. *Green Chem.* **2014**, *16* (3), 950–963.

(12) Palmeros Parada, M.; Osseweijer, P.; Posada Duque, J. A. Sustainable Biorefineries, an Analysis of Practices for Incorporating Sustainability in Biorefinery Design. *Ind Crops Prod* **2017**, *106*, 105–123.

(13) Maity, S. K. Opportunities, Recent Trends and Challenges of Integrated Biorefinery: Part I. *Renew Sustain Energy Rev* **2015**, *43*, 1427–1445.

(14) Pandey, A.; Höfer, R.; Taherzadeh, M.; Nampoothiri, K. M.; Larroche, C. *Industrial Biorefineries And White Biotechnology*; Elsevier, Ed.; Elsevier: Oxford, UK, 2015.

(15) McKeon, T. A.; Hayes, D. G.; Hildebrand, D. F.; Weselake, R. J. *Industrial Oil Crops*; Nikki Levy, 2016.

(16) Zhang, C.; Garrison, T. F.; Madbouly, S. A.; Kessler, M. R. Recent Advances in Vegetable Oil-Based Polymers and Their Composites. *Prog Polym Sci* **2017**, *71*, 91–143.

(17) Montero de Espinosa, L.; Meier, M. A. R. Plant Oils: The Perfect Renewable Resource for Polymer Science?! *Eur Polym J* **2011**, *47* (5), 837–852.

(18) Sharmin, E.; Zafar, F.; Akram, D.; Alam, M.; Ahmad, S. Recent Advances in Vegetable Oils Based Environment Friendly Coatings: A Review. *Ind Crops Prod* **2015**, *76*, 215–229.

(19) Hult, A.; Johansson, M.; Malmström, E. Hyperbranched Polymers. In *Branched Polymers II*; Roovers, J., Ed.; Advances in Polymer Science; Springer Berlin Heidelberg, 1999; Vol. 143, pp 1–34.

(20) Fréchet, J. M. J. Functional Polymers and Dendrimers: Reactivity, Molecular Architecture, and Interfacial Energy. *Science* **1994**, *263*, 1710–1715.

(21) Yan, D.; Gao, C.; Frey, H. *Hyperbranched Polymers: Synthesis, Properties, and Applications*; John Wiley & Sons, Inc.: Hoboken, 2011.

(22) Testud, B. Vegetable Oils as a Platform for the Design of Novel Hyperbranched Polyesters, PhD Thesis, Université de Bordeaux, 2015.

(23) Zheng, Y.; Li, S.; Weng, Z.; Gao, C. Hyperbranched Polymers: Advances from Synthesis to Applications. *Chem Soc Rev* **2015**, *44*, 4091–4130.

(24) Voit, B. New Developments in Hyperbranched Polymers. *J Polym Sci Part A Polym Chem* **2000**, *38* (14), 2505–2525.

(25) Testud, B.; Pintori, D.; Grau, E.; Taton, D.; Cramail, H. Hyperbranched Polyesters by Polycondensation of Fatty Acid-Based AB n -Type Monomers. *Green Chem.* **2017**, *19*, 6–11.

(26) Pramanik, S.; Konwarh, R.; Sagar, K.; Konwar, B. K.; Karak, N. Bio-Degradable Vegetable Oil Based Hyperbranched Poly(Ester Amide) as an Advanced Surface Coating Material. *Prog Org Coatings* **2013**.

(27) Lee, K. W.; Chung, J. W.; Kwak, S.-Y. Synthesis and Characterization of Bio-Based Alkyl Terminal Hyperbranched Polyglycerols: A Detailed Study of Their Plasticization Effect and Migration Resistance. *Green Chem.* **2016**.

(28) Sun, M.; Yin, C.; Gu, Y.; Li, Y.; Xin, Z. Synthesis and Characterization of Hyperbranched Poly(Ester-Amine) by Michael Addition Polymerization. *Des Monomers Polym* **2017**, *2*, 458–467.

(29) Baozhong, S. New Bio-Based Non-Ionic Hyperbranched Polymers as Environmentally Friendly Antibacterial Additives for Biopolymers. *Green Chem* **2018**, *20*, 1238–1249.

(30) Testud, B.; Grau, E.; Pintori, D.; Taton, D.; Cramail, H. New Branched Polymers, Their Preparation Process and Thereof. EU 14306642 A1, 2014.

(31) Son, S.; Park, H.; Shin, E.; Shibasaki, Y.; Kim, B.-S. Architecture-Controlled Synthesis of Redox-Degradable Hyperbranched Polyglycerol Block Copolymers and the Structural Implications of Their Degradation. *J Polym Sci Part A Polym Chem* **2016**, *54* (12), 1752–1761.

(32) Son, S.; Shin, E.; Kim, B. S. Redox-Degradable Biocompatible Hyperbranched Polyglycerols: Synthesis, Copolymerization Kinetics, Degradation, and Biocompatibility. *Macromolecules* **2015**, *48* (3), 600–609.

(33) Shenoi, R. A.; Lai, B. F. L.; Kizhakkedathu, J. N. Synthesis, Characterization, and Biocompatibility of Biodegradable Hyperbranched Polyglycerols from Acid-Cleavable Ketal Group Functionalized Initiators. *Biomacromolecules* **2012**, *13* (10), 3018–3030.

GENERAL INTRODUCTION

This thesis is part of the FunHyBioPol project (W3P20) and was conducted in collaboration with the Laboratoire de Chimie des Polymères Organiques (LCPO), the Laboratoire Charles Coulomb (L2C) and the French Technical Centre of Fats and Oils (ITERG). It was financially supported by the SAS PIVERT, which aims at developing vegetable oil-based chemistry through technology transfer, from research laboratories to industry.

Polymers find applications in various sectors including packaging, building & construction, automotive & aeronautic, electrical & electronics as well as health & safety. Such developments are mainly owed to the low-cost, ease of process and the large range of properties that can be reached with polymeric materials, explaining that approximately 8,300 million tons of plastics have been produced from 1950 to date (330 million tonnes produced in 2015).[1,2]

Nowadays, around 6 % of petroleum consumption (4.9 billion tons per year) are dedicated to the production of "plastics".[3–5] However, in a perspective of reducing greenhouse gas emissions, the replacement of building blocks/monomers from fossil to renewable feedstock has attracted researchers from both the academic and the industrial fields.[6–8] Biomass embodies a sustainable alternative to petroleum, as its regeneration time-scale is much lower in comparison to fossil resources (decades instead of millions of years).[9,10]

The development of efficient bio-refineries, following the principles of green chemistry and processes,[11,12] is required in order to optimize the potential of the biomass to produce power, food, feed and of course chemicals in a sustainable manner.[13–15] Bio-based polymers can hence be expectedly obtained from these processes, that is to say, by (i) using natural polymers directly obtained from biomass (lignin, cellulose, starch) or (ii) polymerizing bio-based building blocks, extracted from biomass.

Among available renewable resources, oilseed biomass represents a promising feedstock owing to the large range of applications of the refinery sub-products.[13–16] Annual production of oilseed accounted to 465 million tons in 2016 and is now expected to grow from 20 % by 2026, due to the high demand in protein meals.[17,18] This, along with a stagnation of the biodiesel demand,

contributes to the increase of the production of vegetable oils, which can be opportunately used as building blocks towards polymer materials.[13–16]

In particular, platforms based on fatty methyl esters (FAMEs), resulting from the transesterification of triglycerides arising from vegetable oils, have been developed for this purpose.[19–21] FAMEs, which display functional groups such as esters, alcohols or double bonds, can be advantageously used or modified for chemical applications such as the synthesis of bio-based polymers, these latter finding applications as additives, plasticizers, sealants, lubricants and food emulsifiers.[16]

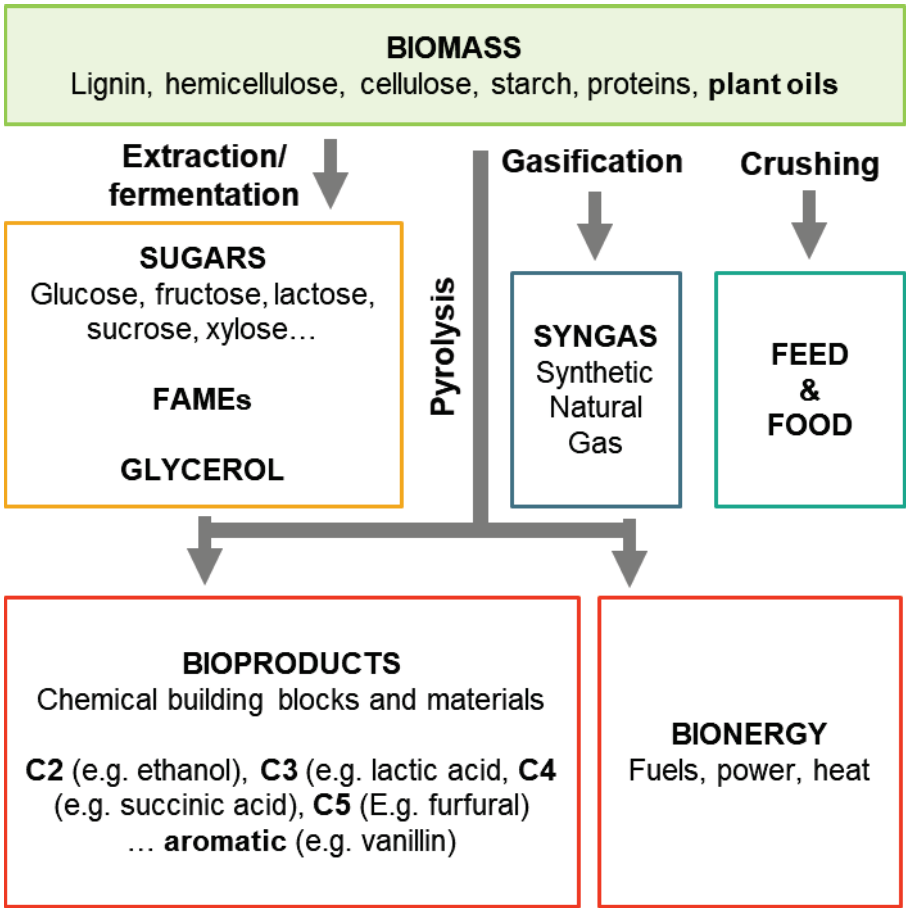

Figure 1. General concept of a biorefinery.

Dendritic polymers, also referred to as highly branched macromolecules, are recognized as one of the three major classes of non cross-linked polymers, together with linear and branched macromolecules (**Figure 2**). The 3D-globular shape imparts to dendritic polymers a low viscosity, good solubility and lack of entanglements, making them attractive for specific applications, e.g. as additives for formulations.[22–24] Among them, hyperbranched polymers are

attracting a major interest regarding their ease of synthesis, high functionality and cost-effective process,[25,26] despite their less regular architecture, broader molecular weight distributions and lower branching compared to dendrimers.[27]

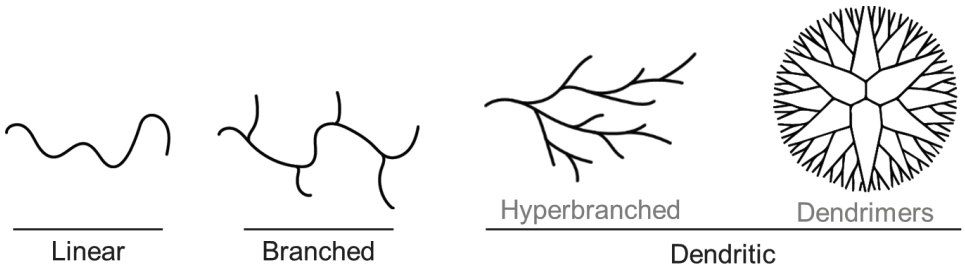

Figure 2. Three major families of thermoplastic polymers, hyperbranched polymers and dendrimers representing two examples of dendritic polymers.

The use of bio-based synthons as precursors of hyperbranched polymers, were reported in a few publications, in particular at the LCPO.[28–32] In the previous HyperBioPol project funded by the SAS PIVERT in 2012, a set of *hb*PEsters from AB_n-type monomers ($n \geq 2$), obtained by functionalization of FAMEs, were developed.[25,28,33] In particular, the polycondensation of methyl 9,10-dihydroxystearate (M2HS), prepared by hydrolysis of epoxidized high oleic sunflower oil, into hyperbranched polyester polyols (*hb*PEster-OH), referred to as M2HS-*hb*PEster, has been investigated.[34] Such synthesis has been scaled up from gram to kilogram.

Throughout this PhD work, we aimed at extending the platform of oily-based hyperbranched polymers, following two main approaches involving the derivatization of M2HS-*hb*PEsters in the one hand and the development of a new class of bio-based hyperbranched polyethers, in the other hand.

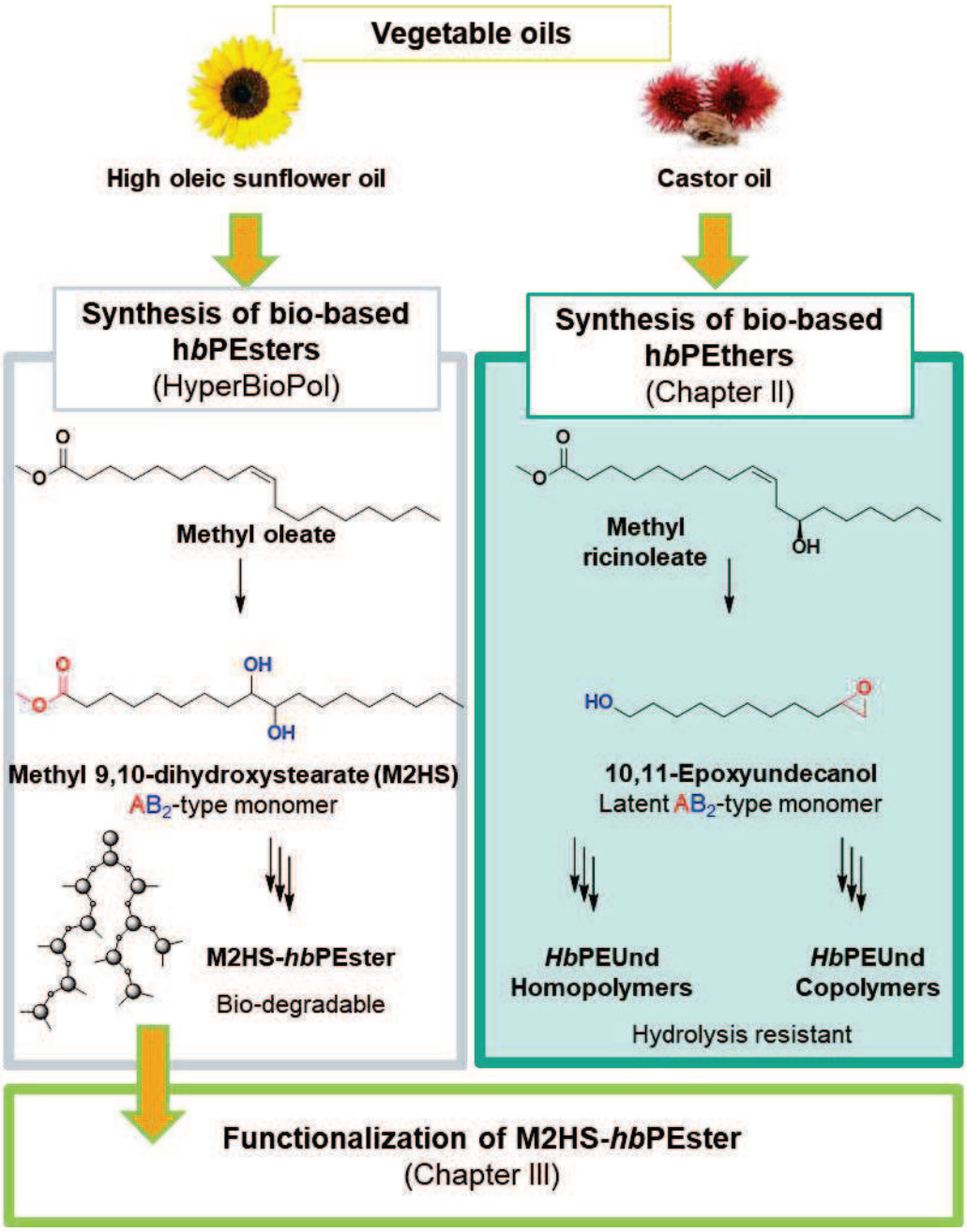

Figure 3. From HyperBioPol to FunHyBioPol project.

After the general features about hyperbranched polymers, an overview of the synthesis, properties and applications of hyperbranched polyethers (*hb*PEthers) will be given in the first Chapter. First, attention will be paid to the chemical pathways, namely aromatic & nucleophilic substitutions and ring-opening polymerization of cyclic monomers (ROP), yielding aromatic and aliphatic *hb*PEthers. Synthesis of hyperbranched polyglycidol (*hb*PG), *via* anionic ring-opening multibranching polymerization (ROMBP) of glycidol will be specifically presented, as this class of polymeric materials has been the topic of intensive research. Copolymerization of

glycidol with other epoxides and functionalization of glycidol-based hyperbranched homo- and copolyethers will be also detailed.

Chapter II describes the synthesis and the subsequent ring-opening multibranching polymerization (ROMPB) of a new bio-based α-epoxy-ω-alcohol, namely, 10,11-epoxyundecanol (EUnd) stemming from castor oil, leading to unprecedented hyperbranched polyethers, that will be denoted as *hb*PEUnd. To the best of our knowledge, EUnd is the only bio-based oxirane, with glycidol, being polymerized through anionic methodology.[35,36]

Emphasis will be focused on the description of the conditions best suited to achieve *hb*PEUnd by ROMBP, as well as the ring-opening multibranching copolymerization (ROMBcP) of EUnd with glycidol forming highly functionalized branched copolyethers.

In the following of the HyperBioPol project, the works presented in Chapter III will investigate the derivatization of the OH groups of M2HS-*hb*PEster, with the objective of broadening the potential applications of these bio-based substrates. The derivatization of M2HS-*hb*PEster with succinic anhydride and acryloyl chloride has thus been undertaken in order to produce water-soluble *hb*PEster-$COOH_x$ or reactive acrylate-terminated *hb*PEster-A_x, respectively. A first part will be dedicated to the functionalization procedure and to the structural characterization of the functionalized *hb*PEsters by ^{1}H NMR, SEC and DSC analyses. Then, specific properties and potential applications of these modified M2HS-*hb*PEster will be discussed.

References

(1) Geyer, R.; Jambeck, J. R.; Law, K. L. Production, Use, and Fate of All Plastics Ever Made. *Sci Adv* **2017**, *3*.

(2) PlasticsEurope. *Plastics - the Facts 2014/2015*; 2015.

(3) PlasticsEurope. Plastics - the Facts 2017: An Analysis of European Plastics Production, Demand and Waste Data. **2017**.

(4) *BP Statistical Review of World Energy 2018*; London, 2018.

(5) *The New Plastics Economy: Rethinking the Future of Plastics & Catalysing Action*; 2017.

(6) Gandini, A. The Irruption of Polymers from Renewable Resources on the Scene of Macromolecular Science and Technology. *Green Chem* **2011**, *13* (5), 1061–1083.

(7) Gandini, A.; Lacerda, T. M.; Carvalho, A. J. F.; Trovatti, E. Progress of Polymers from Renewable Resources: Furans, Vegetable Oils, and Polysaccharides. *Chem Rev* **2016**, *116* (3), 1637–1669.

(8) Brandt-Talbot, A.; Weigand, L. Highlights from the Faraday Discussion: Bio-Resources: Feeding a Sustainable Chemical Industry. *Chem Commun* **2017**, *53*, 12848–12856.

(9) Schneiderman, D. K.; Hillmyer, M. A. 50th Anniversary Perspective : There Is a Great Future in Sustainable Polymers. *Macromolecules* **2017**, *50* (10), 3733–3749.

(10) Okkerse, C.; van Bekkum, H. From Fossil to Green. *Green Chem* **1999**, *1* (2), 107–114.

(11) Anastas, P.; Eghbali, N. Green Chemistry: Principles and Practice. *Chem Soc Rev* **2010**, *39* (1), 301–312.

(12) Sheldon, R. A. Green and Sustainable Manufacture of Chemicals from Biomass: State of the Art. *Green Chem.* **2014**, *16* (3), 950–963.

(13) Palmeros Parada, M.; Osseweijer, P.; Posada Duque, J. A. Sustainable Biorefineries, an Analysis of Practices for Incorporating Sustainability in Biorefinery Design. *Ind Crops Prod* **2017**, *106*, 105–123.

(14) Maity, S. K. Opportunities, Recent Trends and Challenges of Integrated Biorefinery: Part I. *Renew Sustain Energy Rev* **2015**, *43*, 1427–1445.

(15) Pandey, A.; Höfer, R.; Taherzadeh, M.; Nampoothiri, K. M.; Larroche, C. *Industrial Biorefineries And White Biotechnology*; Elsevier, Ed.; Elsevier: Oxford, UK, 2015.

(16) McKeon, T. A.; Hayes, D. G.; Hildebrand, D. F.; Weselake, R. J. *Industrial Oil Crops*; Nikki Levy, 2016.

(17) Ritchie, A.; Roser, M. Meat and Seafood Production & Consumption https://ourworldindata.org/meat-and-seafood-production-consumption.

(18) OECD/FAO. *OECD-FAO Agricultural Outlook 2017-2026. OECD Publishing, Paris,*; 2017.

(19) Zhang, C.; Garrison, T. F.; Madbouly, S. A.; Kessler, M. R. Recent Advances in Vegetable Oil-Based Polymers and Their Composites. *Prog Polym Sci* **2017**, *71*, 91–143.

(20) Montero de Espinosa, L.; Meier, M. A. R. Plant Oils: The Perfect Renewable Resource for Polymer Science?! *Eur Polym J* **2011**, *47* (5), 837–852.

(21) Sharmin, E.; Zafar, F.; Akram, D.; Alam, M.; Ahmad, S. Recent Advances in Vegetable Oils Based Environment Friendly Coatings: A Review. *Ind Crops Prod* **2015**, *76*, 215–229.

(22) Hult, A.; Johansson, M.; Malmström, E. Hyperbranched Polymers. In *Branched Polymers II*; Roovers, J., Ed.; Advances in Polymer Science; Springer Berlin Heidelberg, 1999; Vol. 143, pp 1–34.

(23) Fréchet, J. M. J. Functional Polymers and Dendrimers: Reactivity, Molecular Architecture, and Interfacial Energy. *Science (80-)* **1994**, *263*, 1710–1715.

(24) Yan, D.; Gao, C.; Frey, H. *Hyperbranched Polymers: Synthesis, Properties, and Applications*; John Wiley & Sons, Inc.: Hoboken, 2011.

(25) Testud, B. Vegetable Oils as a Platform for the Design of Novel Hyperbranched Polyesters, PhD Thesis, Université de Bordeaux, 2015.

(26) Zheng, Y.; Li, S.; Weng, Z.; Gao, C. Hyperbranched Polymers: Advances from Synthesis to Applications. *Chem Soc Rev* **2015**, *44*, 4091–4130.

(27) Voit, B. New Developments in Hyperbranched Polymers. *J Polym Sci Part A Polym Chem* **2000**, *38* (14), 2505–2525.

(28) Testud, B.; Pintori, D.; Grau, E.; Taton, D.; Cramail, H. Hyperbranched Polyesters by Polycondensation of Fatty Acid-Based AB n -Type Monomers. *Green Chem.* **2017**, *19*, 6–11.

(29) Pramanik, S.; Konwarh, R.; Sagar, K.; Konwar, B. K.; Karak, N. Bio-Degradable Vegetable Oil Based Hyperbranched Poly(Ester Amide) as an Advanced Surface Coating Material. *Prog Org Coatings* **2013**, *76* (4), 689–697.

(30) Lee, K. W.; Chung, J. W.; Kwak, S.-Y. Synthesis and Characterization of Bio-Based Alkyl Terminal Hyperbranched Polyglycerols: A Detailed Study of Their Plasticization Effect and Migration Resistance. *Green Chem* **2016**, *18* (4), 999–1009.

(31) Sun, M.; Yin, C.; Gu, Y.; Li, Y.; Xin, Z. Synthesis and Characterization of Hyperbranched Poly(Ester-Amine) by Michael Addition Polymerization. *Des Monomers Polym* **2017**, *2*, 458–467.

(32) Baozhong, S. New Bio-Based Non-Ionic Hyperbranched Polymers as Environmentally Friendly Antibacterial Additives for Biopolymers. *Green Chem* **2018**, *20*, 1238–1249.

(33) Testud, B.; Grau, E.; Pintori, D.; Taton, D.; Cramail, H. New Branched Polymers, Their Preparation Process and Thereof. EU 14306642 A1, 2014.

(34) Köckritz, A.; Martin, A. Oxidation of Unsaturated Fatty Acid Derivatives and Vegetable Oils. *Eur J Lipid Sci Technol* **2008**, *110* (9), 812–824.

(35) Son, S.; Shin, E.; Kim, B. S. Redox-Degradable Biocompatible Hyperbranched Polyglycerols: Synthesis, Copolymerization Kinetics, Degradation, and Biocompatibility. *Macromolecules* **2015**, *48* (3), 600–609.

(36) Shenoi, R. A.; Lai, B. F. L.; Kizhakkedathu, J. N. Synthesis, Characterization, and Biocompatibility of Biodegradable Hyperbranched Polyglycerols from Acid-Cleavable Ketal Group Functionalized Initiators. *Biomacromolecules* **2012**, *13* (10), 3018–3030.

CHAPTER I

Synthesis, properties and potential of aromatic and aliphatic hyperbranched polyethers

Keywords: hyperbranched polymers, degree of branching, hyperbranched poly(aryl ether)s, transetherification, aliphatic hyperbranched polyethers, ring-opening polymerization, hyperbranched polyglycidol, copolymerization

TABLE OF CONTENTS

1. HYPERBRANCHED POLYMERS 25

1.1. Introduction to dendritic polymers 25

1.2. Hyperbranched polymers 26

1.3. Introduction to hyperbranched polyethers 30

2. GENERAL OUTLINE OF SYNTHETIC APPROACHES FOR THE PREPARATION OF HYPERBRANCHED POLYETHERS 31

2.1. Synthesis of aromatic hyperbranched polyethers by step-growth polymerization 31

2.2. Synthesis of hyperbranched polyethers by ring-opening polymerization 40

3. RING-OPENING POLYMERIZATION OF GLYCIDOL 54

3.1. Generalities and challenges 54

3.2. Thermal and thermo-rheological properties 61

3.3. Functionalization of hyperbranched polyglycidol: towards original properties .. 62

3.4. Towards innovative technologies 76

4. CONCLUSION AND OBJECTIVES 79

5. REFERENCES 81

1. Hyperbranched Polymers

This bibliographic chapter discusses the main features of hyperbranched polymers in general with a particular focus on hyperbranched polyethers.

1.1. Introduction to dendritic polymers

Dendritic polymers, also referred to as highly branched macromolecules, are recognized as one of the three major classes of non-cross-linked polymers, besides linear and branched macromolecules (**Figure I-1**).

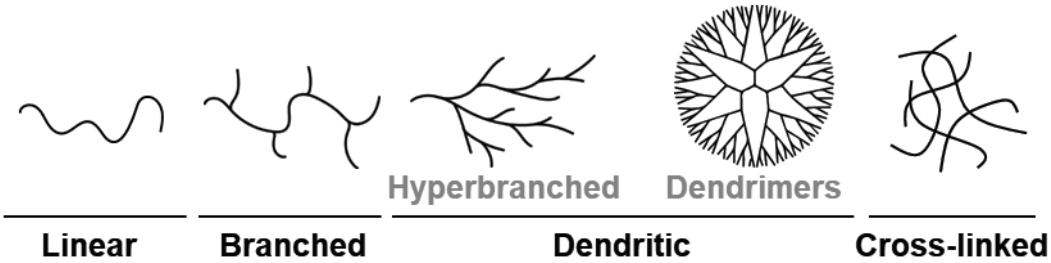

Figure I-1. Main polymeric structures: linear, branched and crosslinked polymers; hyperbranched polymers and dendrimers represent two examples of dendritic polymers.

Dendritic polymers are categorized as follows: (a) dendrons and dendrimers,[1,2] (b) linear-dendritic hybrids,[3] (c) dendronized polymers,[4,5] (d) dendrigrafts and dendrimer-like polymers,[6–8] (e) hyperbranched polymers, (f) hyperbranched polymer brushes, (g) hyperbranched polymer-grafted linear macromolecules and (h) hypergrafts or hyperbranched polymer-like macromolecules,[9] as depicted in **Figure I-2**.[10,11]

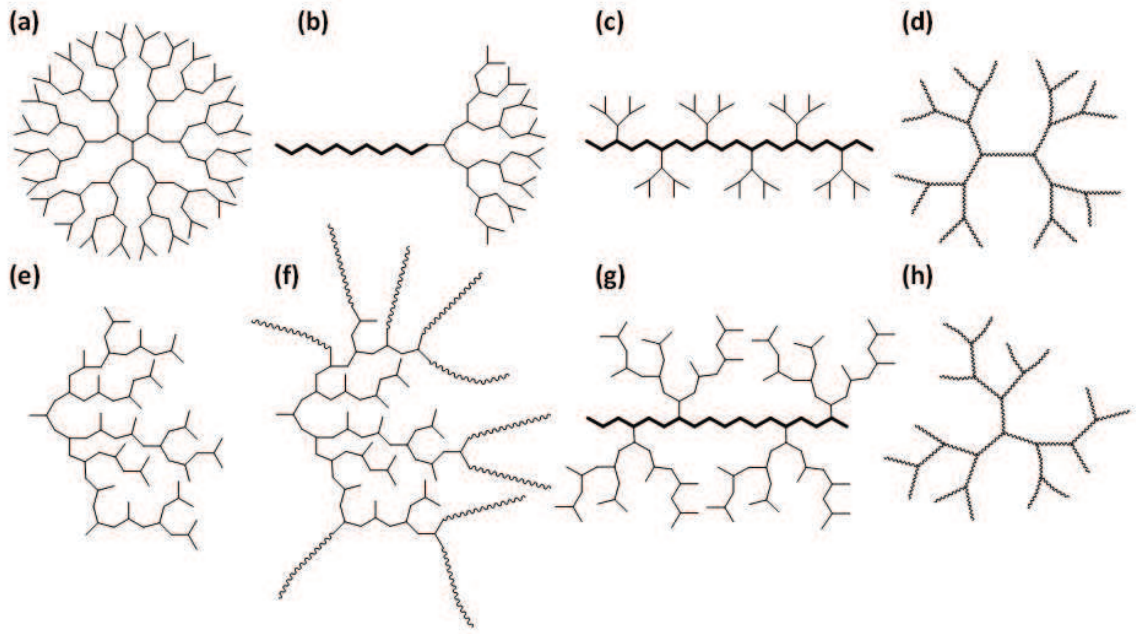

Figure I-2. Dendritic polymers with different structures **(a)** dendrimers, **(b)** linear-dendritic hybrids, **(c)** dendronized polymers, **(d)** dendrimer-like polymers, **(e)** hyperbranched polymers, **(f)** hyperbranched polymer brushes, **(g)** hyperbranched polymer-grafted linear macromolecules and **(h)** hypergrafts polymers.[10,11]

Dendrimers, first reported by Vögtle and coworkers in 1978,[12] are well-defined macromolecules having a perfectly branched and symmetric structure, which can be achieved *via* two main methodologies, namely the divergent[13,14] and the convergent[15,16] multistep approaches (**Figure I-3**).[17,18]

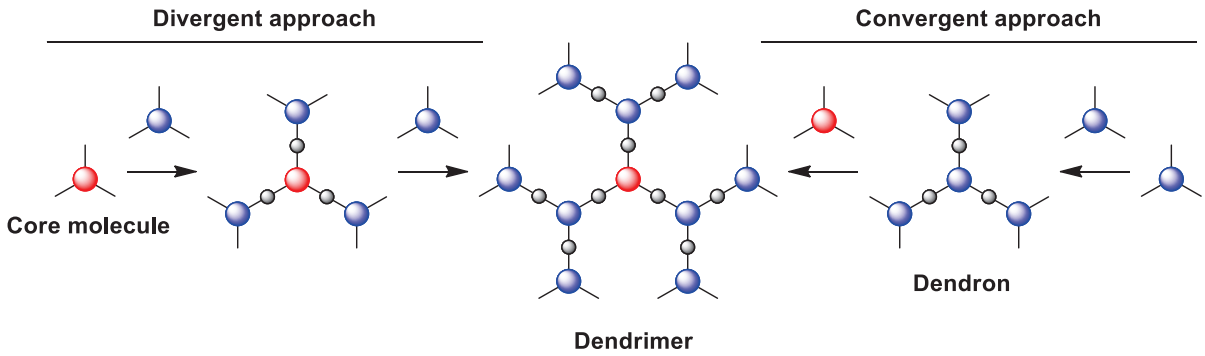

Figure I-3. Dendrimer growth obtained by divergent and convergent approaches.[11]

1.2. Hyperbranched polymers

1.2.1. Generalities

Notions of "highly branched species" and "degree of branching" (DB) were introduced by Flory in the early 1940s.[9–21] Flory later demonstrated that, in contrast to the copolymerization of bi-

(A_2) and trifunctional (B_3) (or tetrafunctional, B_4) monomers, the homopolymerization of AB_n, $_{n\geq2}$-type monomers could prevent the formation of insoluble cross-linked systems, yielding soluble polymers with "branch-on-branch" topologies (**Figure I-4**).[22]

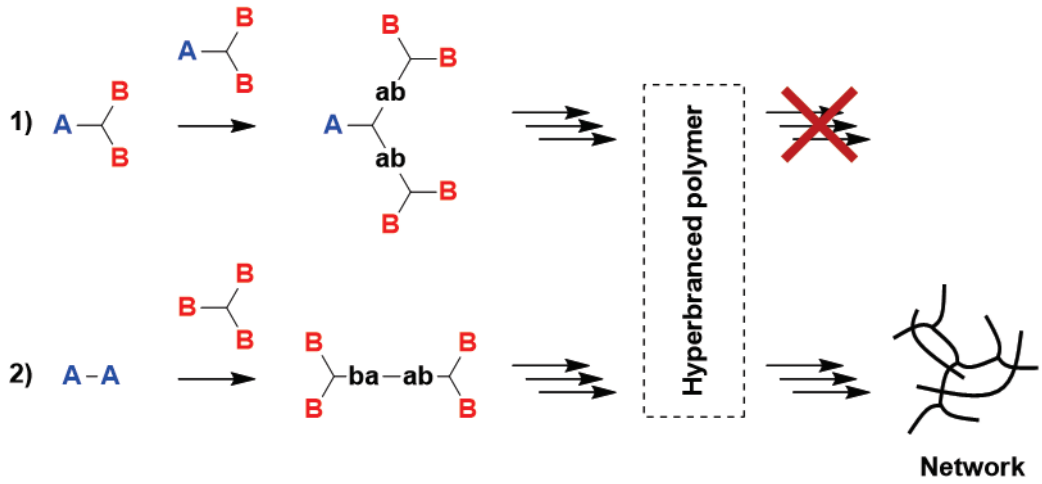

Figure I-4. Synthetic strategy towards hyperbranched polymers and networks according to Flory's approach.

Yet, the terms "hyperbranched polymers" were coined few decades later by Kim and Webster, who reported the first intentional synthesis of hyperbranched polyphenylenes, warranted as a patent in 1987.[23,24] Since then, hyperbranched polymers have been attracting a growing interest regarding their ease of synthesis, modification and wide range of potential applications, as confirmed by the increasing number of publications, from over the past 25 years.[11,25] However, a few examples of hyperbranched polymers synthesized prior to this definition formulated by Kim and Webster, had been reported.[26–28]

1.2.2. Degree of branching

Hyperbranched polymers are usually presented as imperfect but more easily accessible analogues of dendrimers, as their 'one-pot' synthesis affords a much simpler and more economic route to branched materials.[29] Yet, due to statistical growth, control is generally lost over molecular weight and branching accuracy. Hyperbranched polymers show therefore a less regular architecture than dendrimers, with a much broader molecular weight distribution and a lower branching density.

Degree of branching (DB), varying between 0 and 1, is an important parameter of dendritic macromolecules as it quantifies their branching density. As shown in **Figure I-5**, hyperbranched polymers prepared by polymerization of AB_2-type monomers are characterized

by three different subunits, namely terminal (T), linear (L) and dendritic (D) depending on the number of unreacted B groups, *i.e.* 2, 1 and 0, respectively.

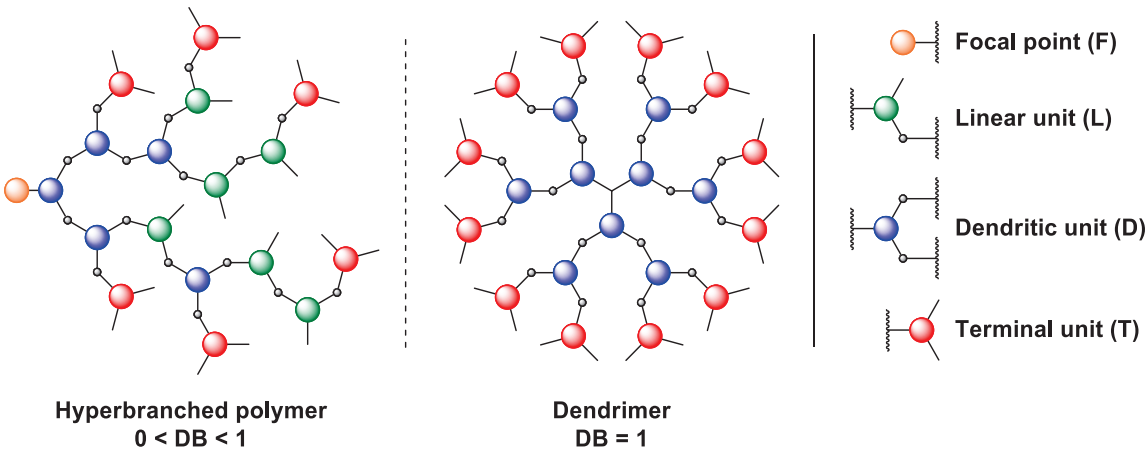

Figure I-5. Different subunits in hyperbranched polymers obtained by polycondensation of AB_2-*type* monomer and dendrimers.

Based on these definitions, DB can be determined according to the two equations proposed by Fréchet[30] and Frey, respectively.[31]

$$DB_{Fréchet} = \frac{D + T}{D + T + L} \qquad \text{(Eq. I-1)}$$

$$DB_{Frey} = \frac{2D}{2D + L} \qquad \text{(Eq. I-2)}$$

While DB of (perfect) dendrimers is equal to 1, DB values reported for randomly branched hyperbranched polymers generally range between 0.4 and 0.8. Both definitions are commonly used and lead to similar results at high conversions. However, if some unreacted AB_2 monomers are included in the calculations, overestimation of the terminal units occurs and the DB coined by Frey tends to be smaller than the one defined by Fréchet.

NMR spectroscopy, most often ^{1}H and invert-gated ^{13}C NMR, is the most useful tool for determining DB, as it enables to distinguish characteristic signals of each repeating unit (T, L and D). In the case of heteroatom-containing hyperbranched polymers, ^{15}N, ^{19}F, ^{29}Si and ^{31}P NMR spectroscopies can also be applied. Two-dimensional NMR (2D NMR) techniques are often required to solve the complex spectra obtained in one dimension. Model compounds, mimicking the linear and dendritic motifs, might be used to correctly assign the characteristic

peaks of each subunit. Other techniques should be mentioned, such as the "degradative approach".[32] Finally, in cases where neither NMR techniques nor degradation is feasible, branching can be estimated by viscometry analysis, based on the Mark-Houwink-Sakurada (MHS) equation:

$$[\eta]=KM^{\alpha} \qquad \text{(Eq. I-3)}$$

with [η] the intrinsic viscosity of the polymer, K and α the MHS constants (α is also referred to as MHS coefficient) and M the molecular weight of the polymer.

Hyperbranched polymers exhibit lower intrinsic viscosity than their linear analogues of same molecular weight, which results in lower values of α, *i.e.* 0.5 to 1 for linear polymers and less than 0.5 for hyperbranched polymers.[33] DB is a parameter of high importance since it impacts many physical and chemical properties of hyperbranched polymers, including their glass transition temperature (T_g), crystallization and melting behaviours, thermal stability, melting/solution viscosity, encapsulation capability, self-assembly behaviour, optoelectronic properties, etc.[34] The main differences between hyperbranched polymers, dendrimers and linear polymers are listed in **Table I-1**. Like dendrimers, hyperbranched polymers exhibit low viscosity,[35,36] high solubility, lack of entanglements and high functionality. Such parameters are often minimized for hyperbranched polymers, as they exhibit irregular architecture characterized by DB value lower than 1, and broad molecular weight distribution (usually $Đ > 2$). Nevertheless, due to their cost-effective synthesis in one-pot, hyperbranched polymers have attracted much industrial attention.

In addition, the high functionality of dendritic polymers, *i.e.* their large number of terminal functional groups, offers the possibility for further modification and opens the scope of potential applications.

Table I-1. Comparison of hyperbranched polymers with linear polymers and dendrimers (inspired from reference [10]).

Polymer	Linear	Hyperbranched	Dendrimer
Topology	1D	3D, irregular	3D, regular
Synthesis	one-step	one-pot	multi-steps
Scaling-up	Easy, already done	Easy, already done	Difficult, limited
Đ	≥ 1	> 2	1
DB	0	0.4-0.8	1
Viscosity	High	Low	Very low
Solubility	Low	High	Very high
Entanglement	Strong	Weak	Very weak or absence
Strength	High	Low	Very Low
Functionality	Chain-ends (2)	Dendritic and Linear units (>> 2)	Dendritic units (>> 2)

1.3. Introduction to hyperbranched polyethers

Hyperbranched polymers based on polyester, polyamide, polyethyleneimine, and polyether, have gained significant importance in macromolecular engineering in the past three decades.[10,29,37–44] In particular, polyethers have been widely used for applications requiring hydrolysis and chemical resistance as well as a good thermal stability. The mobility of the ether bond ensures the processability of these compounds above their glass transition temperature.

Polyethers can be categorized in two main families, namely aliphatic and aromatic polyethers. Aliphatic polyethers represent a spread class of semi-crystalline polymers, which are generally soluble in water and in polar solvents. They are considered as “soft” materials, as their glass transition and melting temperatures are rather low (T_g = -70 to -8 °C, T_m = 60 to 66 °C). In comparison, aromatic polyethers are rigid semi-crystalline materials, exhibiting high T_g (144 to 370 °C) and high T_m (up to 390 °C). Such differences are due to the higher mobility of the aliphatic polyether backbone composed of alkyl chains, in comparison to the strained character induced by the aromatic moieties of the poly(aryl ether)s. For the same reason, aromatic polyethers show a poor solubility in common solvents such as alcohols, chloroform, THF, etc. Different polymerization reaction methods can be implemented to achieve these materials. While aliphatic polyethers are generally obtained by chain-growth polymerization, aromatic polyethers are typically synthesized by step-growth polymerization.

Synthesis of hyperbranched polyethers (*hb*PEthers) has gained increasing popularity as such polymers combine the high thermal and chemical resistance that characterize linear polyethers with the low melt viscosity. The latter feature offers the possibility to further chemically modify the numerous side functional groups. *Hb*PEthers can also be divided into two different families, namely, aromatic[38,44–46] and aliphatic[38,47,48] *hb*PEthers. While rigid hyperbranched poly(aryl ethers) (*hb*P(aryl ether)s) are mostly obtained *via* step-growth polymerization of aromatic compounds,[38,45,494429] aliphatic *hb*PEthers are most often synthesized through cationic ring-opening (CROP) of oxetanes and oxiranes,[29,50–52] or by the anionic ring-opening multibranching polymerization (ROMBP) of oxiranes.[29,50,52]

This chapter gives an overview of the different synthetic routes to *hb*PEthers. The monomer structures and the reaction conditions, as well as the characteristic properties of the dendritic materials synthesized, will be discussed first. In a second part, the synthesis of hyperbranched polyglycidol (*hb*PG) *via* the anionic ring-opening homo- and copolymerization of glycidol will be specifically presented, as this subclass of polymeric materials has been the topic of intensive research efforts.

2. General outline of synthetic approaches for the preparation of hyperbranched polyethers

2.1. Synthesis of aromatic hyperbranched polyethers by step-growth polymerization

Since the early 1990s, the step-growth polymerization of AB_2-*type* and A_2-*type* + B_3-*type* monomers has been widely investigated to achieve aromatic or aromatic-aliphatic *hb*PEthers.[49,53,54] Several aromatic precursors have been specifically designed for this purpose. The resulting polyethers can find applications as additives in coatings. Different methodologies have been explored for the synthesis of *hb*P(aryl ether)s, namely, the homopolymerization of AB_n-*type* monomers (**Figure I-6**), the copolymerization of AB- and AB_n-*type* monomers and the copolymerization of A_2- and B_3-*type* monomers. The main chemical approach involves the nucleophilic aromatic substitution of halogens by nucleophiles (alkoxides or phenoxide). The other approach consists in implementing nucleophilic substitution by transetherification reactions of phenoxides or alkoxides onto aliphatic or benzylic halides.

2.1.1. Polymerization *via* aromatic nucleophilic substitution

2.1.1.1. Mechanism

Several aryl monomers have been designed to be further polymerized by aromatic nucleophilic substitution (S_NAr). In most cases, polymerizations are carried out by S_NAr involving halogens as leaving groups (-F, -Br…), with phenoxides or alkoxides as nucleophiles (**Figure I-6**, **Table I-2**). The latter compounds can be readily generated by deprotonation of corresponding alcohols or phenols in presence of a base (K_2CO_3, NaH, Na…). Alcohols protected by trialkyl silyl ether (-SiR_3) have also been investigated (**Table I-2, entry 6**).[55] S_NAr reactions require the aromatic monomers to be substituted with electron-withdrawing groups (EWG), *i.e.* a halogen,[53,56–58] cyano,[54] trifluoromethane,[49] quinoxaline[53] or maleimide anhydride (**Table I-2**).[55]

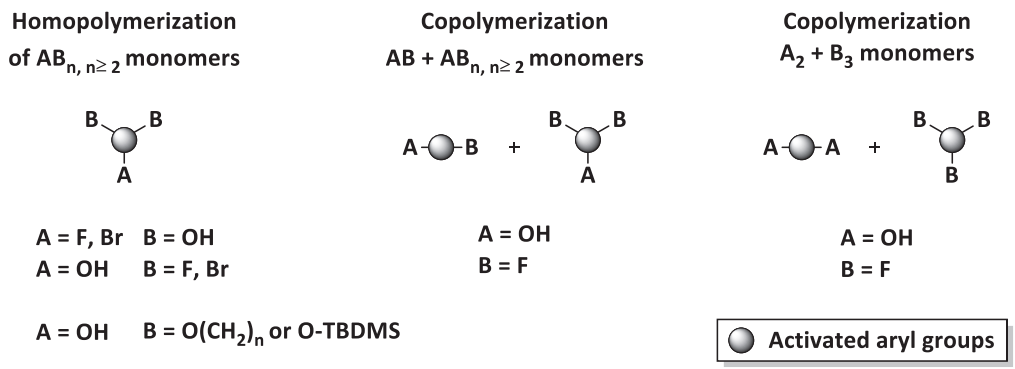

Figure I-6. Methodologies and related monomers employed for *hb*P(aryl ether) synthesis.

A typical example of polymerization of an AB_2-*type* monomer leading to *hb*P(aryl ether) was reported by Srinivisan *et al.*[53] in 1996 (**Figure I-7**). Here, fluoride atom is activated by an EWG heterocycle, *i.e.* quinoxaline. First, potassium carbonate (K_2CO_3) deprotonates a phenol group of the AB_2-*type* monomer, forming a phenoxide. The reaction then occurs in a two-step process involving the addition of the nucleophilic phenoxide, followed by the elimination of the leaving fluoride, causing the precipitation of potassium fluoride salts (KF). Phenoxides arising from the monomer or the growing chain may also be deprotonated by $KHCO_3$, thus forming carbon dioxide (CO_2) and water (H_2O).

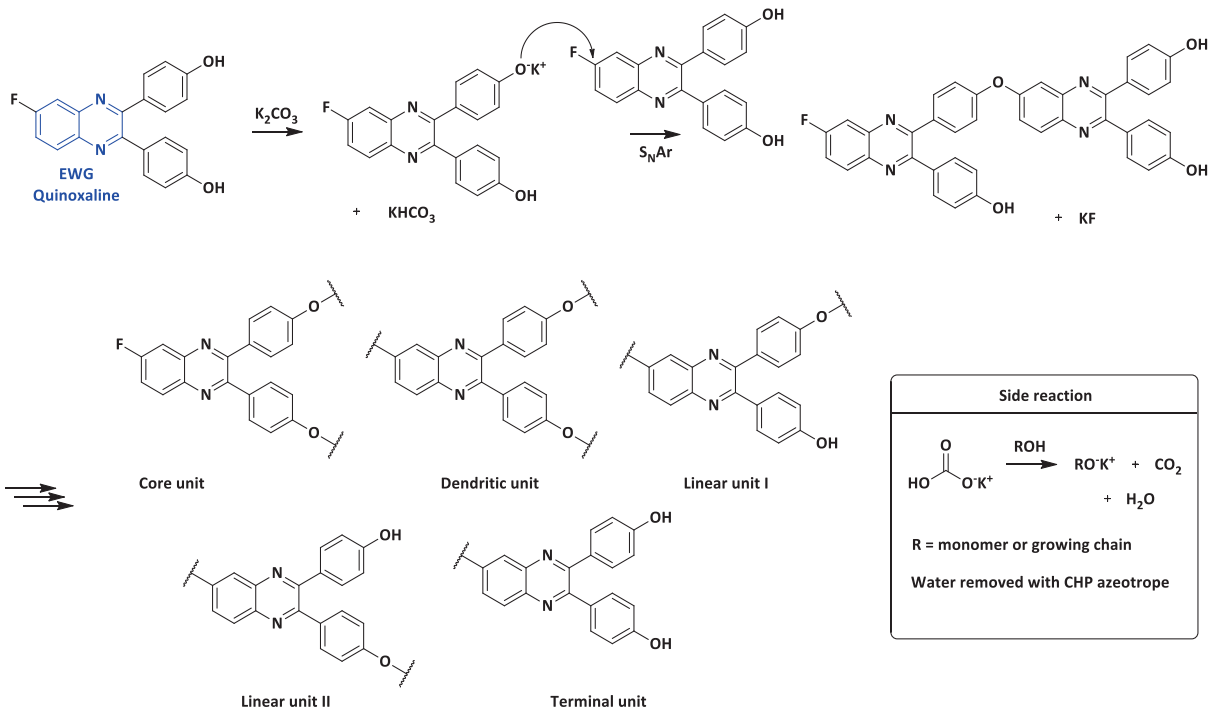

Figure I-7. Heterocycle-activated quinoxaline-based AB_2-*type* monomer for the synthesis of aryl *hb*PEther.[53]

High temperatures, generally ≥ 100 °C, are needed to ensure the S_NAr reaction. Solvents of high boiling points (T_B) must be used, e.g. *N*-Cyclohexyl-2-pyrrolidone (CHP, T_B = 284 °C), *N*-methyl-2-pyrrolidone (NMP, T_B = 203 °C), *N*,*N*'-dimethylacetamide (DMAc, T_B = 165 °C). These solvents are often employed in mixtures with toluene or benzene.

Hyperbranched poly(aryl ether)s obtained by S_NAr exhibit molecular weights ranging from 5,000 to 30,000 g/mol (**Table I-2**), though very low[58] (700 g/mol) and high[49] (500,000 g/mol) molecular weights have also been reported. Related dispersities most often ranged from 1.5 to 3, but increase in molecular weights can result in much higher dispersities (up to 10).[59]

Table I-2. Overview of $AB_{n,\ n\geq2}$-*type* monomers polymerized into aromatic *hb*PEthers *via* aromatic

Entry	Monomer		Conditions
1	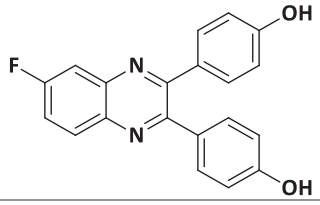	-	K_2CO_3 48 h, in NMP (200 °C), NMP:CHP:toluene (165 °C) or DMPU:toluene (260 °C)
2	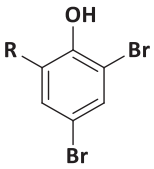	**a. R=H**	NaOH, KOH, cat. $K_3Fe(CN)_6$ 24 h, RT °C, in H_2O:benzene
		b. R=Br	a. conditions but no KOH
3	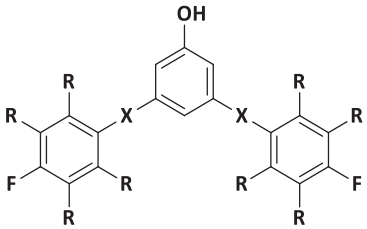	**a. R=H, X=CO**	NaH 0.5-2 h, 100-150 °C, reflux, Ar in DMAc or DMSO
		b. R=F, X=nil	
		c. R=H, X= 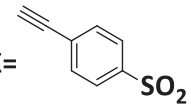	
		d. R=H, X= 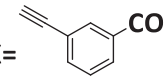	
4	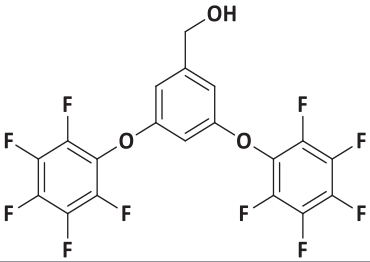	-	Na 45 min-9 h, 40 °C in THF or toluene

5	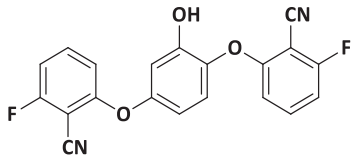	-	1. K_2CO_3, $CaCO_3$ 1.5 h (150 °C) or 8 h (160 °C), N_2 in toluene:DMAc 2. BOP, 3 h, 100 °C, in DMAc
6	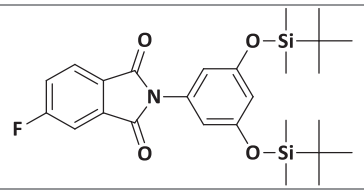	-	cat. CsF 2.5 min, 240 °C in DPS
7	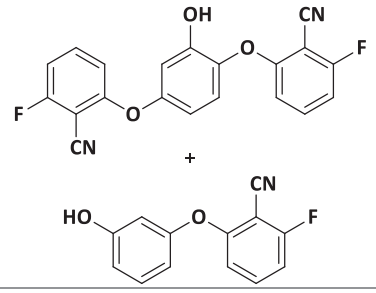	-	1. K_2CO_3, $CaCO_3$ 1.5 h (150 °C) or 8 h (160 °C), N_2 in toluene:DMAc 2. BOP, 3 h, 100 °C, in DMAc
8	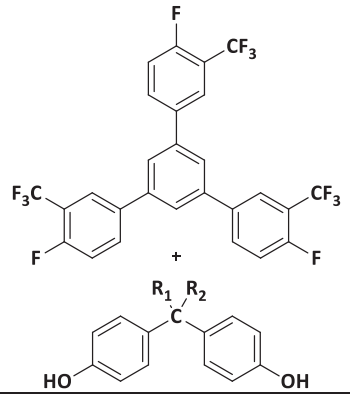	**a. $R_1 = R_2 = CH_3$** **b. $R_1 = R_2 = CF_3$** **c.** 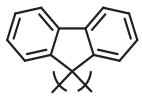 **R_1, R_2**	K_2CO_3 3 h, 150 °C / 3 h, 180 °C, N_2 in NMP:toluene

Determined by [a] SEC in THF, calibration linear PS standard, [b] SEC in $CHCl_3$, calibration linear PS standa
measured, [d] SEC in THF, triple detector system, *determined by ^{1}H NMR, ** using model compounds.

2.1.1.2. Structure and properties

As emphasized above, the DB value characterizes the "tree-like" structure of hyperbranched polymers. Only a few values of DB (0.37-1) have been yet reported for *hb*P(aryl ether)s. It should be noted that high DB, approaching unity as observed with perfect dendrimers (DB = 1), can be obtained in the case of A_2- and B_3-type monomers, *via* a slow addition of B_3.[49] Some authors have discussed concerns for distinguishing the terminal from the linear and the dendritic units, hence calculation of DB may be unresolved in some cases. Model compounds have been devised as a means to determine DB values (0.37-0.66).[54,55]

Viscosity measurements are also useful for *hb*PEther analysis.[54] For instance, whereas a value of 0.40 dL/g has been obtained for a linear polyether, a lower intrinsic viscosity (0.18 dL/g) has been determined for the *hb*PEther analogue (**Table I-2, entry 5**) and related copolymers (**Table I-2, entry 7**). Such comparative study demonstrates the lack of entanglement characterizing the dendritic structures. Low α values of the Mark-Houwink-Sakurada equation account for the compactness of *hb*PEthers. [60]

Linear poly(aryl ethers) are semi-crystalline polymers exhibiting high glass transition temperatures and high T_m due to the rigidity of the aromatic groups. For instance, poly(ether ketone)s have T_g and T_m approaching 150 °C and 400 °C, respectively. Thermal degradation is also enhanced, due to the high thermal stability of ether linkages. The loss degradation temperature at 10 wt.% of poly(ether ketone)s ranges from 550 to 580 °C. In comparison, *hb*P(aryl ether) analogues are amorphous, with lower or equivalent T_g values. For instance, Miller *et al.*[57] have polymerized AB_2-*type* monomers containing one phenolic group and two aryl fluoride groups connected by various spacers, including carbonates, sulfones and tetrafluorophenyl moieties (**Table I-2, entry 3**). While most of the resulting *hb*PEthers show a T_g of 135-150 °C, that featuring sulfone moieties is equal to 230 °C, *i.e.* similar to values of linear poly(ether sulfone)s. Mueller *et al.*[58] have synthesized a pentafluorophenyl-terminated hyperbranched poly(benzyl ether) showing a low T_g of 54 °C, due in this case, to the large number of fluoride terminal groups (**Table I-2, entry 4**).

2.1.2. Polymerization *via* nucleophilic substitution etherification & transetherification

The nucleophilic substitution (trans)etherification can be performed from AB_2-type monomers possessing one nucleophile (A) and two leaving groups (B), or alternatively one leaving group (A) and two nucleophiles (B). This reaction step is typically achieved under basic or acidic conditions (**Figure I-8** and **Figure I-9**)

Table I-3. Overview of AB_2-*type* monomers polymerized into aromatic *hb*PEthers *via* nucleophilic substitution (S_N2) in basic (entries 1-2) or acidic (entries (3-4) conditions.

Entry	Monomer		Conditions	M_n (g/mol) (*Đ*)	Ref
1	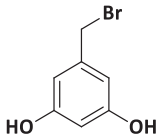	-	1. K_2CO_3, 18-crown-6 51 h, reflux, N_2, in acetone 2. Benzyl bromide 12h, reflux, N_2, in acetone	2,800-14,500[a] (1.5-5.8)	[61]
2	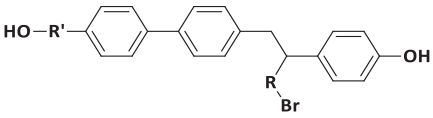 a. R=$(CH_2)_8$ no R' b. R=$(CH_2)_{11}$ no R' c. R=$(CH_2)_{11}$ R'= 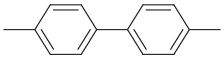 d. R=$(CH_2)_{11}$ R'= 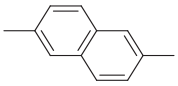	a	1. TBAH, 10M $NaOH_{(aq)}$ 30 min, 80 °C, in o-DCB 2. R_1-Cl or R_2-Br 30 min, 80 °C, N_2, in o-DCB	4,400-41,800[b] (1.6-3.9)	[62]
		b		3,100-27,500b (1.51-2.60) DB = 0.82*	[63]
		c			
		d			
	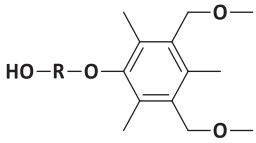 a. R = $(CH_2)_2$ c. R = $(CH_2CH_2O)_{n,\ n=2}$ b. R = $(CH_2)_{2n,\ n=1\text{-}5}$ d. R = 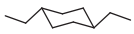	a	pTSA 30 min, 145 °C, N_2 15 min, 145 °C, vac. in bulk	17,800 (5.8)[a] DB = 0.78**	[64]
		b	PCS 2 h, 150 °C, N_2 1 h, 150 °C, vac. in bulk	24,000-90,000[d] (1.7-3.9)	[60]
		c			
		d			
4	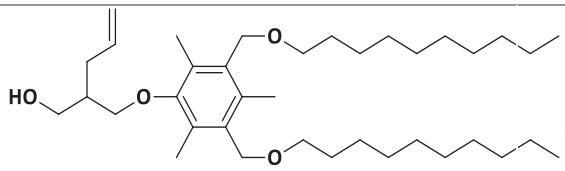		PCS 2h, 150 °C, N_2 45 min, 150 °C, vac. in bulk	12,000[d] (6.0)	[65]

Determined by [a] SEC in THF, calibration linear PS standard, [b] SEC in $CHCl_3$, calibration linear PS standard, [c] SEC in DMAc/LiBr, dn/dc was measured, [d] SEC in THF, triple detector system, * determined by ^{1}H NMR, ** using model compounds.

2.1.2.1. Basic etherification

The basic etherification, also referred to as the Williamson nucleophilic substitution (S_N2) reaction, involves the addition of a phenoxide or alkoxide nucleophile on primary alkyl halide (-Br) derivative (**Table I-3, entries 1-2**). Deprotonation of the phenol/alcohol uses a base such as potassium carbonate (K_2CO_3) or tetrabutylammonium oxide (TBAH). A typical example involving 5-(bromomethyl)-l,3-dihydroxy benzene giving rise to a *hb*P(aryl ether) is depicted in **Figure I-8**.[61] The polymerization is carried out in acetone at 56 °C. Compared to the S_NAr reactions, no water is formed as by-product, however, moisture traces may explain the high dispersities (up to 5.7) obtained in attempts to increase the molecular weights (up to 14,500 g/mol).

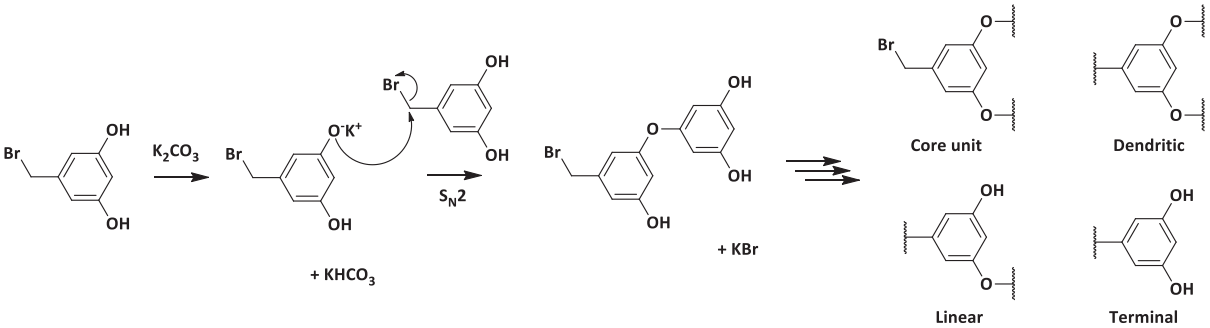

Figure I-8. Polymerization of 5-(bromomethyl)-1,3-dihydroxy benzene *via* etherification under basic conditions.[61]

2.1.2.2. Acidic transetherification

Synthesis of *hb*P(aryl ether)s by acidic nucleophile substitution has been investigated by Ramakrishnan and co-workers in particular from mesitol-based AB_2-*type* monomers (**Table I-3, entries 3-4**).[60,64,65] Polymerizations are carried out at 150 °C using an acid catalyst, e.g. *p*-toluene sulfonic acid or the pyridinium camphor sulfonate (PCS), PCS being more selective with limited side-reactions.

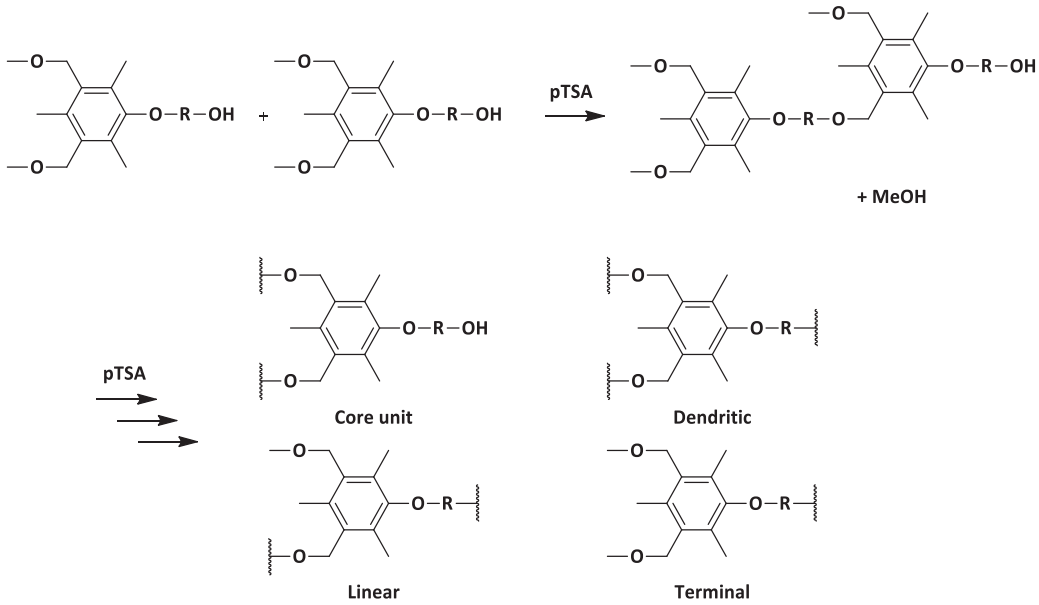

Figure I-9. Polymerization of the mesitol-based AB_2-*type* monomer, incorporating various spacers, *via* transetherification under acidic conditions.[60,64,65]

2.1.2.3. Structure and properties

Similar issues regarding the determination of DB have been encountered. Yet, Percec *et al.*[63] have calculated a DB of 0.82 for compounds shown in **Table I-3, entry 2.d**, as they have been able to distinguish between the different units by ^{1}H NMR spectroscopy, thanks to the resonance induced by the naphthalene substituent (R'). Ramakrishnan and co-workers have resorted to the synthesis of model compounds to estimate a DB of 0.78 by ^{1}H NMR (**Table I-3, entry 3.a**).[64]

Spacers of differing lengths and chemical nature have been introduced in order to tune the transition temperatures. For instance, Percec and co-workers have designed 10-bromo-1-(4-hydroxy-4'-biphenylyl)-2-(4-hydroxyphenyl)decane[62] and (4-hydroxy-4'-biphenylyl)-2-(4-hydroxy-phenyl)hexane[63] *via* multi-step reactions. AB_2-type monomers have been homopolymerized into "willow-like" thermotropic *hb*PEthers (**Table I-3, entry 2** and **Figure I-10**), of high branching density (DB = 0.82). Above their glass transition temperature (25 to 50 °C), chain conformation can switch from gauche to anti. This work eventually represents the first example of hyperbranched polymers exhibiting an enantiotropic nematic mesophase (**Figure I-10**). The transition temperature from the nematic to the isotropic phases can be tuned by grafting alkyl chains or benzyl groups onto phenolate chain ends.

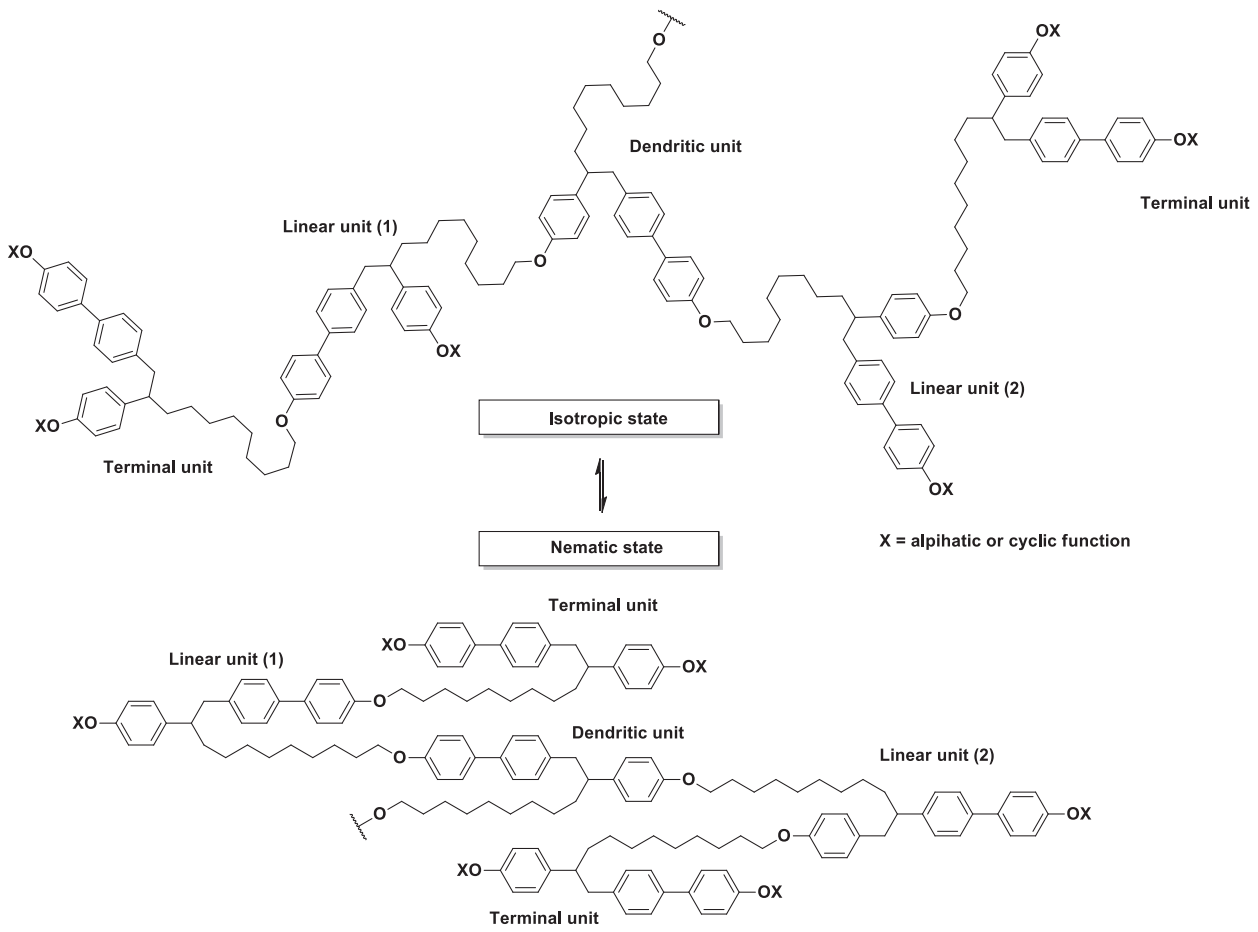

Figure I-10. Transition from the isotropic state to the nematic state of compounds shown in **Table I-3, entry 2**.[62,63]

Ramakrishnan and co-workers have designed several mesitol-based monomers, incorporating spacers of increasing alkyl chain lengths, from C_2 to C_{10}. T_g values have thus been varied from 88 to -18 °C.[60,64,66] Incorporation of flexible oxyethylene segments has led to T_g values of -16 to -8 °C, and a T_g of 77 °C has been determined for compounds featuring a rigid cycloalkane group. Increase of the MHS α coefficient from 0.40 (C_2) to 0.57 (C_{10}) has been noted, indicating a less compact structure for long alkyl chains.

2.2. Synthesis of hyperbranched polyethers by ring-opening polymerization

Ring-opening polymerization of hydroxyl-containing cyclic ethers has been widely investigated to access aliphatic *hb*PEthers. These monomers are indeed considered as latent $AB_{n,\ n\geq2}$-*type* monomers, with A being the cyclic ether and B the hydroxyl functions. The term "latent" lies in the fact that the second OH is created after ring-opening of the epoxide (**Figure I-12**).

Oxiranes or oxetanes, that are, 3- and 4-membered cyclic ethers, have been the most commonly studied in this context, following either cationic, anionic, coordinated or enzymatic polymerization pathways (**Table I-4**). Cationic-ring opening polymerization (CROP) can be typically employed with oxiranes or oxetanes (part 2.2.1). This method is particularly interesting for poly-substituted cyclic ethers, e.g. oxetanes and some specific oxiranes, while the anionic route is generally not adapted for such monomers (**Table I-4**). Anionic conditions referring the ring-opening multibranching polymerization (ROMBP) can be applied to monofunctional oxiranes. Only one report by Huang *et al.*[67] has described the ROMBP of poly-substituted oxirane. Rokicki *et al.*[68] have specifically designed glycerol carbonate as a bio-based AB_2-*type* monomer to derive into *hb*PEthers. Fréchet and co-workers[69,70] have used the so-called proton-transfer polymerization (HTP) to achieve *hb*P(aryl ether)s.

Table I-4. Examples of cyclic ether monomers and their corresponding polymerization approaches.

Cyclic ethers	**Oxiranes**		**Oxetanes**	**5-membered cyclic monomer**
Substitution	Mono-substituted	Poly-substituted	Mono- or poly-substituted	Mono-substituted
Examples	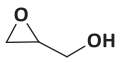 Glycidol	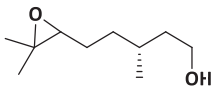 Citronellol oxide	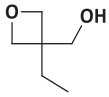 EHMO	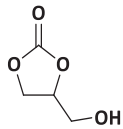 Glycerol carbonate
Polymerization	ROMBP, CROP, coordinated polymerization, enzymatic polymerization	CROP	CROP	ROMBP

As expected, initial reaction conditions have a dramatic impact on macromolecular features of the resulting polyethers. 2,3-Epoxy-1-propanol, known as glycidol, is certainly the most representative example of latent AB_2-*type* monomers. The resulting *hb*PEther derivative is named "hyperbranched polyglycerol" or "hyperbranched polyglycidol" (*hb*PG), a water-soluble and amorphous *hb*PEther showing a high potential in numerous applications. Primary information will be given in the following sections and more details will be presented in part 3 of this chapter.

2.2.1. Cationic ring-opening polymerization

Several types of mono- and poly-substituted oxiranes and oxetanes can undergo a CROP pathway. CROP involves two distinct mechanisms, namely the active chain-end (ACE) and the activated monomer (AM) mechanisms (**Figure I-12**). The former mechanism gives rise to linear units only, while linear and dendritic can be generated *via* the AM mechanism. Competitive occurrence between ACE and AM reactions will affect the amount of dendritic units, *i.e.* the final DB value. Thus, in order to achieve high DB, reaction conditions favouring the AM mechanism must be selected. For instance, some catalysts, such as tin(IV) chloride, have been shown to promote the latter mechanism; DB values up to 0.81 have thus been obtained. In the specific case of CROP of oxetanes, increase of temperature, from -50 to 20 °C, has been found to result in the formation of DB values from 0.09 to 0.49.

*Hb*PEthers obtained by CROP of oxiranes are totaly amorphous, whereas those derived from oxetanes can crystallize depending on DB. A high crystallinity with a high T_m is achieved for low DB, both T_m and crystallinity decreasing for higher DB, leading ultimately to amorphous materials.

2.2.1.1. Glycidol and derivatives

The first example of an aliphatic *hb*PEther synthesized by CROP was described by Goethals *et al*. in 1993.[71] The authors have copolymerized 1,3-dioxolane with glycidol, forming a highly branched polymer. At that time, glycidol has been coined as a “monofer”, as featuring a polymerizable epoxide function and a hydroxyl moiety favouring transfer reactions. The different possible units of the resulting *hb*PG obtained are presented in **Figure I-11**. Two types of linear units, namely the linear 1,2 ($L_{1,2}$) and the linear 1,3 ($L_{1,3}$), can eventually be obtained; the secondary (carbon 2) and the primary (carbon 3) alcohol emanating from the propagation.

In 1995, Tokar *et al*.[72] described the CROP as being the result of both ACE and AM mechanisms (**Figure I-12**). ACE mechanism only yields $L_{1,2}$ units, as the lone pair of the oxygen from the epoxide reacts with C_1 of the activated chain-end, hence resulting in a linear polyglycidol. In contrast, OH groups from either the $L_{1,2}$ (path A) or the T (paths B & C) units react onto the protonated epoxide by the AM mechanism. Thus, $L_{1,2}$, $L_{1,3}$, D and T units can be obtained through the reactions denoted as A, B and C in **Figure I-12**.

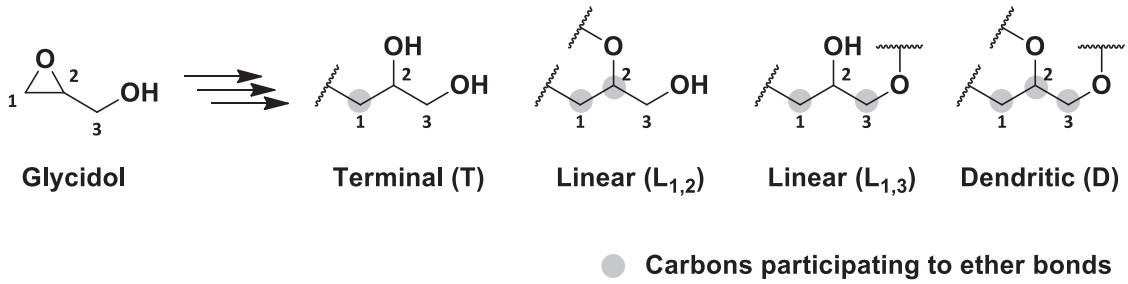

Figure I-11. Different units of hyperbranched polyglycidol and nomenclature.

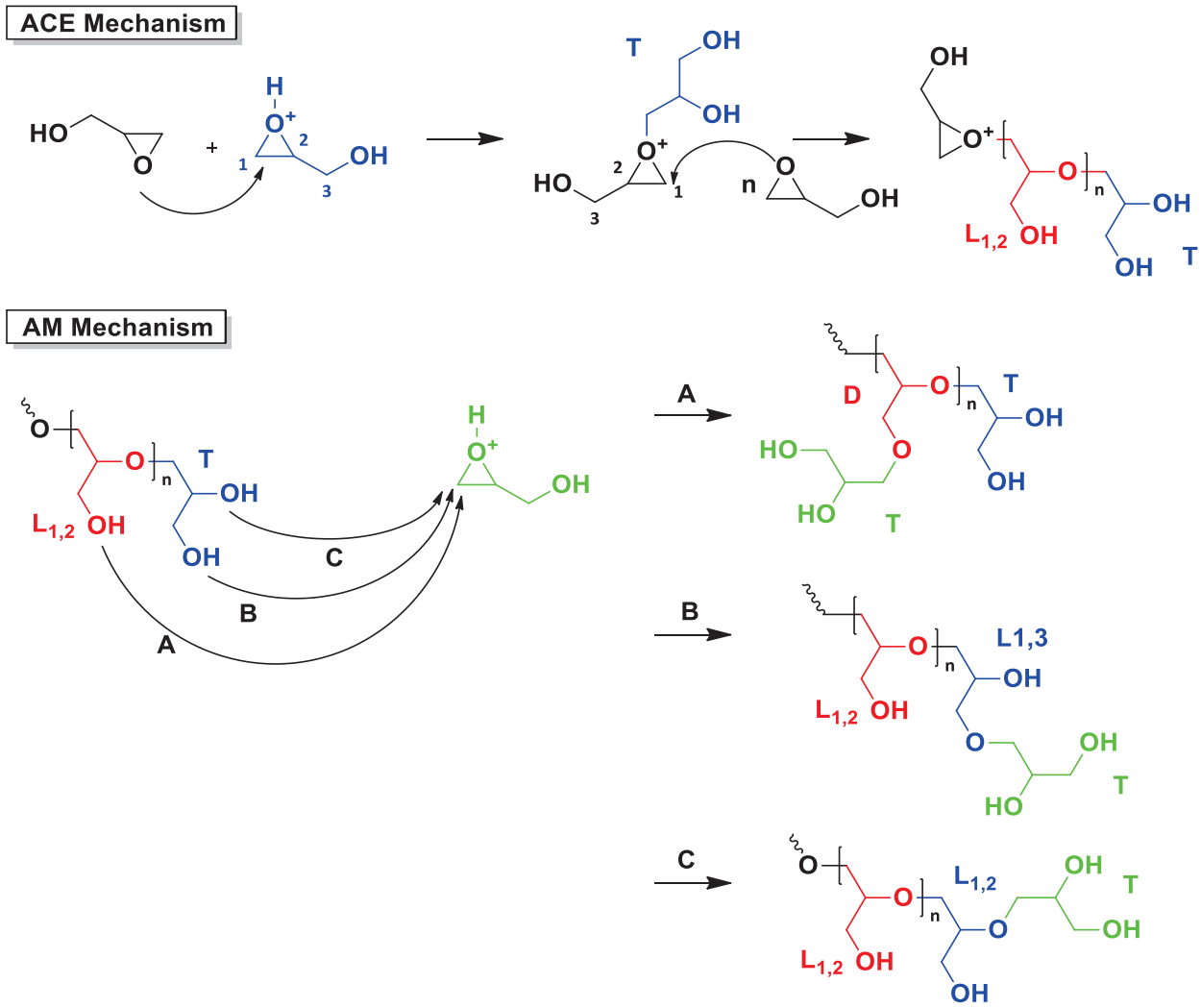

Figure I-12. ACE and AM mechanisms in the CROP of glycidol.

Reaction conditions, including the nature of the catalyst, the temperature or use of a solvent, have been varied by Dworak and co-workers to tune the DB of CROP-derived *hb*PG (**Table I-5, entry 1**).[72,73] For instance, DB as high as 0.81 can be achieved using $SnCl_4$ as catalyst and increasing the temperature to 15 °C.[73] Although molecular weights remain low (500 to

6,000 g/mol), the dispersities can be kept rather low (1.2 < *Đ* < 1.6). Corresponding h*b*PGs can be solubilized in polar solvents, such as water, alcohols, DMF or DMSO.

In recent years, synthesis of *hb*PG of low DB (0.15 to 0.33), have been investigated by Harth and co-workers (**Table I-5, entry 1**).[74,75] In particular, CROP carried out in an aqueous medium containing phosphate buffered saline (PBS) has been reported.[75] Both pH and temperature have been varied to obtain *hb*PG with DB from 0.18 to 0.33, molecular weights ranging from 1,100 to 1,600 g/mol.

Besides glycidol, bio-based latent AB_2-*type* monomers have been purposely designed by Satoh *et al*.[76] For instance, the authors have polymerized citronellol oxide (entry 2) and nopol epoxide (entry 3), in bulk conditions or in solution in DCM, to achieve *hb*PEthers of molecular weights < 2,000 g/mol (**Table I-5**). Dispersities of polyethers derived from citronellol oxide have been found lower (2.0) than those of nopol epoxide *hb*PEthers (2.3-4.7). However, these values are higher than those of *hb*PG. This may be due to side-reactions occurring by transfer of the positive charge into the cycle of nopol oxide (**Figure I-13**), forming vinyl and aromatic moieties; the latter limiting the chain mobility and leading to T_g in the range 73.4-118 °C, for 12 and 32 % of vinyl and aromatic groups, respectively. Lower T_g (-14 to -5 °C) can be achieved for poly(citronellol oxide)s, as the chain mobility is eased by the absence of cycle into the monomer. DB value has not been determined by NMR, owing to the overlapping of peaks due to the different characteristic units. However, the globular compact structure of the polymer has been established by the low values of the MHS coefficient, α, of poly(citronellol oxide)s and poly(nopol epoxide)s: 0.32-0.40 and 0.25-0.45, respectively.

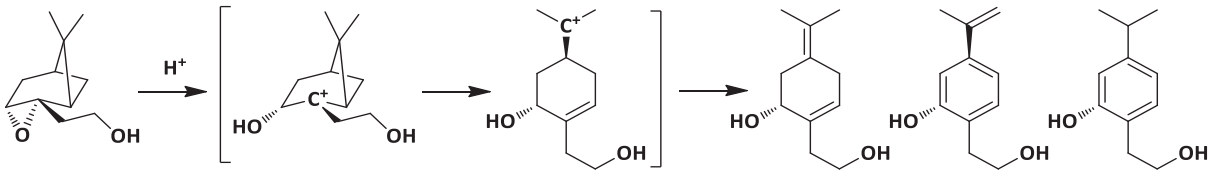

Figure I-13. Formation of aromatic and vinyl groups during CROP of nopol oxide.

Table I-5. Overview of latent $AB_{n,n\geq2}$-*type* monomers polymerized into aliphatic *hb*PEthers by CROP.

Entry	Monomers	Conditions	M_n (g/mol) (*Đ*) DB*	Ref
1	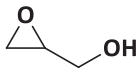 Glycidol	$BF_3.Et_2O$, $SnCl_4$ or $HPF_6.Et_2O$ 3-48 h, -20 to 30 °C, Ar, in bulk or DCM	520-10500[a]	[72]
		$BF_3.Et_2O$, $SnCl_4$, TFA or TFSA -30 to 20°C, Ar, in bulk or DCM	2500-6000[b*] (1.2-1.6) DB = 0.48-0.81	[73]
		$Sn(OTf)_2$ -20 to 40 °C, 1 h to 4 d, N_2, in THF (SMA)	5800-11,000[d] (1.25-1.32) DB = 0.15-0.24	[74]
		PBS (pH = 6) 72 h, 80 °C, in water	1100-1600[c] (1.05-1.21) DB = 0.18-0.33	[75]
2	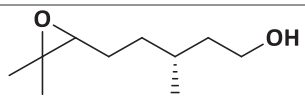 Citronellol oxide	$BF_3.Et_2O$ 120 h, -30 °C, Ar, in DCM	1500-1900[b] (1.6-2.0)	[76]
3	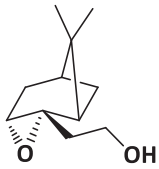 Nopol epoxide	$BF_3.Et_2O$ 24 h, 130 °C, Ar, in bulk	1300-1400[b] (2.3-4.7)	[76]
4	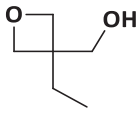 EHMO	$BF_3.Et_2O$ or TFSA 24-45 h at 25, 60 or 130 °C, Ar in bulk DCM, $CHCl_3$ or o-DCB	900-1700[b] (~1.5)	[77,78]
		p-CH_3BTSSbF6 or BTSSbF6 20 min-3 h, 60-160 °C, Ar, in bulk	1200-5300[c] (1.25-1.74) DB = 0.15-0.41	[79]
		$BF_3.Et_2O$ 48 h, -50 to 30°C, N_2, in DCM (SMA 2.3 mL/min)	4700-5400[d] (1.33-1.61) DB = 0.09-0.42	[80]
		$BF_3.Et_2O$ 20 min, 90 °C, N_2, in toluene (SMA 5d/min)	1800[b] (2.3) DB = 0.42	[81]
		$BF_3.Et_2O$ 48 h, -50 to 20 °C, N_2, in DCE	5800-6700[d] (1.34-1.57) DB = 0.14-0.40	[82]
5	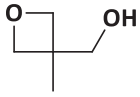 MHMO	$BF_3.Et_2O$ 48 h, -10 to 4 °C, N_2, in DCE	1800-2100[e] (1.38-1.41) DB = 0.33	[83]
		$BF_3.Et_2O$	7000-8900[d] (1.58-1.75)	[82]

		48 h, -50 to 25 °C, N_2, in DCE	DB = 0.15-0.40	
6	MEMO	$BF_3.Et_2O$ 72 h, RT °C, N_2, in DCM	4300-4500[b] (1.16-1.24) DB = 0.16-0.29	[84]
7	BHMO	TFSA 10 days, 50 °C, N_2, in bulk	2000[b]	[85]
8	Glycidol + BHMO	$BF_3.Et_2O$ 24 h, 40 °C, Ar, in DMSO	1400-3300[c] (1.21-1.48)	[86]
9	EHMO + HO-PEG$_{2000}$-OH Core molecule	$BF_3.Et_2O$ 20 h, 90 °C, N_2, in toluene	1600-2400[b] (1.17-1.4) DB = 0.47-0.67	[81]
10	EHMO + BHMO	TFSA 6 days, 25 °C, N_2, in bulk	1500-1800[b]	[85]
11	EHMO + MEMO	$BF_3.Et_2O$ 24 h, 0-5 °C, N_2, in DCM	5600-6800[b] (1.25-1.44) DB = 0.15-0.24	[87]
12	EHMO + Epichlorhydrin	PEHO core synthesis $BF_3.Et_2O$ 48 h, RT °C, N_2, in DCE (SMA)	PEHO core properties 2000-2300[c] (1.20-1.86) DB = 0.41-0.42	[88]

Determined by [a] Vapor pressure osmometry in water, [b] SEC in THF, calibration linear with PS standards ([b*] polymer functionalized with formic acid prior to THF solubilisation, [c] SEC in DMF, calibration linear PEG standard, [d] SEC in DMF, calibration with linear PS standards, [e] MALDI-TOF MS, * Inverse gated ^{13}C NMR.

2.2.1.2. Oxetanes

Various latent $AB_{n,}$-type oxetanes ($n \geq 2$) have served to access *hb*PEthers by CROP. The latter compounds are usually semi-crystalline and most of them are soluble in polar solvents including water, even though, some polymers are too cohesive to be solubilized. The Penczek's group made significant contributions in the early 1990s in this area, by developing the CROP of glycidol.[72] In 1999, new oxetane derivatives were polymerized into aliphatic *hb*PEthers, starting from 3-ethyl-3-(hydroxymethyl)oxetane (EHMO, **Table I-5, entry 4**). Lewis acids, such as boron trifluoride diethyl etherate ($BF_3.Et_2O$) or trifluoromethanesulfonic acid (TFSA), are the preferred catalysts/activators for a CROP pathway. Again, competitive ACE and AM mechanisms strongly affect the DB values. Typically, DB from 0.09 to 0.42 has been determined when increasing temperatures in the range -50 to 20 °C, DB remaining the same (~0.42) for temperatures <20 °C.[79–82] Magnusson *et al.*[79] have reported that the bulk polymerization of EHMO takes place in two steps (**Table I-5, entry 4**). For conversions lower than 30 %, the ACE mechanism is dominant, hence linear units are mostly produced. For higher conversions, dendritic units can form. The so-called slow monomer addition (SMA) can be implemented to reach higher conversions, while maintaining the formation of branched units.[79–81] Oxetane-derived *hb*PEthers with DB up to 0.41 and of molecular weight up to 6700 g/mol have thus been achieved.[79,80,82] The presence of numerous peripheral hydroxyl functions imparts solubility to the resulting *hb*PEHMOs in alcohols, water, DMF and DMSO but not in non-polar solvents.

While hyperbranched polymers are generally amorphous due to the high number of chain ends,[10] DSC analyses has revealed that *hb*PEHMOs are semi-crystalline for DB values < 0.33.[79,80,82] Zhu *et al.*[82] have reported a glass transition temperature around 32-45 °C for DB = 0.40, depending on the thermal history of the sample. The authors have also demonstrated that increasing the DB can retard the crystallisation step and reduce the relative crystallinity, from almost 100 % at DB = 0.14 to approximately 10 % at DB = 0.40.

2.2.1.3. Copolymerization of oxetanes

Properties of the oxetanes-derived *hb*PEthers, e.g. their solubility and crystallinity, can be varied through their copolymerization with a co-monomer. For instance, oxetanes such as (3-methyl-3-hydroxymethyl)oxetane (MHMO, entry 5), 3-{2-[2-(2-methoxyethoxy)ethoxy]-ethoxy}methyl-3'-methyloxetane (MEMO, entry 6) and 3,3-bis(hydroxymethyl)-oxetane (BHMO, entry 7) have been copolymerized with EHMO (**Table I-5**). As BHMO features two OH groups, its copolymerization with EHMO increases the number of terminal hydroxyls on the resulting copolyethers, which can be beneficial for post-functionalization.[85] The water solubility of *hb*PBHMO can be also improved through copolymerization with glycidol, as well as its biocompatibility.[86] In addition, the shorter dangling chains arising from MHMO lead to higher T_m than that of *hb*PEHMO, (116 °C *vs.* 90 °C).[82,83]

Lin *et al.*[84] have synthesized the MEMO AB_2-type monomer by incorporating triethylene glycol into EHMO (**Table I-5, entry 6**). The resulting *hb*PEthers can be functionalized with succinic anhydride and doped with LiTFSI salts, for a use as solid electrolytes in lithium ion batteries. The low T_g of -46.7 °C attests to the high chain mobility. T_g of *hb*PEthers obtained by copolymerization of MHMO with EHMO drop to -64 °C and conductivity is enhanced, from 5.6×10^{-5} S/cm for the MHMO hyperbranched homopolyether, to 8.0×10^{-5} S/cm for the MHMO:EHMO (70:30) copolymer (**Table I-5, entry 11**). By using the semi-crystalline $mPEG_{2000}$ as macroinitiator for EHMO polymerization, semi-crystalline hyperbranched structures can be achieved, with T_m between 35 and 49 °C and crystallinity from 12 to 56 %, for 6 mol% and 29 mol% of PEG, respectively (**Table I-5, entry 9**).[81]

Recently, Zhang *et al.*[88] have reported the synthesis of hyperbranched glycidyl azide polymers (hbGAPs) derived from *hb*PEHMO, for solid propellant purpose. Globular *hb*PEHMOs can be employed as macroinitiators for the polymerization of epichlorohydrin and chlorine groups be further functionalized by azidation, affording *hb*PEHMO with a glycidyl azide units in its shell (**Table I-5, entry 12**). While linear GAPs usually have limited molecular weights, the *hb*PEHMO-*co*-GAP exhibits values approaching 31,000 g/mol ($Đ$ = 1.23) and show improved thermal properties. *Hb*PEHMo-*co*-GAP compounds have also been found compatible with other additives generally used in solid propellant formulations, hence branched structures may be a good alternative to linear GAP-s.

2.2.2. Anionic ring-opening polymerization

2.2.2.1. Synthesis of hyperbranched polyglycerol

The synthesis of linear polyglycerol was extensively investigated in the early 1980s, as this class of polymers combines good water-solubility and hydrolysis resistance.[89] In 1985, Vandenberg highlighted that branched units formed during the CROP of protected glycidol monomers, namely, trimethylsilyl ether (TMSGE) and *tert*-butyl glycidyl ether (TBGE) into linear polyglycerol.[90] The *in situ* formation of glycidol during the polymerization has in fact been considered as a "side reaction" and the highly branched polyglycidol achieved has been viewed as a by-product. This is only much later that the group of Mülhaupt has proposed a convenient synthesis approach to *hb*PG, *via* the direct ROMBP of glycidol, in which glycidol is slowly added onto deprotonated alcohols of a core molecule, typically trimethylol propane (TMP **Figure I-18, part 3**).[91] *Hb*PGs are thus obtained in high yield as viscous transparent liquids with molecular weights ranging from 1,200 to 6,300 g/mol and low dispersities (1.15-1.19). DB values in the range of 0.53-0.59 have been found higher than values obtained in the case of the polycondensation of AB_2 monomers (DB = 0.5), but lower than those obtained from a slow monomer (SMA) addition reaction (0.66).

As mentioned above, Rokicki *et al*.[68] have developed an alternative synthetic pathway to *hb*PGs starting from glycerol carbonate instead of glycidol. Glycerol carbonate is a benign and stable molecule commonly used as solvent, additive or chemical reagent.[92] It can be synthesized from transcarbonation of bio-based glycerol with dimethyl carbonate under mild conditions.[68] In comparison, glycidol is carcinogenic, mutagenic or toxic to reproduction (CMR); it is generally produced by hydrolysis of epichlorohydrin, which is also a CMR substance.[92] Bulk ROP of glycerol carbonate has thus been performed similarly to the ROMBP of glycidol, *i.e.* TMP has been deprotonated at 10 % to initiate the reaction. Either a nucleophilic addition onto the carbonate group (Figure I-14**, reactions 1.a or 1.b**) or the C_1 (Figure I-14**, reactions 2.1 and 2.2**) can take place. Addition on the carbonate is kinetically favoured, however, which reversibly leads to primary (Figure I-14**, reactions 1.a**) and secondary alkoxides (Figure I-14**, reactions 1.b**). Addition on the C1 is irreversible due to carbon dioxide release, forming secondary alkoxides (Figure I-14**, reactions 2.2**). Primary alkoxides propagate onto either C4 (carbonate) or C1, while the addition of the secondary alkoxides is only performed on C1. The fast proton-exchange, relatively to propagation, that occurs during the reaction is crucial for the creation of several terminal, linear and dendritic units (Figure I-14).

As in the case of glycidol polymerization, a slow addition of glycerol carbonate at 2 mL/h prevents the formation of cyclic oligomers, which may be favoured at 170 °C. Only low molecular weight polymers are obtained though, M_n approaching 1,000 g/mol and $Đ = 1.2$. *Hb*P(glycerol carbonate)s of similar molecular weights to those of *hb*PGs had a similar T_g of -19 °C.[91] Unfortunately, DB values have not been provided.

2.2.2.2. Special cases of ring-opening polymerization of oxiranes

Huang *et al*.[67] have reported the ROP of a latent AB_3-type monomer forming *hb*PEther polyol, in presence of the deprotonated form of TMP as initiator (**Figure I-15**). Secondary alkoxides form after opening of the epoxide can either propagate or be protonated by fast proton exchange with the aliphatic hydroxyl functions. Different monomer:TMP initiator ratios (M/TMP), from 5 to 215, have been tested, leading to molecular weights in the range 2,300 to 750,000 g/mol, with low dispersities (1.09-1.15), T_g values from -47 to -30 °C and DB varying between 0.32 and 0.48. Advantage of the numerous hydroxyl end groups in these hyperbranched polyols has been taken as chelate sites and for further sol-gel mineralization of TiO_2 as a segregated network of organic and inorganic phases, named porous anatase nanoparticles.

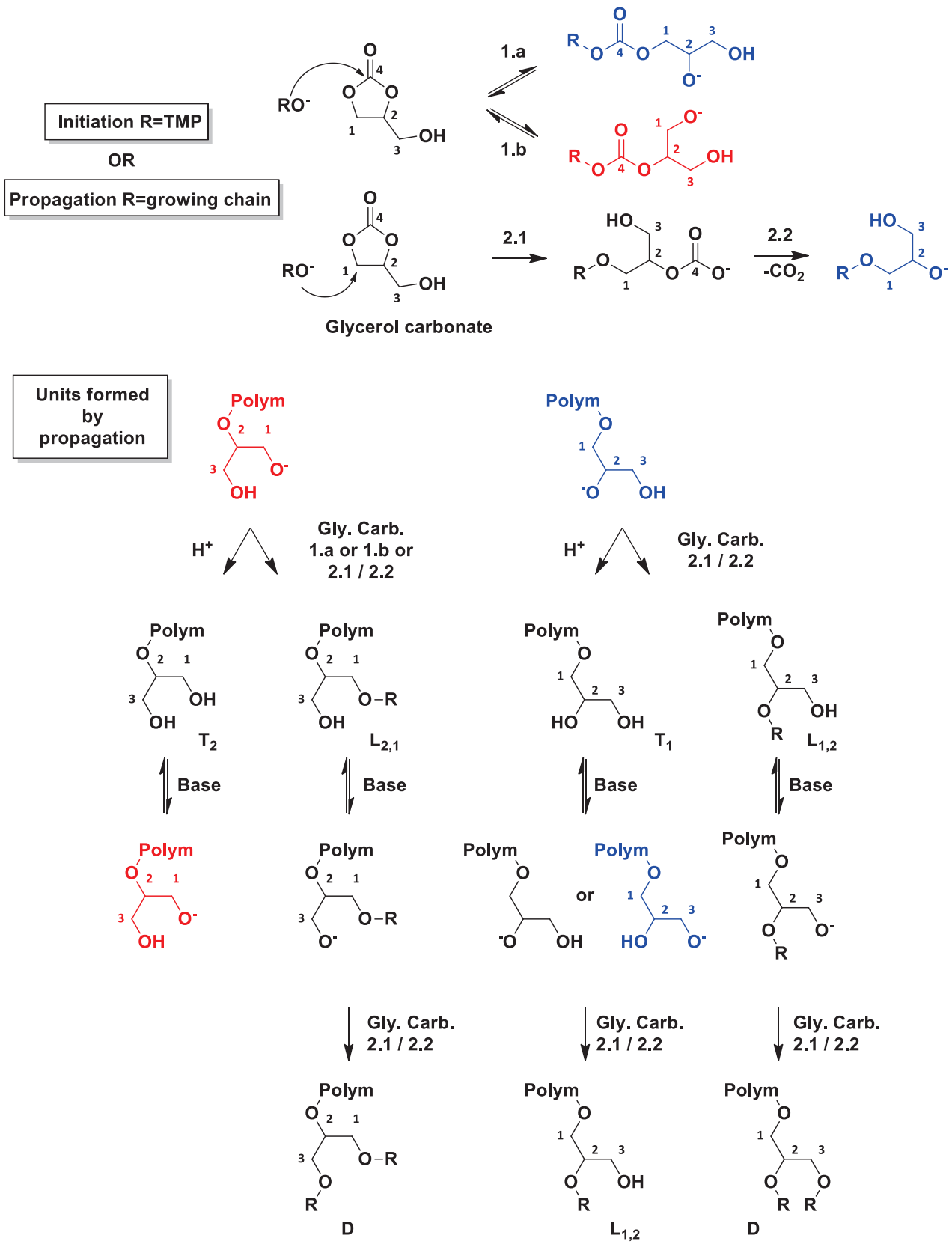

Figure I-14. ROMBP of glycerol carbonate initiated by TMP.

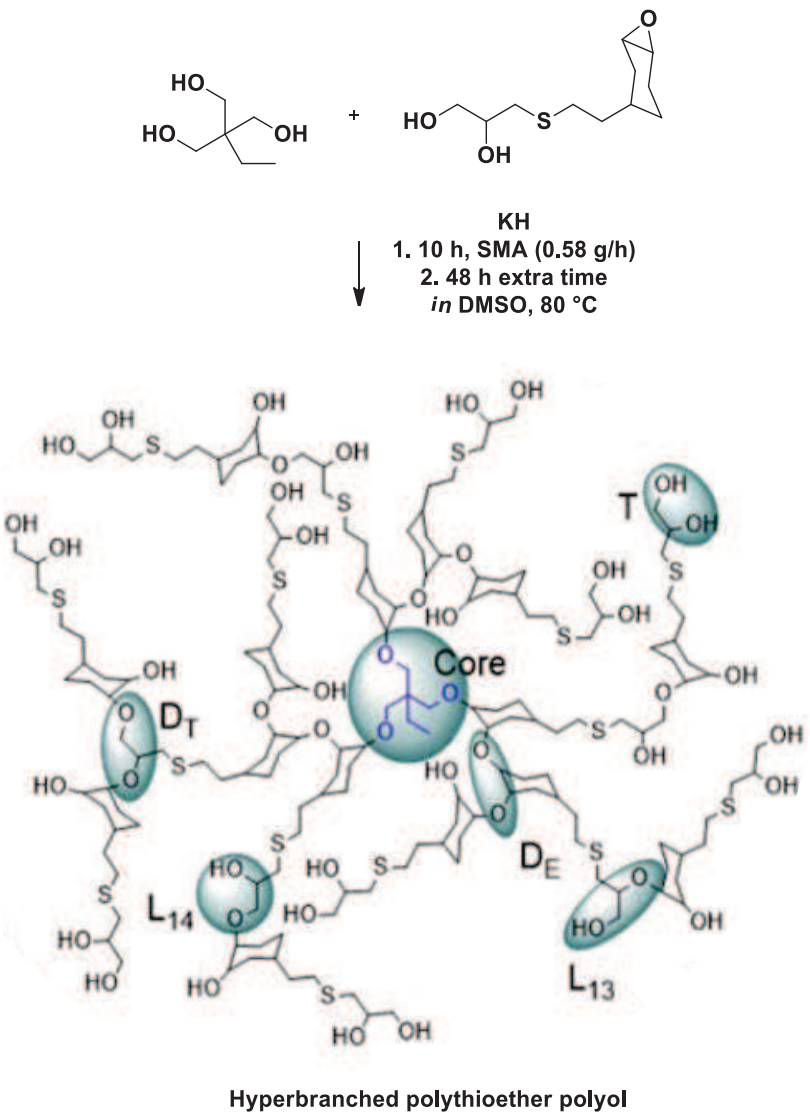

Figure I-15. ROMBP of the latent AB_3-type 3-[2-(7-oxa-bicyclo[4.1.0]hept-3-yl)-ethylsulfanyl]-propane-1,2-diol.[67]

Fréchet and co-workers have investigated the ROP of a latent bis-epoxide A_2B_3-type monomer featuring 2 epoxide moieties and 1 OH *via* HTP, eventually proceeding by a step-growth polymerization mechanism (**Figure I-16**).[69] KOH has been employed to deprotonate the phenolic hydroxyl function of the monomer, and phenoxides thus formed can attack the epoxide functions of another monomer by nucleophilic addition. Fast proton transfer between secondary alkoxide and phenolic alcohol of the monomer has been evidenced, favouring growth of the *hb*P(aryl ether)s. These polymers have been obtained in 98 % yield, with molecular weights between 2400 ($Đ$ = 1.3) and 6200 g/mol ($Đ$ = 12). The dispersity values have been found to dramatically increase when targeting high molecular weights due to the occurrence of cyclization. Resorting to a slow monomer addition process has enabled to prevent this, and high

molecular weights (ca. 23,800 g/mol) with limited dispersity (ca. 2.4) can be achieved after 76 h in THF. Note that the DB value has not been specified in this report.

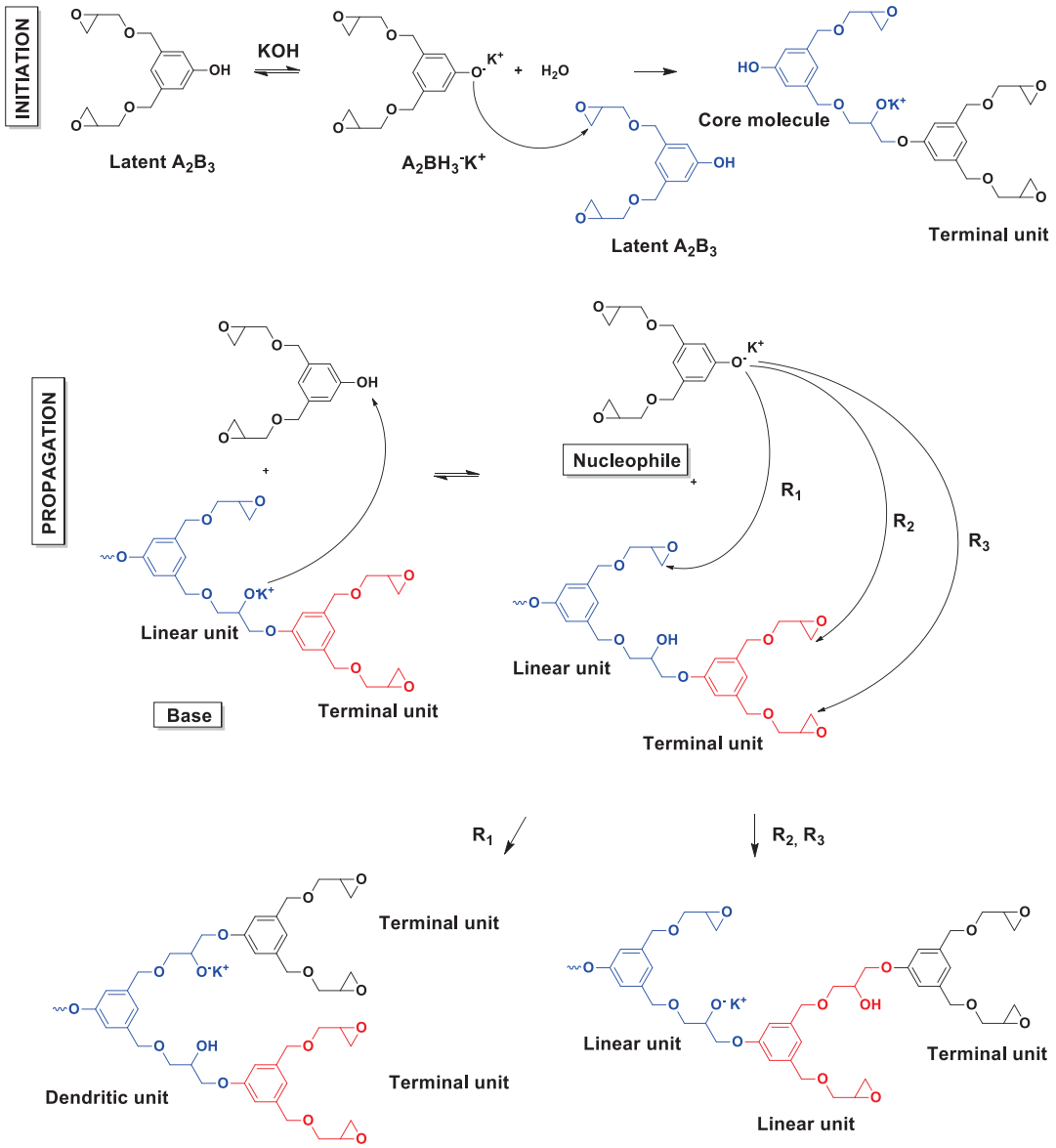

Figure I-16. Synthesis of a hyperbranched epoxy functionalized polymer *via* the proton-transfer polymerization of a phenolic bis-epoxide.

Fréchet and co-workers have also investigated the copolymerization of the latent 1,2,7,8-diepoxyoctane A_2B_2-type monomer with TMP.[70] In this case, tetra-*n*-butylammonium chloride is added onto the epoxide, forming the secondary alkoxide (Figure I-17). Again, fast proton exchange between alkoxides and hydroxyl groups proves crucial to promote the formation of dendritic units. Some cross-linking has yet been noted, especially in the later stages of the reaction. Polymers with molecular weights in the range 1,000-15,000 g/mol have been

obtained in this way. The dispersities drastically increase with molecular weights: for instance, $Đ = 5$ for $M_n = 5{,}000$ g/mol. No value of DB has been reported in this case either.

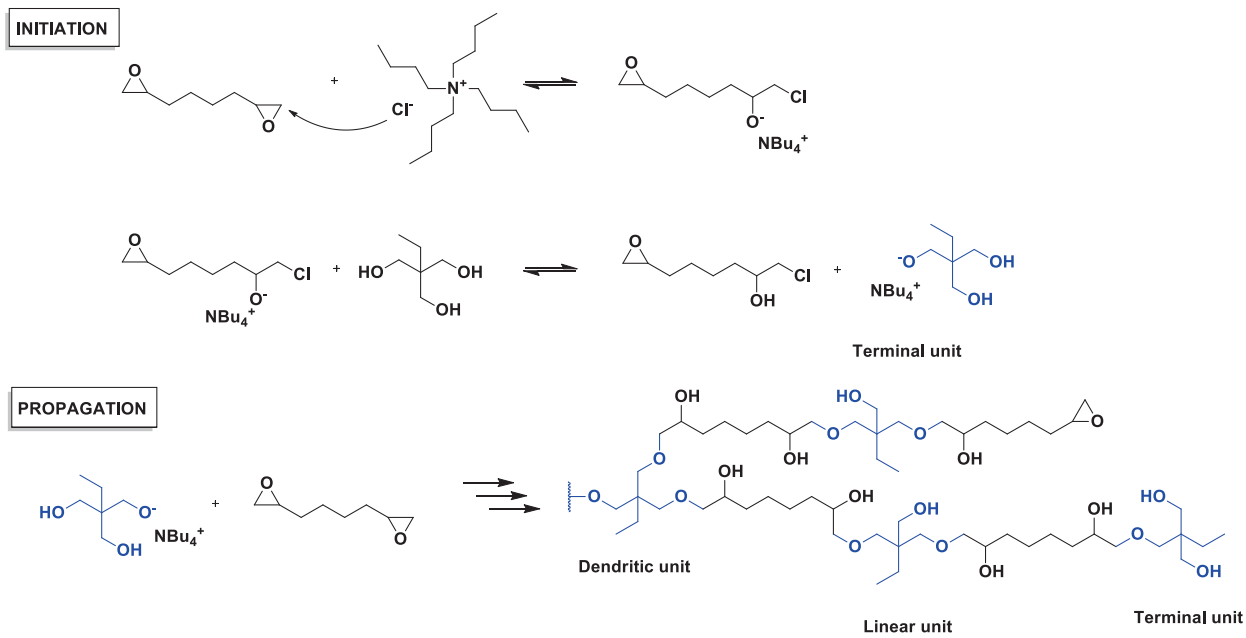

Figure I-17. Synthesis of aliphatic *hb*PEther via the proton-transfer polymerization of an aliphatic bisepoxide with TMP.

3. Ring-opening polymerization of glycidol

3.1. Generalities and challenges

3.1.1. Introduction

Glycidol, also referred as 2,3-epoxy-1-propanol, is a colourless and odourless liquid having a boiling point of 167 °C (1 atm). Glycidol is soluble in water, alcohols and ethers as well as in apolar solvents such as benzene or chloroform.[93] It is mainly produced in Asia (Meryer (Shangaï) Chemical Technology Co., Ltd.; Wako Chemical, Ltd; Nacalai Tesque Inc.; Kanto Chemical Co., Inc.) and in the USA (Acros Organics; HBCChem, Inc.).[94] The British company LGC Group Holdings plc also produces glycidol. No information about the quantity of glycidol produced worldwide has been found or the sale prices trends. However, professionals can easily purchase glycidol to fine chemistry companies or onto e-commerce retail service platforms. The prices approximately vary from \$0.8 / kg to \$300 / kg when ordering few tons or few kilograms of glycidol, respectively!

In 1960, Raciszewski *et al.* have proposed a synthetic pathway to glycidol involving the epoxidation of allyl alcohol using hydrogen peroxide in presence of tungstic acid. The method is now commonly used[95–97] and was first patented in 1983 by Taramasso *et al.*, from Snamprogetti S.p.A.[98] More attention has recently been paid to resort to non-toxic bio-based reagents such as glycerol,[99] glycerol carbonate[100,101] or cyclic carbonate[92,99,101] to obtain glycidol. The Green Epoxy Solutions (GES) pilot plant has recently been inaugurated at the Wilton Centre (Teeside, Northern England), with the objective of producing 10,000-30,000 t/year of glycidol from dimethyl carbonate and glycerol.[102]

Synthesis of "defect-free" linear polyglycerol,[90] *via* ROP of protected glycidol, and of *hb*PG, by the CROP[36-39] or anionic ROMBP[91] of glycidol, has been widely investigated. *Hb*PGs are highly hydrophilic polymers showing a high hydrolysis resistance. In this regard, polyglycidol has been proposed as an alternative to poly(ethylene glycol) for several applications, such as coatings, cosmetic formulation and most of all, pharmaceutical drug delivery area.[51,103] Its globular compact architecture grants *hb*PG a low intrinsic viscosity and an excellent biocompatibility. The great number of hydroxyl groups carried by polyglycidol into its core or at its periphery can be further functionalized to target specific properties.[104–106]

3.1.2. Ring-opening polymerization

In 1999, the Mülhaupt's group[91] thoroughly reinvestigated the ROMBP of glycidol, which had been first reported by Vandenberg few decades before.[90] TMP, used as a core molecule, has been deprotonated at 10 % with a methanol solution of potassium methoxide, before glycidol is slowly added (SMA) over 12 h at 95 °C, in bulk under mechanical stirring. Various TMP/glycidol ratios have been tested to vary the molecular weights. The general polymerization mechanism, which is depicted in **Figure I-18**, uses the deprotonated TMP to initiate the ring-opening of glycidol by nucleophilic addition, generating a secondary alkoxide. The latter active site thus propagates or is protonated by a fast exchange (relatively to propagation) with hydroxylated dormant forms. Therefore, under such conditions, active species often switch from secondary to primary alkoxides, thanks to this proton transfer. Consequence of such a mechanism is the generation of two types of linear units, denoted as $L_{1,2}$ and $L_{1,3}$. The remaining OH of linear units can also be deprotonated and propagate to form dendritic units (**Figure I-18**). The different units of *hb*PG have been clearly distinguished by

^{13}C NMR and quantified by inverted gate ^{13}C NMR. The DB value has also been calculated using either the Fréchet or the Frey equations (DB ≈ 0.56).

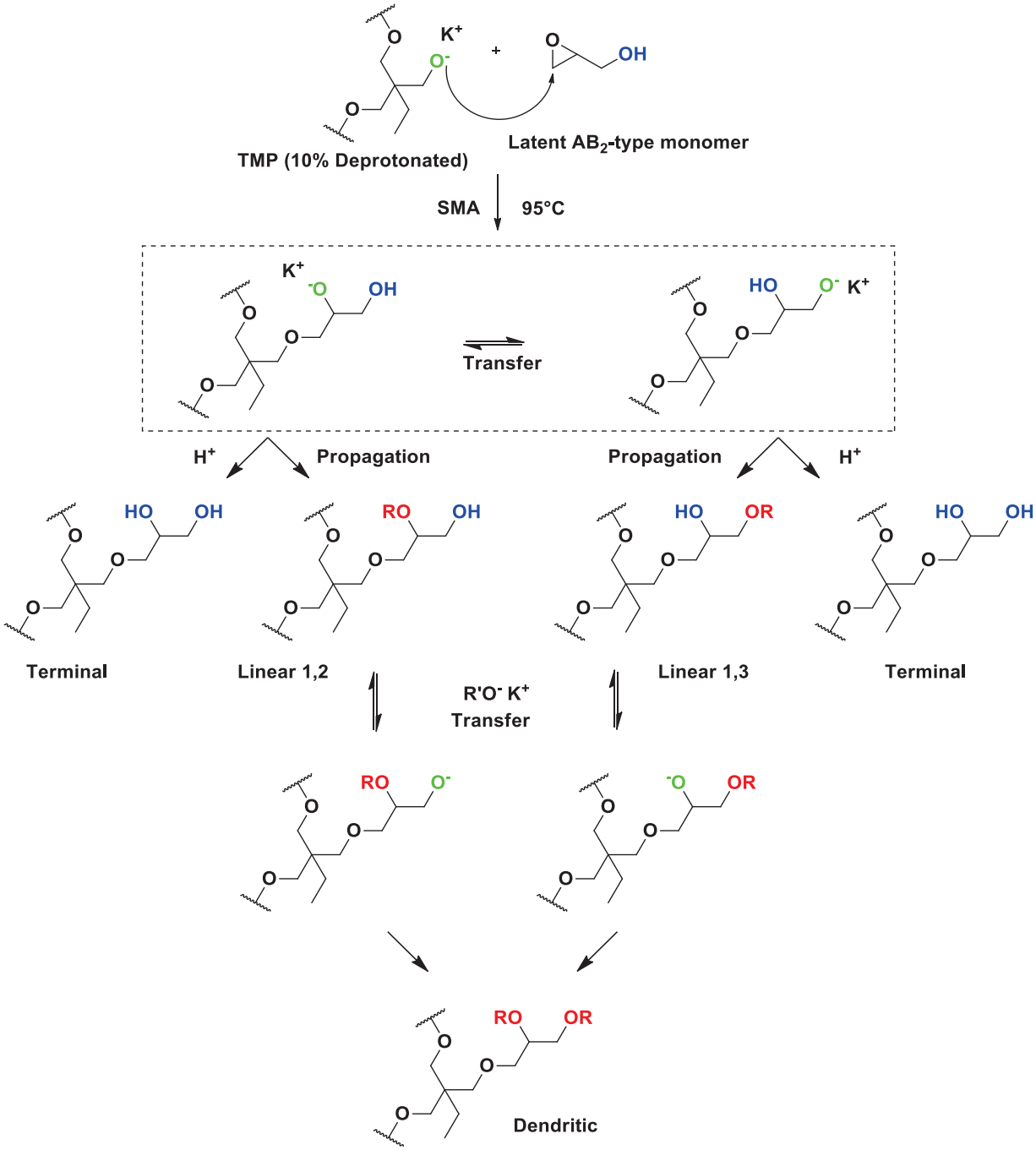

Figure I-18. Mechanism of ROMBP of glycidol.

3.1.3. Self-initiation

While ROMBP is supposed to be initiated by TMP, initiation can also occur directly from the monomer itself (**Figure I-19**).[50,91,107–109] In 2013, Paulus *et al.*[107,109] have demonstrated by modelling the reaction, that this "self-initiation" is mainly thermally induced, *i.e.* the primary alcohol of glycidol directly adds onto another epoxide without being deprotonated. Self-initiation, which takes place at higher molecular weights (M_n > 10,000 g/mol), is responsible for the presence of low molecular weight populations, increasing the dispersities. Nucleophilic addition can occur intramolecularly (**Figure I-20**) or intermolecularly (**Figure I-21**) between the epoxide and a hydroxyl or an alkoxide, respectively, intramolecular reaction leading to cyclic structures. The threshold molecular weight achieved by thermal cyclization has been found close to 10,000 g/mol.

Slow monomer addition is expected to minimize this self-initiation, as few glycidol molecules are incorporated onto the propagating chains. However, at the end of the addition, the reaction does not necessarily reach completion, but viscosity often increases due to the high molecular weights reached. Moreover, as active alkoxide sites are diluted by addition of glycidol, new hydroxyl groups are introduced in the reaction mixture, so that the active sites are less accessible, favouring the thermal self-initiation of glycidol. Therefore, molecular weights cannot be controlled over 6,000 g/mol when *hb*PG is synthesized in bulk.

Wilms and co-workers[110,111] have described the first syntheses of *hb*PGs through the use of microfluidic chipsets, providing a controlled slow addition of the monomer. Molecular weights ranging from 1,100 to 1,600 g/mol and low dispersities ($Đ$ = 1.05-1.15) have been achieved in this way.

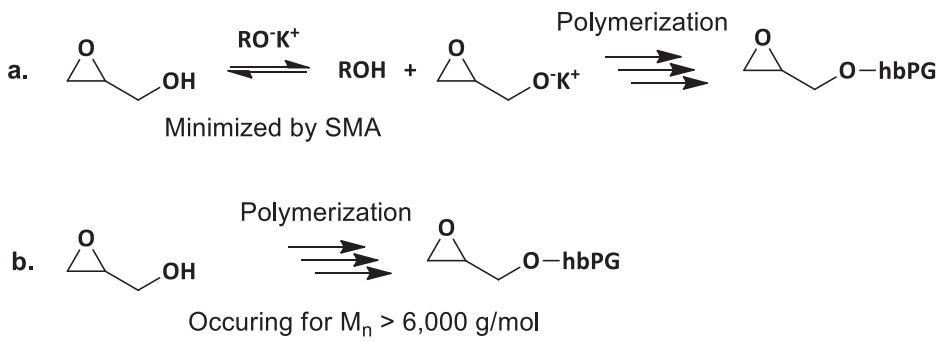

Figure I-19. Self-initiation of the ring-opening polymerization of glycidol, **a.** anionically and **b.** thermally induced.

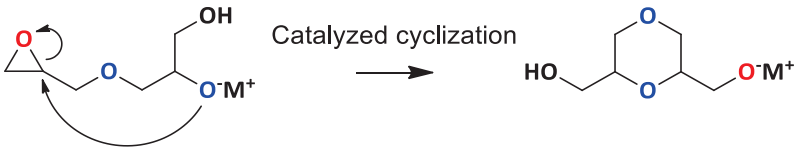

Figure I-20. Intramolecular nucleophilic addition of a self-initiated *hb*PG, leading to cyclic structures.

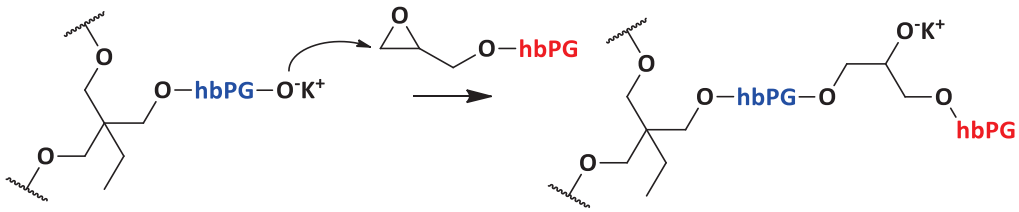

Figure I-21. Intermolecular addition between *hb*PG initiated by TMP and self-initiated *hb*PG.

3.1.4. Use of solvents

Different solvents can be employed for the ROMBP of glycidol as a means to reduce the viscosity of the medium and improve the accessibility of the active sites. (**Figure I-22**). Diglyme and 1,4-dioxane, supposedly playing the role of emulsifiers, prove the most efficient.

In 2001, Kautz *et al.*[112] showed that molecular weight *hb*PG up to 17,000 g/mol can be produced on a large scale (500 g) using the SMA process method described by Sunder *et al.*[91] in 1999. However, M_n values deviate from theoretical ones and dispersities increase upon targeting molecular weights higher than 7,000 g/mol. For instance, compounds of M_n 17,000 g/mol ($Đ = 4.65$) are achieved when targeting values of 11,000 g/mol. The use of diglyme as solvent allows for significant control improvement over M_n values; molecular weights up to 20,000 g/mol ($M_{n,theo} = 17{,}000$ g/mol) can be achieved with a lower dispersity (2.99).

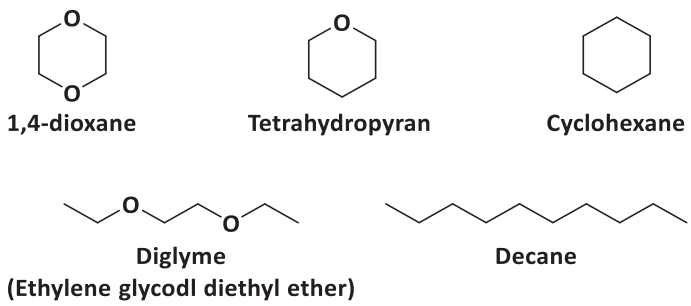

Figure I-22. Solvents investigated for the synthesis of hyperbranched polyglycidol.

Kainthan *et al.*[113] have succeeded in producing *hb*PGs of high M_n (105,000-870,000 g/mol) by using either diglyme or dioxane as solvents, but this is achieved at the expense of the control of the ROMBP process. Molecular weights indeed deviate from targeted values (for instance, for a targeted molecular weight of 70,000 g/mol, a *hb*PG of 870,000 g/mol has been obtained). Reasons for the achievement of such high molecular weight polymers have not been clarified. It has been hypothesized that this is caused by a loss of initiating sites due to residual moisture in the solvent[113] or their emulsifying feature.[107,113,114] Significant differences in dispersities have also been noted depending on the solvent used. While diglyme leads to dispersities between 1.7 and 2.9, use of dioxane gives lower dispersities (1.1-1.4 for M_n = 359,000-670,000 g/mol). Polydisperse compounds can yet be fractionated into a population of low molecular weight (< 1000 g/mol) and another of higher molecular weight (60-90 wt.%, > 1000 g/mol), the latter being not soluble in ethanol.

In 2013, Imran ul-haq *et al.*[114] studied the influence of the solvent nature and the solvent/monomer (S/M) ratio on the polymerization outcomes (**Figure I-22**). The nature of the solvent has been found to have a strong effect on monomer conversion (from 59 to 81%), molecular weight development (M_n range of 5-540 kg/mol) and dispersity ($1.05 < Đ < 2.1$). As Kautz *et al.*[112] and Kainthan *et al.*[113] have reported earlier that polymer chains are not soluble in common solvents, meaning that the polymerization occurs in two distinct phases, the solvent eventually acting as an emulsifier. In contrast to the authors' hypotheses, there seems to be no direct correlation between the dielectric constant (ε_r) of the solvent and the molecular weights, as M_n values decrease in the following order: 1,4-dioxane (M_n = 540,000 g/mol, $\varepsilon_r = 2.2$) > tetrahydropyran (M_n = 160,000 g/mol, $\varepsilon_r = 5.7$) > diglyme (M_n = 48,000 g/mol, $\varepsilon_r = 5.1$) > decane (M_n = 10,000 g/mol, $\varepsilon_r = 2.0$) > cyclohexane (M_n = 5000 g/mol, $\varepsilon_r = 2.0$).

The concentration in glycidol has also a strong influence since molecular weights increase for higher S/M ratios, while dispersities decrease. In dioxane, for instance, increasing the S/M ratio from 0 to 0.25 leads to a dramatic increase of the molecular weights, *i.e.* from M_n = 10 kg/mol, until reaching a plateau at 550 kg/mol. At a S/M ratio of 0.25, molecular weights remain constant, but the dispersity decreases.

Because dioxane has more oxygens, it can develop more interactions with K^+, which may explain the decrease in the kinetics of proton-transfer and a higher nucleophilicity of the anion,

hence to an increase of the molecular weight and a better control of the dispersity. Although diglyme has the same number of oxygen than dioxane, M_n values are lower. The lower accessibility of oxygen atoms of diglyme, in comparison with those of dioxane, may explain these results, dioxane showing a better solubilisation of the polymer chains than non-polar solvents, enabling uniform growth of the polymer.

Surprisingly, the nature and the concentration of the solvents do not show any effect on DB values (0.56-0.59). In addition to the solvent effect, the authors have evidenced that molecular weights increase and dispersity decrease for elevated glycidol:TMP ratios. When increasing reaction time, SEC traces evolve from a bimodal to a monomodal distribution, which may be due to the reaction of oligoglycidols together forming higher molecular weight *hb*PGs. Such intermolecular addition takes place in the core with oligomers made of an epoxide, supporting observations by Paulus *et al.*[107,109] about the occurrence of self-initiated oligomers. Wilms *et al.*[108] have mentioned that solvents such as DMF or DMSO can favour self-initiated ROP of glycidol.

3.1.5. Use of macroinitiators

Wilms *et al.*[108] have proposed a different pathway to achieve *hb*PGs of "high" molecular weights by using "short" *hb*PGs as macroinitiators. This enables a rather good control of molecular weights, from 5,000 to 25,000 g/mol ($Đ$ = 1.38-1.77). Low molecular weight *hb*PGs (500 g/mol, $Đ$ = 1.32 and 1000 g/mol, $Đ$ = 1.4) have thus been used as macroinitiators for the ROMBP of glycidol. Nevertheless, a *hb*PG-1000 precursor appears appropriate to reach high molecular weights and a better control over the ROMBP process. DB values of the *hb*PG-1000 precursor around 0.62 have been determined by inverted gate ^{13}C NMR.

3.1.6. Alternative synthetic routes

To prevent self-initiation of glycidol, Pappuru *et al.*[115] have suggested to use ancillary ligand-supported transition metal complexes as catalysts for the bulk ROMBP of glycidol (**Figure I-23**). Group 5 metal complexes had already been used in the context of ROP of cyclic esters and lactides.[116–118] Both the nature of the metal and the electron withdrawing effect of the R_1 and R_2 substituents on phenoxyl groups have been shown to impact the properties of the final polymer. For instance, niobium (V) chloride gives excellent results as coordinating agents when used with the chloro-substituted benzophazole phenoxide [N,O] ligand L_5.[115]

Polymerization proceeds according to a coordination-insertion mechanism, enabling to minimize transfer reactions. When targeting degree of polymerization (DP_n) from 100 to 300, molecular weights of resulting *hb*PGs have reached expected values (from 10,000 g/mol to 23,000 g/mol) and dispersities have proven higher ($Đ$ = 1.33-1.54) than those obtained by Sunder *et al.*[91]. In this case, DB values vary from 0.45 to 0.53.

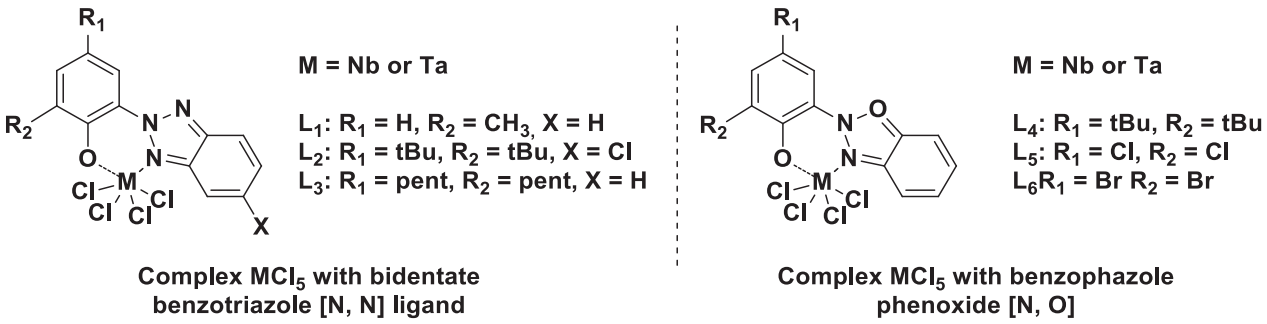

Figure I-23. Platform of ancillary ligand-supported transition metal complexes developed by Pappuru *et al.* for synthesizing hyperbranched polyglycidol.[115]

Soeda *et al.*[119,120] have proposed an enzymatic pathway to synthesize *hb*PGs. Several hydrolase enzymes (10 wt.%) have thus been tested for the ROMBP of glycidol in bulk at 40 °C over 3 days, achieving 99 % conversion using *pseudomonas fluorescens* (lipase AK) and *pseudomonas* sp. (lipase PS).[60] Lipases AK and PS allow giving access to branched oligoglycidols with molecular weights 410 ($Đ$ = 2.2) and 310 g/mol ($Đ$ = 1.7), respectively, but calculation of DB has not been mentioned. Lipase AK can also be used to randomly copolymerize glycidol with glycidyl phenyl ether, leading to oligomers of approximately 350 g/mol.[61]

3.2. Thermal and thermo-rheological properties

As discussed above, *hb*PGs of very distinct molecular weights (from ca. 500 to 1,000,000 g/mol) can be prepared, according to the different procedures. Compounds with $M_n \leq 6{,}000$ g/mol can be synthesized in bulk, as established by Sunder *et al.*,[91] while Wilms *et al.*[108] have shown that *hb*PGs with M_n ranging from 6,000 to 23,000 g/mol can be obtained from hyperbranched oligoglycerols as macroinitiators. Finally, molecular weights in the range 70,000-106,000 g/mol are accessible with the help of dioxane or diglyme as solvent, as reported by Kainthan *et al.*[113]

Reported values of DB of *hb*PGs obtained by ROMBP vary from 0.45 to 0.63.[121] Interestingly, no dependence of DB with molecular weights has been reported.[121] Due to its high compact structure, the intrinsic viscosity of *hb*PG is rather low (0.052 dL/g for 100,000 g/mol) but surprisingly, comparable with the one of linear polyglycidol (0.047 dL/g).[113,122] By comparison, a higher intrinsic viscosity has been reported for PEG of same molecular weight (1.308 dL/g).[122] *Hb*PGs' compactness is also illustrated by the low hydrodynamic radii (R_h), in the range 2.5-5 nm when for M_w between 20,000 and 200,000 g/mol and reaching 7-8 nm for M_w of ca. 1,000 kg/mol,[113] and by the low MHS α coefficient (0.31-0.43).[113]

The compact structure of *hb*PGs also affects their thermo-mechanical properties relatively to linear polyglycerol homologues. Although both linear and hyperbranched PGs are amorphous, the high number of chain ends in *hb*PG leads to slightly lower T_g values (-20 to -15 °C) than linear polyglycidol (-25 to -10 °C).[121,123,124]

The glass transition temperature of *hb*PG can be decreased by post-modification, e.g. by permethylation and trimethylsilylation, as the chain end mobility of *hb*PG is increased when reducing the amount of associating interactions (H-bonding) of the hydroxyl chain ends.[121] Such intramolecular interactions are more pronounced for *hb*PG than for linear PG.

Rheological studies have also demonstrated that *hb*PGs entangle for M_n > 20,000 g/mol *vs.* 10,000 g/mol for linear PG.[80,82] Interestingly, the entanglements molecular weight (6,400 g/mol) is lower than the molecular weight between two branching points (ca. 150 g/mol), meaning that even the branching sections participate to the entanglement.

3.3. Functionalization of hyperbranched polyglycidol: towards original properties

The presence of numerous terminal OH groups in *hb*PGs offers many opportunities for chemical post-modification reactions and for targeting specific properties and original applications. On the other hand, alcohols and protected amines can be employed to initiate the ROMBP, instead of the standard TMP core molecule. Random and sequential ring-opening copolymerization (ROcP) can also be implemented to vary the backbone structure. These different routes aim at modifying the properties of *hb*PGs.

3.3.1. Structural variation of the core molecule

Specific initiation of the ROMBP of glycidol by alcohols, nanoparticles (NPs), modified inorganic surfaces, linear or hyperbranched polyols, biocompatible molecules, or protected amines have been investigated by several research groups, as highlighted in **Figure I-24**.

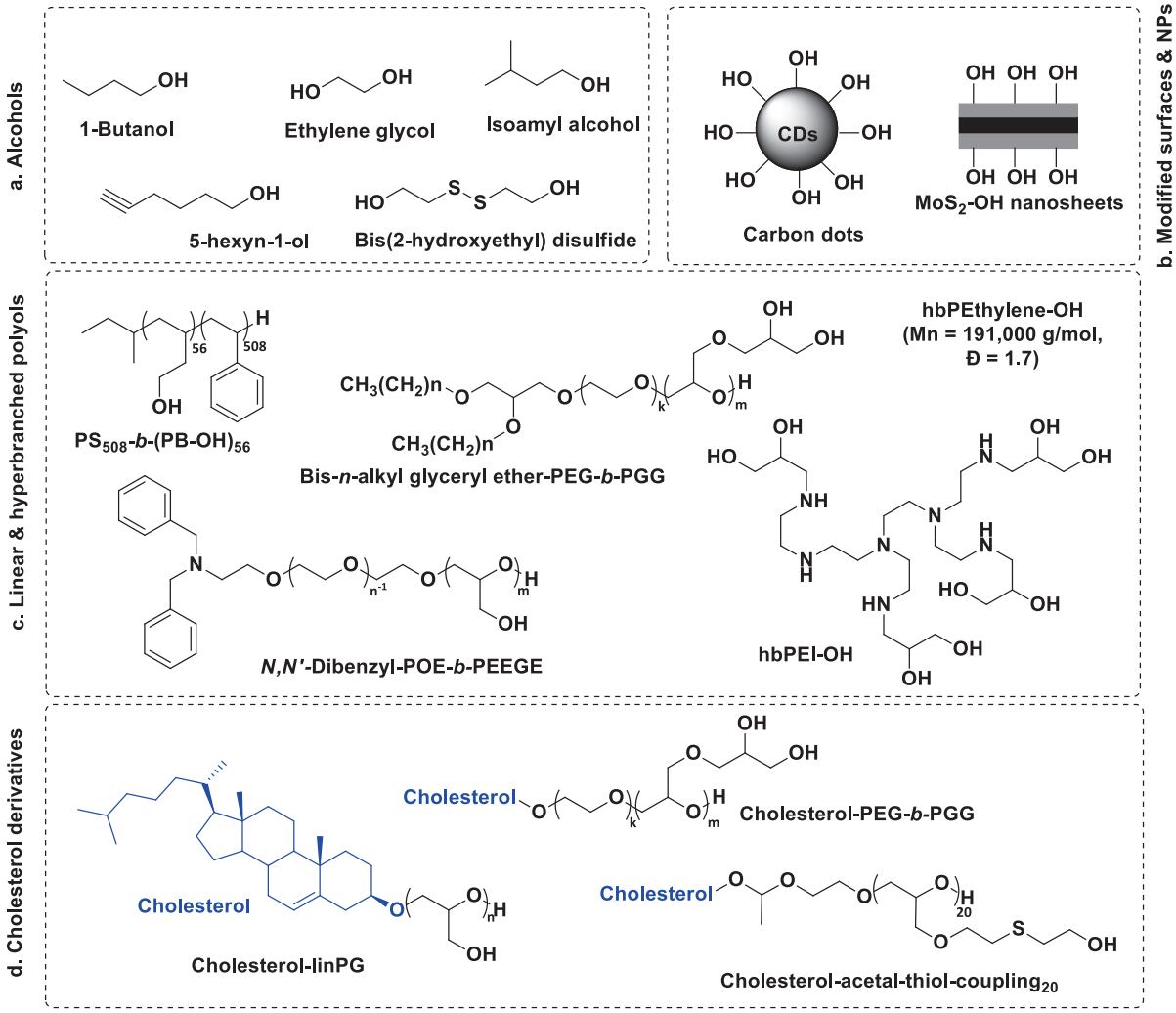

Figure I-24. Different initiating systems or core molecules used for the ROMBP of glycidol.

Initiators other than TMP include isoamyl alcohol,[74] 1-butanol[125] or ethylene glycol[126] (**Figure I-24, entry a**). For instance, Moore *et al.*[127] have used 5-hexyn-1-ol to initiate the ROMBP of glycidol; azido octadecane and azide-fluor 488 have been successfully grafted afterwards onto the resulting *hb*PG (M_n = 17,000-73,000 g/mol), demonstrating the accessibility of the alkyne function at the core. Yeh *et al.*[128] have synthesized *hb*PG featuring a disulfide core molecule. Further cleavage of the disulfide moiety under reducing conditions

affords a thiolated *hb*PG-SH (M_n = 1,600 and 4,300 g/mol). Thin and uniform layers of *hb*PG-SH can be coated on gold NPs (**Figure I-25**), using the thiol core molecule as anchor point. The antifouling feature of the *hb*PGH surface has been evaluated in presence of proteins. Thin layers of *hb*PG-SH have been shown more efficient for preventing the aggregation of proteins than the more traditional PEG-SH coatings.

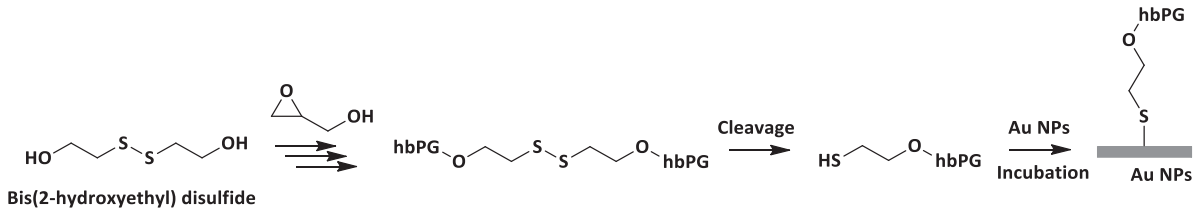

Figure I-25. Synthesis of *hb*PG-SH and grafting to gold nanoparticle surfaces.[128]

Grafting of *hb*PG from both NPs and nanosheet surfaces featuring surface hydroxyl groups has been implemented *via* surface-initiated ROMBP (**Figure I-24, entry b**). As-obtained particles exhibiting fluorescent properties have been found to target cell imaging or biomedical applications. Li *et al.*[129] have designed "hypergrafted" *hb*PG from fluorescent carbon dots of diameter 6.8 nm, obtained from the hydrothermal carbonization of α-cyclodextrin. The numerous hydroxyl groups carried by carbon dots have enabled to initiate the ROMBP of glycidol; resulting carbon dots grafted with *hb*PGs (CD-*g*-*hb*PG) of diameter 71 nm have been achieved, keeping their fluorescent properties. The cell toxicity has been reduced and untargeted cells do not interfere with the CD-*g*-*hb*PG. Inorganic surfaces, such as molybdenum disulphides nanosheets, can be cured to create hydroxylated areas. MoS_2-OH nanosheets have been produced by Huang *et al.*[130] and used for initiation. The fluorescent Rhodamine B dye has been grafted to the hyperbranched hydroxyl groups, forming stable colloidal particles showing good light and thermal properties.

As mentioned, Wilms *et al.*[108] have reported that ROMBP of glycidol can be initiated from macroinitiators. The following examples relate to the use of novel linear and hyperbranched polymers as core molecules (**Figure I-24, entry c**). Barriau *et al.*[131] have grafted *hb*PG from a polystyrene-*b*-poly(hydroxyethyl)ethylene (PS_{508}-*b*-PB-OH_{56}) block copolymer. Approximately 60 to 70 % of OH from (PS_{508}-*b*-PB-OH_{56}) have been found to effectively initiate the polymerization. The as-obtained amphiphilic linear-hyperbranched PS_{508}-*b*-(PB_{56}-*hg*-PG_{280})s have been studied by static and dynamic light scattering, evidencing the formation

of micelle-like structures in various organic solvents. A toluene solution of PS-*hg*-PG copolymer (deposited onto graphite) has been found to phase segregate forming a micelle-like nanostructure constituted of a dense PS core of 4 nm and a *hb*PG shell. Hofmann *et al.*[132] have prepared onion-like architectures based on a hydrophobic bis-*n*-alkyl glyceryl ether-PEG-*b*-PGG core and a hydrophilic *hb*PG shell. Unilamellar liposomes have been prepared by the so-called film hydration method; analyses by TEM, DLS and SANS have revealed the formation of vesicles of 54.2 nm with differing lengths of lipidic-PEG and *hb*PG moieties. For vectorization purpose, the space between the lipophilic core and the hydrophilic shell can affect the protection of the active principle during *in vivo* transportations.

Popeney *et al.*[133] have developed amphiphilic *hb*PEthylene-*b*-*hb*PG of 950,000 g/mol with a dispersity of 1.5. Analysis by dynamic light scattering in water has shown spherical particles with a diameter of 17.5 ± 0.9 nm. The Nile red hydrophobic drug has been successfully incorporated into the hyperbranched polyethylene core and transported into living cells, revealing a plausible use in drug delivery.

Fan *et al.*[134] have modified a commercial hyperbranched polyethylenimine (*hb*PEI, DB = 0.6) to bring hydroxyl functions at the chain ends (*hb*PEI-OH). While neither the *hb*PEI and the *hb*PEI-OH nor the *hb*PG have exhibited fluorescent properties, *hb*PEI-*b*-*hb*PG has been found to emit a blue fluorescent light around 470 nm. Increasing the thickness of the *hb*PG shell, *i.e.* the molecular weight of *hb*PG, has enabled to raise the fluorescence intensity.

Wurm *et al.*[135] have sequentially polymerized ethylene oxide and ethoxyethyl glycidyl ether (EEGE) onto amino-protected *N*,*N*'-dibenzyl-2-as aminoethanol initiator (**Figure I-26**). The EEGE moieties have been further deprotected and the so-formed hydroxyl groups have been deprotonated to initiate the hypergrafting of glycidol. Free amino groups, in α-position, have been finally released by hydrogenation. The resulting α,ω_n-heterotelechelic block copolymers have been covalently coupled with (+)-Biotin pentafluorophenyl ester, forming biotinylated α,ω_n-structure, which has been subsequently complexed with an Avidin protein, as a proof of concept.

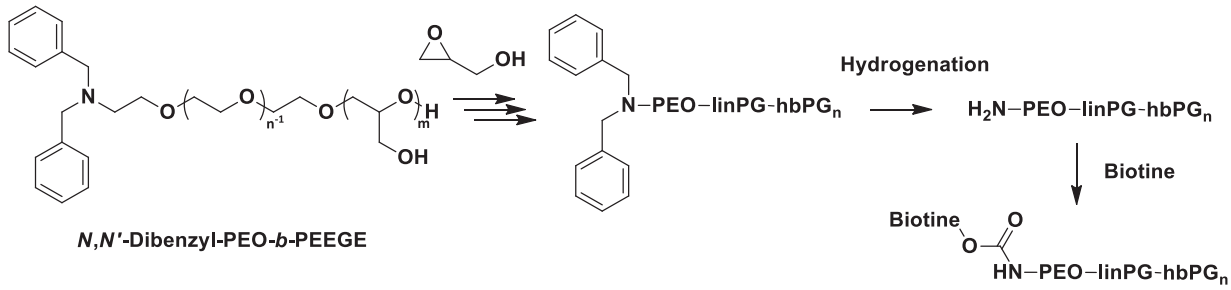

Figure I-26. Synthesis of α,ω$_n$-linear-hyperbranched heterotelechelics, carrying one amino function and n terminal hydroxyl groups and covalent coupling with biotine.[135]

Biocompatible lipids, such as cholesterol and cholesterol derivatives, have also been used as initiators for the ROMBP of glycidol (and glycidol derivatives, **Figure I-24, entry d**). In addition to the aliphatic initiated *hb*PG, Hofmann *et al.*[132] have synthesized cholesterol-based *hb*PG, forming unilamellar vesicles the size of the hydrophobic layer being controlled by molecular weights of PEG, PGG and *hb*PG components. Müller *et al.*[136] have developed several cleavable cholesterol-based *hb*PGs. Depending on the synthetic strategy, the cleavable groups can be either incorporated into the hyperbranched structure or used as core molecules. Random and block copolymers of glycidol and EEGE, Ch-P(GEGE$_x$-*co*-G$_y$) and Ch-P(GEGE$_x$-*b*-G$_y$), respectively, have been synthesized using the cholesterol-initiated linear poly(glycerol) (Ch-linPG$_x$, **Figure I-27, entry a**). Both latent AB$_2$-*type* monomer have contributed to the formation of dendritic units. Many cleavable acetal functions can be introduced into the hyperbranched structures through the use of EEGE monomer, imparting degradability to the hyperbranched compound. Some structures only show one cleavable acetal function, separating the cholesterol moiety from the polymer fraction (**Figure I-27, entry b**). The lipid-hyperbranched polymers can form sterically stabilized liposomes with tuneable acidic degradability and good biocompatibility.

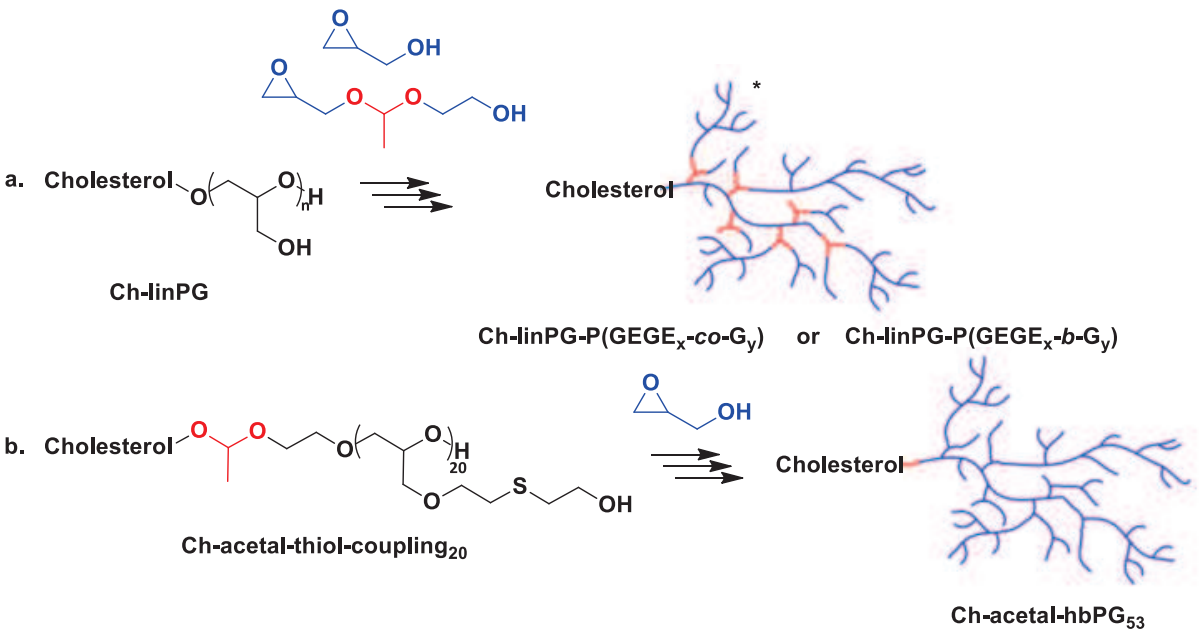

Figure I-27. Cleavable *hb*PG synthesis initiated by cholesterol derivatives.[136]

Deprotonated amines can also initiate the ROMBP of glycidol (**Figure I-28**). Kasza *et al.*[137] have employed phthalimide potassium for that purpose (**Figure I-28, entry a**). Hyperbranched polymers with DB = 0.52-0.56 have thus been obtained with a rather good control of molecular weight (1,400-5,600 g/mol). The phthalimide function at the core can be cleaved with hydrazine to produce amino-monofunctionalized *hb*PGs that can be further derivatized into carboxylic-monofunctionalized *hb*PGs, maleimide-monofunctionalized *hb*PGs and chloroacetamide-monofunctionalized *hb*PGs, which in turn serve to graft proteins, nanoparticles or catalysts. Spears *et al.*[74] have grafted maleimide onto a bovine serum albumin protein (BSA) *via* thiol-ene "click chemistry", which enables to initiate the CROP of glycidol in water (**Figure I-28, entry b**).

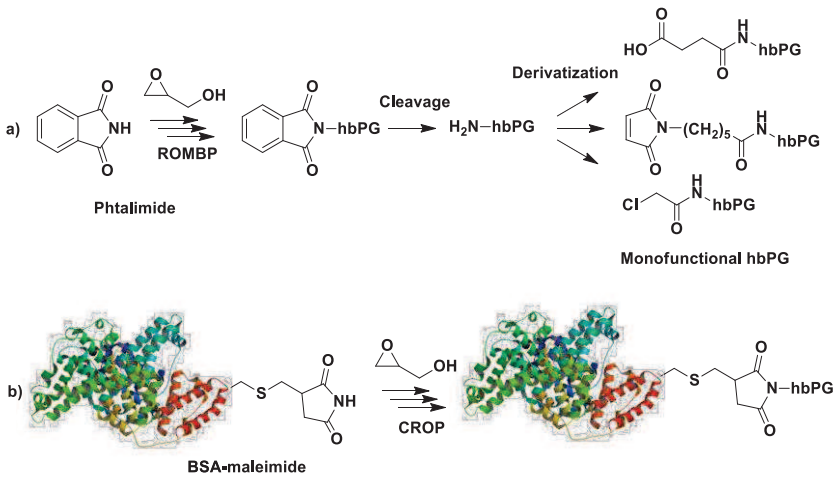

Figure I-28. Synthesis of monofunctional *hb*PG **a)** from phthalimide by ROMBP of glycidol,[137] and **b)** from maleimide-based initiation of CROP of glycidol.[74]

3.3.2. Copolymerization

Anionic ROMBP is particularly adapted to the random and/or sequential copolymerization of involving glycidol and other epoxides. Several co-monomers have been evaluated in order to tune the final properties of the hyperbranched structures. Copolymerization reactions can be initiated with alkoxides (MeOK or CsOH) and monomers must be added by slow addition. *N*-Methyl-2-pyrrolidone (NMP) is most often used as solvent for this purpose, instead of DMSO.

3.3.2.1. Random copolymerization of glycidol with epoxide co-monomers

Not only non-functional but also functional monomer units as well as new dendritic units can be incorporated into the *hb*PG-based structure *via* copolymerization of latent AB-, functional latent AB- and latent AB_2-type co-monomers with glycidol, respectively.

Incorporation of latent AB-type co-monomers

Ethylene oxide and substituted aliphatic epoxides, bearing one to sixteen carbon atoms, have been randomly copolymerized with glycidol (**Figure I-29**). The incorporation of the latter epoxides results in the formation of more hydrophobic hyperbranched copolyethers with long alkyl chains.

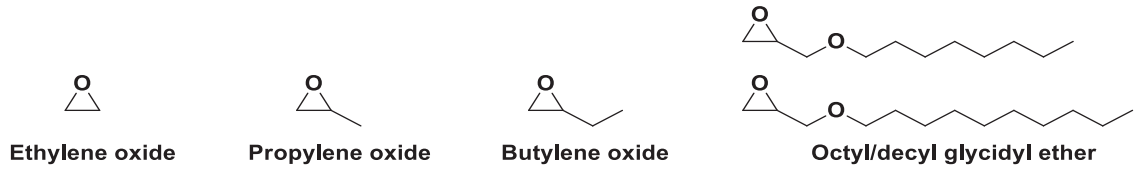

Figure I-29. Latent AB-type co-monomers used for random ROcP with glycidol leading to the formation of non-functional linear moieties.

Most studies have shown that glycidol is more reactive than the other co-monomers, eventually leading to the formation of gradient hyperbranched copolymers, instead of random structures.[138,139] Leibig *et al.*[138] have monitored the random ROcP of glycidol and ethylene oxide (EO), propylene oxide (PO) or butylene oxide (BO), by NMR in DMSO-d_6 (**Figure I-30**). It has been evidenced that glycidol is 6, 30 and 72 times more reactive than EO, PO and BO, respectively (using K^+ as counterion). For instance, during the synthesis of *hb*(PPO-*co*-PG), glycidol is fully consumed at 85 % of the total monomer conversion. This prevents the formation of allyl alcohol, which generally occurs as a side reaction during the homopolymerization of PO.[138,140] Transfer to glycidol can be minimized *via* copolymerization.

Finally, while metal cation does not affect the reactivity of G/PO copolymerization, use of Cs^+ has been found to accelerate (x2) the copolymerization between EO and glycidol as well as the one of BO and glycidol.

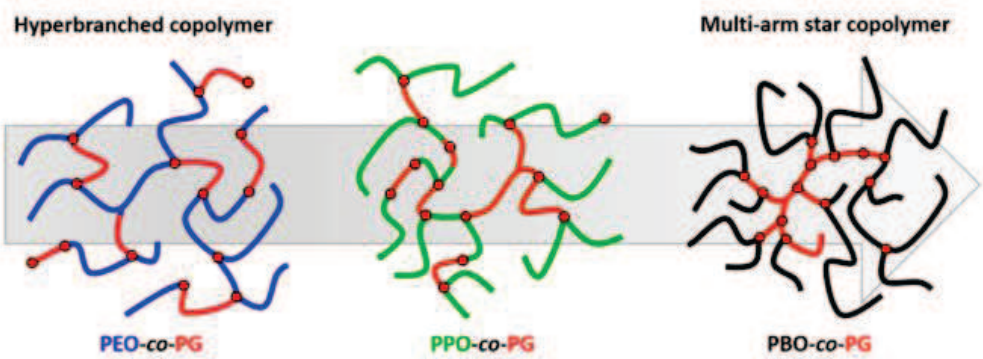

Figure I-30. Gradient hyperbranched copolymers structures.[138,139]

Properties of the hyperbranched copolymers are obviously impacted by incorporation of different contents in co-monomers into the *hb*PG backbone. "Hyperbranched poly(ethylene oxide)s" of DB 0.08 to 0.11 have been obtained by Yao *et al.*[141] after copolymerizing ethylene oxide with a low glycidol fraction (< 10 mol%) in bulk. Semi-crystalline *hb*P(EO-*co*-G) with T_m from 0 to 23 °C and T_g ranging from -64 to -50 °C have been obtained. As expected, the crystalline content, and consequently T_m and T_g values, decrease by increasing DB, *i.e.* upon increasing the glycidol content. The drop in T_m has been explained by the confinement of the PEO segments, as observed by the capillary infiltration of the *hb*(PEO-*co*-PG) into self-ordered anodic aluminium oxide nanopores.

Schömer *et al.*[140] have incorporated up to 97 mol% of PO into the *hb*PG structures, which has made the DB varying from 0.11 to 0.59. In comparison with *hb*PG-*co*-PEO, these copolymers prove fully amorphous with a T_g ranging from -65 to -35 °C, T_g decreasing upon increasing the content in glycidol. Interestingly, such copolymers exhibit a low critical solution temperature (LCST) in the range 24-83 °C, which increases for higher glycidol contents. The precipitation of the hyperbranched copolymer above its LCST is explained by the coil-to-globule transition caused by the segregation of the pendant methyl groups of PPO with the OH of glycidol. Seiwert *et al.*[142] have synthesized hyperbranched poly(butylene oxide)-*co*-polyglycidol with BO content between 26 and 76 mol%. The increase in BO content leads to a decrease of the T_g from -29 °C to -59 °C. No correlation between DB (0.57-0.77), T_g values or the BO content has

been established though. Copolymerization is carried out either *via* the SMA process or in batch. Batch polymerization induces self-initiated polymerization and fractions of unreacted TMP have been recovered. As previously reported by Leibig *et al.*,[138] ROcP of glycidol and BO gives rise to a gradient copolymer with a PBO shell. In contrast, random incorporation of BO is favoured *via* the SMA process. Epoxides featuring long aliphatic chains can also be copolymerized with glycidol. For instance, Misri *et al.*[143] have copolymerized octyl/decyl glycidyl ether (ODGE) acting as spacer into the hyperbranched copolymer backbone.

Incorporation of functional AB-*latent* co-monomers linear units

Several research groups have investigated the ROcP of glycidol with glycidyl ethers or epoxides bearing functional chain ends (**Figure I-31**). In addition to increasing chain mobility, some glycidyl ethers have been subjected to deprotection, releasing hydroxyl groups, which in turn, can be functionalized.

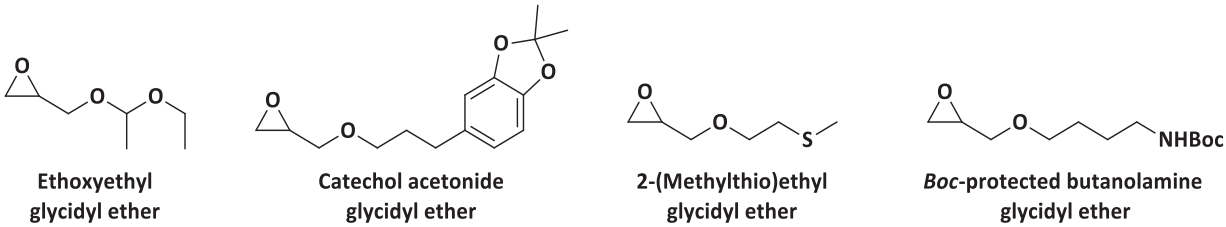

Figure I-31. Functional latent AB-type co-monomers used for random ROcP with glycidol leading to the formation of functional linear moieties.

EEGE has also been copolymerized with glycidol, as reported by Schubert *et al.*[144] The DB can thus be decreased from 0.58 to 0.17 for EEGE contents varying from 10 to 92 mol%. Despite of this, the flexibility of the copolymer is enhanced due to the presence of the long aliphatic chains. The T_g values of *hb*PG-*co*-PEEGE have been found to decrease when the content of EEGE increases. After deprotection of the EEGE moieties, linear glycidol units are obtained, lowering T_g values compared to the parent copolymer.

Other protected co-monomers have been used for ROcP with glycidol, including *Boc*-protected butanolamine glycidyl ether (BBAG).[145] The deprotection of BBAG yields *hb*P(G-*co*-BAG) copolymers containing functional primary amines. Increase in T_g has been noted after the deprotection, due to strong hydrogen bonds developed between the amines and hydroxyl

functions. Amino groups have also been subjected to post functionalization; rhodamine has for instance been successfully conjugated with the *hb*P(G-*co*-BAG).

More unconventional epoxide monomers, such as catechol acetonide glycidyl ether (CAGE)[146] and 2-(methylthio)ethyl glycidyl ether (MTEGE)[139] have also been copolymerized with glycidol. Catechol is well-known to adhere onto almost every surface through the complexation of the OH with ions. The hydroxyl functions of the CAGE monomer have been acetylated prior to ROP and subsequently deprotected. Increasing the amount of CAGE content into *hb*P(G-*co*-CAGE) improves the solubility in apolar solvents, such as Et_2O, while T_g has been found to increase. Networks of *hb*P(G-*co*-CAGE) can next be produced by addition of $FeCl_3$, upon complexation of Fe(III) species with OH groups of catechol moieties (for catechol content > 3 %). Mono-, bis- and tri- catechol complexes form for pH values lower than 5, between 5 and 9, and above 9, respectively. Colour changes, from orange to dark red and black, have been observed. *Hb*P(G-*co*-CAGE) has also been coated onto iron, PTFE and PVC surfaces, reducing the surface hydrophobicity.

Thermoresponsive *hb*P(G-*co*-MTEGE)s with cloud points in aqueous media varying between 29 and 75 °C have also been prepared.[139] Oxidation of the thiol functions into sulfones leads to fully water-soluble compounds, irrespective of the temperature. Post-functionalizations with more common epoxides have been achieved, providing a platform of functional polymers.

Incorporation of latent AB_2-type co-monomers

Over the large range of epoxide monomers copolymerized with glycidol, only a few are eventually of latent AB_2-type, contributing to the formation of dendritic units (**Figure I-32**).

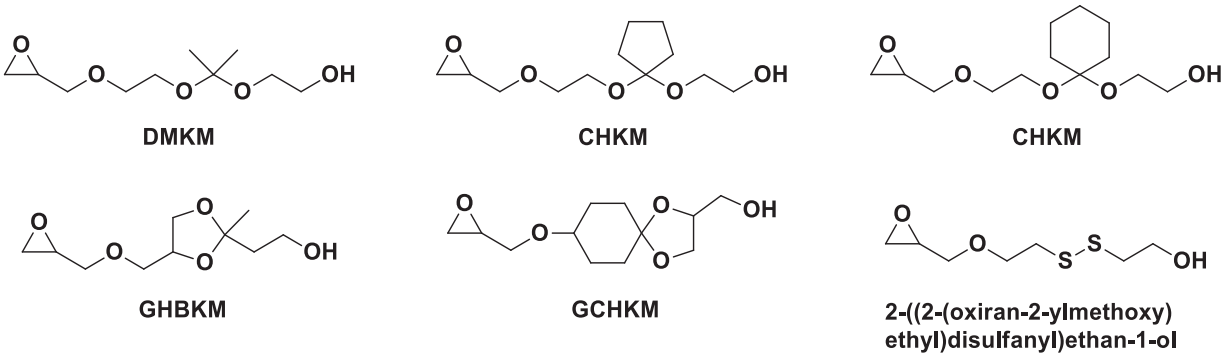

Figure I-32. Functional latent AB_2-type co-monomers used for random ROcP with glycidol leading to the formation of new dendritic moieties.

Shenoi *et al.*[147,148] have developed a platform of five cleavable α-epoxide-ω-hydroxyl ketal monomers. Although low conversions (15-20 %) are achieved by ROMBP of such ketal-containing monomers, use of 33 mol% of glycidol as co-monomer enables to reach conversions up to 70 %. Hence, from 52 to 66 mol% of ketal groups can be incorporated to the hyperbranched structure. All polymers have proven soluble in organic solvents (MeOH, THF…), but only *hb*PEther from DMKM has been found soluble in water. Ketal groups are stable at neutral pH but can be readily cleaved under acidic conditions. The copolymer degradation thus depends on temperature, pH, and structure of the α-epoxide-ω-hydroxyl ketal-containing monomer. The degradation rate increases at higher temperature and lower pH values. The torsion of the ketal groups favours hydrolysis in the following order: acyclic (DMKM) > extracyclic (CPKM and CHKM) > intracyclic (GHBKM and GCHKM). The degradation half-time varies from dozen of minutes to hours or few years accordingly. Both copolymers and degraded products have been shown to be biocompatible with cells and blood.

Son *et al.*[149] have copolymerized glycidol with a disulphide glycidyl ether, namely, 2-((2-(oxiran-2-ylmethoxy)ethyl)disulfanyl)ethan-1-ol (SSG). The as-obtained *hb*P(G-*co*-SSG)s random copolymers have been degraded by exposing the disulphide bond to dithiothreitol (DTT) *via* a reduction process.

3.3.2.2. Sequential copolymerization of glycidol with epoxide co-monomers

Direct use of *hb*PG as multifunctional macroinitiator for the ROcP of another epoxide (**Figure I-33**) has been investigated.

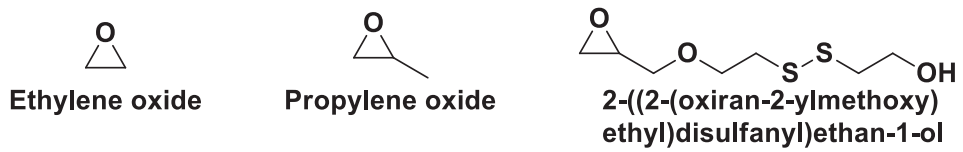

Figure I-33. Co-monomers used for sequential ROcP onto hyperbranched polyglycidol.

The procedure generally starts with the partial deprotonation of the hydroxyl groups of the *hb*PG precursor, forming insoluble aggregates for deprotonated hydroxyls exceeding 5 %, even in DMSO.[150] Although not ensuring good control of the ROP of ethylene oxide, this procedure is adapted to polymerize propylene oxide further, as already observed by Sunder *et al.*[104] All

primary and secondary hydroxyl groups from *hb*PG can indeed initiate the ROP of propylene oxide, forming *hb*PG-*b*-*lin*PPO copolymers containing secondary hydroxyl functions at their chain ends. *Hb*PG-*b*-*lin*PPO remains soluble in DMSO after deprotonating up to 30 % of its hydroxyl functions, which is conveniently used to further polymerize ethylene oxide. Knischka *et al.*[150] have finally synthesized star-like *hb*PEO by grafting PEO from *hb*PG-*b*-*lin*PPO precursors. In their attempts to prepare core-shell *hb*P(G-*b*-SSG), Son *et al.*[151] have noted that cleavage of 10 % of the disulphide internal bonds occurs, forming free thiols. The polymerization of glycidol from a *hb*PSSG core has also been performed. Different platforms of fully redox-degradable gradient and core-shell hyperbranched copolymers have thus been developed.

3.3.3. Post-functionalization of hyperbranched polyglycidol

Post-functionalization of *hb*PG has been widely studied for targeting specific properties. For instance, Sunder *et al.*[104] have succeeded in selectively alkylating either the OH of full molecule or the one of the core of *hb*PG by selective chemical differentiation.[105] Through the use of SMA approach, the core of *hb*PG is constituted of linear and dendritic units while the shell is made of diol-type terminal units. These diols can be first ketalized while the core is further alkylated by alkyl halides. .

Kainthan *et al.*[106] have sequentially grafted octadecane oxide (ODO) and monofunctional PEG oxide (mPEG-oxide) onto *hb*PG (**Figure I-34**). Hydrophobic compounds, such as pyrene or fatty acids being not soluble into the hydrophilic *hb*PG or *hb*PG-PEG, incorporation of C_{18} aliphatic chains at the core of the hyperbranched structure enables the solubilisation of hydrophobic molecules. An anionic fluorescent probe has been encapsulated into so-called unimolecular micelles formed by *hb*PG-C_{18}-PEG. The fluorescent emission has confirmed the encapsulation of the probe, as the latter does not emit in water media due to its quenching.

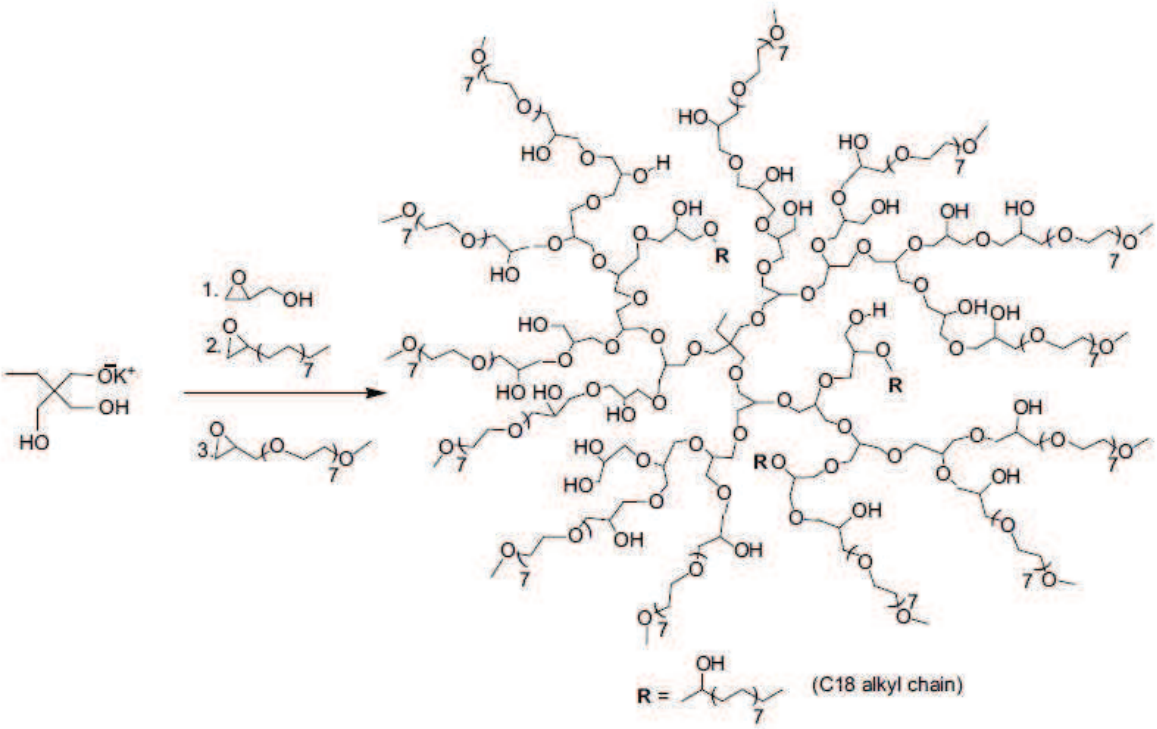

Figure I-34. Functionalization of hyperbranched glycidol with octadecane oxide and polyethylene oxide.[106]

Kurniasih *et al.*[105] have developed a specific approach to co-encapsulate two distinct hydrophobic drugs followed by two different releasing strategies (**Figure I-35**). The "selective chemical differentiation" approach has been implemented to graft bicyclic hydrophobic molecules into the core and hydrophilic mPEG-succinate chains at the periphery. Unimolecular micelles of 10 nm diameter, and functionalized *hb*PG aggregates of diameter 200 nm, form after addition of pyrene first, then of the Nile red. While pyrene can be encapsulated into the hyperbranched backbone, Nile red has been found to be hosted at the interface of the micelles, which brought about their clustering. Aggregates have been disrupted under acidic conditions, releasing Nile red readily upon cleavage of mPEG ester bonds. However, use of *Candida Antarctica* Lipase B is required to split the ester bond of the bicyclic compounds into the core and thus release pyrene guest.

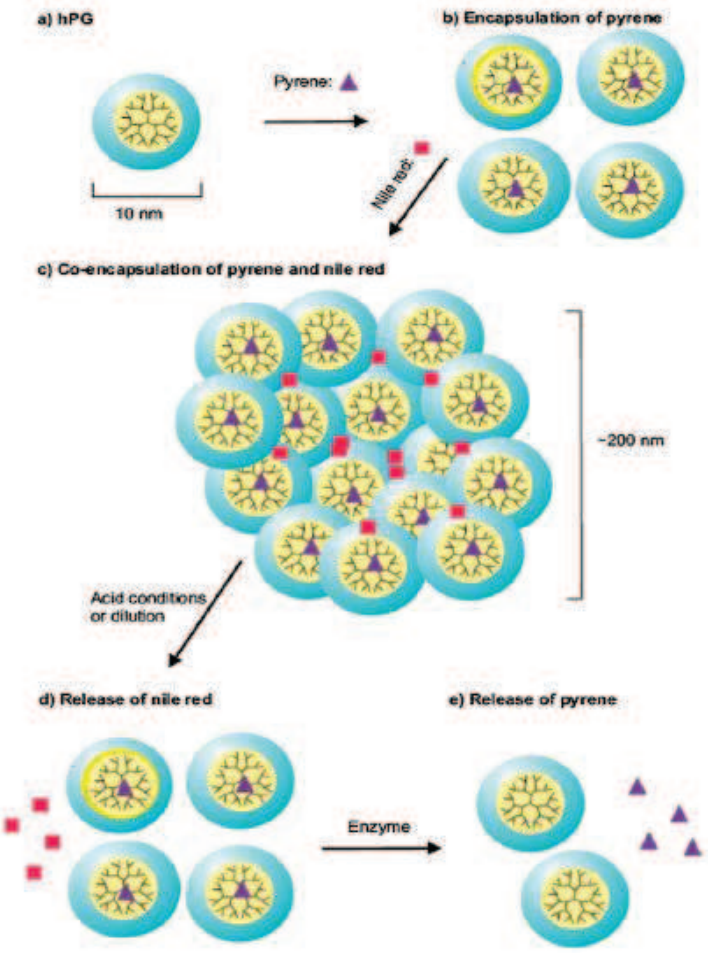

Figure I-35. Encapsulation and release mechanism: **a)** single polymer ca. 10 nm, **b)** encapsulation of pyrene by a unimolecular mechanism, **c)** co-encapsulation of two guest molecules, **d)** release of nile red under acidic conditions, and **e)** release of pyrene in the presence on an enzyme.[105]

3.3.4. Combination of copolymerization and post-functionalization

To extend the range of targeted properties and applications, several modification methods can be combined. For instance, Scharfenberg *et al.*[152] have synthesized *hb*(PG-*co*-PPO) and *hb*(PG-*co*-PBO) copolymers by random ROcP. Polycarbonate-polyether multiarm stars have been finally achieved by initiating the copolymerization of BO (or PO) and CO_2 with the hyperbranched macroinitiator into an autoclave, in presence of (R,R)-(salcy)-CoCl as catalyst and [PPN]Cl as cocatalyst. Depending on the reactivity of co-monomers, arms formed of polyether/polycarbonate (BO as co-monomer) or homopolycarbonates (PO as co-monomer), have thus been generated. The MHS α coefficients of these compounds have been found between 0.08-0.2, which are characteristic values for star and hyperbranched polymers. Phenyl

isocyanate has been subsequently grafted to the biodegradable polycarbonates arms, forming urethane linkages.

The hydrophobic *hb*P(G-*co*-ODGE) produced *via* random ROcP by Misri *et al.*[143] has been post-functionalized, with $mPEG_{400}$-epoxide, to create an amphiphilic hyperbranched derivative.[105,106] *Hb*P(G-*co*-ODGE)-*b*-PEG indeed forms unimolecular micelles of diameter 5.9 nm.

Modified *hb*PGs have also been used as plasticizers for high T_g polymers such as PVC. The grafting of alkyl chain ends onto the parent *hb*PG, *via* transesterification,[153,154] leads to a derivative with a lower T_g. To prevent migration of the *hb*PEther additive, the terminal alkyne *hb*PG has been covalently grafted onto an azide functional PVC. Propargyl alcohol has thus been used to initiate the ROMBP, which has been followed by the post functionalization of the polymer.[98]

3.4. Towards innovative technologies

Many potential applications have been proposed for *hb*PGs and derivatives, in particular as drug delivery systems, surface and nanoparticles coating agents, or curing agents (e.g. for PU synthesis).

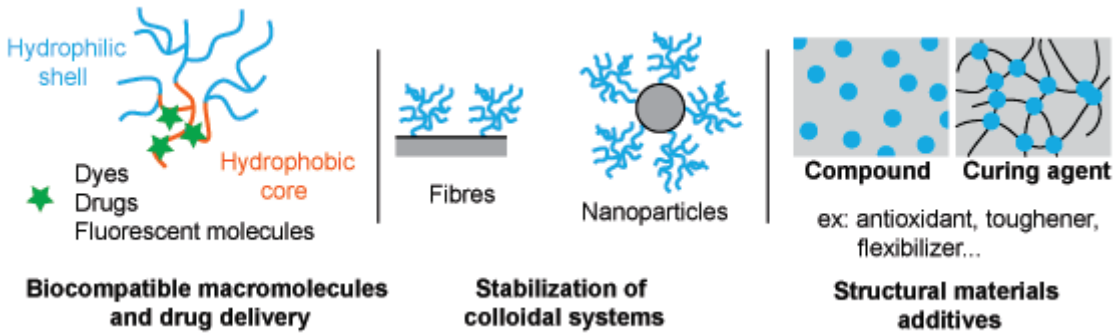

Figure II-36. Examples of applications of *hb*PGs and derivatives.

3.4.1.1. Biocompatible macromolecules and drug delivery

The biomedical field is undoubtedly the main target of *hb*PGs.[155] As amphiphilic derivatives obtained by post-modification can organize into unimolecular micelles in water,[156] guest molecules such as dyes, fluorescent molecules,[155] or drugs[106,122,157] can be encapsulated within their core. Ligands, such as Cu(II) NPs, can also be carried at the periphery of these micelles.[158]

Cleavable units have been incorporated into the core, the shell or at the interface of the core and the shell *via* random or sequential polymerization with suitable co-monomers. The pH or redox degradable properties of the *hb*PG derivatives enable to control the release of the guest molecules, depending on the environment. Due to its low viscosity and water solubility, *hb*PG enhances blood and cell compatibility, which can be further improved by grafting specific biocompatible molecules.[122,156,159] Some groups have taken advantage of this biocompatibility for improving the cold storage of donor organs before transplantation.[160] Application in blood transfusion has also been investigated.[161] The degradation products have appeared poorly cytotoxic.[157] Clinical *in vivo* and *in vitro* tests have outlined the long circulation half-time into blood circulation system,[106,122,157,162] despite the low diameter of the *hb*PG micelles that generally ranges from 2.6 to 10 nm.[122,161] The increase in size (up to 100 or 200 nm) by grafting arms, has allowed prolonging the circulation half-time.[162]

3.4.1.2. Stabilization of colloidal systems

Particles and nanoparticles are generally hydrophobic and are thus hard to solubilize in water. Grafting of *hb*PG onto such materials greatly improves their water solubility by forming stable colloidal dispersions. Several examples involve the ROMBP initiation of raw or modified nanoparticles bearing hydroxyl groups that can be deprotonated by a base. Inorganic NPS such as gold, CdSe-ZnS or Mn-ZnSeS coated with silica,[163] MoS_2 nanosheets,[130] carbon dots (CDs),[129] or carbon fibres,[164] have thus been used as multifunctional initiators for this purpose. Functional cores can also be introduced into *hb*PG and subsequently be grafted onto the particles.[128] This grafting often enhances the colloidal stability of the NPs.[163] The adhesion of epoxy resin onto carbon fibres can also be improved after grafting of *hb*PG onto fibers.[164] As an alternative to the encapsulation of fluorescent compounds into its core,[128,130,165] *hb*PG has been covalently bonded to carbon dots, intrinsically fluorescent.[129] These stabilization properties can be used to enhance ink properties, such as color-fastness to dry and wet rubbing.[125]

3.4.1.3. Structural materials additives

*Hb*PG and its derivatives can conveniently be used as additives of structured matrices. Appropriate molecules make them effective as antioxidants,[166] tougheners[167] or flexibilizers.[168] Post-functionalization of *hb*PG with a phenol antioxidant has for instance been found to delay the oxidation and drastically reduced the chain scission of PVC.[166] Vinyl-functionalized *hb*PGs

have been used as tougheners for vinylester-urethane hybrid resins.[167] Liquid rubber made from the copolymerization of *hb*PG with copolyethers arms have been used as flexibilizers or tougheners, depending on the thermo-mechanical properties, for anhydride-cured epoxy resins.[168] *Hb*PGs with alkyl chain ends successfully plasticizes PVC.[99] To prevent the migration of the dendritic macromolecules, *hb*PG has been covalently linked to a post-modified PVC *via* the core molecule, plasticizing properties being preserved.[98] The high number of functional hydroxyl chain ends is favourable for the formation of structural materials. *Hb*PGs bearing rigid polyether-carbonate arms[152,169] can thus be used as rigid polyols serving for the synthesis of rigid polyurethanes, employed in automotive, housing or civil engineering sectors. PEG-diacrylate has been copolymerized with *hb*PG-acrylate to form networks.[170] The stiffness of the PEG network has been reduced by the incorporation of the hyperbranched moieties. In another study, catechol-functionalized *hb*PG has enabled to generate networks by adding Fe(III) cations; the catechol moieties forming complexes with the metal ions.[146] Reversibly cross-linked hyperbranched polyglycidol have been formed by adding $B(OH)_4^-$ ions into the viscous polymer.[171] Self-healable hydrogels have been similarly achieved by coupling polyacrylamide that carried phenyl boronate functions and *hb*PG.[172] Boronic-ester bonds can link the polyacrylamide to the numerous OH of the hyperbranched polyglycidol at neutral pH.

4. Conclusion and objectives

Due to their specific properties, including their low viscosity, high solubility, and high functionality, as well as their cost-effective synthesis in one-pot, hyperbranched polymers have been showing an increasing interest in the last three decades, from both academic and industrial areas. Several hyperbranched polymers, based on polyester, polyamide, polyethyleneimine, and polyether, have been developed. In particular, polyethers have been found particularly useful for applications requiring hydrolysis and chemical resistance, as well as a good thermal stability. Rigid hyperbranched poly(aryl ether)s exhibiting high T_g have been formed *via* nucleophilic substitution of sterically hindered aromatic monomers at high temperatures. By comparison, synthesis of aliphatic hyperbranched polyethers (*hb*PEthers) is typically achieved by cationic, anionic, coordinated or enzymatic ring-opening polymerizations of hydroxyl-containing oxetanes or oxiranes. Cationic-ring opening polymerization (CROP) is particularly used for poly-substituted monomers such as oxetanes or specific oxiranes. In contrast, their polymerization is not favoured by an anionic route. *Hb*PEthers derived from oxetanes, representing the most important class of *hb*PEthers synthesized through CROP, can be either amorphous or semi-crystalline, with a solubility that drastically vary depending on the constitutive monomer units.

Hyperbranched polyglycidol (*hb*PG) is certainly the *hb*PEther the most studied nowadays, showing a high potential in numerous applications owing to its high water-solubility, amorphous feature and high number of OH groups available for post-functionalization. Mainly synthesized following the so-called anionic ring-opening multi-branching polymerization (ROMBP), CROP, coordination-insertion and enzymatic ROP can also be performed, yielding *hb*PGs of molecular weights ranging from 500 to 1,000,000 g/mol, with DB of 0.45-0.63 and T_g varying between -20 and -15°C. Random and sequential copolymerization of glycidol with other epoxides can also be implemented to achieve a large palette of hyperbranched systems, with tunable properties, e.g. viscosity, compatibility, crystallinity, finding interest as additives in structural materials, as reactive polyols for the synthesis of hybrid polymer resins and as surface modifier for imagery applications.

In recent years, the Cramail's team at the LCPO has been developing versatile platforms of epoxidized fatty acids, enabling new advances in bio-based hyperbranched polymer synthesis.[11,173] Yet, only a few studies have employed bio-based monomers for this purpose.[68,76]

To the best of our knowledge, no study has been dedicated to the design of hyperbranched polyethers derived from fatty acids. In the next chapters, will be reported the synthesis of hyperbranched polyethers by ROMBP of latent AB_2-type α-epoxy-ω-hydroxy monomers derived from ricinoleic oil. Hydrophobic, semi-crystalline polyethers have been obtained in this way by ROMBP. Random and sequential copolymerization will be also described, with the aim at tuning the properties of the resulting copolyethers. As seen in this chapter, post-modification is also a powerful tool for tuning the properties of the hyperbranched materials. In the last chapter, examples of post-modification of fatty acid-derived *hb*PEsters will be discussed. Depending on the nature of the functionalization, such hydrophobic *hb*PEsters can be made water-soluble or used as toughener for PMMA.

5. References

(1) Newkome, G. R.; Moorefield, C. N.; Vögtle, F. *Dendrimers and Dendrons: Concepts, Synthesis, Applications*; WILEY-VCH Verlag GmbH, 2004.

(2) Tomalia, D. A.; Christensen, J. B.; Boas, U. *Dendrimers, Dendrons and Dendritic Polymers: Discovery, Applications and the Future*; Cambridge University Press, 2012.

(3) Gitsov, I. Hybrid Linear Dendritic Macromolecules: From Synthesis to Applications. *J Polym Sci Part A Polym Chem* **2008**, *46* (16), 5295–5314.

(4) Schlüter, A. D.; Rabe, J. P. Dendronized Polymers: Synthesis, Characterization, Assembly at Interfaces and Manipulation. *Angew Chemie Int Ed* **2000**, *39*, 864–883.

(5) Frauenrath, H. Dendronized Polymers—building a New Bridge from Molecules to Nanoscopic Objects. *Prog Polym Sci* **2005**, *30* (3–4), 325–384.

(6) Taton, D.; Feng, X.; Gnanou, Y. Dendrimer-like Polymers: A New Class of Structurally Precise Dendrimers with Macromolecular Generations. *New J Chem* **2007**, *31* (7), 1097.

(7) Konkolewicz, D.; Monteiro, M. J.; Perrier, S. Dendritic and Hyperbranched Polymers from Macromolecular Units: Elegant Approaches to the Synthesis of Functional Polymers. *Macromolecules* **2011**, *44*, 7067–7087.

(8) Teertstra, S. J.; Gauthier, M. Dendrigraft Polymers: Macromolecular Engineering on a Mesoscopic Scale. *Prog Polym Sci* **2004**, *29* (4), 277–327.

(9) Hutchings, L. R. DendriMacs and HyperMacs - Emerging as More than Just Model Branched Polymers. *Soft Matter* **2008**, *4* (11), 2150–2159.

(10) Yan, D.; Gao, C.; Frey, H. *Hyperbranched Polymers: Synthesis, Properties, and Applications*; John Wiley & Sons, Inc.: Hoboken, 2011.

(11) Testud, B. Vegetable Oils as a Platform for the Design of Novel Hyperbranched Polyesters, PhD Thesis, Université de Bordeaux, 2015.

(12) Buhleier, E.; Wehner, W.; Vögtle, F. 'Cascade'- and 'Nonskid-Chain-like' Syntheses of Molecular Cavity Topologies. *Synthesis (Stuttg)* **1978**, *2*, 155–158.

(13) Tomalia, D. A.; Baker, H.; Dewald, J.; Hall, M.; Kallos, G.; Martin, S.; Roeck, J.; Ryder, J.; Smith, P. A New Class of Polymers: Starburst-Dendritic Macromolecules. *Polym J* **1985**, *17* (1), 117–132.

(14) Newkome, G. R.; Yao, Z.; Baker, G. R.; Gupta, V. K. Cascade Molecules: A New Approach to Micelles. A [27]-Arborol. *J Org Chem* **1985**, *50* (3), 2003–2004.

(15) Hawker, C.; Fréchet, J. M. J. A New Convergent Approach to Monodisperse Dendritic Macromolecules. *J Chem Soc Chem Commun* **1990**, *15*, 1010–1013.

(16) Hawker, C.; Fréchet, J. M. J. Preparation of Polymers with Controlled Molecular Architecture. A New Convergent Approach to Dendritic Macromolecules. *J Am Chem Soc* **1990**, *112* (21), 7638–7647.

(17) Voit, B. I. Dendritic Polymers: From Aesthetic Macromolecules to Commercially Interesting Materials. *Acta Polym* **1995**, *46* (2), 87–99.

(18) Tomalia, D. A.; Fréchet, J. M. J. Discovery of Dendrimers and Dendritic Polymers: A Brief Historical Perspective. *J Polym Sci Part A Polym Chem* **2002**, *40* (16), 2719–2728.

(19) Flory, P. J. Molecular Size Distribution in Three Dimensional Polymers. I. Gelation. *J Am Chem Soc* **1941**, *63* (11), 3083–3090.

(20) Flory, P. J. Molecular Size Distribution in Three Dimensional Polymers. II. Trifunctional Branching Units. *J Am Chem Soc* **1941**, *63* (11), 3091–3096.

(21) Flory, P. J. Molecular Size Distribution in Three Dimensional Polymers. III. Tetrafunctional

Branching Units. *J Am Chem Soc* **1941**, *63* (11), 3096–3100.

(22) Flory, P. J. Molecular Size Distribution in Three Dimensional Polymers. VI. Branched Polymers Containing A-R-B,-, Type Units. *J Am Chem Soc* **1952**, *74* (1932), 2718–2723.

(23) Kim, Y. H. Hyperbranched Polyarylenes. U.S. 4857630, 1987.

(24) Kim, Y. H.; Webster, O. W. Hyperbranched Polyphenylenes. *Macromolecules* **1992**, *25* (21), 5561–5572.

(25) Zheng, Y.; Li, S.; Weng, Z.; Gao, C. Hyperbranched Polymers: Advances from Synthesis to Applications. *Chem Soc Rev* **2015**, *44*, 4091–4130.

(26) Kienle, R. H.; Hovey, A. G. The Polyhydric Alcohol-Polybasic-Acid Reaction. I.Glycerol-Phtalic Anhdydride. *J Am Chem Soc* **1929**, *51* (2), 509–519.

(27) Kienle, R. H.; Van Der Meulen, P. A.; Petke, F. E. The Polyhydric Alcohol-Polybasic Acid Reaction. III. Further Studies of the Glycerol-Phthalic Anhydride Reaction. *J Am Chem Soc* **1939**, *61* (9), 2258–2268.

(28) Kricheldorf, H. R.; Zang, Q.-Z.; Schwarz, G. New Polymer Syntheses: 6. Linear and Branched Poly(3-Hydroxy-Benzoates). *Polymer (Guildf)* **1982**, *23* (12), 1821–1829.

(29) Voit, B. New Developments in Hyperbranched Polymers. *J Polym Sci Part A Polym Chem* **2000**, *38* (14), 2505–2525.

(30) Hawker, C.; Lee, R.; Fréchet, J. M. J. One-Step Synthesis of Hyperbranched Dendritic Polyesters. *J Am Chem Soc* **1991**, *4588* (113), 4583–4588.

(31) Frey, H.; Hölter, D.; Burgath, A. Degree of Branching in Hyperbranched Polymers. *Acta Polym* **1997**, *48* (1-2), 30–35.

(32) Kambouris, P.; Hawker, C. J. A Versatile New Method for Structure Determination in Hyperbranched Macromolecules. *J Chem Soc Perkin Trans 1* **1993**, No. 22, 2717–2721.

(33) Simon, P. F. W.; Müller, A. H. E.; Pakula, T. Characterization of Highly Branched Poly(Methyl Methacrylate) by Solution Viscosity and Viscoelastic Spectroscopy. *Macromolecules* **2001**, *34* (6), 1677–1684.

(34) Zhu, X.; Zhou, Y.; Yan, D. Influence of Branching Architecture on Polymer Properties. *J Polym Sci Part B Polym Phys* **2011**, *49* (18), 1277–1286.

(35) Hult, A.; Johansson, M.; Malmström, E. Hyperbranched Polymers. In *Branched Polymers II*; Roovers, J., Ed.; Advances in Polymer Science; Springer Berlin Heidelberg, 1999; Vol. 143, pp 1–34.

(36) Fréchet, J. M. J. Functional Polymers and Dendrimers: Reactivity, Molecular Architecture, and Interfacial Energy. *Science (80-)* **1994**, *263*, 1710–1715.

(37) Sun, F.; Luo, X.; Kang, L.; Peng, X.; Lu, C. Synthesis of Hyperbranched Polymers and Their Applications in Analytical Chemistry. *Polym Chem* **2015**, *6* (8), 1214–1225.

(38) Zheng, Y.; Li, S.; Weng, Z.; Gao, C. Hyperbranched Polymers: Advances from Synthesis to Applications. *Chem Soc Rev* **2015**, *44* (12), 4091–4130.

(39) Wilms, D.; Stiriba, S.-E.; Frey, H. Hyperbranched Polyglycerols: From the Controlled Synthesis of Biocompatible Polyether Polyols to Multipurpose Applications. *Acc Chem Res* **2010**, *43* (1), 129–141.

(40) Higashihara, T.; Segawa, Y.; Sinananwanich, W.; Ueda, M. Synthesis of Hyperbranched Polymers with Controlled Degree of Branching. *Polym J* **2012**, *44* (1), 14–29.

(41) Gao, C.; Yan, D. Hyperbranched Polymers: From Synthesis to Applications. *Prog Polym Sci* **2004**, *29* (3), 183–275.

(42) Frey, H. Degree of Branching in Hyperbranched Polymers. 2. Enhancement of the Db: Scope

and Limitations. *Acta Polym* **1997**, *48* (8), 298–309.

(43) Yates, C. R.; Hayes, W. Synthesis and Applications of Hyperbranched Polymers. *Eur Polym J* **2004**, *40* (7), 1257–1281.

(44) Voit, B. I.; Lederer, A. Hyperbranched and Highly Branched Polymer Architectures—Synthetic Strategies and Major Characterization Aspects. *Chem Rev* **2009**, *109* (11), 5924–5973.

(45) Chen, H.; Kong, J. Hyperbranched Polymers from $A_2 + B_3$ Strategy: Recent Advances in Description and Control of Fine Topology. *Polym. Chem.* **2016**, *7* (22), 3643–3663.

(46) Jikei, M.; Kakimoto, M. Hyperbranched Polymers: A Promising New Class of Materials. *Prog Polym Sci* **2001**, *26* (8), 1233–1285.

(47) Herzberger, J.; Niederer, K.; Pohlit, H.; Seiwert, J.; Worm, M.; Wurm, F. R.; Frey, H. Polymerization of Ethylene Oxide, Propylene Oxide, and Other Alkylene Oxides: Synthesis, Novel Polymer Architectures, and Bioconjugation. *Chem Rev* **2016**, *116* (4), 2170–2243.

(48) Weiss, M. E. R. A Kinetic Model for the Anionic Ring-Opening Polymerization of Glycidol, PhD Thesis, Freien Universität Berlin, 2012.

(49) Banerjee, S.; Komber, H.; Ha, L.; Voit, B. Synthesis and Characterization of Hyperbranched Poly (Arylene Ether)s from a New Activated Trifluoro B3 Monomer Adopting an A2 + B3 Approach. *Macromol Chem Phys* **2009**, *210*, 1272–1282.

(50) Klein, R.; Wurm, F. R. Aliphatic Polyethers: Classical Polymers for the 21st Century. *Macromol Rapid Commun* **2015**, *36* (12), 1147–1165.

(51) Calderón, M.; Quadir, M. A.; Sharma, S. K.; Haag, R. Dendritic Polyglycerols for Biomedical Applications. *Adv Mater* **2010**, *22* (2), 190–218.

(52) Schömer, M.; Schüll, C.; Frey, H. Hyperbranched Aliphatic Polyether Polyols. *J Polym Sci Part A Polym Chem* **2013**, *51* (5), 995–1019.

(53) Srinivasan, S.; Twieg, R.; Hedrick, J. L.; Hawker, C. J. Heterocycle-Activated Aromatic Nucleophilic Substitution of AB2 Poly(Aryl Ether Phenylquinoxaline) Monomers. 3. *Macromolecules* **1996**, *29* (26), 8543–8545.

(54) Jikei, M.; Nishigaya, K.; Matsumoto, K. Synthesis of Hyperbranched Poly(Ether Nitrile)s as Supporting Polymers for Palladium Nanoparticles. *Polym J* **2016**, *48* (9), 941–948.

(55) Thompson, D. S.; Markoski, L. J.; Moore, J. S. Rapid Synthesis of Hyperbranched Aromatic Polyetherimides. *Macromolecules* **1999**, *32*, 4764–4768.

(56) Kim, Y. H. Highly Branched Aromatic Polymers Prepared by Single Step Syntheses. *Macromol Symp* **1994**, *77* (1), 21–33.

(57) Miller, T. M.; Neenan, T. X.; Kwock, E. W.; Stein, S. M. Dendritic Analogs of Engineering Plastics: A General One-Step Synthesis of Dendritic Polyaryl Ethers. *J Am Chem Soc* **1993**, *115* (1), 356–357.

(58) Mueller, A.; Kowalewski, T.; Wooley, K. L. Synthesis , Characterization , and Derivatization of Hyperbranched Polyfluorinated Polymers. *Macromolecules* **1998**, *31*, 776–786.

(59) Yan, D.; Zhou, Z. Molecular Weight Distribution of Hyperbranched Polymers Generated from Polycondensation of AB2 Type Monomers in the Presence of Multifunctional Core Moieties. *Macromolecules* **1999**, *32* (3), 819–824.

(60) Behera, G. C.; Ramakrishnan, S. Controlled Variation of Spacer Segment in Hyperbranched Polymers: From Densely Branched to Lightly Branched Systems. *Macromolecules* **2004**, *37* (26), 9814–9820.

(61) Uhrich, K. E.; Hawker, C. J.; Frechet, J. M. J.; Turner, S. R. One-Pot Synthesis of Hyperbranched Polyethers. *Macromolecules* **1992**, *25* (18), 4583–4587.

(62) Percec, V.; Kawasumi, M. Synthesis and Characterization of a Thermotropic Nematic Liquid Crystalline Dendrimeric Polymer. *Macromolecules* **1992**, *25* (15), 3843–3850.

(63) Percec, V.; Chu, P.; Kawasumi, M. Toward 'Willowlike' Thermotropic Dendrimers. *Macromolecules* **1994**, *27* (16), 4441–4453.

(64) Jayakannan, M.; Ramakrishnan, S. A Novel Hyperbranched Polyether by Melt Transetherification. *Chem Commun* **2000**, No. 19, 1967–1968.

(65) Roy, R. K.; Ramakrishnan, S. Single-Step Synthesis of Internally Functionalizable Hyperbranched Polyethers. *J Polym Sci Part A Polym Chem* **2013**, *51* (19), 4125–4135.

(66) Roy, R. K.; Ramakrishnan, S. Single-Step Synthesis of Internally Functionalizable Hyperbranched Polyethers. *J Polym Sci Part* **2013**, *51*, 4125–4135.

(67) Huang, X.; Hoang, T. T. K.; Lee, H. R.; Park, H.; Cho, J. K.; Kim, Y.; Kim, I. Controlled Synthesis of Hyperbranched Polythioether Polyols and Their Use for the Fabrication of Porous Anatase Nanospheres. *J Polym Sci Part A Polym Chem* **2015**, *53* (22), 2557–2562.

(68) Rokicki, G.; Rakoczy, P.; Parzuchowski, P.; Sobiecki, M. Hyperbranched Aliphatic Polyethers Obtained from Environmentally Benign Monomer: Glycerol Carbonate. *Green Chem* **2005**, *7* (7), 529.

(69) Chang, H.; Fréchet, J. M. J. Proton-Transfer Polymerization: A New Approach to Hyperbranched Polymers. *J Am Chem Soc* **1999**, *121* (10), 2313–2314.

(70) Emrick, T.; Chang, H.-T.; Fréchet, J. M. J. An $A_2 + B_3$ Approach to Hyperbranched Aliphatic Polyethers Containing Chain End Epoxy Substituents. *Macromolecules* **1999**, *32* (19), 6380–6382.

(71) Goethals, E. J.; Trossaert, G. G.; Hartmann, P. J.; Engelen, K. Branched Polymers by Cationic Ring-opening Polymerization. *Macromol Symp* **1993**, *73* (1), 77–89.

(72) Tokar, R.; Kubisa, P.; Penczek, S.; Dworak, A. Cationic Polymerization of Glycidol: Coexistence of the Activated Monomer and Active Chain End Mechanism. *Macromolecules* **1994**, *27*, 320–322.

(73) Dworak, A.; Walach, W.; Trzebicka, B. Cationic Polymerization of Glycidol. Polymer Structure and Polymerization Mechanism. *Macromol Chem Phys* **1995**, *196*, 1963–1970.

(74) Spears, B. R.; Waksal, J.; McQuade, C.; Lanier, L.; Harth, E. Controlled Branching of Polyglycidol and Formation of Protein–glycidol Bioconjugates via a Graft-from Approach with "PEG-like" Arms. *Chem Commun* **2013**, *49* (24), 2394.

(75) Spears, B. R.; Marin, M. A.; Montenegro-Burke, J. R.; Evans, B. C.; McLean, J.; Harth, E. Aqueous Epoxide Ring-Opening Polymerization (AEROP): Green Synthesis of Polyglycidol with Ultralow Branching. *Macromolecules* **2016**, *49* (6), 2022–2027.

(76) Satoh, T.; Kinugawa, Y.; Tamaki, M.; Kitajyo, Y.; Sakai, R.; Kakuchi, T. Synthesis, Structure, and Characteristics of Hyperbranched Polyterpene Alcohols. *Macromolecules* **2008**, *41* (14), 5265–5271.

(77) Bednarek, M.; Biedron, T.; Helinski, J.; Kaluzynski, K.; Kubisa, P.; Penczek, S. Branched Polyether with Multiple Primary Hydroxyl Groups : Polymerization of 3-Ethyl-3-Hydroxymethyloxetane. *Macromol Rapid Commun* **1999**, *20*, 369–372.

(78) Bednarek, M.; Kubisa, P.; Penczek, S. Multihydroxyl Branched Polyethers . 2 . Mechanistic Aspects of Cationic Polymerization of 3-Ethyl-3- (Hydroxymethyl) Oxetane. *Macromolecules* **2001**, *34*, 5112–5119.

(79) Magnusson, H.; Malmström, E.; Hult, A. Influence of Reaction Conditions on Degree of Branching in Hyperbranched Aliphatic Polyethers from 3-Ethyl-3-(Hydroxymethyl)Oxetane. *Macromolecules* **2001**, *34* (17), 5786–5791.

(80) Mai, Y.; Zhou, Y.; Yan, D.; Lu, H. Effect of Reaction Temperature on Degree of Branching in Cationic Polymerization of 3-Ethyl-3-(Hydroxymethyl)Oxetane. *Macromolecules* **2003**, *36*, 9667–9669.

(81) Rahm, M.; Westlund, R.; Eldsäter, C.; Malmström, E. Tri-Block Copolymers of Polyethylene Glycol and Hyperbranched Poly-3-Ethyl-3-(Hydroxymethyl)Oxetane through Cationic Ring Opening Polymerization. *J Polym Sci Part A Polym Chem* **2009**, *47* (22), 6191–6200.

(82) Zhu, Q.; Wu, J.; Tu, C.; Shi, Y.; He, L.; Wang, R.; Zhu, X.; Yan, D. Role of Branching Architecture on the Glass Transition of Hyperbranched Polyethers. *J Phys Chem B* **2009**, *113* (17), 5777–5780.

(83) Yan, D.; Hou, J.; Zhu, X.; Kosman, J. J.; Wu, H. S. A New Approach to Control Crystallinity of Resulting Polymers: Self-Condensing Ring Opening Polymerization. *Macromol Rapid Commun* **2000**, *21* (9), 557–561.

(84) Lin, Y.; Zeng-Guo, F.; Yu-Mei, Z.; Feng, W.; Shi, C.; Guo-Qing, W. Synthesis and Application as Polymer Electrolyte of Hyperbranched Polyether Made by Cationic Ring-Opening Polymerization of 3-{2-[2-(2-Hydroxyethoxy)Ethoxy]Ethoxymethyl}-3′-Methyl-Oxetane. *J Polym Sci Part A Polym Chem* **2006**, *44* (11), 3650–3665.

(85) Chen, Y.; Bednarek, M.; Kubisa, P.; Penczek, S. Synthesis of Multihydroxyl Branched Polyethers by Cationic Copolymerization of 3,3-Bis(Hydroxymethyl)Oxetane and 3-Ethyl-3-(Hydroxymethyl)Oxetane. *J Polym Sci Part A Polym Chem* **2002**, *40* (12), 1991–2002.

(86) Christ, E.-M.; Hobernik, D.; Bros, M.; Wagner, M.; Frey, H. Cationic Copolymerization of 3,3-Bis(Hydroxymethyl)Oxetane and Glycidol: Biocompatible Hyperbranched Polyether Polyols with High Content of Primary Hydroxyl Groups. *Biomacromolecules* **2015**, *16* (10), 3297–3307.

(87) Lin, Y.; Peng, G.; Feng, W.; Ying, B.; Zeng-guo, F. Synthesis and Application as Polymer Electrolyte of Hyperbranched Copolyethers Derived from Cationic Ring-Opening Polymerization. **2007**, *48*, 1550–1556.

(88) Zhang, G.; Zhang, T.; Li, J.; Luo, Y. Core-Shell Type Multi-Arm Azide Polymers Based on Hyperbranched Copolyether as Potential Energetic Materials in Solid Propellants. *Polym Int* **2018**, *67* (1), 68–77.

(89) Taton, D.; Le Borgne, A.; Sepulchre, M.; Spassky, N. Synthesis of Chiral and Racemic Functional Polymers from Glycidol and Thioglycidol. *Macromol Chem Phys* **1994**, *195* (1), 139–148.

(90) Vandenberg, E. J. Polymerization of Glycidol and Its Derivatives: A New Rearrangement Polymerization. *J Polym Sci Polym Chem Ed* **1985**, *23* (4), 915–949.

(91) Sunder, A.; Hanselmann, R.; Frey, H.; Mülhaupt, R. Controlled Synthesis of Hyperbranched Polyglycerols by Ring-Opening Multibranching Polymerization. *Macromolecules* **1999**, *32* (13), 4240–4246.

(92) Gade, S. M.; Munshi, M. K.; Chherawalla, B. M.; Rane, V. H.; Kelkar, A. A. Synthesis of Glycidol from Glycerol and Dimethyl Carbonate Using Ionic Liquid as a Catalyst. *Catal Commun* **2012**, *27*, 184–188.

(93) Haynes, W. M. *CRC Handbook of Chemistry and Physics: A Ready-Reference Book of Chemical and Physical Data*, 84th ed.; CRC Press LLC, 2004.

(94) Research, T. M. Glycidol Market - Global Industry Analysis, Size, Share, Growth, Trends, and Forecast 2017 - 2025 https://www.transparencymarketresearch.com/glycidol-market.html.

(95) Wróblewska, A.; Milchert, E. Technological Parameters of the Epoxidation of Allyl Alcohol with Hydrogen Peroxide over TS-1 and TS-2 Catalysts. *Chem Pap* **2002**, *56* (3), 150–157.

(96) Wróblewska, A.; Fajdek, A. Epoxidation of Allyl Alcohol to Glycidol over the Microporous TS-1 Catalyst. *J Hazard Mater* **2010**, *179* (1–3), 258–265.

(97) Hutchings, G. J.; Lee, D. F.; Minihan, A. R. Epoxidation of Allyl Alcohol to Glycidol Using Titanium Silicalite TS-1: Effect of the Reaction Conditions and Catalyst Acidity. *Catal Letters* **1996**, *39* (1–2), 83–90.

(98) Taramasso, M.; Perego, G.; Notari, B. Preparation of Porous Crystalline Synthetic Material Comprised of Silicon and Titanium Oxides. U.S. 4410501, 1983.

(99) Bruson, H. A.; Riener, T. W.; River, R. Method of Preparing Glycidol. U.S. 2636040A, 1953.

(100) Malkemus, J. D.; Currier, V. A.; Bell, J. B. Method for Preparing Glycidol. U.S. 2856413A, 1958.

(101) Yoo, J.-W.; Mouloungui, Z.; Gaset, A. Method for Producing an Epoxide, in Particular of Glycidol, and Installation for Implementation. U.S. 6316641, 2001.

(102) Doyle, A. Green glycidol pilot plant in the UK https://www.thechemicalengineer.com.

(103) Kainthan, R. K.; Gnanamani, M.; Ganguli, M.; Ghosh, T.; Brooks, D. E.; Maiti, S.; Kizhakkedathu, J. N. Blood Compatibility of Novel Water Soluble Hyperbranched Polyglycerol-Based Multivalent Cationic Polymers and Their Interaction with DNA. *Biomaterials* **2006**, *27* (31), 5377–5390.

(104) Sunder, A.; Mülhaupt, R.; Frey, H. Hyperbranched Polyether-Polyols Based on Polyglycerol: Polarity Design by Block Copolymerization with Propylene Oxide. *Macromolecules* **2000**, *33* (2), 309–314.

(105) Kurniasih, I. N.; Liang, H.; Kumar, S.; Mohr, A.; Sharma, S. K.; Rabe, J. P.; Haag, R. A Bifunctional Nanocarrier Based on Amphiphilic Hyperbranched Polyglycerol Derivatives. *J Mater Chem B* **2013**, *1* (29), 3569.

(106) Kainthan, R. K.; Mugabe, C.; Burt, H. M.; Brooks, D. E. Unimolecular Micelles Based On Hydrophobically Derivatized Hyperbranched Polyglycerols: Ligand Binding Properties. *Biomacromolecules* **2008**, *9* (3), 886–895.

(107) Paulus, F.; Weiss, M. E. R.; Steinhilber, D.; Nikitin, A. N.; Schütte, C.; Haag, R. Anionic Ring-Opening Polymerization Simulations for Hyperbranched Polyglycerols with Defined Molecular Weights. *Macromolecules* **2013**, *46* (21), 8458–8466.

(108) Wilms, D.; Wurm, F.; Nieberle, J.; Böhm, P.; Kemmer-Jonas, U.; Frey, H. Hyperbranched Polyglycerols with Elevated Molecular Weights: A Facile Two-Step Synthesis Protocol Based on Polyglycerol Macroinitiators. *Macromolecules* **2009**, *42* (9), 3230–3236.

(109) Paulus, F.; Weiss, M. E. R.; Steinhilber, D.; Nikitin, A. N.; Schütte, C.; Haag, R. Anionic Ring-Opening Polymerization Simulations for Hyperbranched Polyglycerols with Defined Molecular Weights. *Macromolecules* **2013**, *46* (21), 8458–8466.

(110) Wilms, D.; Klos, J.; Frey, H. Microstructured Reactors for Polymer Synthesis: A Renaissance of Continuous Flow Processes for Tailor-Made Macromolecules? *Macromol Chem Phys* **2008**, *209* (4), 343–356.

(111) Wilms, D.; Nieberle, J.; Klos, J.; Löwe, H.; Frey, H. Synthesis of Hyperbranched Polyglycerol in a Continuous Flow Microreactor. *Chem Eng Technol* **2007**, *30* (11), 1519–1524.

(112) Kautz, H.; Sunder, A.; Frey, H. Control of the Molecular Weight of Hyperbranched Polyglycerols. *Macromol Symp* **2001**, *163* (1), 67–74.

(113) Kainthan, R. K.; Muliawan, E. B.; Hatzikiriakos, S. G.; Brooks, D. E. Synthesis, Characterization, and Viscoelastic Properties of High Molecular Weight Hyperbranched Polyglycerols. *Macromolecules* **2006**, *39* (22), 7708–7717.

(114) Imran ul-haq, M.; Shenoi, R. A.; Brooks, D. E.; Kizhakkedathu, J. N. Solvent-Assisted Anionic Ring Opening Polymerization of Glycidol: Toward Medium and High Molecular Weight Hyperbranched Polyglycerols. *J Polym Sci Part A Polym Chem* **2013**, *51* (12), 2614–2621.

(115) Pappuru, S.; Chakraborty, D.; Ramkumar, V. Nb and Ta Benzotriazole or Benzoxazole Phenoxide Complexes as Catalysts for the Ring-Opening Polymerization of Glycidol to Synthesize Hyperbranched Polyglycerols. *Dalt Trans* **2017**, *46* (47), 16640–16654.

(116) Perumal, G.; Pappuru, S.; Chakraborty, D.; Nandkumar, A. M.; Kumar, D.; Doble, M. Synthesis and Characterization of Curcumin Loaded PLA — Hyperbranched Polyglycerol Electrospun Blend for Wound Dressing Applications. *Mater Sci Eng C* **2017**, *76*, 1196–1204.

(117) Clowes, L.; Redshaw, C.; Hughes, D. L. Vanadium-Based Pro-Catalysts Bearing Depleted 1 ,3-Calix[4] Arenes for Ethylene or ε-Caprolactone Polymerization. *Inorg Chem* **2011**, *50*, 7838–7845.

(118) Pappuru, S.; Chokkapu, E. R.; Chakraborty, D.; Ramkumar, V. Group (IV) Complexes Containing the Benzotriazole Phenoxide Lignad as Catalysts for the Ring-Opening Polymerization of Lactides, Epoxides and as Precatalysts for the Polymerization of Ethylene. *Dalt Trans* **2013**, *42* (46), 16412–16427.

(119) Soeda, Y.; Toshima, K.; Matsumura, S. Novel Enzyme-Catalyzed Ring-Opening Polymerization of Glycidol. *Chem Lett* **2001**, No. 1, 76–77.

(120) Soeda, Y.; Okamoto, T.; Toshima, K.; Matsumura, S. Enzymatic Ring-Opening Polymerization of Oxiranes and Dicarboxylic Anhydrides. *Macromol Biosci* **2002**, *2* (9), 429–436.

(121) Schubert, C.; Osterwinter, C.; Tonhauser, C.; Schömer, M.; Wilms, D.; Frey, H.; Friedrich, C. Can Hyperbranched Polymers Entangle? Effect of Hydrogen Bonding on Entanglement Transition and Thermorheological Properties of Hyperbranched Polyglycerol Melts. *Macromolecules* **2016**, *49* (22), 8722–8737.

(122) Imran ul-haq, M.; Lai, B. F. L.; Chapanian, R.; Kizhakkedathu, J. N. Influence of Architecture of High Molecular Weight Linear and Branched Polyglycerols on Their Biocompatibility and Biodistribution. *Biomaterials* **2012**, *33* (35), 9135–9147.

(123) Tonhauser, C.; Wilms, D.; Korth, Y.; Frey, H.; Friedrich, C. Entanglement Transition in Hyperbranched Polyether-Polyols. *Macromol Rapid Commun* **2010**, *31* (24), 2127–2132.

(124) Osterwinter, C.; Schubert, C.; Tonhauser, C.; Wilms, D.; Frey, H.; Friedrich, C. Rheological Consequences of Hydrogen Bonding: Linear Viscoelastic Response of Linear Polyglycerol and Its Permethylated Analogues as a General Model for Hydroxyl-Functional Polymers. *Macromolecules* **2015**, *48* (1), 119–130.

(125) Żołek-Tryznowska, Z.; Tryznowski, M.; Królikowska, J. Hyperbranched Polyglycerol as an Additive for Water-Based Printing Ink. *J Coatings Technol Res* **2015**, *12* (2), 385–392.

(126) Goodwin, A.; Baskaran, D. Inimer Mediated Synthesis of Hyperbranched Polyglycerol via Self-Condensing Ring-Opening Polymerization. *Macromolecules* **2012**, *45* (24), 9657–9665.

(127) Moore, E.; Zill, A. T.; Anderson, C. A.; Jochem, A. R.; Zimmerman, S. C.; Bonder, C. S.; Kraus, T.; Thissen, H.; Voelcker, N. H. Synthesis and Conjugation of Alkyne-Functional Hyperbranched Polyglycerols. *Macromol Chem Phys* **2016**, *217* (20), 2252–2261.

(128) Yeh, P.-Y. J.; Kainthan, R. K.; Zou, Y.; Chiao, M.; Kizhakkedathu, J. N. Self-Assembled Monothiol-Terminated Hyperbranched Polyglycerols on a Gold Surface: A Comparative Study on the Structure, Morphology, and Protein Adsorption Characteristics with Linear Poly(Ethylene Glycol)S. *Langmuir* **2008**, *24* (9), 4907–4916.

(129) Li, S.; Guo, Z.; Feng, R.; Zhang, Y.; Xue, W.; Liu, Z. Hyperbranched Polyglycerol Conjugated Fluorescent Carbon Dots with Improved in Vitro Toxicity and Red Blood Cell Compatibility for Bioimaging. *RSC Adv* **2017**, *7* (9), 4975–4982.

(130) Huang, B.; Wang, D.; Wang, G.; Zhang, F.; Zhou, L. Enhancing the Colloidal Stability and Surface Functionality of Molybdenum Disulfide (MoS 2) Nanosheets with Hyperbranched Polyglycerol for Photothermal Therapy. *J Colloid Interface Sci* **2017**, *508*, 214–221.

(131) Barriau, E.; García Marcos, A.; Kautz, H.; Frey, H. Linear-Hyperbranched Amphiphilic AB Diblock Copolymers Based on Polystyrene and Hyperbranched Polyglycerol. *Macromol Rapid Commun* **2005**, *26* (11), 862–867.

(132) Hofmann, A. M.; Wurm, F.; Huhn, E.; Nawroth, T.; Langguth, P.; Frey, H. Hyperbranched Polyglycerol-Based Lipids via Oxyanionic Polymerization: Toward Multifunctional Stealth Liposomes. *Biomacromolecules* **2010**, *11* (3), 568–574.

(133) Popeney, C. S.; Lukowiak, M. C.; Böttcher, C.; Schade, B.; Welker, P.; Mangoldt, D.; Gunkel, G.; Guan, Z.; Haag, R. Tandem Coordination, Ring-Opening, Hyperbranched Polymerization for the Synthesis of Water-Soluble Core–Shell Unimolecular Transporters. *ACS Macro Lett* **2012**, *1* (5), 564–567.

(134) Fan, Y.; Cai, Y.-Q.; Fu, X.-B.; Yao, Y.; Chen, Y. Core-Shell Type Hyperbranched Grafting Copolymers: Preparation, Characterization and Investigation on Their Intrinsic Fluorescence Properties. *Polymer (Guildf)* **2016**, *107*, 154–162.

(135) Wurm, F.; Klos, J.; Räder, H. J.; Frey, H. Synthesis and Noncovalent Protein Conjugation of Linear-Hyperbranched PEG-Poly(Glycerol) α,ω n -Telechelics. *J Am Chem Soc* **2009**, *131* (23), 7954–7955.

(136) Müller, S. S.; Fritz, T.; Gimnich, M.; Worm, M.; Helm, M.; Frey, H. Biodegradable Hyperbranched Polyether-Lipids with in-Chain PH-Sensitive Linkages. *Polym. Chem.* **2016**, *7* (40), 6257–6268.

(137) Kasza, G.; Kali, G.; Domján, A.; Petho, L.; Szarka, G.; Iván, B. Synthesis of Well-Defined Phthalimide Monofunctional Hyperbranched Polyglycerols and Its Transformation to Various Conjugation Relevant Functionalities. *Macromolecules* **2017**, *50* (8), 3078–3088.

(138) Leibig, D.; Seiwert, J.; Liermann, J. C.; Frey, H. Copolymerization Kinetics of Glycidol and Ethylene Oxide, Propylene Oxide, and 1,2-Butylene Oxide: From Hyperbranched to Multiarm Star Topology. *Macromolecules* **2016**, *49* (20), 7767–7776.

(139) Seiwert, J.; Herzberger, J.; Leibig, D.; Frey, H. Thioether-Bearing Hyperbranched Polyether Polyols with Methionine-Like Side-Chains: A Versatile Platform for Orthogonal Functionalization. *Macromol Rapid Commun* **2017**, *38*, 1600457.

(140) Schömer, M.; Seiwert, J.; Frey, H. Hyperbranched Poly(Propylene Oxide): A Multifunctional Backbone-Thermoresponsive Polyether Polyol Copolymer. *ACS Macro Lett* **2012**, *1* (7), 888–891.

(141) Yao, Y.; Suzuki, Y.; Seiwert, J.; Steinhart, M.; Frey, H.; Butt, H.-J.; Floudas, G. Capillary Imbibition, Crystallization, and Local Dynamics of Hyperbranched Poly(Ethylene Oxide) Confined to Nanoporous Alumina. *Macromolecules* **2017**, *50* (21), 8755–8764.

(142) Seiwert, J.; Leibig, D.; Kemmer-Jonas, U.; Bauer, M.; Perevyazko, I.; Preis, J.; Frey, H. Hyperbranched Polyols via Copolymerization of 1,2-Butylene Oxide and Glycidol: Comparison of Batch Synthesis and Slow Monomer Addition. *Macromolecules* **2016**, *49* (1), 38–47.

(143) Misri, R.; Wong, N. K. Y.; Shenoi, R. A.; Lum, C. M. W.; Chafeeva, I.; Toth, K.; Rustum, Y.; Kizhakkedathu, J. N.; Khan, M. K. Investigation of Hydrophobically Derivatized Hyperbranched Polyglycerol with PEGylated Shell as a Nanocarrier for Systemic Delivery of Chemotherapeutics. *Nanomedicine Nanotechnology, Biol Med* **2015**, *11* (7), 1785–1795.

(144) Schubert, C.; Schömer, M.; Steube, M.; Decker, S.; Friedrich, C.; Frey, H. Systematic Variation of the Degree of Branching (DB) of Polyglycerol via Oxyanionic Copolymerization of Glycidol with a Protected Glycidyl Ether and Its Impact on Rheological Properties. *Macromol Chem Phys* **2018**, 1700376.

(145) Song, S.; Lee, J.; Kweon, S.; Song, J.; Kim, K.; Kim, B.-S. Hyperbranched Copolymers Based on Glycidol and Amino Glycidyl Ether: Highly Biocompatible Polyamines Sheathed in Polyglycerols. *Biomacromolecules* **2016**, *17* (11), 3632–3639.

(146) Niederer, K.; Schüll, C.; Leibig, D.; Johann, T.; Frey, H. Catechol Acetonide Glycidyl Ether (CAGE): A Functional Epoxide Monomer for Linear and Hyperbranched Multi-Catechol Functional Polyether Architectures. *Macromolecules* **2016**, *49* (5), 1655–1665.

(147) Shenoi, R. A.; Lai, B. F. L.; Imran ul-haq, M.; Brooks, D. E.; Kizhakkedathu, J. N. Biodegradable Polyglycerols with Randomly Distributed Ketal Groups as Multi-Functional Drug Delivery Systems. *Biomaterials* **2013**, *34* (25), 6068–6081.

(148) Shenoi, R. A.; Narayanannair, J. K.; Hamilton, J. L.; Lai, B. F. L.; Horte, S.; Kainthan, R. K.; Varghese, J. P.; Rajeev, K. G.; Manoharan, M.; Kizhakkedathu, J. N. Branched Multifunctional Polyether Polyketals: Variation of Ketal Group Structure Enables Unprecedented Control over Polymer Degradation in Solution and within Cells. *J Am Chem Soc* **2012**, *134* (36), 14945–14957.

(149) Son, S.; Shin, E.; Kim, B. S. Redox-Degradable Biocompatible Hyperbranched Polyglycerols: Synthesis, Copolymerization Kinetics, Degradation, and Biocompatibility. *Macromolecules* **2015**, *48* (3), 600–609.

(150) Knischka, R.; Lutz, P. J.; Sunder, A.; Mülhaupt, R.; Frey, H. Functional Poly(Ethylene Oxide) Multiarm Star Polymers: Core-First Synthesis Using Hyperbranched Polyglycerol Initiators. *Macromolecules* **2000**, *33* (2), 315–320.

(151) Son, S.; Park, H.; Shin, E.; Shibasaki, Y.; Kim, B.-S. Architecture-Controlled Synthesis of Redox-Degradable Hyperbranched Polyglycerol Block Copolymers and the Structural Implications of Their Degradation. *J Polym Sci Part A Polym Chem* **2016**, *54* (12), 1752–1761.

(152) Scharfenberg, M.; Seiwert, J.; Scherger, M.; Preis, J.; Susewind, M.; Frey, H. Multiarm Polycarbonate Star Polymers with a Hyperbranched Polyether Core from CO 2 and Common Epoxides. *Macromolecules* **2017**, *50* (17), 6577–6585.

(153) Lee, K. W.; Chung, J. W.; Kwak, S. Y. Structurally Enhanced Self-Plasticization of Poly(Vinyl Chloride) via Click Grafting of Hyperbranched Polyglycerol. *Macromol Rapid Commun* **2016**, *37* (24), 2045–2051.

(154) Lee, K. W.; Chung, J. W.; Kwak, S.-Y. Synthesis and Characterization of Bio-Based Alkyl Terminal Hyperbranched Polyglycerols: A Detailed Study of Their Plasticization Effect and Migration Resistance. *Green Chem* **2016**, *18* (4), 999–1009.

(155) Mugabe, C.; Matsui, Y.; So, A. I.; Gleave, M. E.; Heller, M.; Zeisser-Labouèbe, M.; Heller, L.; Chafeeva, I.; Brooks, D. E.; Burt, H. M. In Vitro and In Vivo Evaluation of Intravesical Docetaxel Loaded Hydrophobically Derivatized Hyperbranched Polyglycerols in an Orthotopic Model of Bladder Cancer. *Biomacromolecules* **2011**, *12* (4), 949–960.

(156) Du, C.; Mendelson, A. A.; Guan, Q.; Chapanian, R.; Chafeeva, I.; da Roza, G.; Kizhakkedathu, J. N. The Size-Dependent Efficacy and Biocompatibility of Hyperbranched Polyglycerol in Peritoneal Dialysis. *Biomaterials* **2014**, *35* (5), 1378–1389.

(157) Kainthan, R. K.; Janzen, J.; Kizhakkedathu, J. N.; Devine, D. V.; Brooks, D. E. Hydrophobically Derivatized Hyperbranched Polyglycerol as a Human Serum Albumin Substitute. *Biomaterials* **2008**, *29* (11), 1693–1704.

(158) Albrecht, R.; Fehse, S.; Pant, K.; Nowag, S.; Stephan, H.; Haag, R.; Tzschucke, C. C. Polyglycerol-Based Copper Chelators for the Transport and Release of Copper Ions in Biological Environments. *Macromol Biosci* **2016**, *16* (3), 412–419.

(159) Kainthan, R. K.; Hester, S. R.; Levin, E.; Devine, D. V; Brooks, D. E. In Vitro Biological Evaluation of High Molecular Weight Hyperbranched Polyglycerols. *Biomaterials* **2007**, *28* (31), 4581–4590.

(160) Li, S.; Liu, B.; Guan, Q.; Chafeeva, I.; Brooks, D. E.; Nguan, C. Y.; Kizhakkedathu, J. N.; Du, C. Cold Preservation with Hyperbranched Polyglycerol-Based Solution Improves Kidney Functional Recovery with Less Injury at Reperfusion in Rats. *Am J Transl Res* **2017**, *9* (2), 429–

441.

(161) Chapanian, R.; Constantinescu, I.; Brooks, D. E.; Scott, M. D.; Kizhakkedathu, J. N. Invivo Circulation, Clearance, and Biodistribution of Polyglycerol Grafted Functional Red Blood Cells. *Biomaterials* **2012**, *33* (10), 3047–3057.

(162) Deng, Y.; Saucier-Sawyer, J. K.; Hoimes, C. J.; Zhang, J.; Seo, Y. E.; Andrejecsk, J. W.; Saltzman, W. M. The Effect of Hyperbranched Polyglycerol Coatings on Drug Delivery Using Degradable Polymer Nanoparticles. *Biomaterials* **2014**, *35* (24), 6595–6602.

(163) Panja, P.; Das, P.; Mandal, K.; Jana, N. R. Hyperbranched Polyglycerol Grafting on the Surface of Silica-Coated Nanoparticles for High Colloidal Stability and Low Nonspecific Interaction. *ACS Sustain Chem Eng* **2017**, *5* (6), 4879–4889.

(164) Gao, B.; Zhang, J.; Hao, Z.; Huo, L.; Zhang, R.; Shao, L. In-Situ Modification of Carbon Fibers with Hyperbranched Polyglycerol via Anionic Ring-Opening Polymerization for Use in High-Performance Composites. *Carbon N Y* **2017**, *123*, 548–557.

(165) Dong, C.; Liu, Z.; Liu, J.; Wu, C.; Neumann, F.; Wang, H.; Schäfer-Korting, M.; Kleuser, B.; Chang, J.; Li, W.; et al. A Highly Photostable Hyperbranched Polyglycerol-Based NIR Fluorescence Nanoplatform for Mitochondria-Specific Cell Imaging. *Adv Healthc Mater* **2016**, *5* (17), 2214–2226.

(166) Kasza, G.; Stumphauser, T.; Nádor, A.; Osváth, Z.; Szarka, G.; Domján, A.; Mosnáček, J.; Iván, B. Hyperbranched Polyglycerol Nanoparticles Based Multifunctional, Nonmigrating Hindered Phenolic Macromolecular Antioxidants: Synthesis, Characterization and Its Stabilization Effect on Poly(Vinyl Chloride). *Polymer (Guildf)* **2017**, *124*, 210–218.

(167) Karger-Kocsis, J.; Fröhlich, J.; Gryshchuk, O.; Kautz, H.; Frey, H.; Mülhaupt, R. Synthesis of Reactive Hyperbranched and Star-like Polyethers and Their Use for Toughening of Vinylester-Urethane Hybrid Resins. *Polymer (Guildf)* **2004**, *45* (4), 1185–1195.

(168) Fröhlich, J.; Kautz, H.; Thomann, R.; Frey, H.; Mülhaupt, R. Reactive Core/Shell Type Hyperbranched Blockcopolyethers as New Liquid Rubbers for Epoxy Toughening. *Polymer (Guildf)* **2004**, *45* (7), 2155–2164.

(169) Scharfenberg, M.; Hofmann, S.; Preis, J.; Hilf, J.; Frey, H. Rigid Hyperbranched Polycarbonate Polyols from CO2 and Cyclohexene-Based Epoxides. *Macromolecules* **2017**, *50* (16), 6088–6097.

(170) Pedron, S.; Pritchard, A. M.; Vincil, G. A.; Andrade, B.; Zimmerman, S. C.; Harley, B. A. C. Patterning Three-Dimensional Hydrogel Microenvironments Using Hyperbranched Polyglycerols for Independent Control of Mesh Size and Stiffness. *Biomacromolecules* **2017**, *18* (4), 1393–1400.

(171) Gosecki, M.; Zgardzinska, B.; Gosecka, M. Temperature-Induced Changes in the Nanostructure of Hydrogels Based on Reversibly Cross-Linked Hyperbranched Polyglycidol with B(OH)4-Ions. *J Phys Chem C* **2016**, *120* (32), 18323–18332.

(172) Gosecki, M.; Kazmierski, S.; Gosecka, M. Diffusion-Controllable Biomineralization Conducted in Situ in Hydrogels Based on Reversibly Cross-Linked Hyperbranched Polyglycidol. *Biomacromolecules* **2017**, *18* (10), 3418–3431.

(173) Testud, B.; Pintori, D.; Grau, E.; Taton, D.; Cramail, H. Hyperbranched Polyesters by Polycondensation of Fatty Acid-Based ABn-Type Monomers. *Green Chem* **2017**, *19*, 259–269.

CHAPTER II

From 10,11-epoxyundecanol to vegetable oil-based hyperbranched polyethers

Keywords : Ring-opening multibranching polymerization, hyperbranched, polyethers, 10,11-epoxyundecanol, bio-based monomer, copolymerization.

TABLE OF CONTENTS

1. INTRODUCTION 93

2. SYNTHESIS OF 10,11-EPOXYUNDECANOL 96

3. RING-OPENING MULTIBRANCHING POLYMERIZATION OF 10,11-EPOXYUNDECANOL 98

3.1. Methodology 98

3.2. Characterization of *hb*PEUnd by NMR spectroscopy 102

3.3. Polymerization conditions 111

3.4. Properties 125

4. RING-OPENING COPOLYMERIZATION OF 10,11-EPOXYUNDECANOL AND GLYCIDOL 127

4.1. Random copolymerization of 10,11-epoxyundecanol and glycidol 127

4.2. Sequential polymerization of 10,11-epoyxundecanol and glycidol 134

5. CONCLUSIONS 144

6. REFERENCES 146

7. EXPERIMENTAL AND SUPPORTING INFORMATION 150

7.1. Chemicals 150

7.2. Protocols 150

7.3. NMR 156

1. Introduction

This chapter deals with the synthesis of a new bio-based α-epoxy-ω-alcohol, namely, 10,11-epoxyundecanol (EUnd) stemming from castor oil and its subsequent ring-opening multibranching polymerization (ROMPB), forming unprecedented hyperbranched polyethers. These will be denoted as *hb*PEUnd (**Figure II-1**) later in this chapter. As it contains both an epoxy and a primary hydroxyl group, EUnd can indeed be regarded as a latent AB_2–*type* monomer. We here describe the best suited conditions to achieve *hb*PEUnd by ROMBP (**Figure II-1**), as well as the ring-opening multibranching copolymerization (ROMBcP) of EUnd with another AB_2–*type* monomer called glycidol, forming functionalized branched copolyethers.

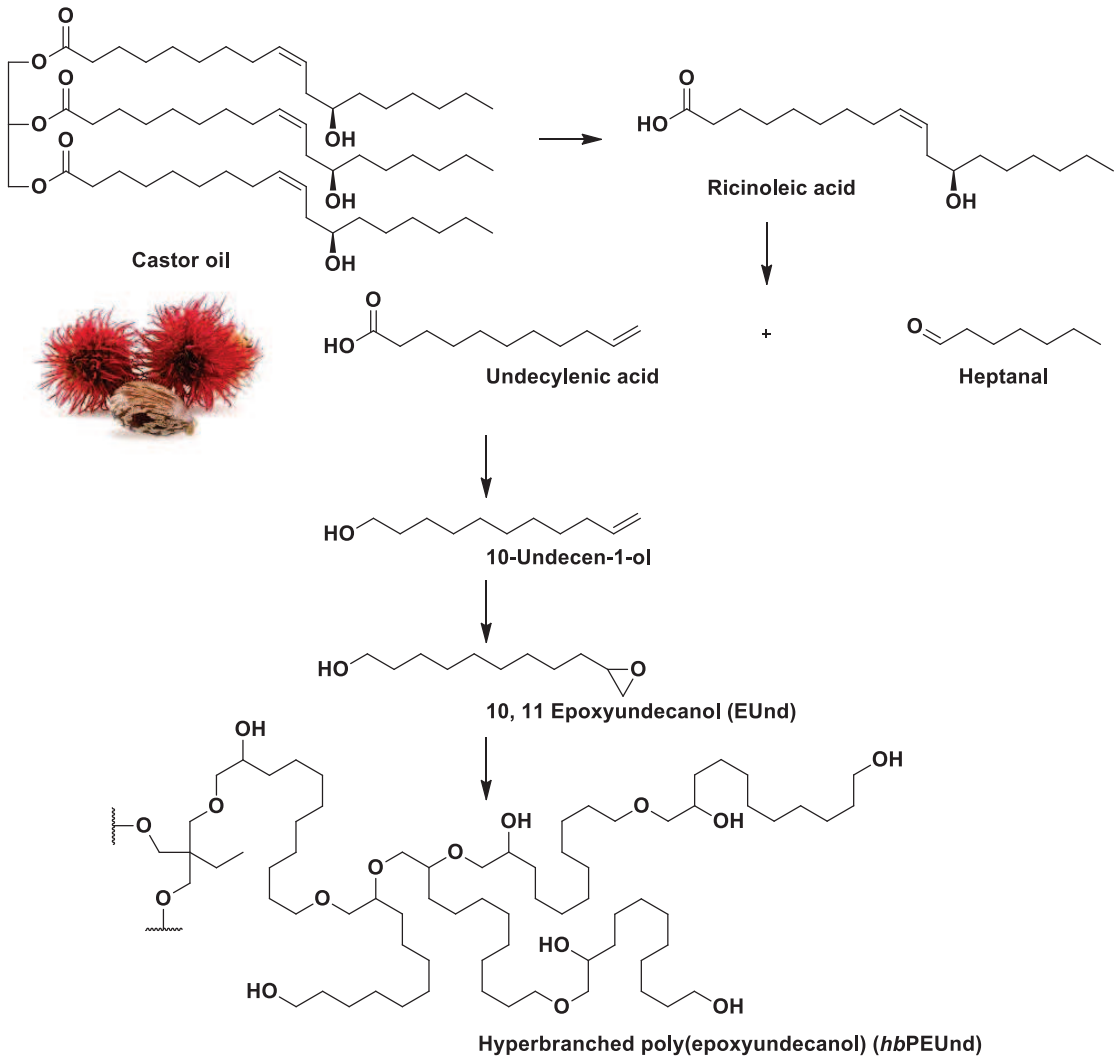

Figure II-1. From castor oil to bio-based *hb*PEthers derived from EUnd.

As emphasized in the bibliographic chapter of this manuscript, the polymerization of glycidol into hyperbranched polyethers has been extensively described in the literature, since the pioneer

works by Vandeberg.[1] In particular, Mülhaupt and coworkers have reconsidered this synthetic approach as an efficient means to achieve highly branched functionalized polyether polyols, referred to as hyperbranched polyglycidols.[2–4] With the exception of glycidol, the ROMBP of which has been intensively investigated by the groups of Frey,[2,5] Haag[6,7] and Dworak[8–10], the synthesis of hyperbranched polyethers from AB_n-*latent* type monomers ($n \geq 2$), featuring both a hydroxyl-function and an epoxide, is not so covered.[11,12] Kizhakkedathu and coworkers have resorted to cleavable ketal-containing monomers for this purpose.[13,14] Therefore, synthesis of α-epoxy-ω-hydroxyl monomers arising from a bio-resource appears highly desirable.[15,16]

In a general context of uncertain supply of petroleum resources, combined with environmental concerns, several attempts have been made to valorise biomass as a sustainable source of carbon.[17–22] Among available renewable resources, vegetable oils and their derivatives, *i.e.* fatty acid methyl esters (FAMEs), represent a promising feedstock for the polymer industry owing to their abundant availability, relatively low cost and inherent degradability.[23–25] However, only a few research groups have focused on the synthesis of vegetable oil-based aliphatic polyethers, including compounds exhibiting a linear architecture. Related works have mainly concerned the acid- or metal-catalyzed ring-opening polymerization of epoxidized FAMEs and derivatives of AB-type.[26–29] To the best of our knowledge, however, no studies have been dedicated to the design of hyperbranched polyethers derived from plant oils. In addition, synthesis and polymerization of new bio-based epoxy functional monomers may broaden the scope of polyether synthesis by imparting innovative properties.[15]

In this chapter, we report the synthesis of hyperbranched polyethers by ROMBP of latent AB_2-*type* α-epoxy-ω-hydroxyl monomers derived from vegetable oils. A versatile platform of epoxidized fatty acids has been developed in the frame of the "HyperBioPol project".[30,31] Various unsaturated fatty acids can be obtained by saponification of triglycerides arising from vegetable oils, as illustrated in **Figure II-2**. Unsaturated double bonds carried by fatty acids are generally internal (**Figure II-2**, entries 1-6), hence corresponding epoxides are characterized by a 1,2 substitution pattern showing a poor reactivity in polymerization reactions. In contrast, both 9-decenoic acid and 10-undecenoic acid, which can be obtained by cross-metathesis with ethylene – *via* a so-called ethenolysis reaction – and by cracking of ricinoleic acid, respectively, are naturally occurring monocarboxylic acids featuring an unsaturation in terminal position, as

shown in **Figure II-2**. The latter precursor can be readily transformed to achieve new AB_2-*latent* type monomers.

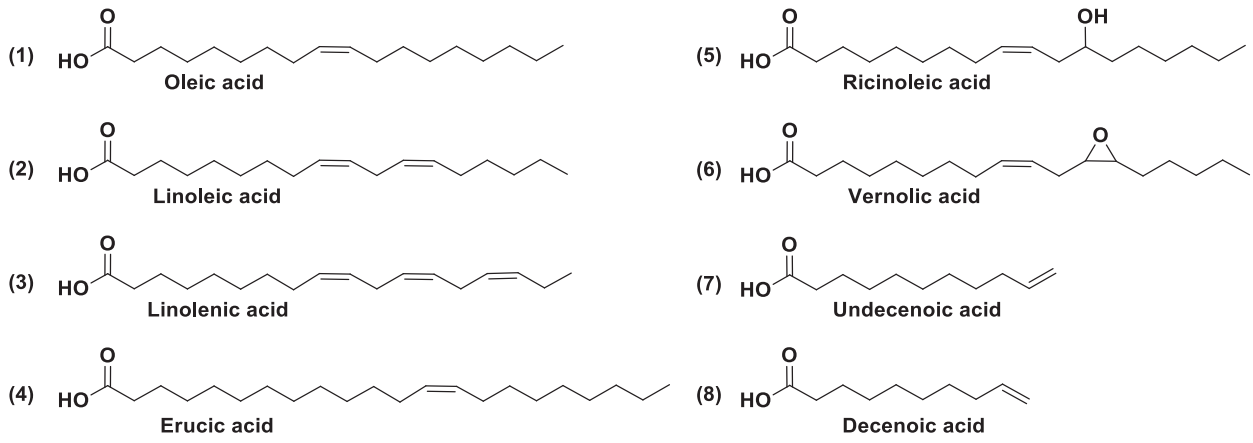

Figure II-2. Common unsaturated fatty acids obtained by saponification of triglycerides.

In the present study, a novel bio-based α-epoxy-ω-hydroxyl AB_2–*type* monomer was thus designed by a two-step synthetic procedure, involving the reduction of undecenoïc acid, followed by the epoxidation of the 10-undencen-1-ol α-alkene-ω-hydroxyl intermediate. The latter step was carried out in presence of *m*-chloroperbenzoic acid (mCPBA), leading to the targeted EUnd. Different polymerization conditions were then implemented, inspired by typical procedures developed for the ROMBP of glycidol.[2,5,32,33] In particular, trimethylolpropane (TMP) was used as a trifunctional initiating core molecule.

Due to its long aliphatic chain between the epoxide and the hydroxyl moieties, we anticipated that EUnd would exhibit a lower reactivity, compared to glycidol, and expectedly polymerize into a hydrophobic polyEUnd, while polyglycidol is highly hydrophilic. Thus, various experimental parameters were examined, including the initial monomer/TMP ratio (M/TMP), the extent of deprotonation of TMP, the nature of the solvent, and the way the monomer was added in the reaction mixture (batch *vs.* slow monomer addition). These varying conditions allowed us to achieve novel hyperbranched polyethers of apparent molecular weights up to 11,300 g/mol, with a dispersity (*Đ*) ranging from 1.8 to 6.9. Random and sequential ring-opening multibranching copolymerization (ROMBcP) of EUnd and glycidol were also investigated. Copolymers having gradient and core-shell structures combining the properties of

both polyglycidol (hydrophilic, amorphous) and polyEUnd (hydrophobic, semi-crystalline) comonomers were generated in this way.

2. Synthesis of 10,11-epoxyundecanol

Reaction of 10-undecen-1-ol in presence of mCPBA led to full conversion of the double bond into the epoxide, after stirring overnight at room temperature (**Figure II-3**). EUnd was thus obtained as a colourless slightly viscous liquid after several washings to remove mCPBA. The chemical structure of EUnd was determined by ^{1}H and ^{13}C NMR spectroscopy (**Figure II-4** and **Figure II-5**).

After reaction, it can be seen on corresponding ^{1}H NMR spectra (**Figure II-4)** that multiplets attributed to the protons of the double bond (positions 1 and 2) shifted, from 4.98 ppm to 2.84 and 2.39 ppm, and from 5.82 ppm to 2.68 ppm, respectively, attesting to the completion of the epoxidation step. This result is congruent with those obtained by ^{13}C NMR spectroscopy (**Figure II-5**). One can indeed notice shifts of the peaks ascribed to carbon atoms in positions 1 and 2, from 114.23 to 47.10 ppm, and from 139.32 to 52.44 ppm, respectively. In addition, these NMR analyses confirm that mCPBA was totally removed from EUnd, as no peak could be detected between 7.5 and 8.5 ppm by ^{1}H NMR (**Figure II-4.b**) and between 120 and 140 ppm by ^{13}C NMR (**Figure II-5.b**).

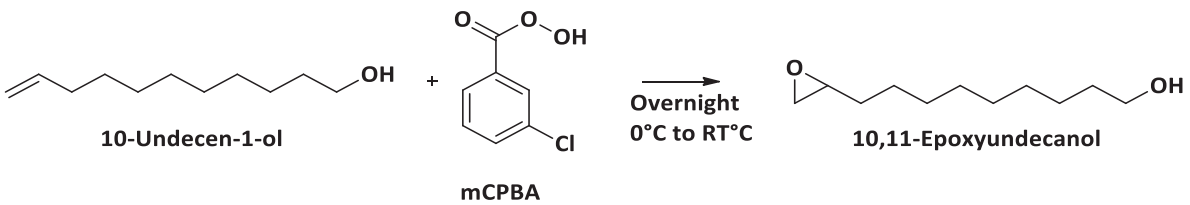

Figure II-3. Synthesis of EUnd from 10-undencenol.

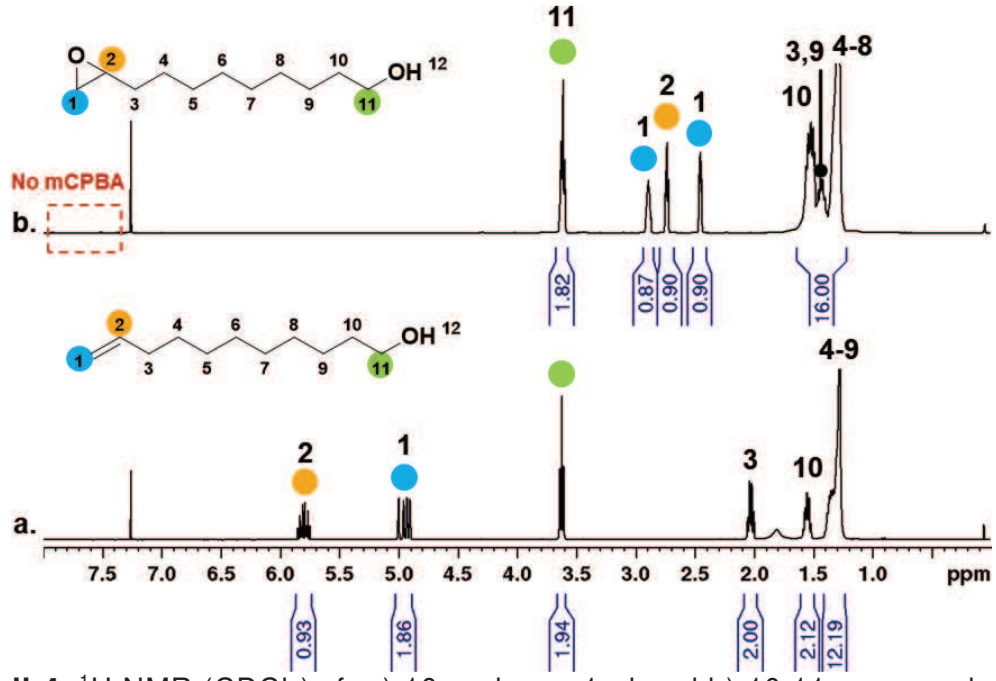

Figure II-4. ^{1}H NMR ($CDCl_3$) of: a) 10-undecen-1-ol and b) 10,11-epoxyundecanol.

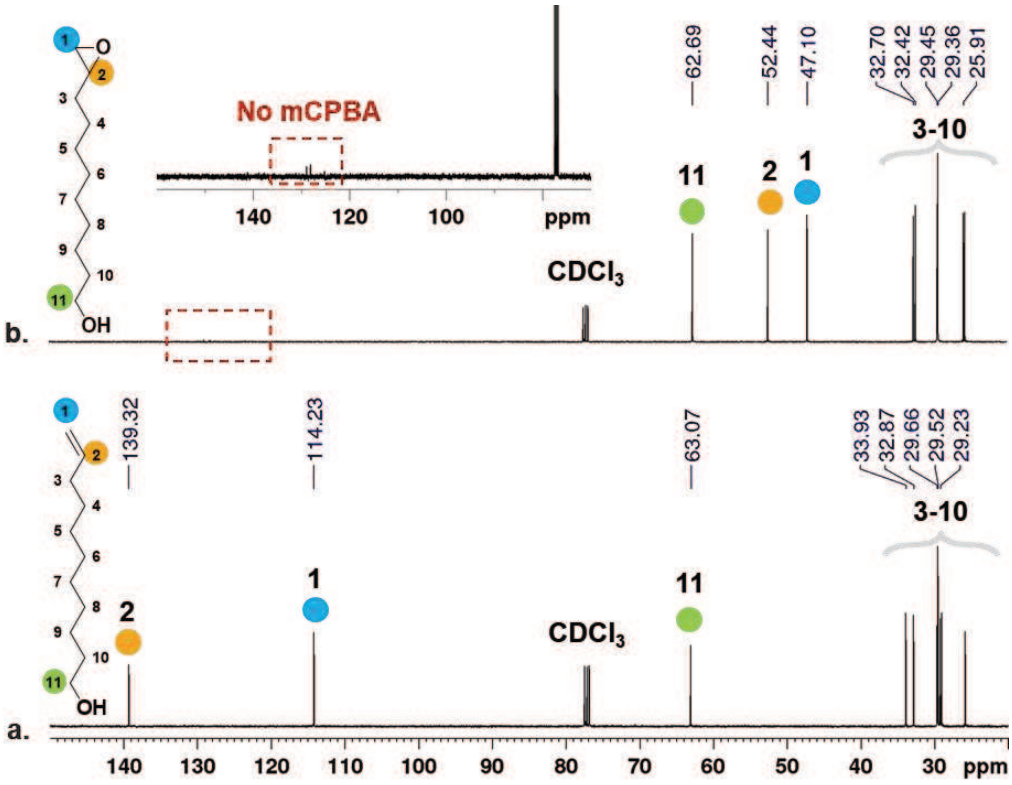

Figure II-5 . ^{13}C NMR ($CDCl_3$) of: a) 10-undecen-1-ol and b) 10,11-epoxyundecanol.

3. Ring-opening multibranching polymerization of 10,11-epoxyundecanol

3.1. Methodology

To polymerize EUnd, we drew on the conditions set up by Sunder *et al.*,[2] in the case of the ROMBP of glycidol. Therefore, not only semi-batch experiments (SBA, sequential additions of monomer aliquots), but also the so-called "slow-monomer addition" (SMA) procedure were implemented, for comparison purpose. As mentioned, trimethylolpropane (TMP) served as a trifunctional initiator core (**Figure II-6**) that was partially deprotonated using potassium methoxide (MeOK). The TMP/MeOK ratio was also varied to investigate the influence of this parameter on the molar mass of the resulting polyethers. Reactions were carried out either in bulk, or in solution in dioxane, DMSO or DMF.

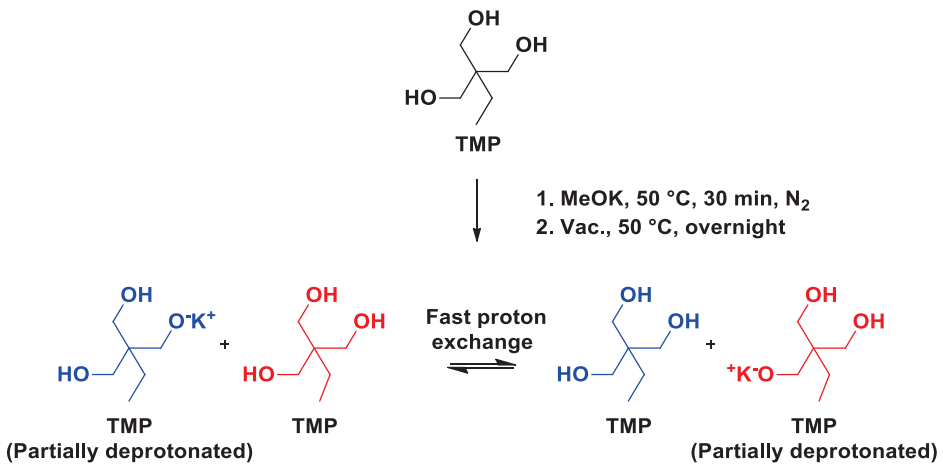

Figure II-6. Fast proton exchange between partially deprotonated TMP.

The general polymerization procedure is depicted in the supporting information. Similarly to ROMBP of glycidol, the deprotonated TMP initiates the ring-opening of EUnd by nucleophilic addition, generating a secondary alkoxide. The latter active site can either directly propagate, or be protonated owing to a fast proton exchange with a hydroxylated dormant form.[2,34] Under such conditions, active species thus often switch from secondary to primary alkoxides. Consequence of such a mechanism is the generation of two types of linear units, denoted as $L_{1,2}$ and $L_{1,11}$. The remaining OH from a linear unit can also be deprotonated and propagate to form dendritic units (**Figure II-7**).

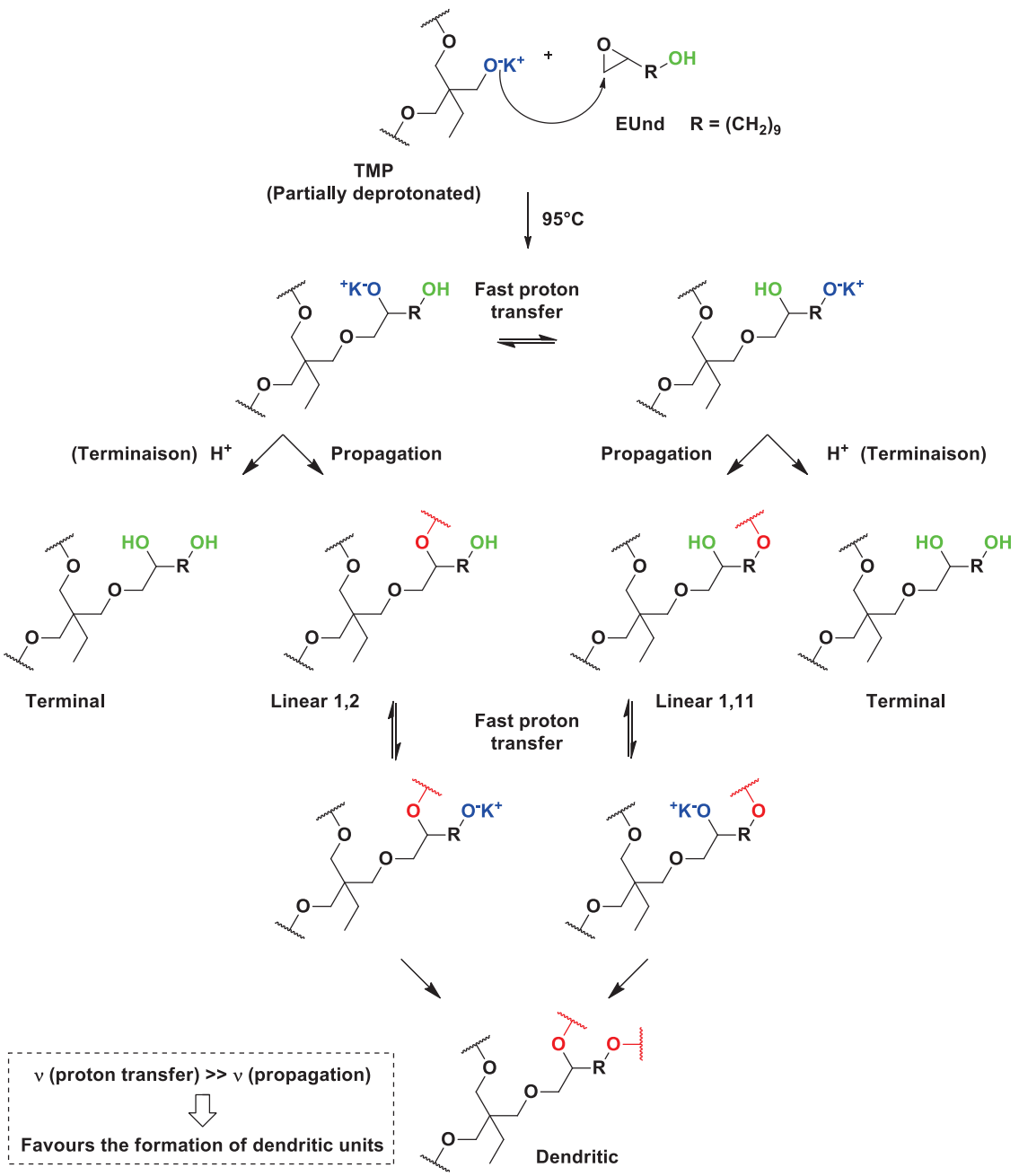

Figure II-7. Synthesis of *hb*PEUnd by reaction of EUnd with TMP as initiator.

For all experiments, the reaction mixture was stirred at 95 °C until reaching maximal conversion, *i.e.* until no evolution of the conversion of EUnd was noted, which was monitored by ^{1}H NMR (**Figure II-7**), using the following equation II-1:

$$\text{Conversion} = \frac{I_2(t_0) - I_2(t)}{I_2(t_0)} \qquad \text{(Eq. II-1)}$$

where $I_2(t_0)$ and $I_2(t)$ correspond to the integral of the peak of proton (2) at t_0 and at t (**Figure II-7**).

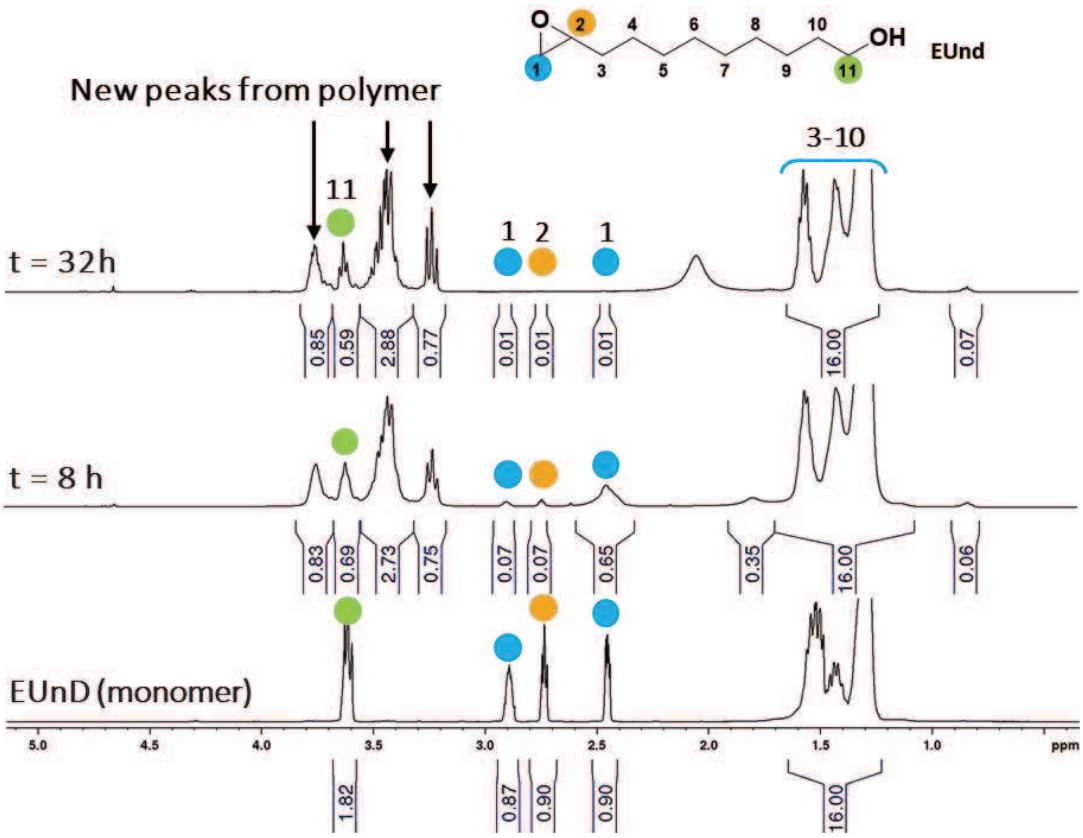

Figure II-8. Monitoring of the conversion of EUnd by ^{1}H NMR ($CDCl_3$) at M/TMP = 50 and TMP deprotonation = 10 %.

Molecular weights of the resulting polymers were determined either by SEC in chloroform, on the basis of a calibration using linear PS standards, or by SEC in DMF using a d*n*/d*c* = 0.049. Typical SEC traces obtained in chloroform for polymers synthesized by ROMBP of EUnd is illustrated in **Figure II-8**. Although ROMBP is known as a chain-growth polymerization, the chromatogram obtained at 70 % of conversion displays conventional pattern of step-growth polymerization, as a multimodal distribution is observed with discrete peaks due to the formation of different oligomers. Such a feature has been described by Weiss *et al.*[6], in the case of ROMBP of glycidol, and would be the result of a self-initiation of the polymerization by the monomer (**Figure II-10**).

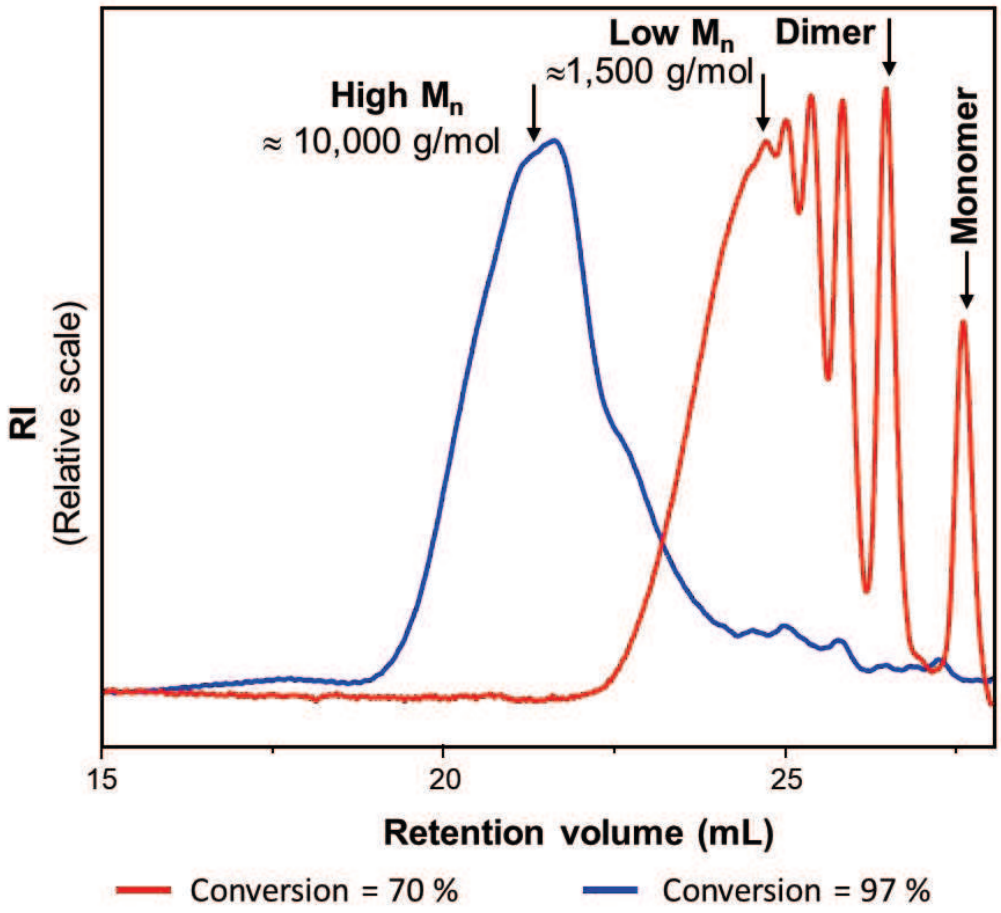

Figure II-9. SEC-RI traces ($CHCl_3$, PS standard calibration) of polymer obtained by ROMBP of EUnd.

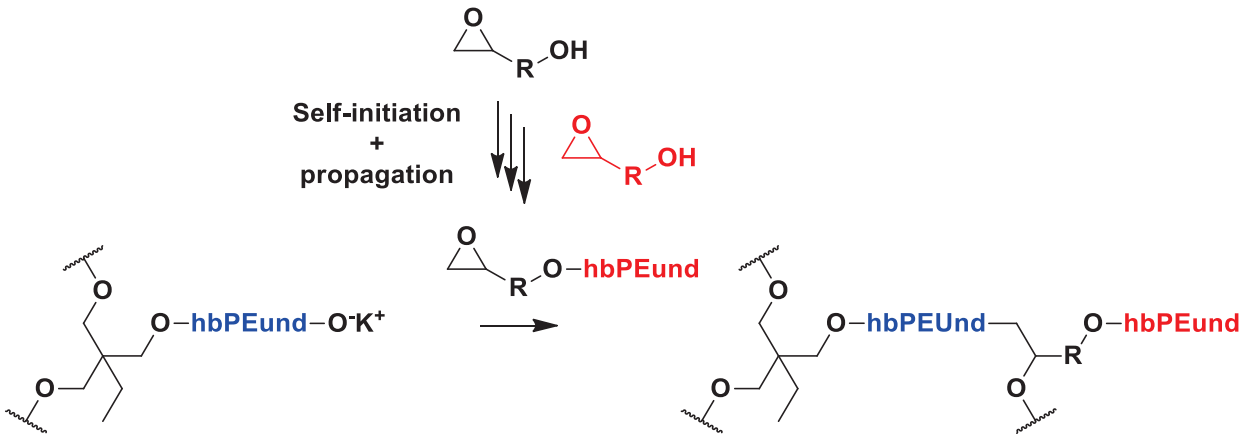

Figure II-10. Step-growth polymerization of EUnd induced by self-initiation.

3.2. Characterization of *hb*PEUnd by NMR spectroscopy

3.2.1. Units nomenclature and peaks assignment

Poly(epoxyundecanol)s (polyEUnds) synthesized under the different conditions discussed above were analysed by NMR spectroscopy, including by ^{1}H, ^{13}C, DEPT-135, HSQC and COSY. These analyses were indispensable to know the distinctive signals of the different constitutive units of the polymers resulting from the ROMBP of EUnd, namely, dendritic, linear and terminal units (**Figure II-7** and **Figure II-11**).

The ^{1}H and ^{13}C NMR spectra of a typical polymer are shown in **Figure II-11**, together with the different possible units and the corresponding assignments. These were made with the aid of HSQC, COSY and DEPT-135 analyses (see supporting information, **Figure SI.II-51** and **Figure SI.II-52**) by comparing the peaks with those of model molecules (**part 3.2.2: Figure II-14** and **Figure II-16**).

To simplify the reading, the following nomenclature was used taking the dendritic and the terminal units as references:

- For the dendritic unit (D), α, β, γ and ω positions are called d1, d2, d3 and d11.
- For the terminal unit (T), α, β, γ and ω positions are called t1, t2, t3 and t11.
- For the linear 1,11 unit (L1,11), α, β and γ are called t1, t2 and t3, as the electronic environment of protons (or carbons) in α, β and γ positions of L1,11 and T units are equivalent. The ω-position is called d11, the electronical environment of protons (or carbon) in ω-position being similar to that of protons (or carbon) in ω-position of D unit.
- For the linear 1,2 unit (L1,2), α, β, γ and ω positions are called d1, d2, d3 and t11. The same reasoning as for the (L1,11) unit applies.

Three examples of nomenclature are provided below:

A proton situated in position d3 on a dendritic unit will be written H-D-d3.

A carbon situated in position t10 of a linear 1,11 unit will be written C-L1,11-t10.

A carbon situated in position 5 of a linear 1,2 unit will be written C-L1,2-5.

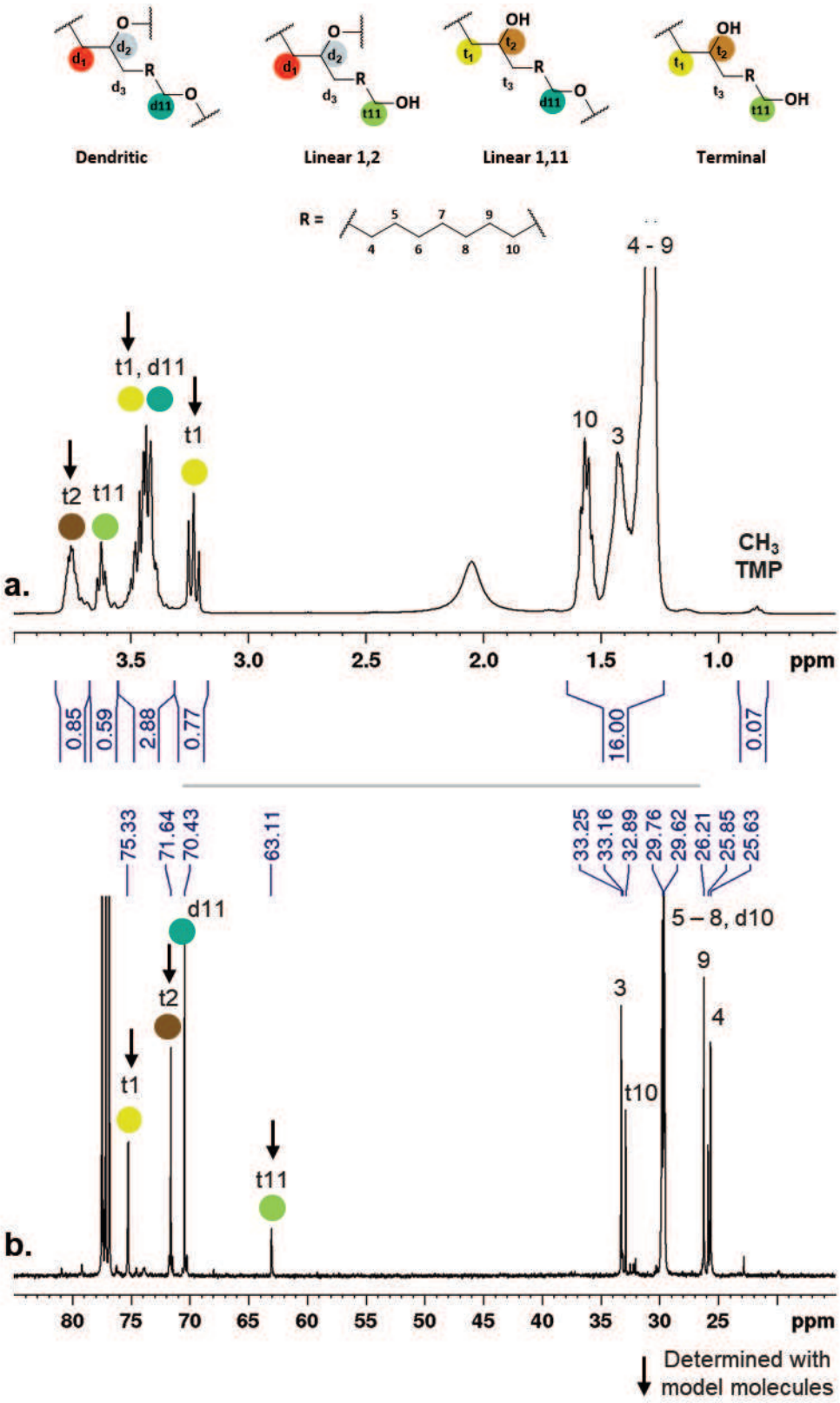

Figure II-11. **a.** ^{1}H NMR ($CDCl_3$) and **b.** ^{13}C NMR of a polymer obtained by ROMBP of EUnd at M/TMP = 50 and TMP deprotonation = 10 %.

As can be seen on the NMR spectra, all peaks of protons and carbon atoms from L1,11 and T units were successfully assigned. Unfortunately, the same was not true in the case of protons and carbon atoms in position d1, d2 and d3 of D and L1,2; these units could not be clearly identified. However, values of integrals due to protons in position t1, t2, t11 and d11 suggested that D and L1,2 (30 %) units did form (**Figure II-11.a**).

3.2.2. Attempts to determine the degree of branching

The transfer reaction, namely the proton-exchange, is the key-step for the production of dendritic structures *via* ROMBP (**Figure II-7** and **Figure II-12**). After the ring-opening of the epoxide by nucleophilic substitution of C1, a secondary alkoxide is formed on C2. T or L12 units can be produced by termination or propagation, respectively. Fast proton exchange can also lead to the formation of a primary alkoxide on C11, while T or L111 units can be produced by termination or propagation of the primary alkoxide, respectively.

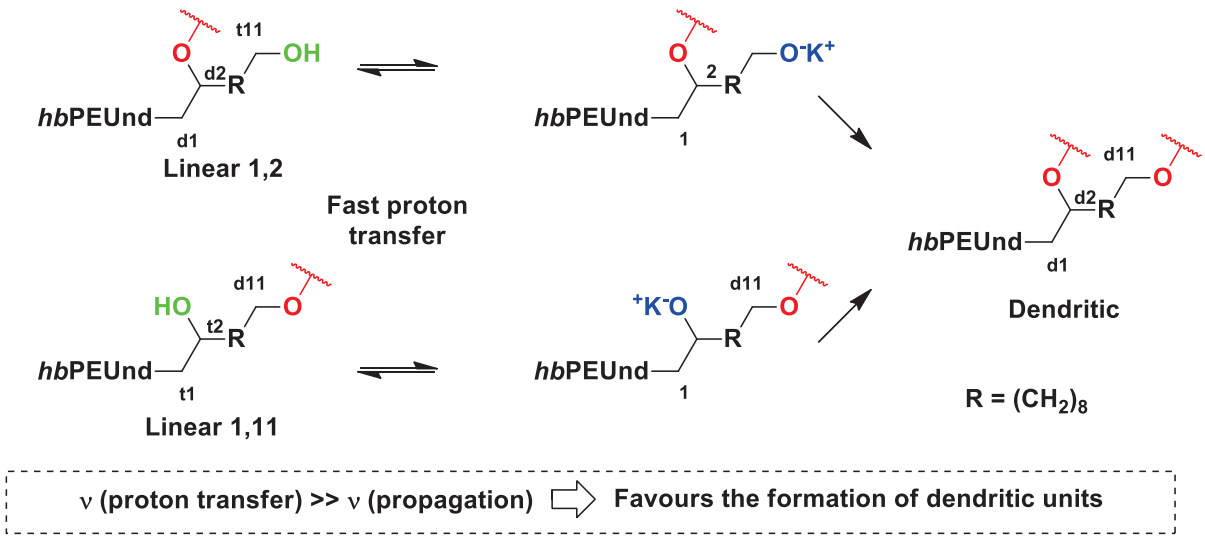

Figure II-12. Proton transfer of hydroxyl functions from linear units and propagation yielding dendritc units.

The decrease in intensity of the peak t11 (I_{t11}; Eq. II-3) together with the increase in intensity of the peak t2 (I_{t2}; Eq. II-2) is a strong indication that such a proton exchange between secondary and primary hydroxyl groups did occur (**Figure II-11** and **Figure II-12**). The following equations express the contribution of the different units in these peak integrals:

$$I_{t2} = \frac{I_{3-10}}{16} \times \left(L_{1,11} + T\right) \qquad \text{(Eq. II-2)}$$

$$I_{t11} = \frac{I_{3-10}}{16} \frac{L_{1,2} + T + x(EUnd)}{2} \qquad \text{(Eq. II-3)}$$

"x(EUnd)" corresponding to the molar ratio of the 10,11-epoxyundecanol monomer into the mixture, which is equal to 1-conversion, *i.e.* equal to 0 for 100 % of conversion.

As the contribution of the monomer should not be taken into account for conversion lower than 100 %, I'_{t11} was used (Eq. II-4) instead of I_{t11}:

$$I'_{t11} = I_{t11} - \frac{I_{3-10}}{16} \frac{EUnd}{2} = I_{t11} - \frac{I_{3-10}}{16} \frac{(1 - \text{conversion})}{2} \qquad \text{(Eq. II-4)}$$

The mean value of the I_{t2}/I'_{t11} ratio was found, whatever the experimental conditions, to be equal to 2.7±0.3, *i.e.* 73 % ± 2.1 % of the OH of the PEUnd are estimated to correspond to secondary alcohols. Given that EUnd monomer only contains primary OH, it can be assumed that transfer occurred during the reaction, and that the primary alkoxides mainly participated in the propagation step. Therefore, these calculations suggest that dendritic units can be achieved from the ROMBP of EUnd.

As emphasized in the bibliographic chapter, the degree of branching (DB) of hyperbranched polymers is an important parameter of such structures. For low molecular weight polymers, the "Frey equation (DB_{Frey})" is most often employed:

$$DB_{Frey} = \frac{2D}{2D + L} \qquad \text{(Eq. II-5)}$$

where D and L are the molar ratio of the dendritic and the linear units of the polymer, respectively. These ratios are generally determined by ^{1}H NMR or by inverted gate ^{13}C NMR spectroscopy.[2,14] Unfortunately, it was not here possible to directly determine the degree of branching of such polyethers on the basis of the different NMR analyses. This was due to the presence of long alkyl chains between the two hypothetical propagating alkoxides, namely, those directly deriving from the primary hydroxyl of EUnd (position 11), and those resulting from ring-opening reactions of the epoxy (position 2) (**Figure II-8**). Indeed, the chemical shifts of typical protons could not be distinguished from signals characterizing the different units

constituting these polyethers (**Figure II-11** and **Figure II-12**). For example, d11 protons could not be differentiated from protons attributed to the dendritic and to the linear 1,11 units. The same was true for d1, t2, t1 and t2; protons d1 and d2 could not be distinguished from those of the dendritic and the linear 1, 2 units, and the same applied for t1 and t2, relatively to the protons due to the terminal and the linear 1,11 units. As a matter of fact, and despite many efforts, the proportion of each type of units of such polyethers could not be determined.

Model molecules mimicking the different units, *i.e.* exhibiting a structural similarity with the expected constitutive units of *hb*PEUnd, were yet purposely synthesized (see ESI) and further probed by NMR spectroscopy.[35] In **Figure II-13**, D^m, $L111^m$, $L12^m$ and T^m represent the model molecules corresponding to the dendritic (D), the linear 1,11 (L111), the linear 1,2 (L12) and the terminal (T) units, respectively. The numbering and the nomenclature of the different atoms in these model molecules are analogous to that previously presented for the polyethers.

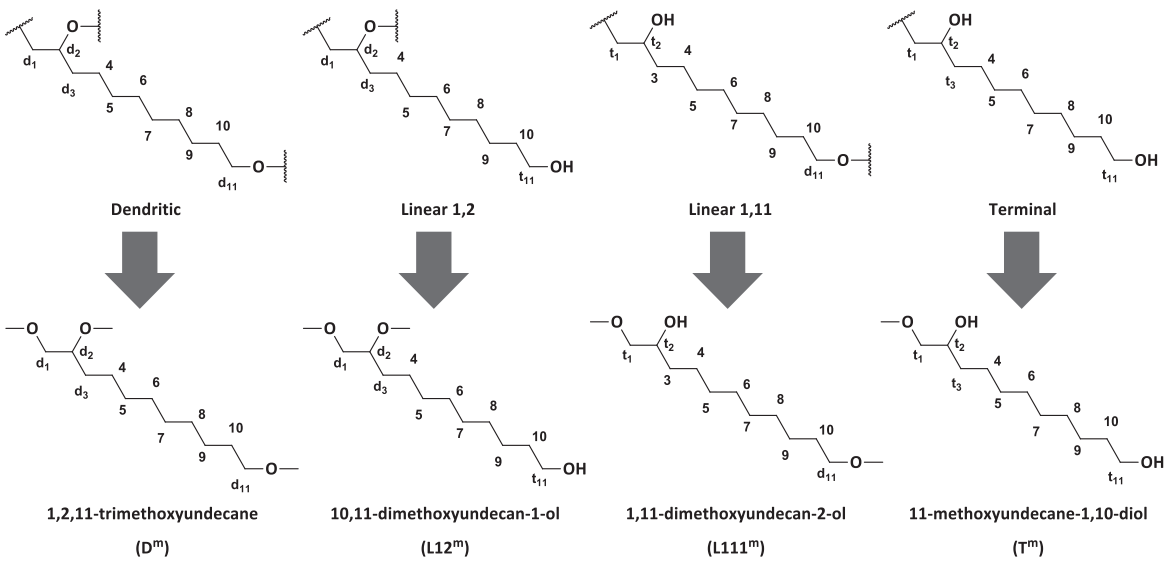

Figure II-13. Model molecules and their corresponding units of *hb*PEUnd.

The ^1H and ^{13}C NMR spectra obtained in $CDCl_3$ of these model molecules are provided in **Figure II-14** and **Figure II-16** with the corresponding assignments (see Figure II-15), based on HSQC and COSY analysis (**ESI, Figure SI.II-53** to **Figure SI.II-62**).

Figure II-14 evidences that, depending on the constitutive units, protons having a similar environment could be shifted or not. For instance, protons due to H-D^m-d1 show the same chemical shift than those of H-$L12^m$-d1. Likewise, D^m and $L12^m$ protons exhibit the same

electronic environment, namely, a methoxy group on C_β (see Figure II-15). Interestingly, the chemical shift of H-T^m-t11 (3.59 ppm) differs from that of H-L12^m-t11 (3.64 ppm). We reasoned that this chemical shift difference could be useful to differentiate the four model molecules, and consequently the four constitutive units of *hb*PEUnd. A better differentiation was nonetheless observed through analyses of the different compounds by ^{13}C NMR spectroscopy.

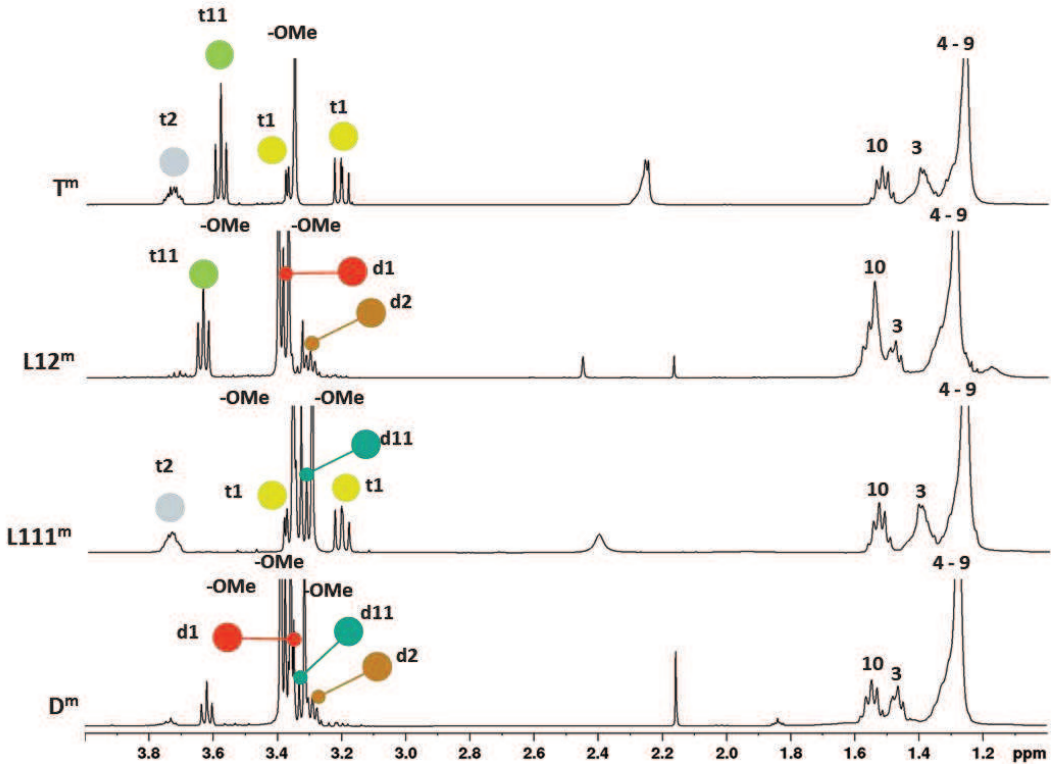

Figure II-14. ^{1}H NMR ($CDCl_3$) of the model molecules of the *hb*PEUnd units.

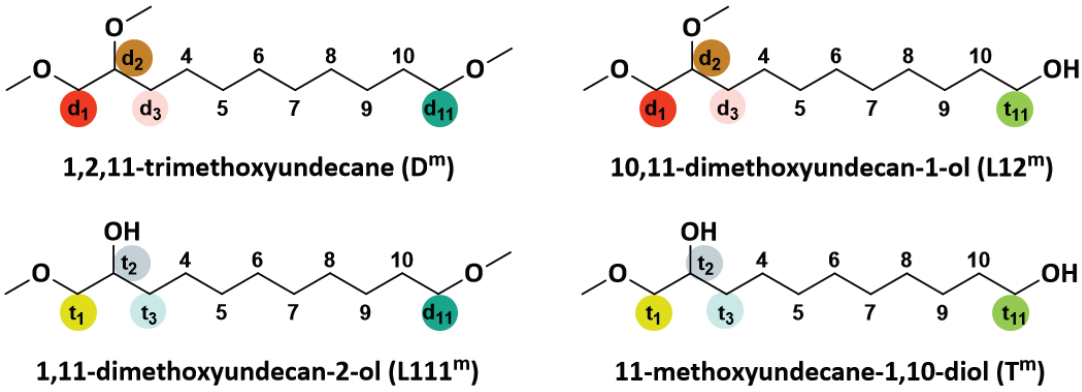

Figure II-15. Model molecules of the dendritic (D^m), the linear 1,2 (L12^m), the linear 1,11 (L111^m) and the terminal (T^m) units, with corresponding assignments.

All peaks of the different carbon atoms, *i.e.* those in α, β, γ and ω positions, were assigned on the ^{13}C NMR spectrum of each model molecule (**Figure II-16**). **Figure II-17** and **Figure II-18** are the enlarged regions of **Figure II-16**, from 61 to 82 ppm and from 25 to 34 ppm, respectively. Differences in chemical shifts are noted between the aforementioned carbon atoms of the four different model compounds, as summarized in **Table II-1**. However, C_1, C_2, C_3 and C_{11} atoms of *hb*PEUnd led to singlet peaks only, hampering a quantification of the different units by this means.

Table II-1. Model molecules of the *hb*PEUnd units and chemical shift differences from ^{13}C NMR ($CDCl_3$).

Entry	Mol. A	Mol. B	C analysed	Chemical shift Mol. A *(ppm)*	Chemical shift Mol. B *(ppm)*
1	D^m	$L12^m$	d2	80.23	80.26
2	D^m	$L111^m$	d11	73.09	73.05
3	T^m	$L111^m$	t2	70.32	70.36
4	T^m	$L12^m$	t11	62.96	63.22
5	T^m	$L111^m$	t3	33.20	33.24
6	T^m	$L12^m$	t10	32.82	32.94

A series of middle chain peaks were also observed on the ^{13}C NMR spectrum of the obtained polyethers. We hypothesized that some of these peaks, from positions 4 to 10, were eventually shifted depending on the constitutive units they originated from. Unfortunately, it was impossible to distinguish the corresponding carbon atoms from these model molecules, *i.e.* carbon atoms from positions 4 to 9, for T^m and $L12^m$, and from positions 4 to 10 for D^m and $L111^m$.

Therefore, and despite several attempts to differentiate the constitutive units of poly(EUnd), including by NMR characterizations and through the use of model compounds, it was not possible to fully establish their branched structure and calculate their degree of branching. Such concerns in the determination of DB of hyperbranched polymers have already been reported in the literature, as discussed in details in chapter I.[15,36,37] As described in the following section, it was yet possible to evaluate whether the growth of the polymer chains took place from both the secondary and the primary alkoxide groups.

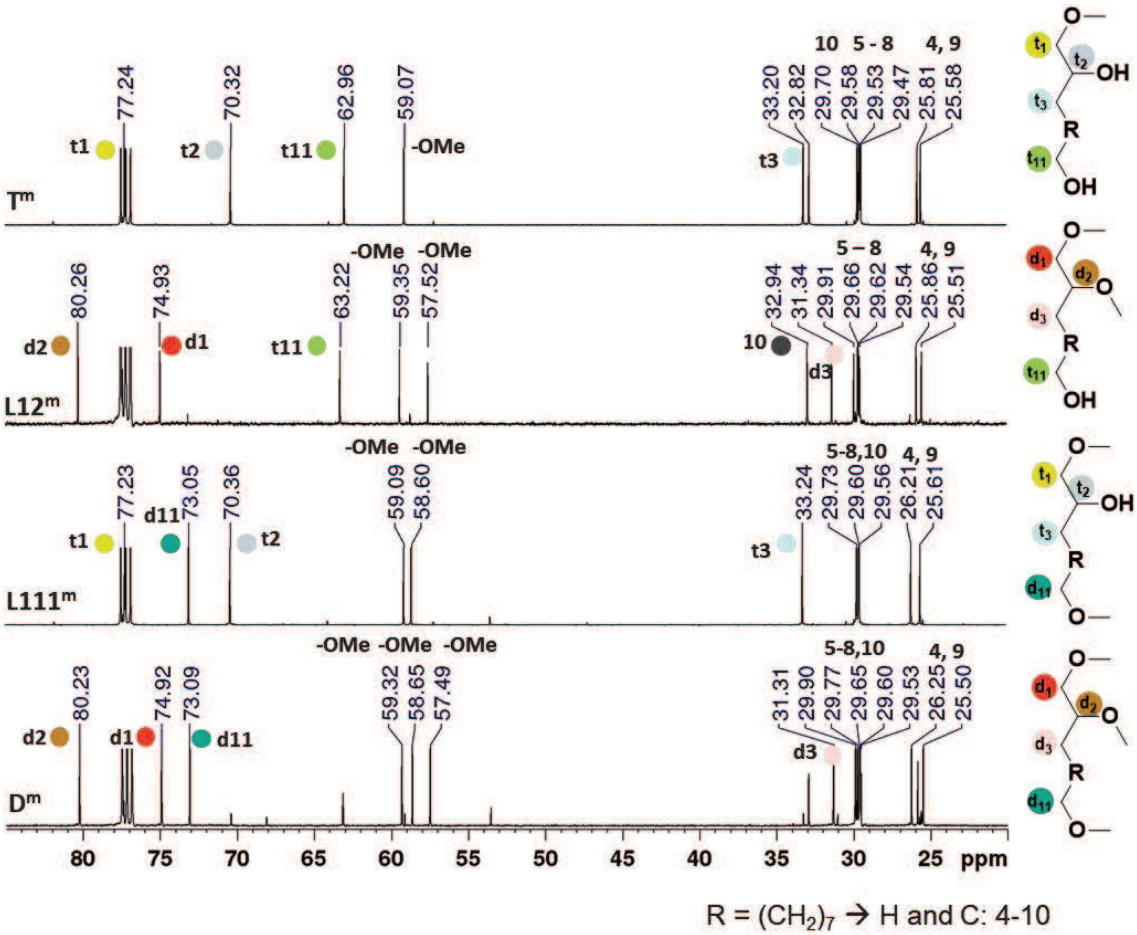

Figure II-16. ^{13}C NMR ($CDCl_3$) of the model molecules of the *hb*PEUnd units.

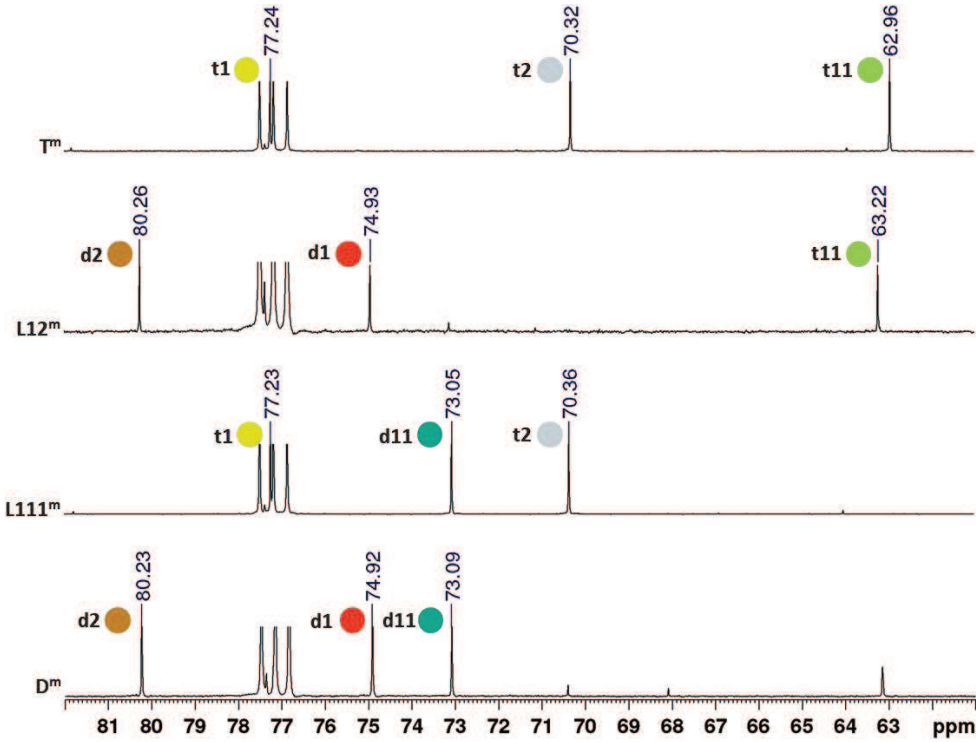

Figure II-17. ^{13}C NMR ($CDCl_3$) of the model molecules from 61 to 82 ppm.

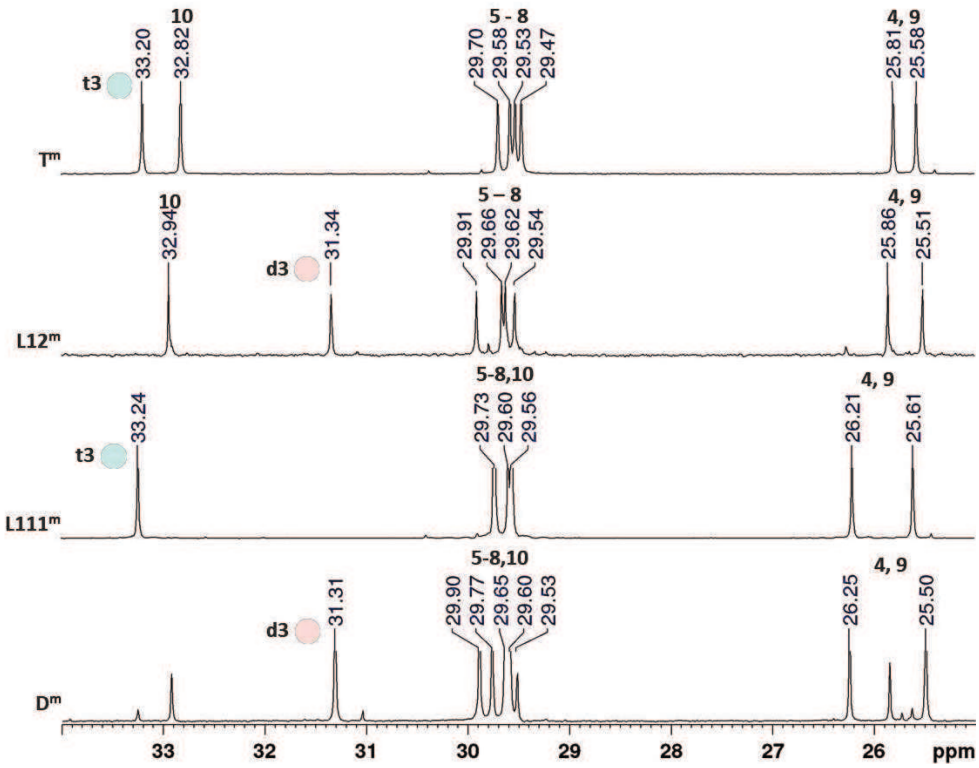

Figure II-18. ^{13}C NMR ($CDCl_3$) of the model molecules from 25 to 34 ppm.

3.3. Polymerization conditions

3.3.1. Influence of M/TMP at a TMP deprotonation of 10 %

Partial deprotonation of alkoxides, typically from 10 to 30 %, is generally sufficient to ensure the ROP of oxiranes, including functional monomers such as glycidol.[38] As already discussed, this is due to the very fast exchange of protons between active alkoxides and dormant hydroxyl groups, relatively to propagation.[5,39] Moreover, deprotonated TMP tends to aggregate for an extent of deprotonation higher than 30 %, leading to heterogeneous reaction mixtures causing a slow initiation. Low extent of deprotonation thus allows minimizing the aggregation of anionic propagating species, ensuring growth from all hydroxyl groups and favouring a better control of the degree of branching and of the dispersity of the resulting polymer.[2,5,32] Preliminary experiments were thus performed using a TMP deprotonation of 10 %, using M/TMP ratio varying from 5 to 200. These conditions enabled the formation of polyethers with molecular weights ranging from 2,200 to 11,400 g/mol and a nearly complete conversion of the EUnd monomer (**Table II-2**). As a general trend, and as expected, polymerization proved faster at lower M/TMP ratios, owing to a higher concentration in alkoxide active species.[5] For instance, the polymerization was complete after 8h of reaction using an initial M/TMP ratio equal to 5. For higher ratio, *i.e.* for M/TMP ratios of 10, 20 and 50, the polymerization went to completion at 24 h. The monomer conversion was found to slightly decrease above these ratios (**Table II-2**).

Table II-2. Results of ROMBP of EUnd at TMP deprotonation = 10 %, using different M/TMP ratios.

Entry	M/TMP	$M_{n,th.}$ [a] *(g/mol)*	$M_{n,exp}$ [b] *(g/mol)*	*Đ* [b]	Conv. (8 h)[c] *(%)*	Conv. (24 h) [c] *(%)*
1	5	900	3,100 (2,700)	6.7 (2.7)	100	-
2	10	1900	5,800 (4,200)	6.6 (12.7)	93	100
3	20	3700	6,900 (4,800)	3.9 (7.2)	83	95
4	50	9000	11,400 (8,000)	2.4 (2.7)	91	97
5	100	16,600	3,400 (2,700)	2.7 (3.1)	78	89
6	200	26,000	1,700 (1,700)	1.7 (1.5)	63	70

Polymerizations carried out in bulk at 95 °C under nitrogen with TMP deprotonated at 10 % before addition of 0.5 mL of monomer per aliquots of 100 µL every 3 min.
[a] Theoretical molecular weight calculated according to the conversion of the monomer into *hb*PEUnd $M_{n,th}$ = (M/TMP) x M(EUnd) x conversion.[b] Determined via SEC-RI in Chloroform + 1 % TEA using linear PS standard calibration (Determined via SEC-RI/Visco in Chloroform +

1 % TEA using universal calibration).[c] Calculated from ^{1}H NMR by comparison of the epoxide proton peaks of the monomer with the proton peaks of the aliphatic backbone.

The evolution profile of apparent molecular weights as a function of the M/TMP ratio is shown in **Figure II-20**. As expected, higher molecular weights were achieved as the M/TMP ratio increased. The highest apparent M_n value was found equal to 11,400 g/mol, using a M/TMP ratio of 50. M/TMP ratios higher than 50 inevitably led to lower molecular weights, as can be seen in **Figure II-20**. Formation of low molecular weight polyethers might be ascribed to the thermal self-initiation of the polymerization by the monomer itself, which might be favoured by poor concentration in active sites when increasing the M/TMP ratios (**Figure II-21**).

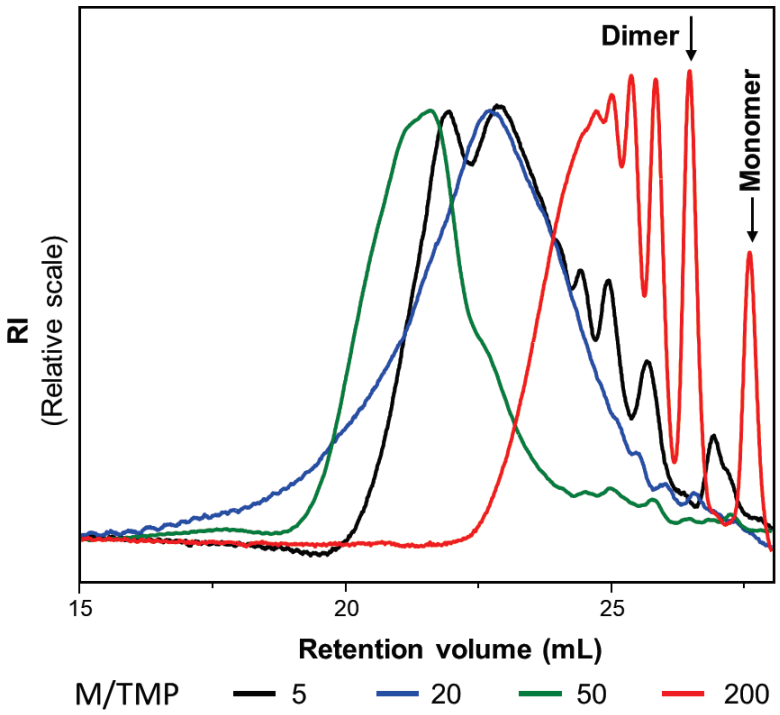

Figure II-19. SEC-RI traces ($CHCl_3$) of *hb*PEUnd obtained from polymerization conducted at TMP deprotonation = 10 %, at different M/TMP ratios.

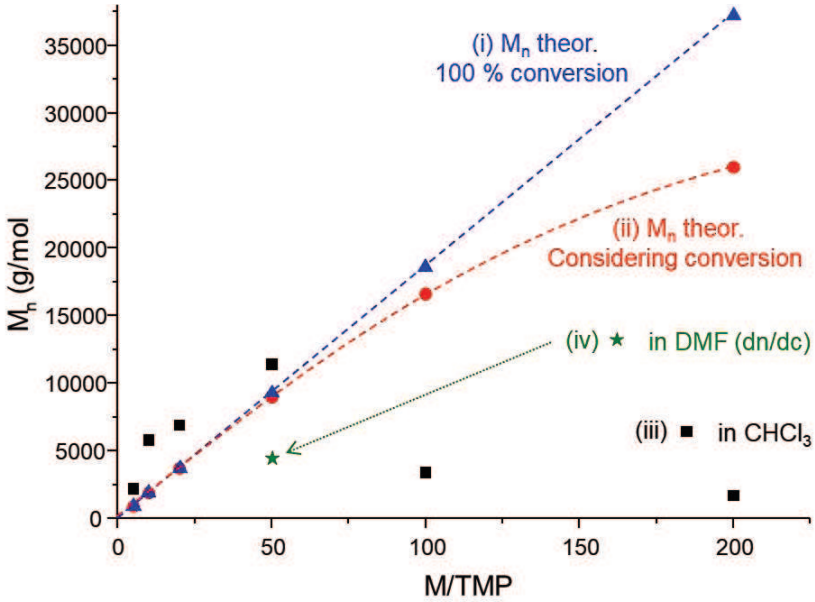

Figure II-20. M_n of *hb*PEUnd plotted versus M/TMP ratio at TMP deprotonation = 10 %, with M_n determined via **(iii)** ■ SEC-RI ($CHCl_3$, PS calibration) and **(iv)** ★ SEC-RI (DMF, using dn/dc).

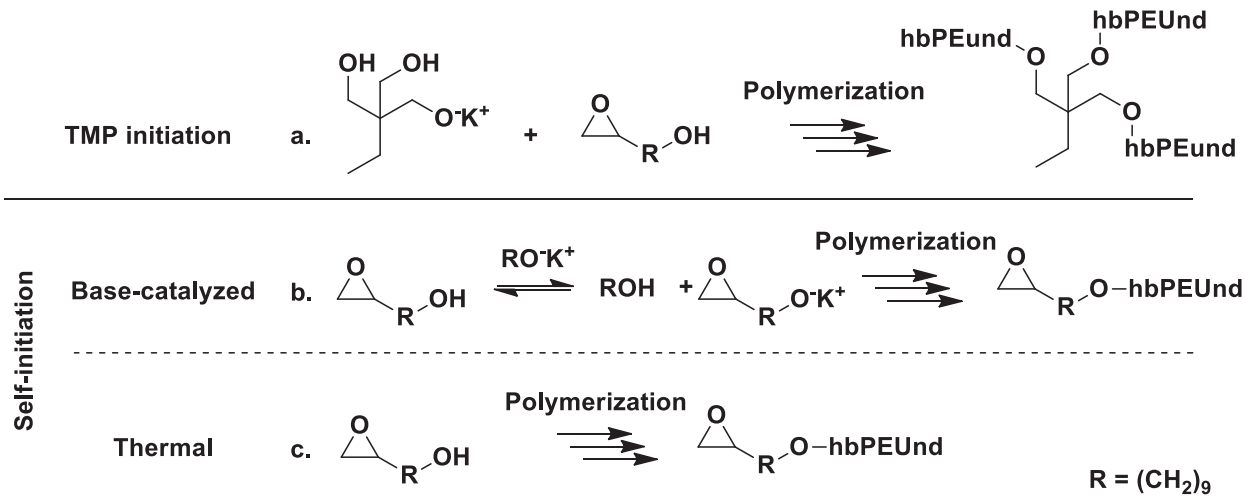

Figure II-21. Representation of the ROMBP **a.** initiation by TMP and **b.** base-catalyzed self-intiation (by EUnd) and **c.** thermal self-intiation (by EUnd).

3.3.2. Influence of TMP deprotonation

The study was performed, on the one hand, at M/TMP = 20 for extents of deprotonation of TMP varying from 2 to 10 % and, on the other hand, at M/TMP = 50 for extents of deprotonation 10 to 95 %, keeping constant the overall concentration in monomer. The concentration in active sites, compared to the number of hydroxyl functions, was reduced for low deprotonation ratios;

a M/TMP ratio equal to 20 was used for practical reasons, *i.e.* for adding reasonable quantities (V > 5 µL) of the MeOK solution.

The effect of TMP deprotonation was evaluated, from 2 to 10 %, using an initial M/TMP ratio equal to 20 (**Table II-3**). Conversion of the EUnd monomer was thus assessed by ^{1}H NMR spectroscopy following these different conditions, and results are summarized in **Figure II-22**. A TMP deprotonation ratio threshold of 5 % appeared necessary to reach a monomer conversion ≥ 90 %. Higher molecular weights, reaching an apparent maximum M_n value of 6,900 g/mol were obtained for high TMP deprotonation ratio, giving a high concentration of active alkoxides (**Figure II-23**).[5,39] As mentioned, however, this also caused aggregation of alkoxides derived from TMP, leading to the formation of a white precipitate in the reaction mixture. These aggregates were solubilized by further addition of the EUnd monomer, enabling to achieve high monomer conversion (up to 99 %). The effect of the extent of TMP deprotonation on the molecular weight is illustrated in **Figure II-24**. While molecular weight was expected to remain constant, it was found to increase upon increasing the extent of deprotonation of TMP. The deviation might be ascribed to side reactions, as already discussed.

Table II-3. Results of the ROMBP of EUnd at M/TMP = 20, at different extents of TMP deprotonation.

Entry	TMP deprotonation *(%)*	$M_{n,th.}$ [a] *(g/mol)*	$M_{n,exp}$ [b] *(g/mol)*	*Đ* [b]	Conversion [c] *(%)*
1	2	410	900	11	11
2	5	3,300	3,200	1.8	89
3	7	3,500	3,300	2.3	95
4	10	3,700	6,900	3.9	99

Polymerizations carried out in bulk at 95 °C under nitrogen with TMP deprotonated at 10 % before addition of 0.5 mL of monomer per aliquots of 100 µL every 3 min.
[a] Theoretical molecular weights calculated according to the conversion of the monomer into hbPEther: $M_{n,th}$ = (M/TMP) x M(EUnd) x conversion.
[b] Determined via SEC-RI/Viscometry in Chloroform + 1 % TEA using universal calibration (Determined via SEC-RI in Chloroform + 1 % TEA using linear PS standard calibration).
[c] Calculated from ^{1}H NMR by comparison of the epoxide proton peaks of the monomer with the proton peaks of the aliphatic backbone.

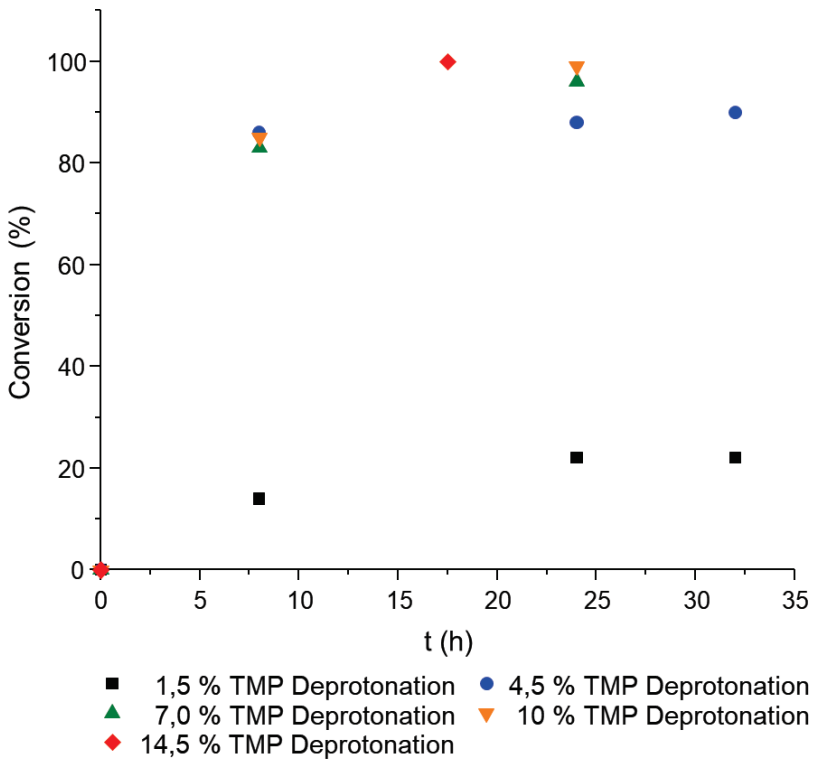

Figure II-22. Monitoring of EUnd conversion during its ROMBP in bulk at M/TMP = 20, at different extents of TMP deprotonation.

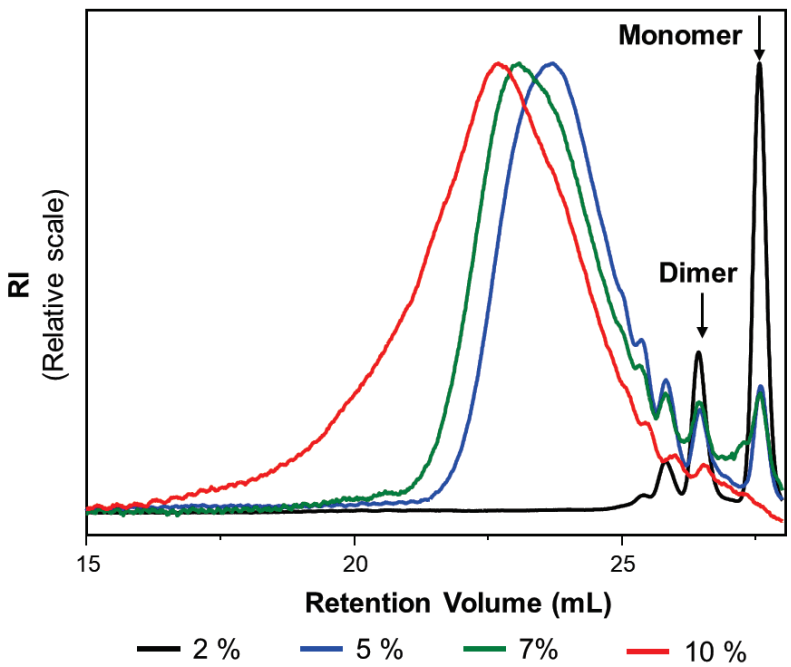

Figure II-23. SEC-RI traces ($CHCl_3$) of *hb*PEUnd obtained from polymerization conducted at M/TMP = 20, at different extents of TMP deprotonation.

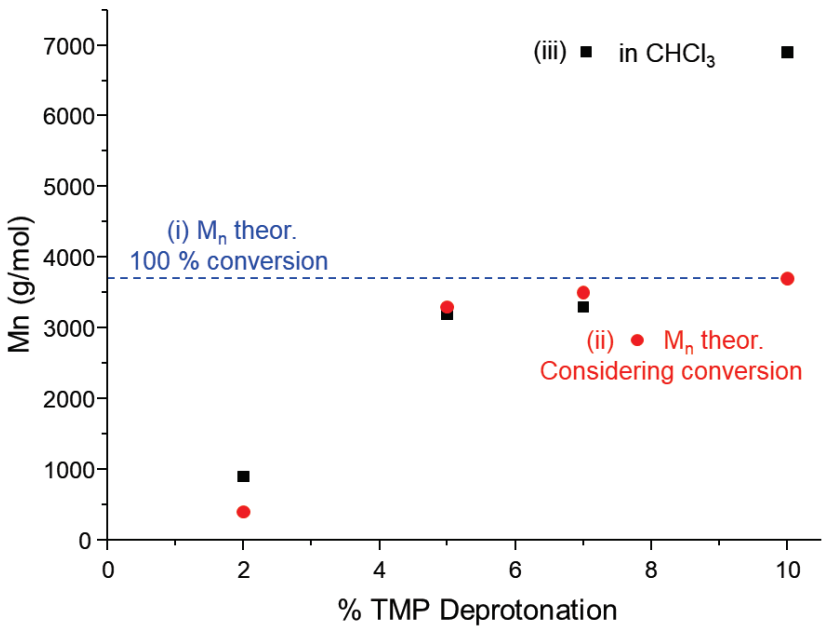

Figure II-24. M_n of *hb*PEUnd plotted versus the extent of TMP deprotonation at M/TMP = 20, with M_n determined *via* (iii) ■ SEC-RI (in $CHCl_3$, PS calibration).

The effect of the extent of TMP deprotonation was also investigated, using ratios in the range 10 - 95 %. In this case, an initial EUnd/TMP ratio of 50 was employed in order to achieve high molecular weights. Corresponding results are given in **Table II-4**, **Figure II-25** and **Figure II-26**. Monomer conversions > 90 % could be reached within 2 h for TMP deprotonation higher than 50 %. For lower extent of deprotonation, almost full conversion was achieved after 7 h. The highest M_n value, which was found equal to 11,400 g/mol, was obtained for a TMP deprotonation ratio of 10. Again, TMP deprotonation > 30 mol.% led to strong aggregation of as-obtained alkoxides. Therefore, while for TMP deprotonation between 10 to 30 %, aggregates could be solubilized by subsequent addition of EUnd in 30 min, around 2 h were necessary in the case of 95 % of TMP deprotonation.

The evolution of the molecular weight regarding the ratio of TMP deprotonation is illustrated in **Figure II-27**. Despite the high conversions obtained for higher ratios of TMP deprotonation, the molecular weights remained lower than the theoretical values, indicating that the self-initiation of the monomer probably still occurred. The persistence of aggregates for TMP deprotonation ratios higher than 30 %, along with the disrupting of stirring might explain these results.

In order to improve the solubility of the growing chains and achieve a homogeneous reaction mixture, other experimental conditions were investigated, including the increase of the M/TMP ratio (from 50 to 200), the use of polar solvents and the implementation of a slow-monomer addition (SMA). The results obtained are presented in section 3.3.3.

Table II-4. Results of the ROMBP of EUnd at M/TMP = 50, at different extents of TMP deprotonation.

Entry	TMP deprot. (%)	$M_{n,th.}$ [a] (g/mol)	$M_{n,exp}$ [b] (g/mol)	Đ [b]	Conversion [c] (%)
1	10	9,000	11,400	2.4	97
2	30	9,000	6,300	2.3	97
3	50	9,300	6,700	2.3	100
4	70	8,600	6,800	2.2	92
5	95	9,300	5,400	2.7	98

The polymerizations were carried out in bulk at 95 °C under nitrogen with M/TMP = 50. 0.5 mL of monomers were added per aliquots of 100 µL every 3 min.
[a] Theoretical molecular weight calculated according to the conversion of the monomer into hbPEther: $M_{n,th}$ = (M/TMP) x M(EUnd) x conversion.
[b] Determined via SEC-RI in Chloroform + 1 % TEA using linear PS standard calibration.
[c] Calculated from ^{1}H NMR by comparison of the epoxide proton peaks of the monomer with the proton peaks of aliphatic backbone.

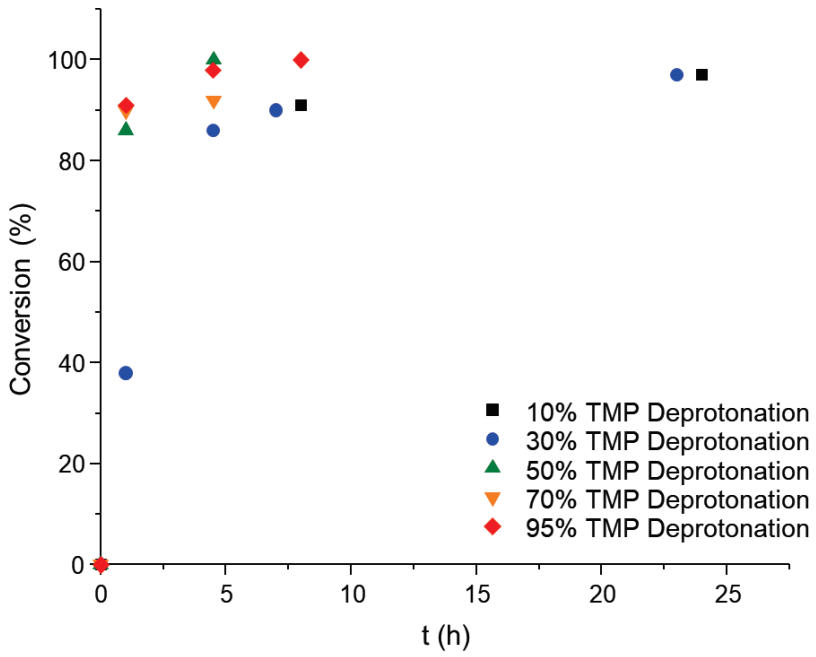

Figure II-25. Monitoring of EUnd conversion during its ROMBP in bulk at M/TMP = 50, at different extents of TMP deprotonation.

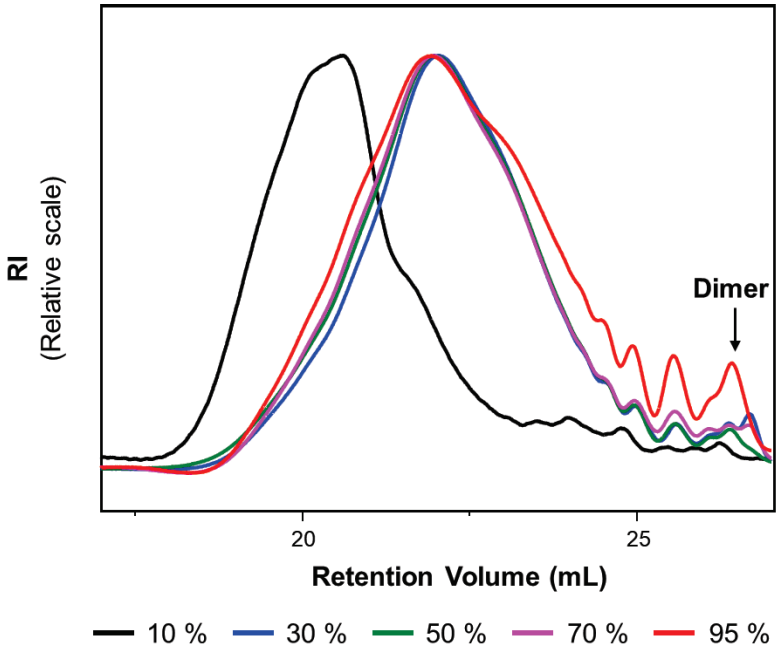

Figure II-26. SEC-RI traces ($CHCl_3$) of *hb*PEUnd obtained from polymerization conducted at M/TMP = 50, at different extents of TMP deprotonation.

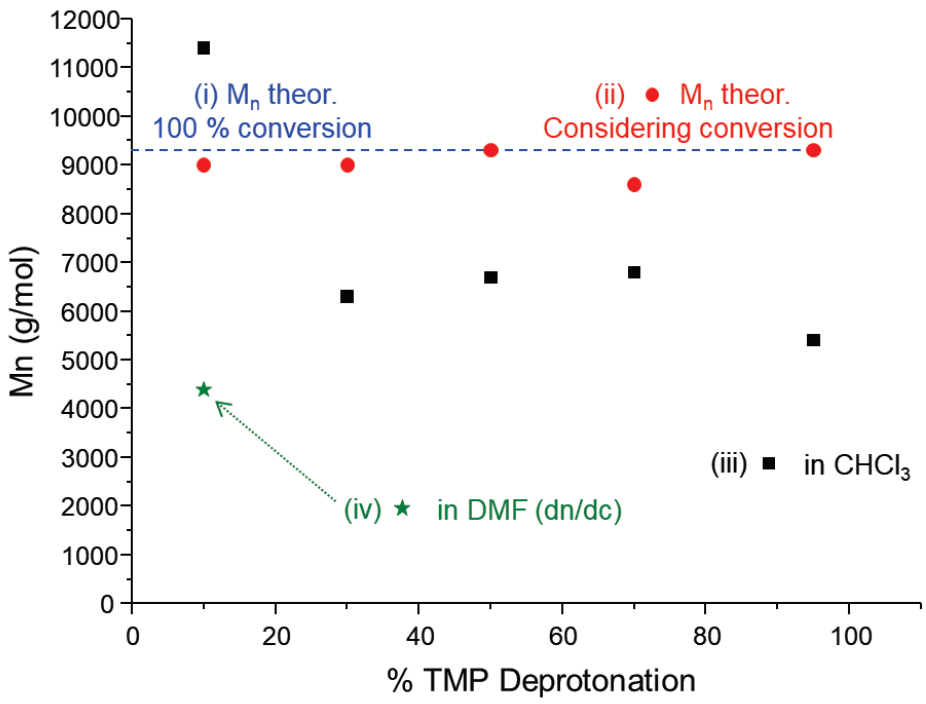

Figure II-27. M_n of *hb*PEUnd plotted versus the extent of TMP deprotonation at M/TMP = 50, with M_n determined via
■ SEC-RI ($CHCl_3$, PS calibration) ★ SEC-RI (DMF, using dn/dc).

3.3.3. Solvent effect and influence of the method of monomer addition

Different solvents were tested for the ROMBP of EUnd in order to minimize the aggregation phenomenon before addition of the monomer. Aprotic and polar solvents, such as DMSO and DMF, can be used for anionic ROP of epoxides, as they can better dissociate active species and enhance their reactivity.[40] In the case of the ROMBP of glycidol, however, these solvents were suspected to favour the self-initiation of the monomer, contributing to the development of multimodal molecular weight distributions.[5] For this reason, less polar solvents as diglyme or dioxane are generally preferred, in particular to achieve high molecular weight polymers with narrower dispersities.[32,33,41] Preliminary polymerization experiments using EUnd performed in different solvents (DMF, DMSO and dioxane) gave a poor monomer conversion (ca. 25 %) only, in comparison to bulk conditions. Further attempts were then carried out in concentrated media by adding dried dioxane (0.3 mL/mL of monomer). In this case, TMP was deprotonated up to 95 %, so that the number of active sites remained high for the polymerization. Similarly to the case of the polymerization of glycidol, alkoxides thus formed were not soluble in dioxane, the latter acting as an emulsifier. EUnd was added in stages using aliquots of 100 µL every 3 minutes; corresponding data are collected in **Table II-5**, time dependence of monomer conversion is depicted in **Figure II-28** and SEC traces are provided in **Figure II-29**. The evolution of the molecular weight regarding the M/TMP ratio is illustrated in **Figure II-30**.

Monomer conversion > 90 % could be reached within 2.5 h, for TMP deprotonation higher than 50 % in dioxane, *i.e.* the polymerization rate was slightly lower than that observed under solvent-free conditions. For higher M/TMP ratios, around 15 h of reactions were necessary to overpass 90 % monomer conversion. The highest apparent molecular weight of 17,200 g/mol was obtained for a TMP deprotonation ratio of 50, when carrying out the polymerization in dioxane (**Figure II-29**). It is important to note that the molecular weight, as determined by SEC, was likely underestimated in this case, as some populations of polymer chains were eluted from the column beyond the higher limit of molecular weights (50,000 g/mol; **Figure II-29**, peak*). The solvent-free ROMBP at M/TMP = 50 led to lower molecular weights (11,000 g/mol) with a dispersity lower than 2.0. However, and as already noted in bulk reactions mentioned above, M/TMP ratios > 50 generated polyethers with molecular weights deviating from those expected. Use of little amounts of dioxane was yet shown to favour the formation of higher molecular weight polymer, reaching 17,200 g/mol for a M/TMP = 50. As discussed by Kainthan *et al.*,[33] polymerization under such conditions is not controlled. No explanation has

yet been proposed, but one could hypothesize that the heterogeneity of the reactive mixture might explain this feature.[41]

Table II-5. Results of the ROMBP of EUnd conducted (1) in bulk and (2-4) in dioxane, at TMP deprotonation = 95 %, at different M/TMP ratios.

Entry	M/TMP	$M_{n,th.}$ [a] *(g/mol)*	$M_{n,exp}$ [b] *(g/mol)*	*Đ* [b]	Conversion [c] *(%)*
1	50	8,800	11,000	1.9	95
2	50	9,300	17,220	15.3	100
3	100	17,500	8,900	2.1	94
4	200	35,700	11,300	2.2	96

The polymerizations were carried out in bulk (entry 1) or in dioxane (entry 2-4, 0.3 mL/mL of monomer) at 95 °C under nitrogen with TMP deprotonated at 95 %. 1.0 mL of monomer was added per aliquots of 100 µL every 3 min.
[a] Theoretical molecular weight calculated according to the conversion of the monomer into *hb*PEther: $M_{n,th}$ = (M/TMP) x M(EUnd) x conversion.
[b] Determined via SEC in DMF using d*n*/d*c* = 0.049.
[c] Calculated from ^{1}H NMR by comparison of the epoxide proton peaks of the monomer with the proton peaks of aliphatic backbone.

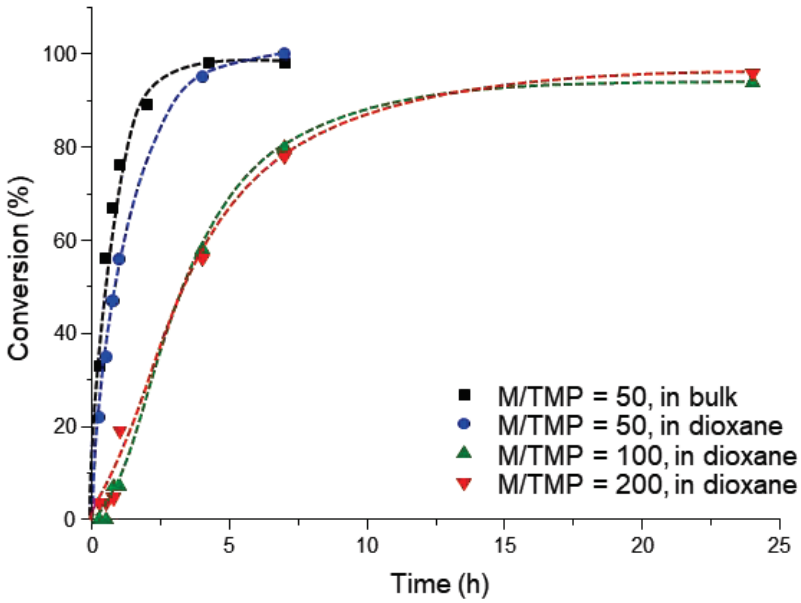

Figure II-28. Monitoring of EUnd conversion during its ROMBP conducted in bulk or in dioxane, at TMP deprotonation = 95 %, at different M/TMP ratios.

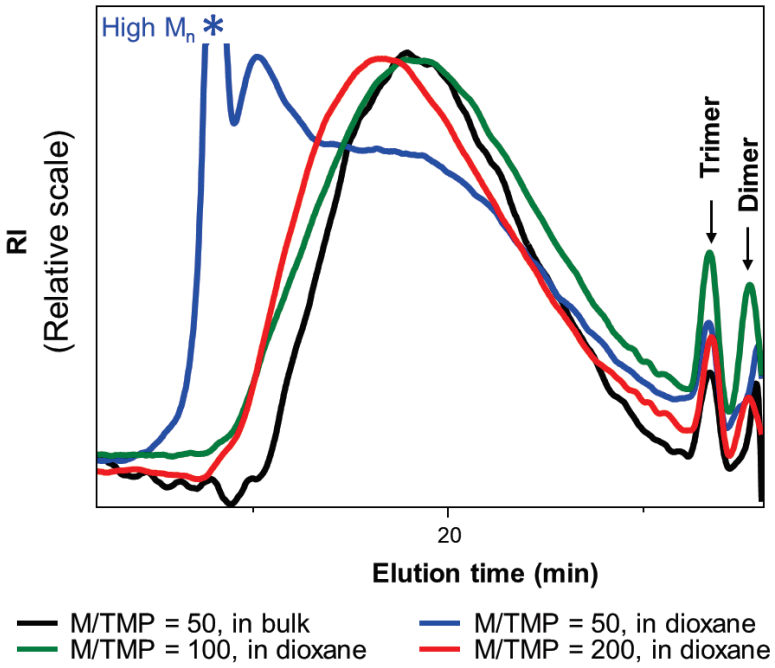

Figure II-29. SEC-RI traces (in DMF) of *hb*PEUnd obtained from polymerization conducted in bulk or in dioxane, at TMP deprotonation equal to 95 %, at different M/TMP ratios.

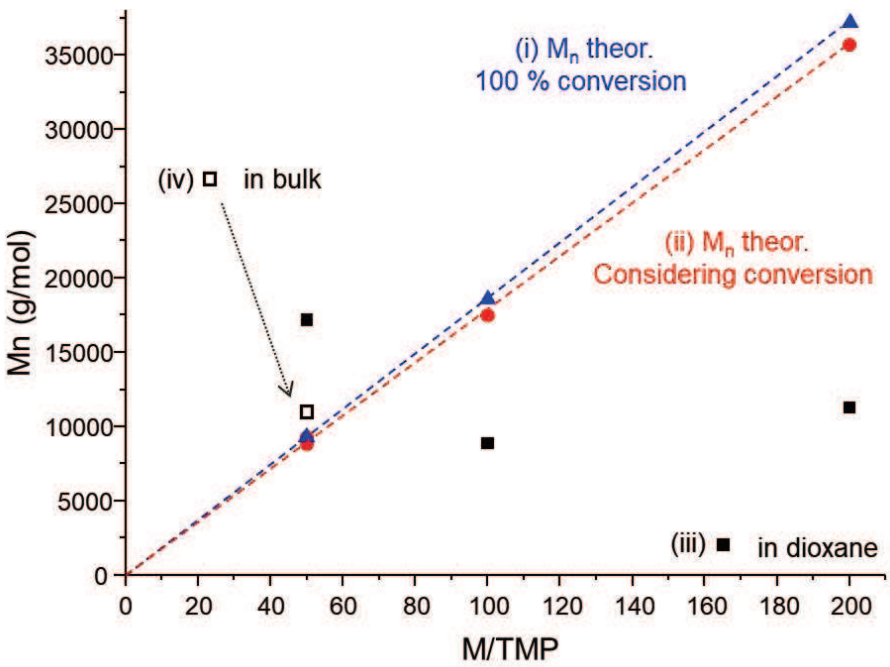

Figure II-30. M_n of *hb*PEUnd plotted versus M/TMP ratio at TMP deprotonation = 95 %. The polymerizations were carried out (iii) in dioxane (0.3 mL/mL of monomer) or (iv) in bulk.

In a new series of experiments, polymerizations were conducted at an extent of deprotonation of TMP equal to 95 %, from a M/TMP ratio of 200. Reactions were carried out either in bulk (**Table II-6**, entry 1), or in dioxane at a concentration S/M = 0.3 mL/mL, (entry 2) or at S/M = 1 mL/mL (entry 3). The monomer was thus introduced *via* a SBA process, *i.e.* by adding aliquots of 100 µL every 3 minutes, or *via* SMA with the aim at preventing self-initiation of the monomer.[2,34] Results of monomer conversion *vs.* time, as determined by ^{1}H NMR spectroscopy, are shown in **Figure II-31**, and corresponding SEC traces using DMF as solvent are given in **Figure II-32**.

Reactions performed in solution in dioxane proved faster than those implemented in bulk. In the latter case, indeed, monomer conversion hardly reached 80 % after 70 h of reaction, while in dioxane, 80 % could be attained after 20 h of reaction. This may be ascribed to a decrease in viscosity of the mixture upon using dioxane, favouring proton exchange between active alkoxides and dormant hydroxyls, and propagation of the growing chains.[33,41,42] However, the S/M ratio was also found to play an important role toward the polymerization kinetics. Higher reaction rates were indeed achieved under concentrated medium, monomer conversion higher than 80 % being obtained after approximately 10 and 20 h, for S/M ratio of 0.3 and 1 mL/mL, respectively. Consequently, higher molecular weights, ca. 11,000 g/mol, could be obtained *via* polymerization in dioxane (*vs.* 8,000 g/mol in bulk). No significant influence of the monomer concentration was noticed; the molecular weights were found equal to 11,300 and 10,800 g/mol for S/M = 0.3 mL/mL and S/M = 1 mL/mL, respectively. Despite the slow addition of the monomer (**Table II-6**, entry 4), the kinetics proved particularly slow and the reaction did not reach completion even after 90 h (53 %), giving a molecular weight as low as 500 g/mol.

Table II-6. Results of the ROMBP of EUnd in bulk or in dioxane *via* SBA or SMA at TMP deprotonation = 95 % and M/TMP = 200.

Entry	Solvent *(S:M mL/mL)*	Monomer addition	$M_{n,th.}$ [a] *(g/mol)*	$M_{n,exp}$ [b] *(g/mol)*	*Đ* [b]	Conv. [c] *(%)*
1	Bulk	SBA	30,500	8000	1.8	82
2	Dioxane (0.3:1)	SBA	35,700	11,300	2.2	96
3	Dioxane (1:1)	SBA	37,200	10,800	1.8	100
4	Dioxane (1:1)	SMA (2 mL/h)	19,700	500	3.1	53

The polymerizations were carried out in bulk or in dioxane at 95 °C under nitrogen with TMP deprotonated at 95 % and M/TMP equal to 200. 1.0 mL of monomer was added by semi-batch addition (SBA, per aliquots of 100 µL every 3 min) or by slow-monomer addition (SMA, 2 mL/h).

[a] Theoretical molecular weight calculated according to the conversion of the monomer into *hb*PEther: $M_{n,th}$ = (M/TMP) x M(EUnd) x conversion.

[b] Determined via SEC in DMF using d*n*/d*c* = 0.049.

[c] Calculated from ^{1}H NMR by comparison of the epoxide proton peaks of the monomer with the proton peaks of aliphatic backbone.

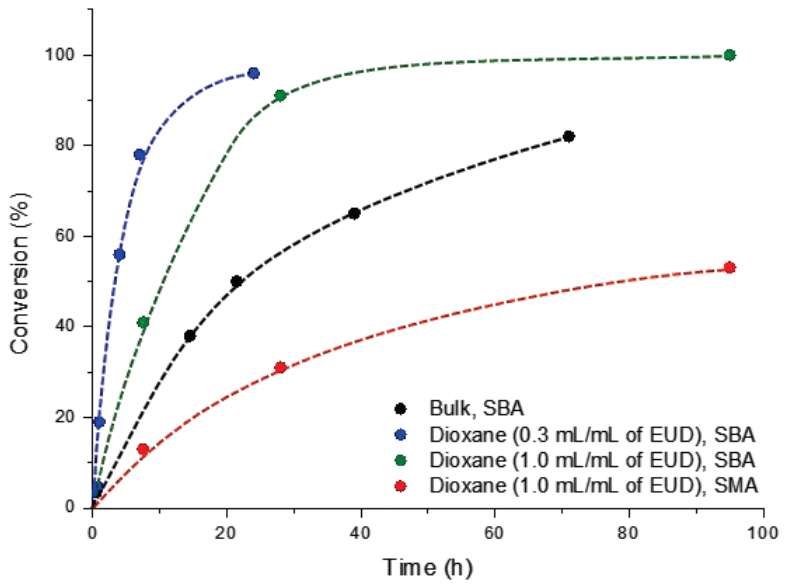

Figure II-31. Monitoring of EUnd conversion during its ROMBP conducted in bulk or in dioxane *via* SBA or SMA, at TMP deprotonation = 95 % and at M/TMP = 200.

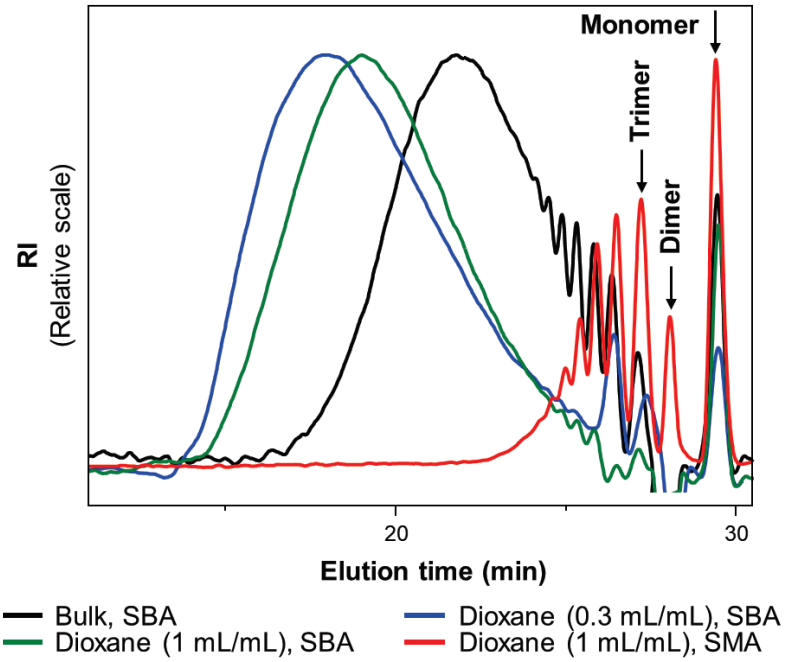

Figure II-32. SEC-RI traces (in DMF) of *hb*PEUnd obtained from polymerization conducted in bulk or in dioxane *via* SBA or SMA, at TMP deprotonation = 95 % and at M/TMP = 200.

In summary, the ring-opening polymerization of a new latent bio-based AB_2-*type* monomer, namely, 10,11-epoxyundecnaol can be conducted in bulk or in concentrated solutions, preferentially in dioxane, at 95 °C, as a means to achieve bio-sourced hyperbranched polyether polyols. Optimization of the experimental conditions, involving semi-continuous addition process of the monomer, use of a trifunctional core molecule (TMP) and partial deprotonation of the latter, enables the formation of polymers with a maximum apparent molecular weight (M_n) of 10,000 g/mol ($hbPEUnd_{10k}$), *i.e.* corresponding to an average degree of polymerization of 50, with a dispersity lower than 2. Such polymers can be synthesized in bulk within 7 h by using M/TMP = 50 and an extent of deprotonation of TMP of 95 %. For similar M/TMP and TMP deprotonation ratios, addition of dioxane leads to the formation of polymers with molecular weights that deviate from theoretical values and exhibit significantly higher dispersities; in the latter case, dioxane is suspected to act as an "emulsifier" of the polymerization process.[33,41] Upon increasing the M/TMP ratio (up to 200), self-initiation of the monomer probably occurred as a side reaction,[6] limiting the accessible molecular weights. Use of a slow monomer addition process does not enable to suppress side reactions, as the addition rate (2 mL/h) is presumably still too important relatively to the rate of polymerization of that monomer.

3.4. Thermal properties

Unlike amorphous hyperbranched polyglycidols, polyethers obtained from EUnd show semi-crystalline properties, with melting points around 85 °C.[43,44] The crystallinity of these *hb*PEUnds can be correlated to the presence of long aliphatic sequences in their structure. This feature had been observed with *hb*PEsters, synthesized by polycondensation of methyl 10,11-dihydroxyundecanoate (M2HU-*hb*PEster); these latter exhibiting melting points around 50 °C.[30,31,45]

TGA analysis of *hb*PEUnds indicated a multi-stage degradation profile with a first stage at 365 °C and a second around 460 °C (**Figure II-33** and **Figure II-34**), which is in agreement with values classically observed for polyethers.[46,47] By comparison, and as expected, the degradation of M2HU-*hb*PEsters started at lower temperatures (200-230 °C), the thermal stability of ester bonds being generally lower than the one of ethers.

As already discussed, the limitation of molecular weights (10,000 g/mol) restricts somehow the possibility to vary the polymer properties. Nevertheless, these might be tuned either through the copolymerization involving EUnd and other epoxides, or by post-modifying the parent *hb*PEUnds.

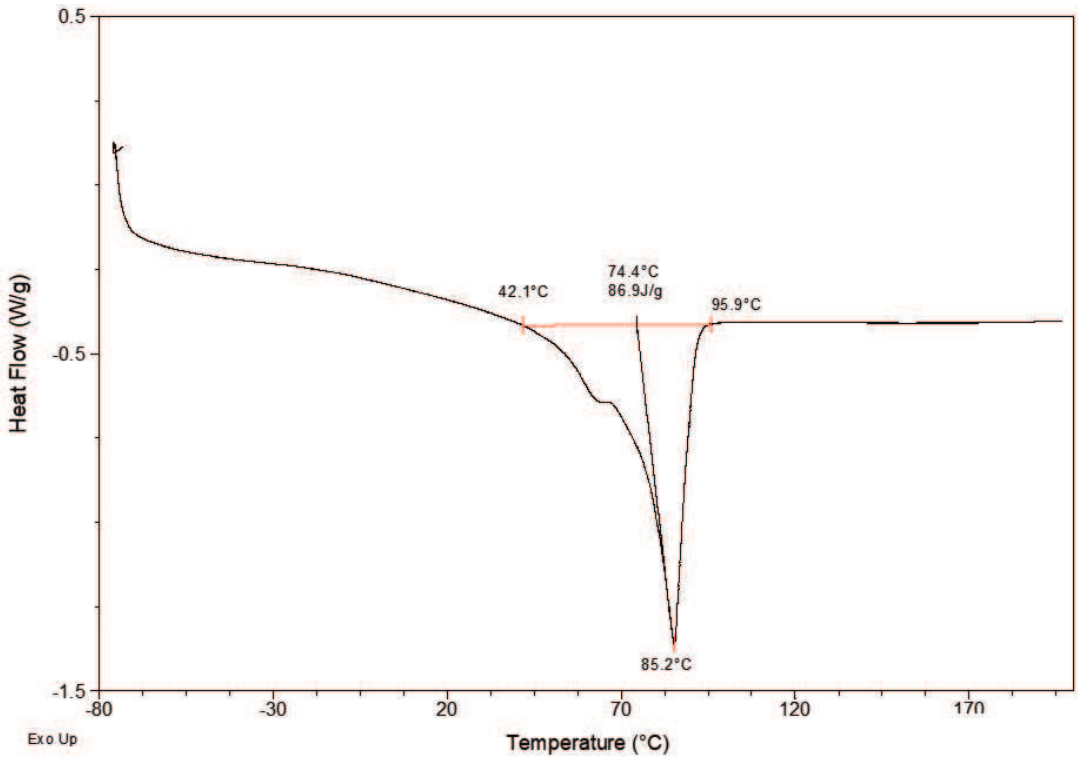

Figure II-33. DSC of polyether obtained from ROMBP of EUnd conducted in bulk at M/TMP = 50 and TMP deprotonation = 10 %.

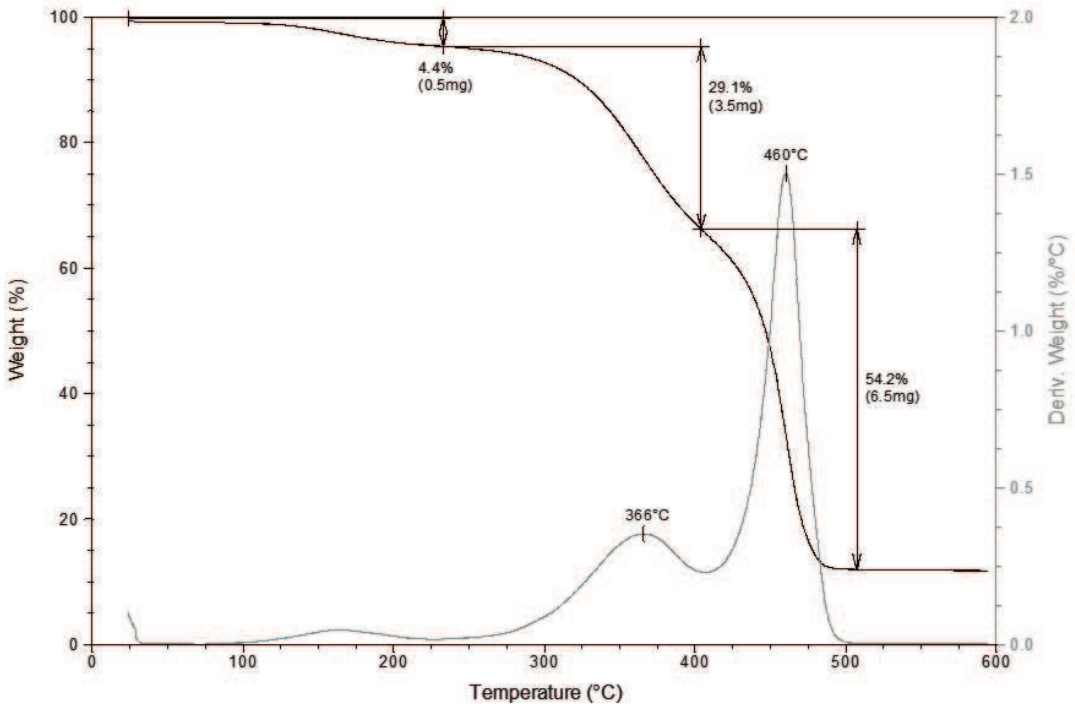

Figure II-34. TGA of polyether obtained from ROMBP of EUnd conducted in bulk at M/TMP = 50 and TMP deprotonation = 10 %.

4. Ring-opening copolymerization of 10,11-epoxyundecanol and glycidol

Random,[48–52] and sequential[3,53] anionic copolymerizations of glycidol with oxirane comonomers have been widely investigated in the literature. However, while the use of latent AB_2-type comonomer would lead to the synthesis of fully hyperbranched copolymers, only few examples have been reported due to the lack of this type of monomer.[11–14] In this part, we implemented random and sequential ring-opening multibranching copolymerizations (ROMBcP) of EUnd and glycidol in order to manipulate the physico-chemical properties of the resultant hyperbranched polyether polyols. Therefore, synthesis of semi-crystalline gradient copolymers, named *hb*P(G-*co*-EUnd) and block copolymers, called *hb*PG-*b*-*hb*PEUnd and *hb*PEUnd-*b*-*hb*PG, was attempted (**Figure II-35**). These syntheses and related characterizations of the as-obtained copolymers are detailed in the following part.

4.1. Random copolymerization of 10,11-epoxyundecanol and glycidol

On the one hand, EUnd leads to a crystalline hydrophobic polyether and, on the other hand, polyglycidol is an amorphous hydrophilic polyether. Copolymerizations were implemented by mixing the two monomers at different ratios, with the objective to form gradient copolymers. The gradient structure indeed stems from the higher kinetics rate of glycidol in comparison to EUnd. In all cases, copolymers of low molecular weights (1,500 and 1,900 g/mol) were obtained as waxy viscous liquid. Such oligomers were found to be soluble in common polar and non-polar solvents and dispersible in water.

4.1.1. Methodology

The random copolymerization of EUnd and glycidol was performed using the conditions that were optimized for ROMBP of EUnd. Namely, reactions were conducted in bulk, at M/TMP = 50 and at TMP deprotonation = 10 %. Two glycidol:EUnd comonomer molar ratios, of 0.50:0.50 and 0.67:0.33, were tested in order to vary the proportion of hydrophilic and hydrophobic moieties. The resulting copolymers obtained are denoted as *hb*P($G_{0.50}$-*co*-$EUnd_{0.50}$) and *hb*P($G_{0.67}$-*co*-$EUnd_{0.30}$), respectively. The general procedure of the random copolymerization of EUnd and glycidol is depicted in the supporting information. As in the case of the homopolymerization of EUnd, the conversion of EUnd and glycidol into *hb*P(G-*co*-EUnd) was monitored by ^{1}H NMR (**Figure II-36**).

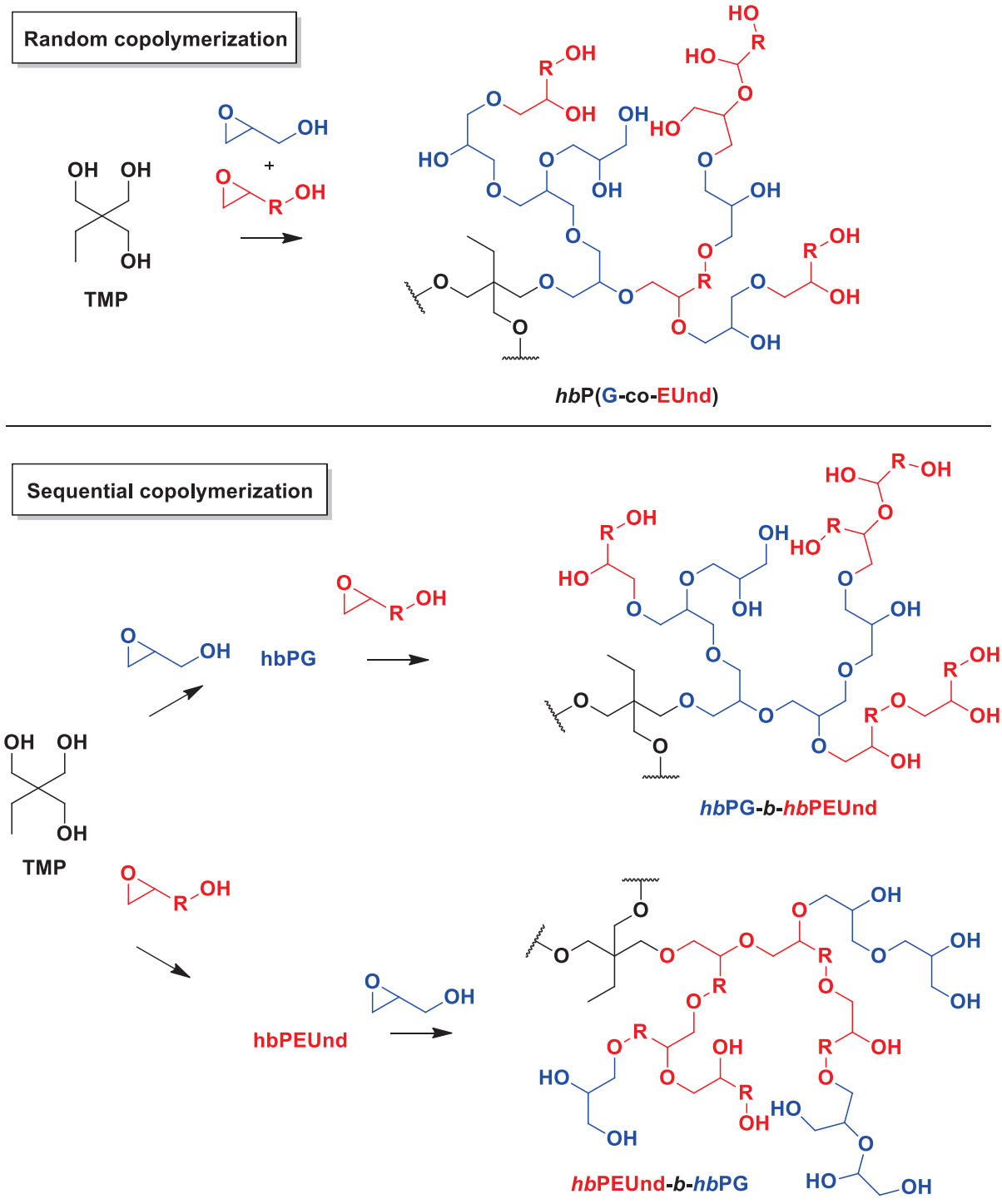

Figure II-35. Random and sequential ROMBcP of EUnd and glycidol.

The sixteen protons of the peaks 3-10 were used as standards. EUnd conversion was calculated by comparing the integrals of the peaks **1** and **2** with the integral of the peaks **3-10**. Glycidol conversion rate was calculated comparing the integrals of the peaks **c** with the integral of the peaks **3-10**.

The molecular weights and the dispersities of the copolymers obtained were measured by SEC in chloroform using PS standards and a universal calibration (**Figure II-37**). DSC was performed to determine their glass transition temperature and their melting point.

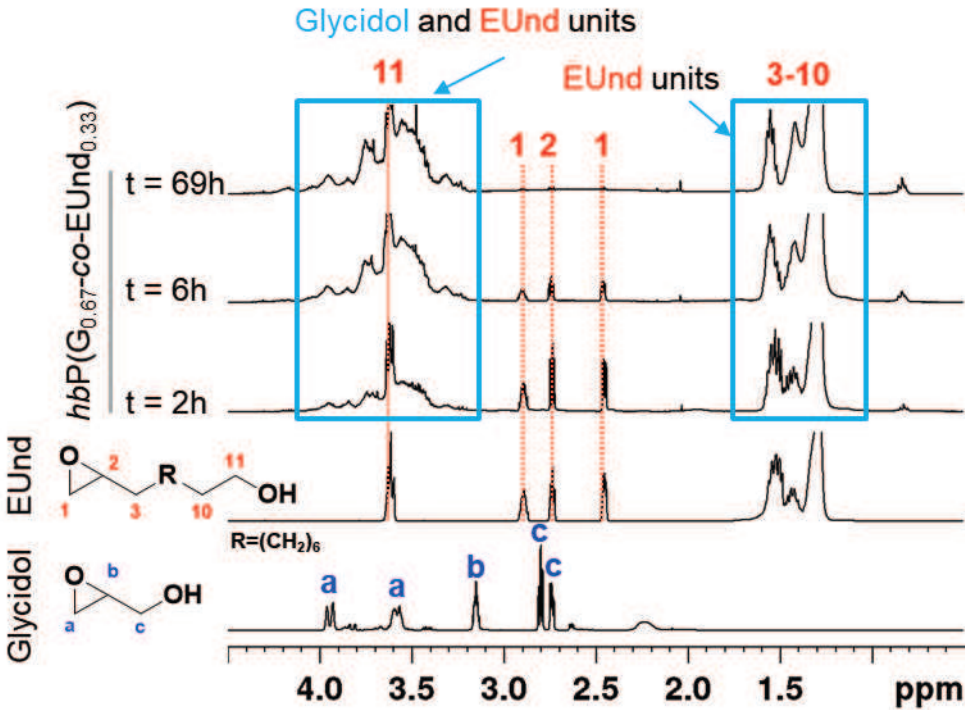

Figure II-36. Monitoring of the conversion of glycidol and EUnd by ^{1}H NMR ($CDCl_3$). ROMBcP was conducted in bulk, at glycidol:EUnd = 0.67:0.33, M/TMP = 50 and TMP deprotonation = 10 %.

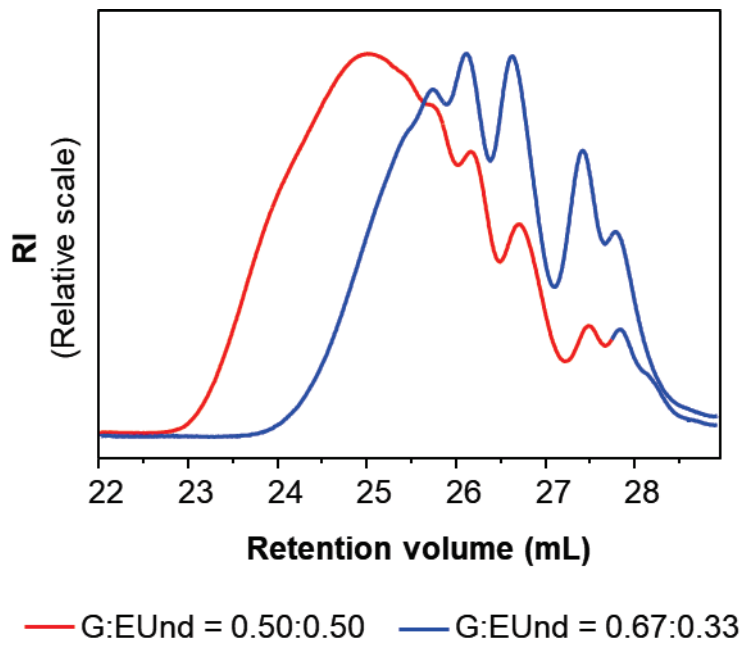

Figure II-37. SEC-RI traces (in $CHCl_3$) of polyethers obtained by random ROMBcP of glycidol (G) and EUnd conducted in bulk, at M/TMP = 50, at TMP deprotonation = 10 % and at different glycidol:Eund ratios.

4.1.2. Characterization of the *hb*P(G-*co*-EUnd)

Monitoring by NMR confirmed that conversion of glycidol was much faster than the one of EUnd (**Figure II-36** and **Figure II-38**). Indeed, while glycidol was fully consumed after 2 h, only 40 % of EUnd was polymerized in the same period of time. The higher reactivity of glycidol suggests that the ROMBcP process takes place in a two-step process, involving glycidol conversion in the first 2 h with a low fraction of EUnd incorporated. The latter monomer mainly polymerised in a second stage, until a conversion up to 93% after 70h (**Figure II-38** and **Table II-7**). As observed for the ROMBP of EUnd, low molecular weights were produced. The higher molecular weight of 1,900 g/mol was reached for a glycidol:EUnd ratio of 0.50:0.50, *i.e.* for the highest proportion of EUnd.

Table II-7. Results of the random ROMBcP of glycidol and EUnd conducted in bulk, at M/TMP = 50, TMP deprotonation = 10 %.

Entry	Glycidol:EUnd (%)	M_n [a] (g/mol)	M_n [b] (g/mol)	Đ [a]	Đ [b]	EUnd Conv.[c] (%)	Glycidol Conv. [c] (%)
1	0:1	8,000	11,400	2.7	2.4	97	-
2	0.50:0.50	1,900	1,800	2.4	1.7	93	100
3	0.67:0.33	1,500	1,000	1.6	1.5	87	100

Polymerizations were carried out in bulk at 95 °C under nitrogen. 1 mL of the comonomer mixture was added per aliquots of 100 µL every 3 min.
[a] Determined via SEC-RI/Visco in Chloroform + 1 % TEA using universal calibration.
[b] Determined via SEC-RI in Chloroform + 1% TEA using linear PS standard calibration.
[c] Calculated from ^{1}H NMR by comparison of the epoxide proton peaks of the monomers with the proton peaks of alkane backbone of EUnd units (peaks 3-10).

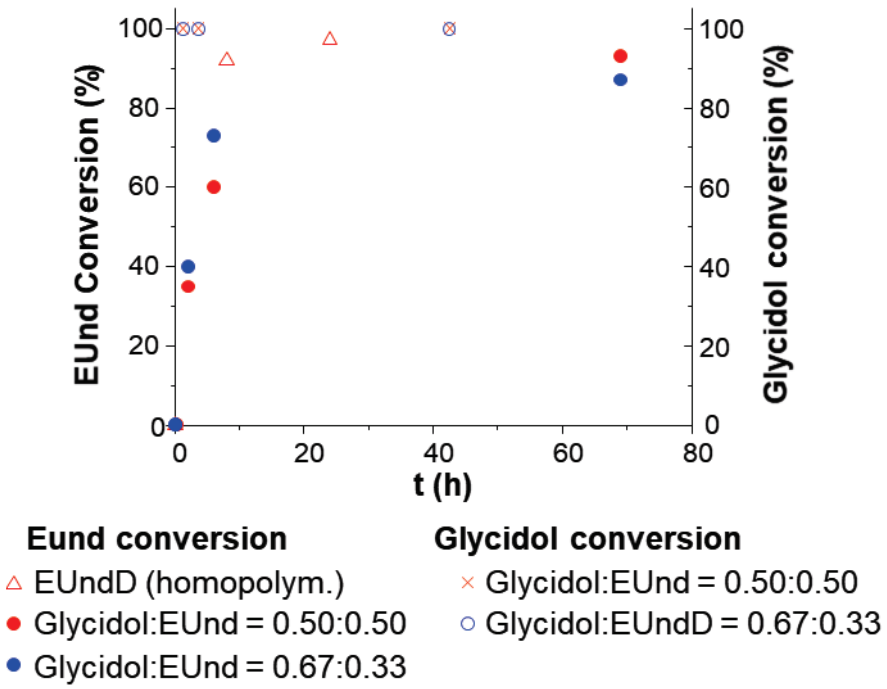

Figure II-38. Monitoring of EUnd and glycidol conversion during the homopolymerization of EUnd and the random copolymerization of EUnd and glycidol (at different glycidol/EUnd ratios).

The difference in reactivity between the two comonomers is expected to yield hyperbranched copolyethers with a core-shell type structure. The core would thus be mostly composed of hydrophilic glycidol units, while the shell would be constituted of hydrophobic *hb*PEUnd.

The structure of the different copolymers was determined by ^{1}H NMR spectroscopy (**Figure II-39**) in $CDCl_3$. The diagnostic peaks of the *hb*P($G_{0.50}$-*co*-$EUnd_{0.50}$) and *hb*P($G_{0.67}$-*co*-$EUnd_{0.33}$) copolymers derived from *hb*PEUnd are assigned on the NMR spectra. These assignments are based on NMR spectra of the respective homopolyethers, *hb*PEUnd and *hb*PG, discussed in section 3.2 (**Figure II-11**) and in the supporting information (**Figure SI.II-65**). The integrals of the peaks I at δ = 3.1-4.1 ppm, and II at δ = 1.1-1.7 ppm were used to determine the proportion of glycidol and EUnd in the copolymers according to equations (Eq. II-6) and (Eq. II-7). Hence, *hb*P($G_{0.50}$-*co*-$EUnd_{0.50}$) contains 54 % of glycidol and 46 % of EUnd, while *hb*P($G_{0.67}$-*co*-$EUnd_{0.33}$) is composed of 63 % of glycidol and 37 % of EUnd. These calculated values are in very good agreement with the expected values based on the initial molar ratio in the comonomer feed.

$$\text{EUnd fraction} = \frac{5}{16} \cdot \frac{I_{II}}{I_I} \qquad \text{(Eq. II-6)}$$

$$\text{Glycidol fraction} = 1 - \text{EUnd fraction} \qquad \text{(Eq. II-7)}$$

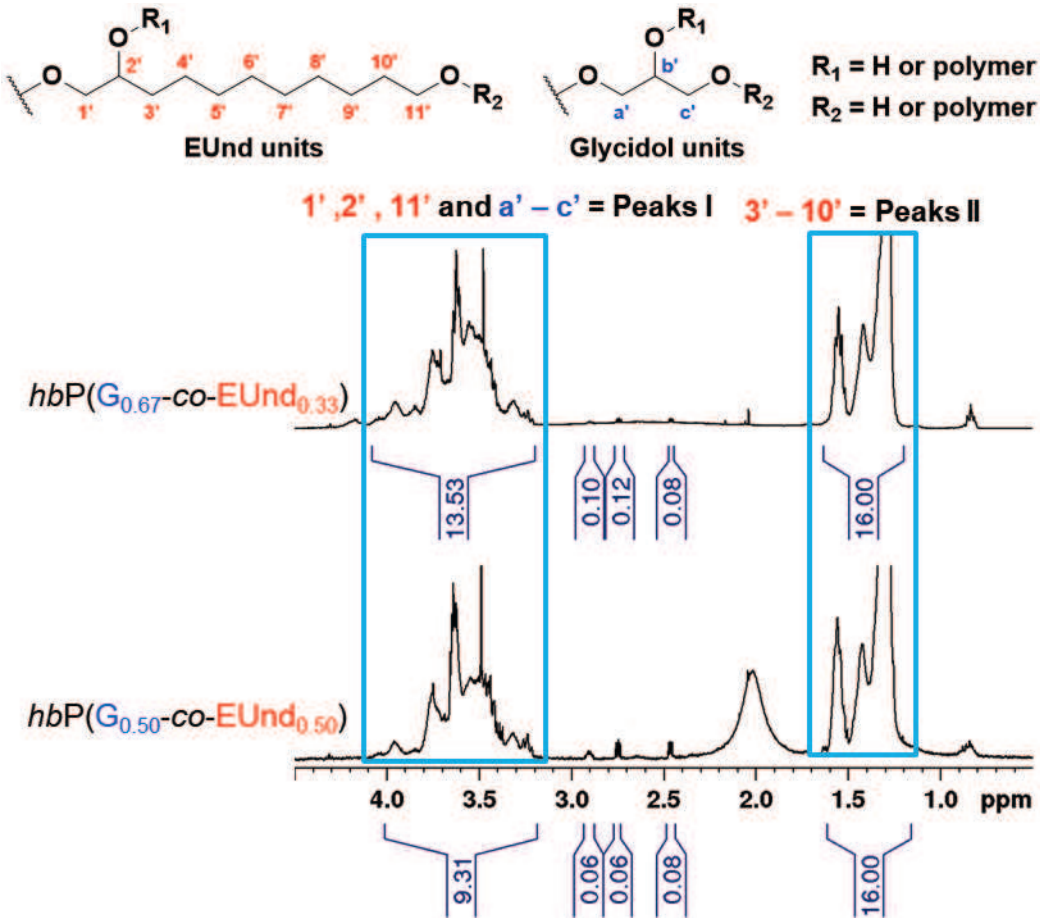

Figure II-39. ^{1}H NMR ($CDCl_3$) of *hb*P($G_{0.5}$-*co*-$EUnd_{0.5}$) and *hb*P($G_{0.7}$-*co*-$EUnd_{0.3}$).

4.1.3. Properties of the *hb*P(G-*co*-EUnd)

As already mentioned, *hb*PG is known as a highly hydrophilic polymer and is only soluble in polar solvents, such as water, alcohols, DMF and DMSO. In contrast, *hb*PEUnd is only soluble in chloroform or in hot DMF (T > 40 °C). Interestingly, the copolymers obtained by ROMBcP of EUnd and glycidol proved soluble in many common organic solvents, including chloroform, methanol, acetone, THF, and also dispersible in water. No difference of solubility was noticed by the naked eye when varying the proportions of EUnd and glycidol into the copolymers.

As expected, the incorporation of glycidol into the *hb*PEUnd structure also modified its thermal properties (**Figure II-40**). As a general trend, the melting point was found to decrease from 70 °C (*hb*PEUnd) to 33±5 °C (*hb*P(G-*co*-EUnd) and a glass transition was clearly visible around -18±6 °C. This can be explained by both the increase of mobility due to the incorporation of glycidol and the low molecular weight of the copolymers. For the same reasons, the glass transition and the melting temperatures were lower for higher contents in glycidol: T_g = -22 °C and T_m = 29 °C for 67 % of glycidol and T_g = -14 °C and T_m = 36 °C for 50 % of glycidol. A decrease of the crystallinity was also observed for a higher content in glycidol.

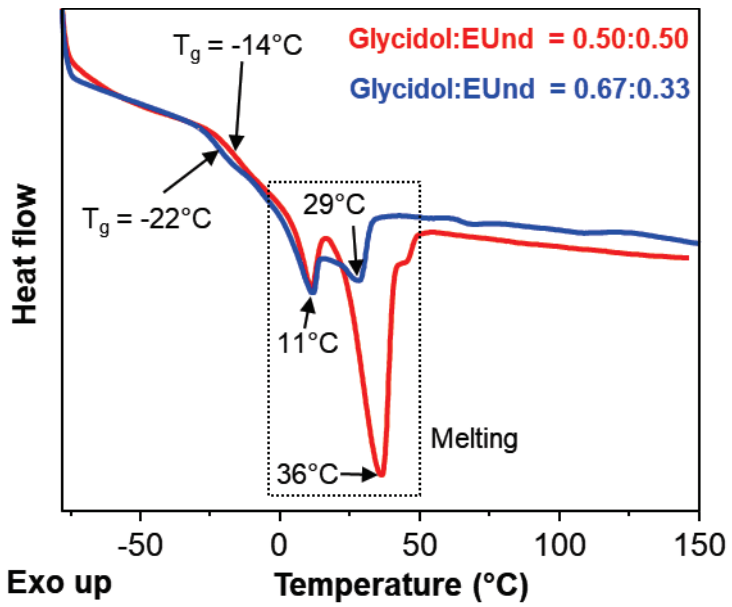

Figure II-40. DSC of polyether obtained from ROMBcP of EUnd and glycidol conducted in bulk at M/TMP = 50 and TMP deprotonation = 10 % at different glycidol:EUnd ratios.

4.2. Sequential polymerization of 10,11-epoyxundecanol and glycidol

The following section describes preliminary results obtained in our attempts to sequentially copolymerize EUnd and glycidol in a one pot process, to reach hyperbranched copolymers having a core-shell structure.

4.2.1. Formation of *hb*PEUnd-*b*-*hb*PG and *hb*PG-*b*-*hb*PEUnd

Synthesis of two compounds was achieved using a glycidol:EUnd comonomer molar ratio of 0.67:0.33. The procedures of these sequential copolymerizations are depicted in the supporting information.

These syntheses required the use of *N*-methyl-2-pyrrolidone (NMP) as solvent to prevent any phase segregation of the two blocks. This is particularly challenging, as the second monomer is expected to polymerize from the first block and not only homopolymerize. One prerequisite to perform the sequential copolymerization is thus to ensure the good miscibility of the two blocks during the copolymerization.[39-41] High extent of TMP deprotonation was used to fasten the polymerization of EUnd, which was shown to be slower in presence of a solvent (see section 3.3.3). The conversion of EUnd and glycidol was monitored by ^{1}H NMR, as exemplified in **Figure II-41** and **Figure II-42** with the example of the synthesis of *hb*PEUnd-*co*-*hb*PG. The conversion of EUnd was assessed as previously discussed (**Figure II-41**), while that of glycidol was determined by comparing the integral of the peaks $\mathbf{a_1}$ with the integral of peaks **3-10** (**Figure II-42**). NMR spectra obtained for *hb*PG-*co*-*hb*PEUnd are given in **Figure II-43** and **Figure II-44**. In all cases, full conversion was obtained for both comonomers.

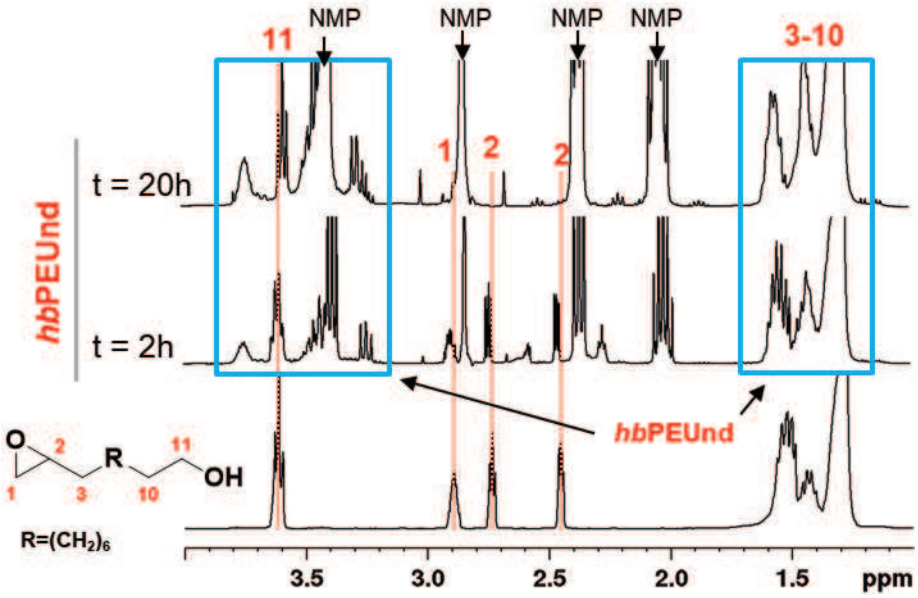

Figure II-41. Monitoring of the conversion of EUnd by ^{1}H NMR ($CDCl_3$). ROMBP was conducted in NMP, at EUnd/TMP = 200 and TMP deprotonation = 95 %.

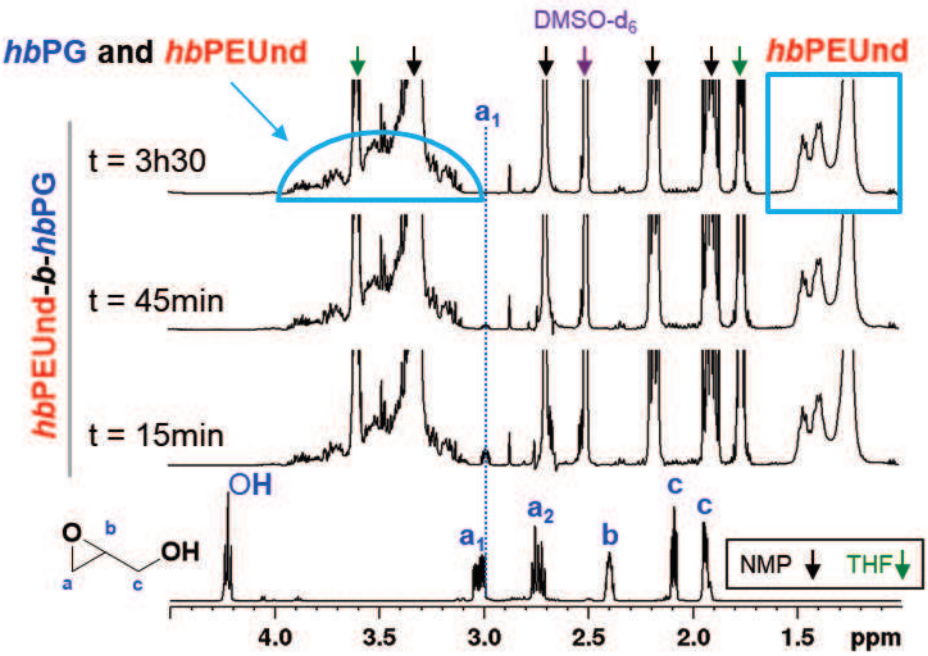

Figure II-42. Monitoring of the conversion of glycidol by ^{1}H NMR (DMSO-d_6). ROMBP of glycidol from *hb*PEUnd was conducted in NMP, at glycidol/OH(*hb*PEUnd) = 200 and at OH(*hb*PEUnd) deprotonation = 5 %.

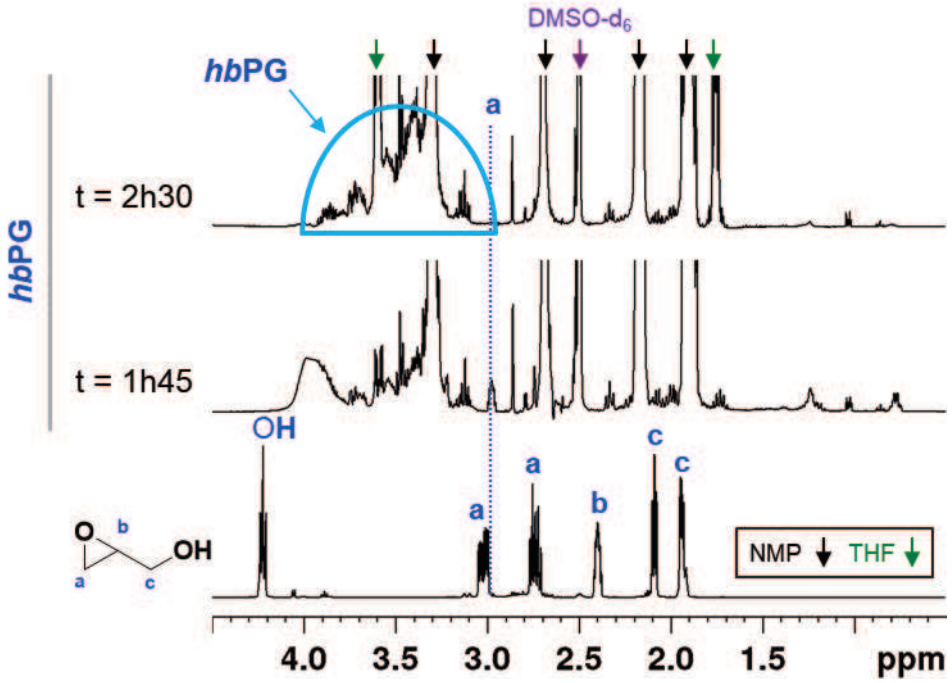

Figure II-43. Monitoring of the conversion of glycidol by ^{1}H NMR (DMSO-d_6). ROMBP was conducted in NMP, at glycidol/TMP = 200 and TMP deprotonation = 95 %.

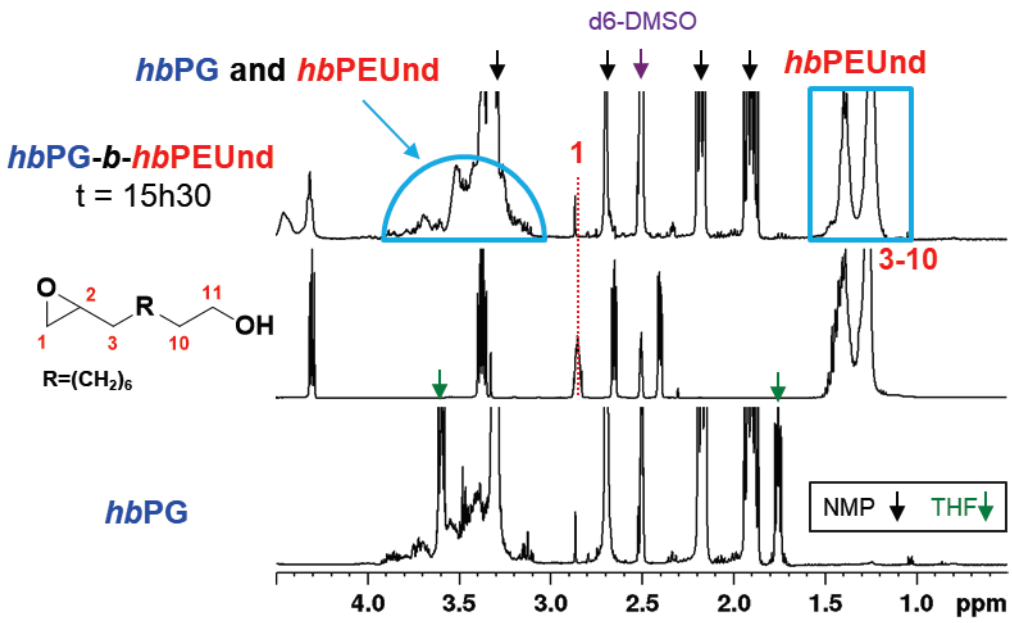

Figure II-44. Monitoring of the conversion of EUnd by ^{1}H NMR (DMSO-d_6). ROMBP of EUNd from *hb*PG was conducted in NMP, at EUnd/OH(*hb*PG) = 200 and at OH(*hb*PG) deprotonation = 5 %.

The formation of the block copolymers was also monitored by SEC in DMF (**Figure II-45** and **Figure II-46**). In the case of *hb*PEUnd-*b*-*hb*PG synthesis, the SEC traces showed the molecular weight increase after polymerization of glycidol, confirming the grafting of polyglycidol onto the *hb*PEUnd core (**Figure II-45**). However, the presence of populations of low molecular weight is also noted (**Figure II-45**, t = 26 min). Unfortunately, the superimposition of the peak coming from the salts present in DMF, used as the SEC solvent, does not permit the calculation of the molecular weight of the low M_n population (peak at 26 min).

The chromatograms obtained for the synthesis of *hb*PG-*b*-*hb*PEUnd indicates that polymers of higher molecular weights were formed (**Figure II-46**). However, low molecular weight polymers were still present in the mixture and, as in the case of *hb*PEUnd-*b*-*hb*PG, their peaks are not clearly distinguishable due to the presence of salts eluted at the same retention time (t =27 min).

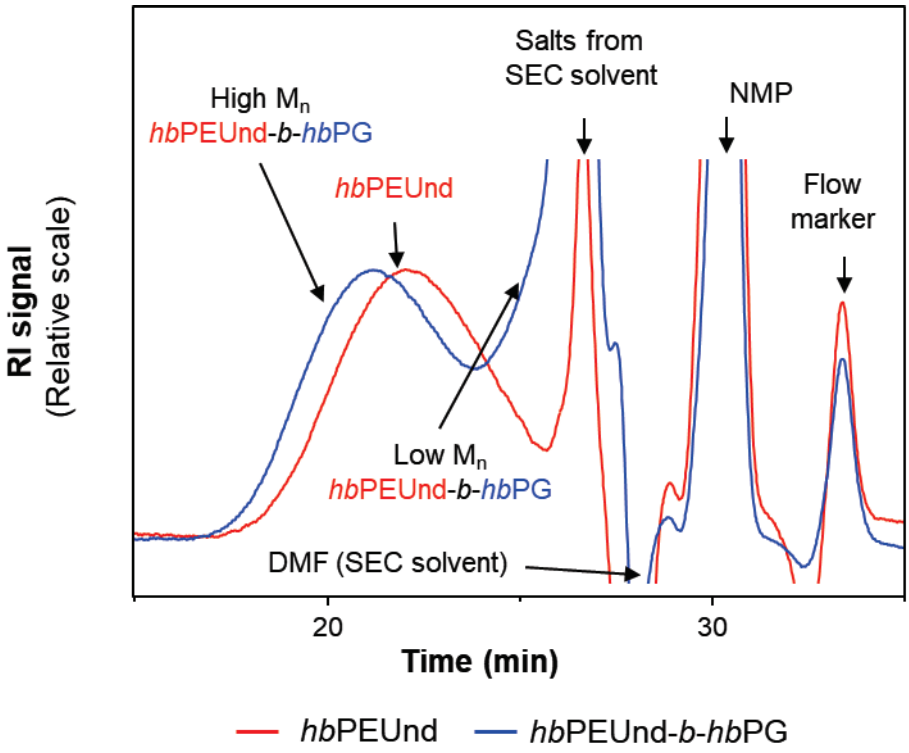

Figure II-45. SEC-RI traces (in DMF) of copolymers obtained by sequential ROMBP of EUnd followed by polymerization of glycidol onto the *hb*PEUnd formed.

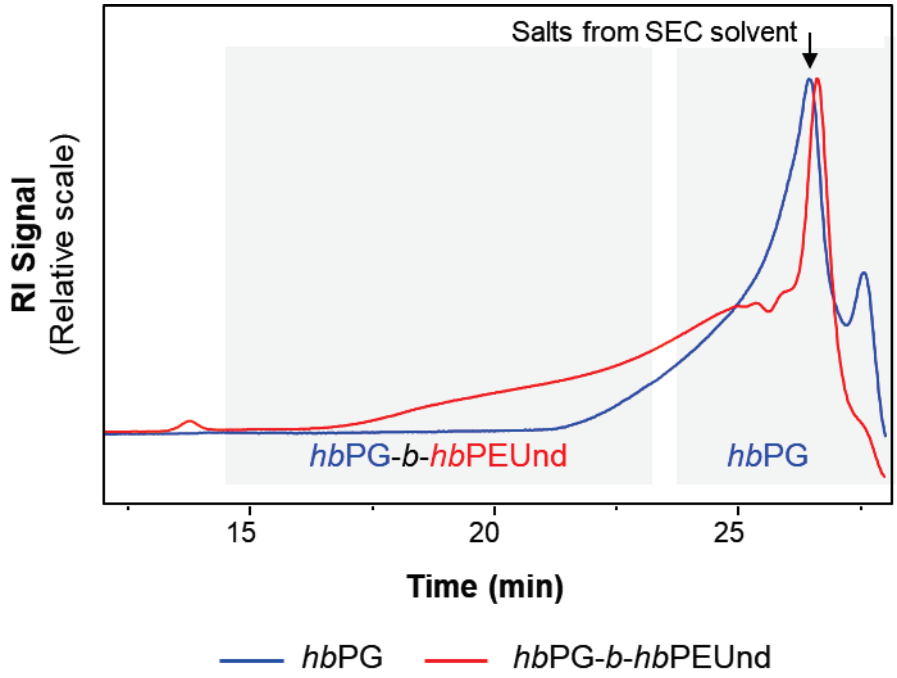

Figure II-46. SEC-RI traces (DMF) of polymers obtained by ROMBP of glycidol followed by the polymerization of EUnd onto the *hb*PG formed.

4.2.2. Characterization of *hb*PEUnd-*b*-*hb*PG and *hb*PG-*b*-*hb*PEUnd

The following characterization was performed on *hb*PEUnd-*b*-*hb*PG and *hb*PG-*b*-*hb*PEUnd fractions, obtained after removal of NMP by precipitation. Such a purification also caused the fractionation of the compound, *i.e.* elimination of the low molecular weight fraction. The composition, the molecular weights, the T_g and the T_m of the different fractions are given in **Table II-8**.

Table II-8. Structure and properties of the different fractions of *hb*PEUnd-*b*-*hb*PG and *hb*PG-*b*-*hb*PEUnd.

Entry	Sample	Glycidol:EUnd [a]	M_n [b] (*g/mol*)	*Đ* [b]	T_g [c] (*°C*)	T_m [c] (*°C*)	Yield [d] (*%*)
	*hb*PEUnd-*b*-*hb*PG						
1	F1	0.65:0.35	21,500	1.1	-	66	15
2	F2	0.70:0.30	15,400	1.2	-	64	7
3	F3	0.80:0.20	9,000	1.2	-6	72	12
4	*hb*PG-*b*-*hb*PEUnd	0.63:0.37	16,200	1.5	-7	23/36	50

Polymerizations were carried out in NMP at 95 °C under nitrogen by subsequent addition of comonomers by SMA (2 mL/h). [a] Calculated from ^{1}H NMR according to equation (Eq. II-6 and Eq. II-7 presented in page 132). [b] Determined via SEC-RI in DMF using linear PS standard calibration. [c] Determined *via* DSC. [d] Calculated after precipitation in diethyl ether, centrifugation and evaporation of diethyl ether.

Three fractions – named F1, F2 and F3 – were recovered (34% yield) after precipitation of *hb*PEUnd-*b*-*hb*PG in diethyl ether, followed by centrifugation (**Table II-8**, entries 1-3). Although the first fraction recovered contained the expected copolymers with a glycidol:EUnd composition of 0.65:0.35, the content in glycidol was higher in the two others, 70 % in F2 and 80 % in F3 (**Table II-8**, entries 1-3 and **Figure II-47**). Alongside, the molecular weight of the polymers decreased, from 21,500 g/mol (F1) to 9,000 g/mol (F3), with increasing the proportion of glycidol into the copolymer (**Table II-8**, entries 1-3 and **Figure II-48**). However, additional precipitation/centrifugation step would be required to fully remove NMP and low molecular weight polymers from F3 (**Figure II-47**) and F2 (**Figure II-48**), respectively. It is most likely that polyglycidol of low molecular weight formed during the copolymerization.

By comparison, only one fraction of *hb*PG-*b*-*hb*PEUnd was collected by precipitation/centrifugation with 50 % yield (**Table II-8**, entry 4). This purification step could be improved to fully remove the NMP (**Figure II-47**) and to reach higher yields. The ratio of incorporated glycidol and EUnd units of 0.63:0.37 is in agreement with the comonomer feed ratios (0.67:0.33), confirming that EUnd and glycidol properly copolymerized (**Table II-8**, entry 4 and **Figure II-47**). The broad multimodal peak obtained by SEC after purification, seemed to support that the copolymerization occurred (**Figure II-49**), even though polyglycidol of low molecular weight probably formed as well.

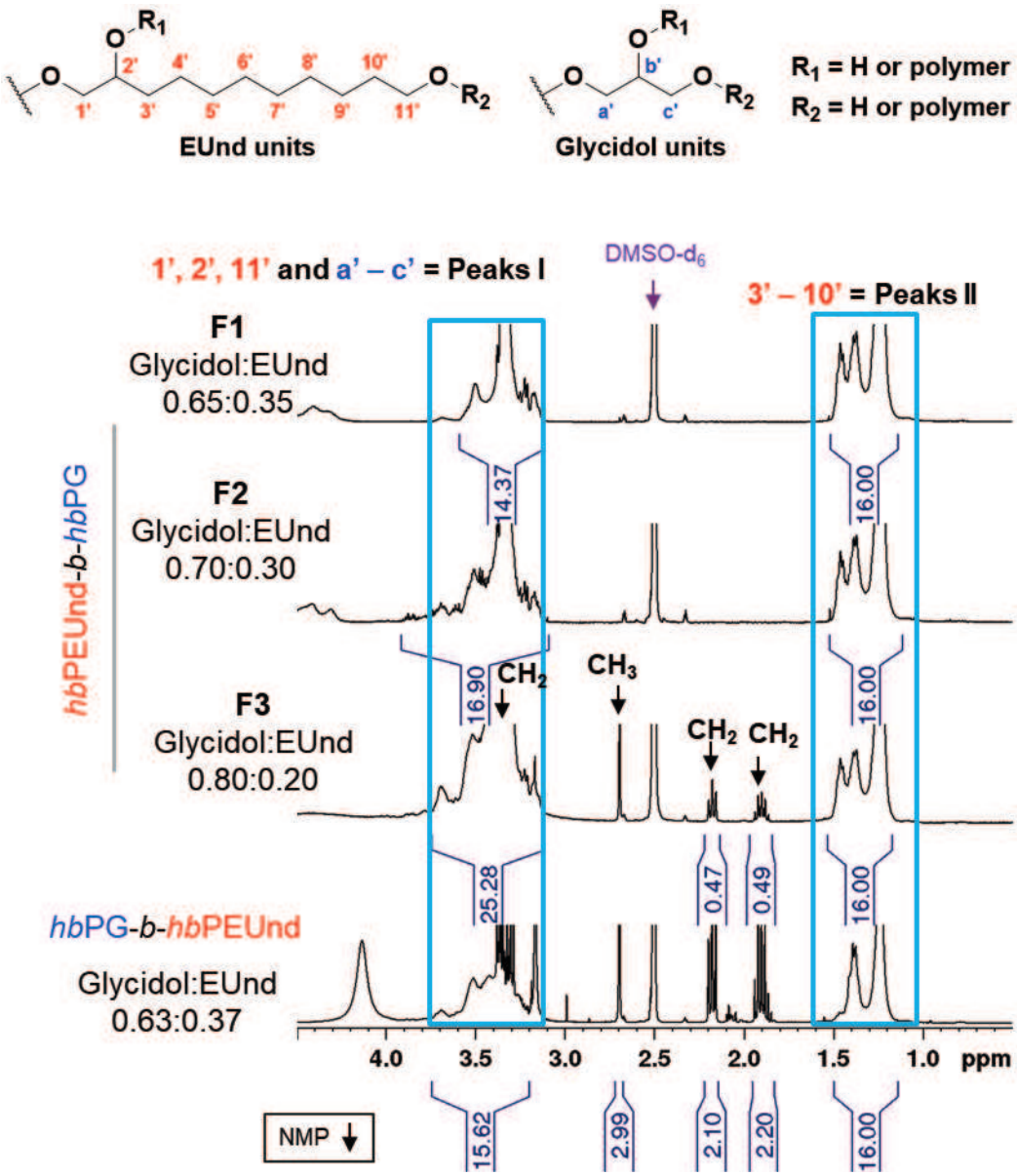

Figure II-47. ^{1}H NMR (DMSO-d_6) of *hb*PEUnd-*b*-*hb*PG and *hb*PG-*b*-*hb*PEUnd fractions obtained after purification by precipitation in diethyl ether and centrifugation.

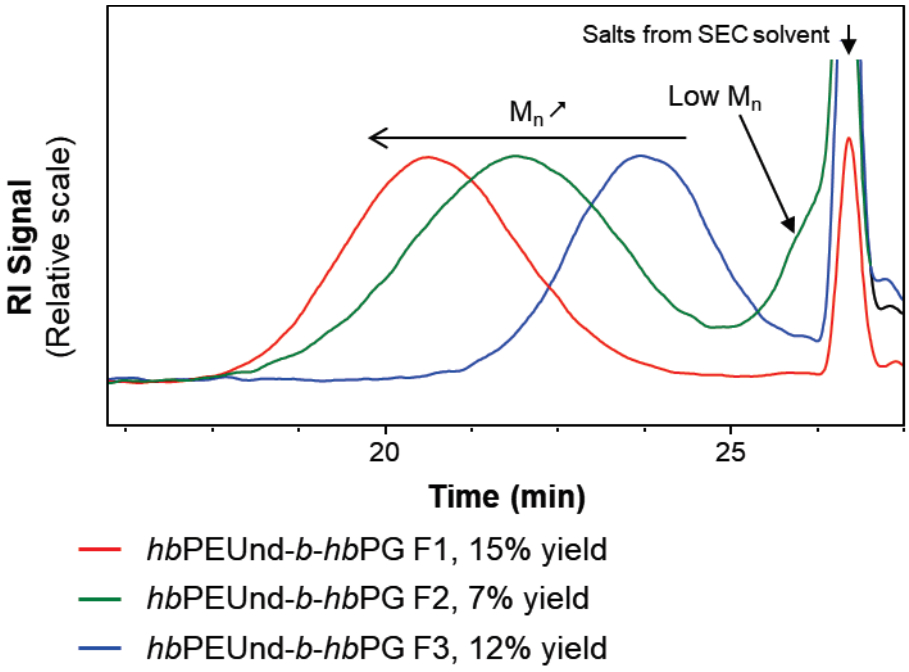

Figure II-48. SEC-RI traces (DMF) of *hb*PEUnd-*b*-*hb*PG fractions obtained after precipitation in diethyl ether and centrifugation.

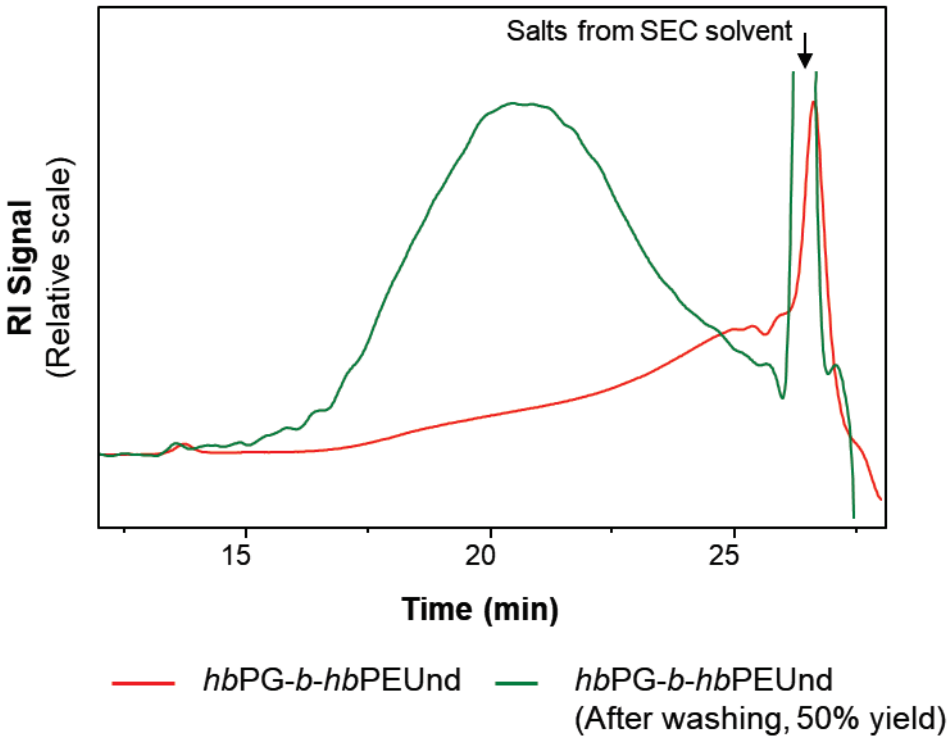

Figure II-49. SEC-RI traces (DMF) of *hb*PG-*b*-*hb*PEUnd before and after precipitation in diethyl ether and centrifugation.

4.2.3. Properties of *hb*PEUnd-*b*-*hb*PG and *hb*PG-*b*-*hb*PEUnd

The three fractions of *hb*PEUnd-*b*-*hb*PG were recovered as turbid waxes, with a similar aspect than the *hb*P(G-*co*-EUnd) obtained by random copolymerization of glycidol and EUnd. *Hhb*PG-*b*-*hb*PEUnd had a similar texture, but was found brownish. The solubility of these copolymers were quite different: while *hb*P(G-*co*-EUnd) were found to be soluble in a large number of common organic solvents and dispersible in water, *hb*PEUnd-*b*-*hb*PG fractions and *hb*PG-*b*-*hb*PEUnd were both soluble only in DMF and methanol (**Table II-9**).

Table II-9. Solubility of polyethers obtained from homo- and copo- ROMBP of EUnd and glycidol.

Sample	Water	Methanol	DMF	THF	$CHCl_3$
***hb*PEUnd**	n.s	n.s	S (T>40 °C)	n.s	S
***hb*PG**	S	S	S	S	n.s
***hb*P(G-*co*-EUnd)**	d	S	S	S	S
***hb*PEUnd-*b*-*hb*PG**	n.s	S	S	n.s	n.s
***hb*PG-*b*-*hb*PEUnd**	n.s	S	S	n.s	n.s

n.s: not souble, S: soluble, d: dispersible. Experiments performed at 1 mg/mL on ca. 10 mg samples.

As expected, the copolymers proved semi-crystalline due to the presence of the amorphous *hb*PG block and of the semi-crystalline *hb*PEUnd block. However, some differences were noted on the DSC thermograms depending on the structure and the composition of the copolymers (**Figure II-50**). For instance, the glass transition of *hb*PEUnd-*b*-*hb*PG was not easily visible on F1 and F2, but was found at -6 °C for F3, *i.e.* when increasing the proportion of glycidol. By comparison, *hb*PG-*b*-*hb*PEUnd which has the same glycidol content than F1, showed a T_g value of -7 °C, corresponding to the glass transtion of the *hb*PG core. In addition, the melting temperature of *hb*PG-*b*-*hb*PEUnd (23-36 °C) was 30 °C lower than the melting temperature of F1 from *hb*PEUnd-*b*-*hb*PG (66 °C). This might be explained by the lower size of the *hb*PEUnd shell of *hb*PG-*b*-*hb*PEUnd in comparison to the *hb*PEUnd core of *hb*PEUnd-*b*-*hb*PG.

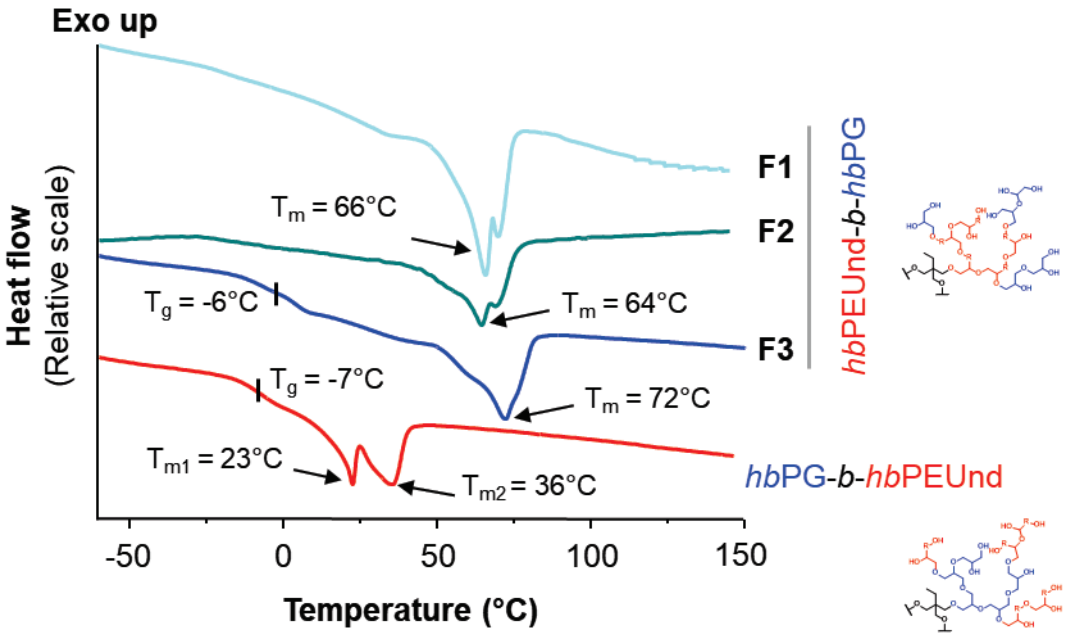

Figure II-50. DSC of *hb*PEUnd-*b*-*hb*PG and *hb*PG-*b*-*hb*PEUnd fractions obtained after purification by precipitation in diethyl ether and centrifugation.

In summary, random and sequential copolymerization of EUnd and glycidol thus enabled the formation of hyperbranched copolyethers having an amphiphilic structure, a differing melting temperatures (decreasing with the incorporation of glycidol) and a clearly visible glass transition. The modification of these features, the variation of the consistence of the polymer (from solid to viscous liquid), as well as the NMR spectra and SEC traces confirmed that copolymerization actually occurred. However, the latter analyses indicated that EUnd and glycidol often homopolymerized, homopolyethers thus generated requiring further purification. Even though more optimization of the reaction conditions is required, this work paves the way to the development of a platform of amphiphilic copolyethers, showing tunable properties.

5. Conclusions

In this chapter, the synthesis of a novel family of bio-based hyperbranched polyol polyethers involving ring-opening multibranching polymerizations was described. Unlike the well-established hyperbranched polyglycidol, hyperbranched polyethers synthesized from the bio-based 10,11-epoyxundecanol (EUnd) exhibit semi-crystalline properties and are hydrophobic. Synthesis can be achieved either in bulk or in presence of a solvent at 95 °C. Polymerization in bulk is particularly relevant from the perspective of an industrial development based on solvent-free conditions and energy savings. Several parameters, including the monomer/initiator ratio (M/TMP), the extent of TMP deprotonation or the use of solvent, were tested in order to promote the synthesis of *hb*PEUnd of high molecular weights. However, the raise of molecular weights, related to a higher M/TMP ratio, only occurred for M/TMP lower than 50. Therefore, *hb*PEUnds of 10,000 g/mol as a maximum were achieved which limited the possibilities of evaluating the properties of the molecular weights on the polymer properties. Even though the hyperbranched architecture of polyEUnd could not be totally further quantified, this work represents one of the rare example of anionic ring-opening polymerization of oxirane bearing long aliphatic chains. The random and sequential copolymerization of EUnd with glycidol enabled to extend the properties of the polyEUnd, for instance, the solubility could be manipulated in organic solvent and possibility to disperse the resulting copolyethers in water. The thermal properties could also be tuned by incorporating glycidol units. Thus, the glass transition can be modulated and the melting temperature reduced from 85 to 30 °C.

Further experiments should be performed in order to optimize the homopolymerization of EUnd and the characterization of the (co)polymers obtained, For instance, the study of the Mark-Houwink-Sakura α coefficient on a panel of polyEUnds would be interesting to confirm its dendritic structure. Copolymerization is a rather powerful tool for tuning the properties of polymers. Therefore, there is still room to develop a versatile platform of copolyethers having different compositions and topologies. The development of a platform of bio-based synthons, from vegetable oils or lignocellulosic resources, as precursors for the synthesis of aromatic and aliphatic *hb*PEthers, *via* cationic ring-opening polymerization, for instance, is also an interesting option. Finally, post-functionalization of hydroxyl chain ends of these hyperbranched (co)polyethers allows to further vary their properties, in bulk or in solution. The next chapter will discuss a method for modifying the hydroxyl groups of the hyperbranched polymer polyols.

6. References

(1) Vandenberg, E. J. Polymerization of Glycidol and Its Derivatives: A New Rearrangement Polymerization. *J Polym Sci Polym Chem Ed* **1985**, *23* (4), 915–949.

(2) Sunder, A.; Hanselmann, R.; Frey, H.; Mülhaupt, R. Controlled Synthesis of Hyperbranched Polyglycerols by Ring-Opening Multibranching Polymerization. *Macromolecules* **1999**, *32* (13), 4240–4246.

(3) Sunder, A.; Mülhaupt, R.; Frey, H. Hyperbranched Polyether-Polyols Based on Polyglycerol: Polarity Design by Block Copolymerization with Propylene Oxide. *Macromolecules* **2000**, *33* (2), 309–314.

(4) Karger-Kocsis, J.; Fröhlich, J.; Gryshchuk, O.; Kautz, H.; Frey, H.; Mülhaupt, R. Synthesis of Reactive Hyperbranched and Star-like Polyethers and Their Use for Toughening of Vinylester-Urethane Hybrid Resins. *Polymer (Guildf)* **2004**, *45* (4), 1185–1195.

(5) Wilms, D.; Wurm, F.; Nieberle, J.; Böhm, P.; Kemmer-Jonas, U.; Frey, H. Hyperbranched Polyglycerols with Elevated Molecular Weights: A Facile Two-Step Synthesis Protocol Based on Polyglycerol Macroinitiators. *Macromolecules* **2009**, *42* (9), 3230–3236.

(6) Paulus, F.; Weiss, M. E. R.; Steinhilber, D.; Nikitin, A. N.; Schütte, C.; Haag, R. Anionic Ring-Opening Polymerization Simulations for Hyperbranched Polyglycerols with Defined Molecular Weights. *Macromolecules* **2013**, *46* (21), 8458–8466.

(7) Kurniasih, I. N.; Liang, H.; Kumar, S.; Mohr, A.; Sharma, S. K.; Rabe, J. P.; Haag, R. A Bifunctional Nanocarrier Based on Amphiphilic Hyperbranched Polyglycerol Derivatives. *J Mater Chem B* **2013**, *1*, 3569.

(8) Goethals, E. J.; Trossaert, G. G.; Hartmann, P. J.; Engelen, K. Branched Polymers by Cationic Ring-opening Polymerization. *Macromol Symp* **1993**, *73* (1), 77–89.

(9) Tokar, R.; Kubisa, P.; Penczek, S.; Dworak, A. Cationic Polymerization of Glycidol: Coexistence of the Activated Monomer and Active Chain End Mechanism. *Macromolecules* **1994**, *27*, 320–322.

(10) Dworak, A.; Walach, W.; Trzebicka, B. Cationic Polymerization of Glycidol. Polymer Structure and Polymerization Mechanism. *Macromol Chem Phys* **1995**, *196*, 1963–1970.

(11) Son, S.; Shin, E.; Kim, B. S. Redox-Degradable Biocompatible Hyperbranched Polyglycerols: Synthesis, Copolymerization Kinetics, Degradation, and Biocompatibility. *Macromolecules* **2015**, *48* (3), 600–609.

(12) Son, S.; Park, H.; Shin, E.; Shibasaki, Y.; Kim, B.-S. Architecture-Controlled Synthesis of Redox-Degradable Hyperbranched Polyglycerol Block Copolymers and the Structural Implications of Their Degradation. *J Polym Sci Part A Polym Chem* **2016**, *54* (12), 1752–1761.

(13) Shenoi, R. A.; Lai, B. F. L.; Imran ul-haq, M.; Brooks, D. E.; Kizhakkedathu, J. N. Biodegradable Polyglycerols with Randomly Distributed Ketal Groups as Multi-Functional Drug Delivery Systems. *Biomaterials* **2013**, *34* (25), 6068–6081.

(14) Shenoi, R. A.; Narayanannair, J. K.; Hamilton, J. L.; Lai, B. F. L.; Horte, S.; Kainthan, R. K.; Varghese, J. P.; Rajeev, K. G.; Manoharan, M.; Kizhakkedathu, J. N. Branched Multifunctional Polyether Polyketals: Variation of Ketal Group Structure Enables Unprecedented Control over Polymer Degradation in Solution and within Cells. *J Am*

Chem Soc **2012**, *134* (36), 14945–14957.

(15) Satoh, T.; Kinugawa, Y.; Tamaki, M.; Kitajyo, Y.; Sakai, R.; Kakuchi, T. Synthesis, Structure, and Characteristics of Hyperbranched Polyterpene Alcohols. *Macromolecules* **2008**, *41* (14), 5265–5271.

(16) Rokicki, G.; Rakoczy, P.; Parzuchowski, P.; Sobiecki, M. Hyperbranched Aliphatic Polyethers Obtained from Environmentally Benign Monomer: Glycerol Carbonate. *Green Chem* **2005**, *7* (7), 529.

(17) Sheldon, R. A. The E Factor 25 Years on: The Rise of Green Chemistry and Sustainability. *Green Chem.* **2017**, *9* (1), 903–906.

(18) Sheldon, R. A. The E Factor 25 Years on: The Rise of Green Chemistry and Sustainability. *Green Chem.* **2016**.

(19) Sheldon, R. A. Green and Sustainable Manufacture of Chemicals from Biomass: State of the Art. *Green Chem.* **2014**, *16* (3), 950–963.

(20) Dunn, J. B.; Biddy, M.; Jones, S.; Cai, H.; Benavides, P. T.; Markham, J.; Tao, L.; Tan, E.; Kinchin, C.; Davis, R.; et al. Environmental, Economic, and Scalability Considerations and Trends of Selected Fuel Economy-Enhancing Biomass-Derived Blendstocks. *ACS Sustain Chem Eng* **2017**, *6* (1), 561–569.

(21) Kümmerer, K. Sustainable Chemistry: A Future Guiding Principle. *Angew Chemie Int Ed* **2017**, *56*, 2–4.

(22) Lambert, S.; Wagner, M. Environmental Performance of Bio-Based and Biodegradable Plastics: The Road Ahead. *Chem Soc Rev* **2017**, *46* (August), 6855–6871.

(23) Zhang, C.; Garrison, T. F.; Madbouly, S. A.; Kessler, M. R. Recent Advances in Vegetable Oil-Based Polymers and Their Composites. *Prog Polym Sci* **2017**, *71*, 91–143.

(24) Montero de Espinosa, L.; Meier, M. A. R. Plant Oils: The Perfect Renewable Resource for Polymer Science?! *Eur Polym J* **2011**, *47* (5), 837–852.

(25) Sharmin, E.; Zafar, F.; Akram, D.; Alam, M.; Ahmad, S. Recent Advances in Vegetable Oils Based Environment Friendly Coatings: A Review. *Ind Crops Prod* **2015**, *76*, 215–229.

(26) Lligadas, G.; Ronda, J. C.; Galià, M.; Biermann, U.; Metzger, J. O. Synthesis and Characterization of Polyurethanes from Epoxidized Methyl Oleate Based Polyether Polyols as Renewable Resources. *J Polym Sci Part A Polym Chem* **2006**, *44* (1), 634–645.

(27) Warwel, S.; Wiege, B.; Fehling, E.; Kunz, M. Ring-Opening Polymerization of Oleochemical Epoxides.Pdf. **2000**, *36*, 8–16.

(28) Warwel, S.; Brüse, F.; Demes, C.; Kunz, M. Polymers and Polymer Building Blocks from Meadowfoam Oil. *Ind Crops Prod* **2004**, *20* (3), 301–309.

(29) Ahmadi, R.; Ullah, A. Microwave-Assisted Rapid Synthesis of a Polyether from a Plant Oil Derived Monomer and Its Optimization by Box-Behnken Design. *RSC Adv* **2017**, *7* (45), 27946–27959.

(30) Testud, B. Vegetable Oils as a Platform for the Design of Novel Hyperbranched Polyesters, PhD Thesis, Université de Bordeaux, 2015.

(31) Testud, B.; Pintori, D.; Grau, E.; Taton, D.; Cramail, H. Hyperbranched Polyesters by

Polycondensation of Fatty Acid-Based ABn-Type Monomers. *Green Chem* **2017**, *19*, 259–269.

(32) Kautz, H.; Sunder, A.; Frey, H. Control of the Molecular Weight of Hyperbranched Polyglycerols. *Macromol Symp* **2001**, *163* (1), 67–74.

(33) Kainthan, R. K.; Muliawan, E. B.; Hatzikiriakos, S. G.; Brooks, D. E. Synthesis, Characterization, and Viscoelastic Properties of High Molecular Weight Hyperbranched Polyglycerols. *Macromolecules* **2006**, *39* (22), 7708–7717.

(34) Paulus, F.; Weiss, M. E. R.; Steinhilber, D.; Nikitin, A. N.; Schütte, C.; Haag, R. Anionic Ring-Opening Polymerization Simulations for Hyperbranched Polyglycerols with Defined Molecular Weights. *Macromolecules* **2013**, *46* (21), 8458–8466.

(35) García, J. I.; Pires, E.; Aldea, L.; Lomba, L.; Perales, E.; Giner, B. Ecotoxicity Studies of Glycerol Ethers in Vibrio Fi Scheri : Checking the Environmental Impact of Glycerol-Derived Solvents †. **2015**, 4326–4333.

(36) Thompson, D. S.; Markoski, L. J.; Moore, J. S. Rapid Synthesis of Hyperbranched Aromatic Polyetherimides. *Macromolecules* **1999**, *32*, 4764–4768.

(37) Jikei, M.; Nishigaya, K.; Matsumoto, K. Synthesis of Hyperbranched Poly(Ether Nitrile)s as Supporting Polymers for Palladium Nanoparticles. *Polym J* **2016**, *48* (9), 941–948.

(38) Herzberger, J.; Niederer, K.; Pohlit, H.; Seiwert, J.; Worm, M.; Wurm, F. R.; Frey, H. Polymerization of Ethylene Oxide, Propylene Oxide, and Other Alkylene Oxides: Synthesis, Novel Polymer Architectures, and Bioconjugation. *Chem Rev* **2016**, *116* (4), 2170–2243.

(39) Six, J.-L. Synthèse et Caratérisation de Poly(Oxide d'éthylène)s à Structure Dendritique, Université Bordeaux I, 1996.

(40) Brocas, A. L.; Mantzaridis, C.; Tunc, D.; Carlotti, S. Polyether Synthesis: From Activated or Metal-Free Anionic Ring-Opening Polymerization of Epoxides to Functionalization. *Prog Polym Sci* **2013**, *38* (6), 845–873.

(41) Imran ul-haq, M.; Shenoi, R. A.; Brooks, D. E.; Kizhakkedathu, J. N. Solvent-Assisted Anionic Ring Opening Polymerization of Glycidol: Toward Medium and High Molecular Weight Hyperbranched Polyglycerols. *J Polym Sci Part A Polym Chem* **2013**, *51* (12), 2614–2621.

(42) Kautz, H.; Sunder, A.; Frey, H. Control of the Molecular Weight of Hyperbranched Polyglycerols. *Macromol Symp* **2001**, *163*, 67–73.

(43) Schubert, C.; Osterwinter, C.; Tonhauser, C.; Schömer, M.; Wilms, D.; Frey, H.; Friedrich, C. Can Hyperbranched Polymers Entangle? Effect of Hydrogen Bonding on Entanglement Transition and Thermorheological Properties of Hyperbranched Polyglycerol Melts. *Macromolecules* **2016**, *49* (22), 8722–8737.

(44) Tonhauser, C.; Wilms, D.; Korth, Y.; Frey, H.; Friedrich, C. Entanglement Transition in Hyperbranched Polyether-Polyols. *Macromol Rapid Commun* **2010**, *31* (24), 2127–2132.

(45) Testud, B.; Grau, E.; Pintori, D.; Taton, D.; Cramail, H. New Branched Polymers, Their Preparation Process and Thereof. EU 14306642 A1, 2014.

(46) Olabisi, O.; Adewale, K. *Handbook of Thermoplastics*, 2nd ed.; CRC Press, Taylor & Francis Group: Boca Raton, 2015.

(47) Gnanou, Y.; Fontanille, M. *Organic and Physical Chemistry of Polymers*; 2007.

(48) Leibig, D.; Seiwert, J.; Liermann, J. C.; Frey, H. Copolymerization Kinetics of Glycidol and Ethylene Oxide, Propylene Oxide, and 1,2-Butylene Oxide: From Hyperbranched to Multiarm Star Topology. *Macromolecules* **2016**, *49* (20), 7767–7776.

(49) Seiwert, J.; Herzberger, J.; Leibig, D.; Frey, H. Thioether-Bearing Hyperbranched Polyether Polyols with Methionine-Like Side-Chains: A Versatile Platform for Orthogonal Functionalization. *Macromol Rapid Commun* **2017**, *38*, 1600457.

(50) Schömer, M.; Seiwert, J.; Frey, H. Hyperbranched Poly(Propylene Oxide): A Multifunctional Backbone-Thermoresponsive Polyether Polyol Copolymer. *ACS Macro Lett* **2012**, *1* (7), 888–891.

(51) Yao, Y.; Suzuki, Y.; Seiwert, J.; Steinhart, M.; Frey, H.; Butt, H.-J.; Floudas, G. Capillary Imbibition, Crystallization, and Local Dynamics of Hyperbranched Poly(Ethylene Oxide) Confined to Nanoporous Alumina. *Macromolecules* **2017**, *50* (21), 8755–8764.

(52) Niederer, K.; Schüll, C.; Leibig, D.; Johann, T.; Frey, H. Catechol Acetonide Glycidyl Ether (CAGE): A Functional Epoxide Monomer for Linear and Hyperbranched Multi-Catechol Functional Polyether Architectures. *Macromolecules* **2016**, *49* (5), 1655–1665.

(53) Knischka, R.; Lutz, P. J.; Sunder, A.; Mülhaupt, R.; Frey, H. Functional Poly(Ethylene Oxide) Multiarm Star Polymers: Core-First Synthesis Using Hyperbranched Polyglycerol Initiators. *Macromolecules* **2000**, *33* (2), 315–320.

(54) Schubert, C.; Schömer, M.; Steube, M.; Decker, S.; Friedrich, C.; Frey, H. Systematic Variation of the Degree of Branching (DB) of Polyglycerol via Oxyanionic Copolymerization of Glycidol with a Protected Glycidyl Ether and Its Impact on Rheological Properties. *Macromol Chem Phys* **2018**, 1700376.

(55) Seiwert, J.; Herzberger, J.; Leibig, D.; Frey, H. Thioether-Bearing Hyperbranched Polyether Polyols with Methionine-Like Side-Chains: A Versatile Platform for Orthogonal Functionalization. *Macromol Rapid Commun* **2017**, *38*, 1600457.

7. Experimental and supporting information

7.1.Chemicals

All reagents and solvents were used as received, unless otherwise mentioned. 3-Chloroperbenzoic acid (mCPBA, < 77 %), potassium methoxide (MeOK, 95 %), sodium hydride (NaH, 95 %), iodomethane (MeI, 99 %), ethyl vinyl ether (99%), glycidol (96 %) and potassium bis(trimethylsilyl)amide (KHMDS, 95 %) were obtained from Sigma Aldrich. 10-Undecen-1-ol (99 %) and trimethylol propane (TMP, 98 %) were supplied from abcr GmbH.

Glycidol and solvents used for polymerization were always dried over CaH_2 and distilled prior to use. THF was dried over a sodium and toluene over butyl lithium. TMP and 10,11-epoxyundecanol (EUnd) were *via* toluene heteroazeotrope.

7.2. Protocols

7.2.1. Synthesis of EUnd

In an Erlenmeyer, 15 g of mCPBA (67 mmol) was dissolved/suspended in 250 mL of dichloromethane (DCM). The mixture was cooled down to 0 – 5 °C and 8 g of 10-undecen-1-ol (47 mmol) were added to the solution. The reaction medium was allowed to warm to room temperature and let for stirring overnight. After completion – the reaction was monitored by ^{1}H NMR –, the solution was cooled to -20 °C to precipitate the residual mCPBA. The mixture was then filtrated and washed with cold DCM and the filtrate was collected and poured in a separating funnel. The DCM organic phase was washed three times with 100 mL of saturated Na_2CO_3, four times with 100 mL of saturated $NaHCO_3$ and twice with 200 mL of saturated brine. DCM was then evaporated and the EUnd was isolated by flash chromatography using cyclohexane:ethyl acetate as eluents. The fractions of pure EUnd were gathered and the solvents were evaporated overnight under vacuum and then dried with a toluene azeotrope under inert atmosphere.

7.2.2. Standard procedure for the ROMBP of EUnd in dioxane (0.3 mL/mL), at M/TMP = 50 and at 10 % of TMP deprotonation

7.2.2.1. Initiator preparation

In a Schlenk flask, 768 µL of TMP solution in methanol (0.1 mmol, 17.5 mg/mL) and 140 µL of MeOK solution in methanol (0.03 mmol, 0.015 g/mL) were poured under a nitrogen flow. The mixture was stirred for at least 30 min at 50 °C and methanol was then removed under vacuum overnight at 50 °C. 0.3 mL of dioxane were added; the solution was stirred until being homogeneous (ca. 30 min).

7.2.2.2. Monomer addition

"Semi-batch" addition (SBA)

In a Schlenk flask, 1 mL of EUnd (5.0 mmol) was added – by aliquots of 100 µL every 3 min in order to simulate a slow monomer addition – under a nitrogen flow into the reaction medium. The reactants were stirred at 95 °C until reaching full conversion (or until no conversion evolution was observed anymore). The reaction was quenched with methanol. When used, solvents were removed by evaporation.

Slow monomer addition (SMA)

In a Schlenk flask, 1 mL of EUnd (5 mmol) was added - at a 2 mL/h flow using a syringe pump – under a nitrogen flow into the reaction medium. The reactants were stirred at 95 °C until reaching full conversion (or until no conversion evolution was observed anymore). The reaction was quenched with methanol. When used, solvents were removed by evaporation.

7.2.3. Synthesis of the model molecules

7.2.3.1. Terminal unit model molecule (T_m) – 11-methoxyundecane-1,10-diol

In a Schlenk flask, 3 mL of MeOH (74 mmol) and 0.12 g KOH (2.1 mmol) were stirred 15 min at 60 °C. The temperature was increased at 70 °C and 2 mL of EUnd (10 mmol) were added dropwise to the solution, which was let for stirring 1 h. HCl was added dropwise until reaching a pH of 7. The mixture was then filtrated and methanol was removed from the filtrate, which was solubilized in DCM. The organic phase was washed three times with water. DCM was finally evaporated to yield transparent viscous liquid.

7.2.3.2. Dendritic unit model molecule (D_m) – 1,2,11-trimethoxyundecane

In a Schlenk flask, 2.2 mL of a solution of NaH in THF (4.6 mmol, 0.05 g/mL) was cooled at 0 °C and 0.5 g of T_m (2.3 mmol) were added dropwise. The reaction medium was allowed to warm to room temperature and let for stirring for 2 h, during which the solution turned from grey to white. 0.5 mL of MeI (7.9 mmol) were added to the reactive mixture, which was heated at 60 °C and let for stirring overnight. The reaction was then quenched using a solution of saturated NH_4Cl. The product was solubilized in DCM and washed three times with water in a separating funnel. DCM was finally evaporated yielding a transparent viscous liquid.

* THF was delivered from a column solvent purification apparatus.

7.2.3.3. Linear 1,11 model molecule ($L111_m$) – 1,11-dimethoxyundecan-2-ol

11-methoxyundec-1-ene

In a Schlenk flask, 2.9 mL of a solution of NaH in THF (6.0 mmol, 0.05 g/mL) was cooled at 0 °C and 1 g of 10-undecen-1-ol (2.9 mmol) was added dropwise. The reaction medium was allowed to warm to room temperature and let for stirring for 2 h, during which the solution turned from grey to white. 0.6 mL of MeI (9.5 mmol) were added to the reactive mixture, which was heated to 60 °C overnight. The reaction was then quenched using a solution of saturated NH_4Cl. The product was solubilized in DCM and washed three times with water in a separating funnel. DCM was finally evaporated yielding a transparent viscous liquid.

2-(9-methoxynonyl)oxirane

11-methoxyundec-1-ene was epoxidized with mCPBA, following the same procedure as for epoxidation of 10-undecen-1-ol.

1,11-dimethoxyundecan-2-ol

In a Schlenk flask, 3 mL of MeOH (74 mmol) and 0.12 g KOH (2.1 mmol) were stirred 15 min at 60 °C. The temperature was increased at 70 °C and 0.42 g of 2-(9-methoxynonyl)oxirane (2.1 mmol) were added dropwise to the solution, which was let for stirring for 1 h. HCl was added dropwise until reaching a pH of 7. The mixture was then filtrated and methanol was removed from the filtrate, which was solubilized in DCM. The organic phase was washed three times with water. DCM was finally evaporated to yield transparent viscous liquid.

7.2.3.4. Linear 1,2 model molecule ($L12_m$) – 10,11-dimethoxyundecan-1-ol

2-(9-(1-ethoxyethoxy)nonyl)oxirane

In a Schlenk flask, 1 mL of EUnd (5.0 mmol), 2 mL of ethyl vinyl ether (ca. 20 mmol) were stirred at 0 °C. 0.1 g of *p*-toluenesulfonic acid were added in small quantities to the reactive mixture, which was allowed to warm to room temperature and let under stirring for 3 h. The reaction was quenched by addition of 1 mL of saturated $NaHCO_3$ solution.

11-(1-ethoxyethoxy)-1-methoxyundecan-2-ol

In a Schlenk flask, 3 mL of MeOH (74 mmol) and 0.12 g KOH (2.1 mmol) were stirred 15 min at 60 °C. The temperature was increased at 70 °C and 0.54 g of 2-(9-(1-ethoxyethoxy)nonyl)oxirane (2.1 mmol) were added dropwise to the solution, which was let for stirring for 1 h. HCl was added dropwise until reaching a pH of 7. The mixture was then filtrated and methanol was removed from the filtrate, which was solubilized in DCM. The organic phase was washed three times with water. DCM was finally evaporated to yield transparent viscous liquid.

10,11-dimethoxyundecan-1-ol

In a Schlenk flask, 2 mL of a solution of NaH in THF (4.2 mmol, 0.05 g/mL) was cooled at 0 °C and 0.5 g of 11-(1-ethoxyethoxy)-1-methoxyundecan-2-ol (1.7 mmol) were added dropwise. The reaction medium was allowed to warm to room temperature and let for stirring for 2 h, the solution turned from grey to brown and white. 0.5 mL of MeI (7.9 mmol) were added to the reactive mixture, which was heated at 60 °C and let for stirring overnight. The reaction was then quenched using a solution of saturated NH_4Cl. Three phases formed. The upper, containing the product, was collected in flask from which THF was evaporated, yielding a transparent viscous liquid.

7.2.4. Standard procedure for the random copolymerization of EUnd and glycidol into *hb*P($G_{0.67}$-*co*-$EUnd_{0.33}$)

In a Schlenk flask, 1.69 mL of TMP solution in methanol (0.22 mmol, 17.5 mg/mL) and 310 µL of MeOK solution in methanol (0.07 mmol, 0.015 g/mL) were poured under a nitrogen flow. The mixture was stirred for at least 30 min at 50 °C and methanol was then removed under vacuum overnight at 50 °C.

A mixture containing 0.75 mL of EUnd (3.8 mmol) and 0.48 mL of glycidol (7.3 mmol) was added – by aliquots of 100 µL every 3 min in order to simulate a slow monomer addition – under a nitrogen flow into the reaction medium. The reactants were stirred at 95 °C until reaching full conversion (or until no conversion evolution was observed anymore). The reaction was quenched with methanol.

7.2.5. Standard procedure for the sequential copolymerization of EUnd and glycidol into *hb*PEUnd-*b*-*hb*PG

In a Schlenk flask, 192 µL of TMP solution in methanol (0.025 mmol, 17.5 mg/mL) and 330 µL of MeOK solution in methanol (0.71 mmol, 0.015 g/mL) were poured under a nitrogen flow. The mixture was stirred for 30 min at 50 °C and methanol was then removed under vacuum overnight at 50 °C. 2 mL of NMP were added; the solution was mechanically stirred until being homogeneous (ca. 45 min).

Into this reaction medium, 0.1 mL of EUnd (0.5 mmol) was added - at a 2 mL/h flow using a syringe pump – under a nitrogen flow. The reactants were stirred at 95 °C for 1 h, *i.e.* until reaching full conversion (or until no conversion evolution was observed anymore). 0.2 mL of KHMDS solution in THF (0.05 mmol, 0.048 g/mL) were added in order to deprotonate 10 % of the OH of polyEUnd formed for 30 min.

Then, 0.9 mL of EUnd (4.5 mmol) was slowly added (2 mL/h) and the reaction mixture was let under stirring for 21 h. 0.83 mL of KHMDS solution in THF (0.2 mmol, 0.048 g/mL) and 0.5 mL of NMP were added before 30 min of stirring.

Finally, 0.66 mL of glycidol was incorporated (2 mL/h) to the reaction, which was stirred for 4h30 and quenched with methanol. The product precipitated in diethyl ether and collected after centrifugation as a turbid wax. The procedure was repeated 3 times, yielding 3 fractions representing 35 w% of the total mass of comonomers incorporated.

7.2.6. Standard procedure for the sequential copolymerization of EUnd and glycidol into *hb*PG-*b*-*hb*PEUnd

In a Schlenk flask, 383 µL of TMP solution in methanol (0.050 mmol, 17.5 mg/mL) and 210 µL of MeOK solution in methanol (0.045 mmol, 0.015 g/mL) were poured under a nitrogen flow. The mixture was stirred for 30 min at 50 °C and methanol was then removed under vacuum overnight at 50 °C. 1 mL of NMP were added; the solution was mechanically stirred until being homogeneous (ca. 30 min).

Into this reaction medium, 0.18 mL of glycidol (2.7 mmol) was added - at a 2 mL/h flow using a syringe pump – under a nitrogen flow. The reactants were stirred at 95 °C for 2 h, *i.e.* until reaching full conversion (or until no conversion evolution was observed anymore). 1.12 mL of KHMDS solution in THF (0.27 mmol, 0.048 g/mL) were added in order to deprotonate 5 % of the OH of *hb*PG. 2mL of NMP were added to enhance the solubility of the salts (1h30 of stirring).

Then, 0.48 mL of glycidol (7.3 mmol) was slowly added (2 mL/h) and the reaction mixture was let under stirring for 3h30. 0.96 mL of KHMDS solution in THF (0.2 mmol, 0.048 g/mL) were added, followed by 30 min of stirring).

Finally, 1 mL of EUnd was incorporated (2 mL/h). The reaction was let under stirring for 15h30, before being quenched with methanol. The product was precipitated in diethyl ether and collected after centrifugation as a brownish wax in 50 % yield.

7.3. NMR

7.3.1. *Hb*PEUnd

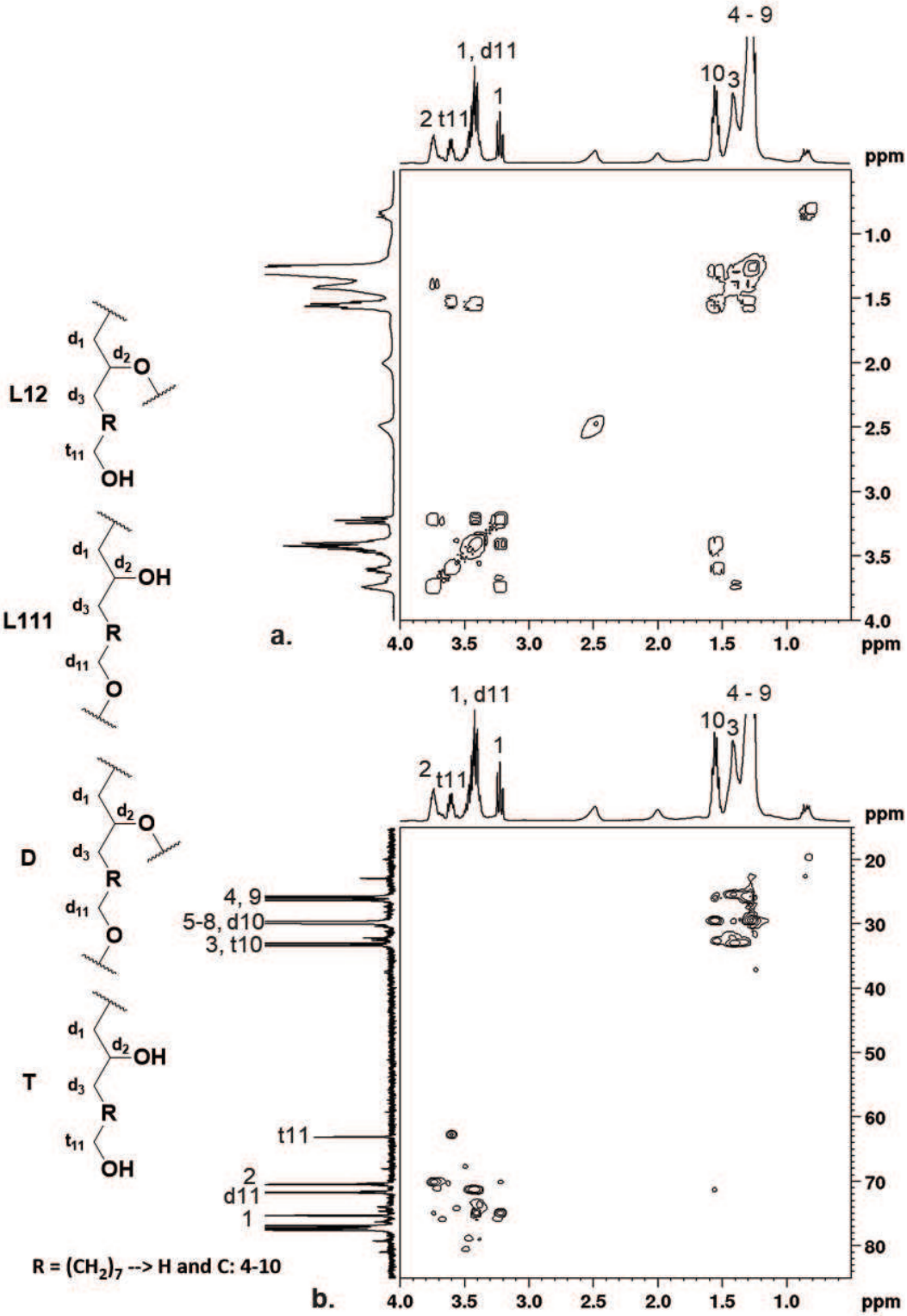

Figure SI.II-51. a. COSY and b. HSQC traces of polymer obtained by ROMBP of EUnd, in bulk, at M/TMP = 50 and at TMP deprotonation = 10 %.

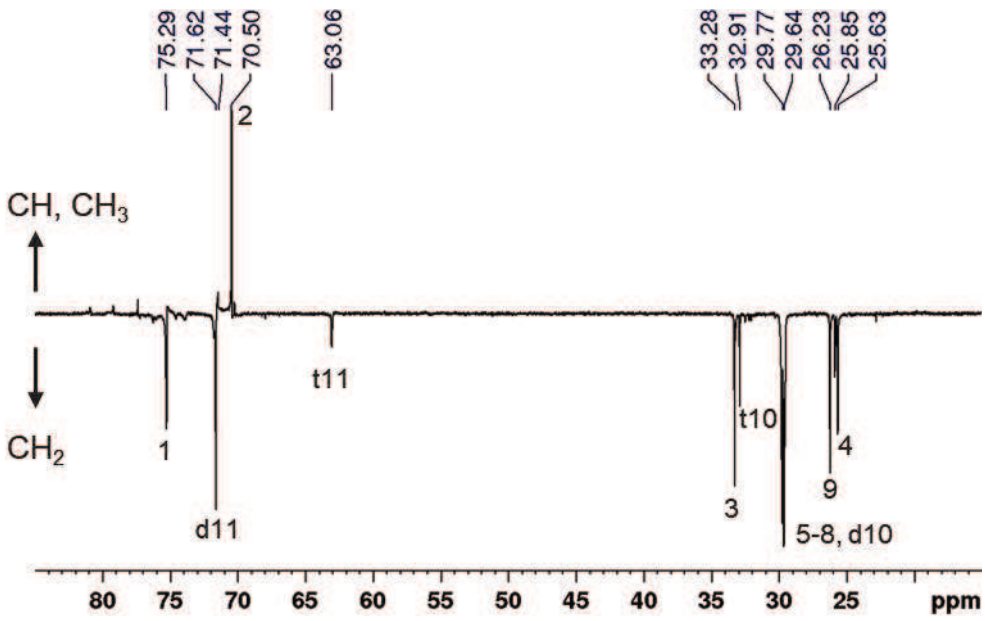

Figure SI.II-52. DEPT-135 traces of polymer obtained by ROMBP of EUnd, in bulk, at M/TMP = 50 and at TMP deprotonation = 10 %.

7.3.2. Model molecules

7.3.2.1. Terminal unit model molecule (T_m) – 11-methoxyundecane-1,10-diol

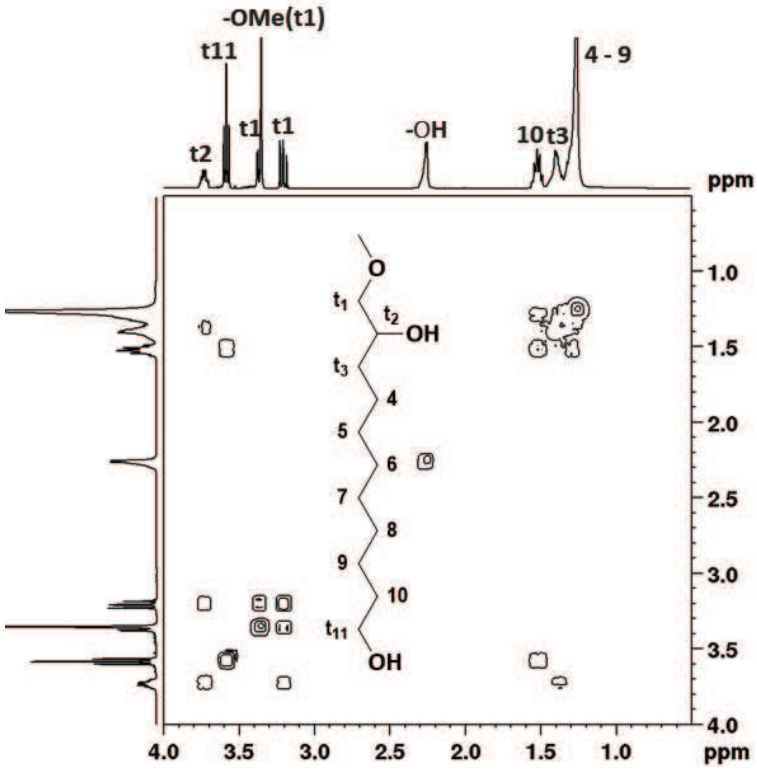

Figure SI.II-53. COSY spectrum of T_m.

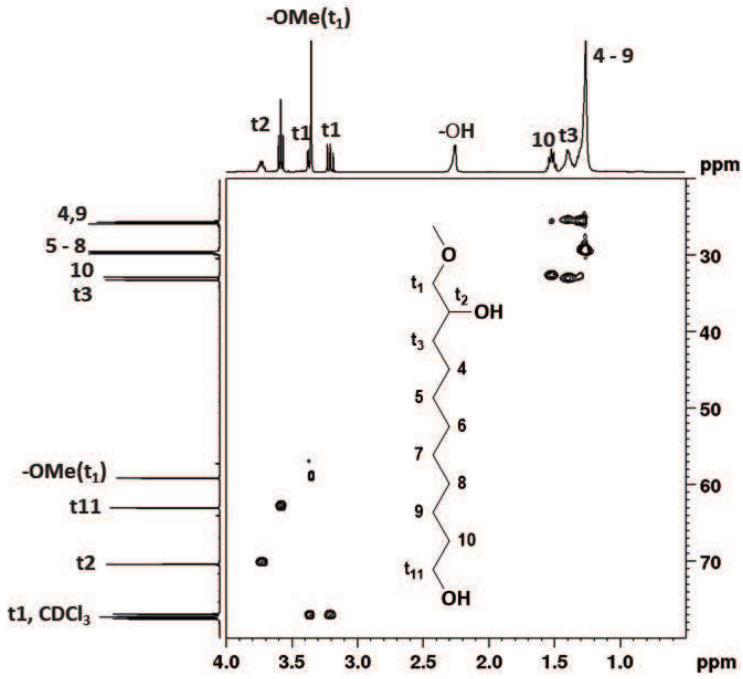

Figure SI.II-54. HSQC spectrum of T_m.

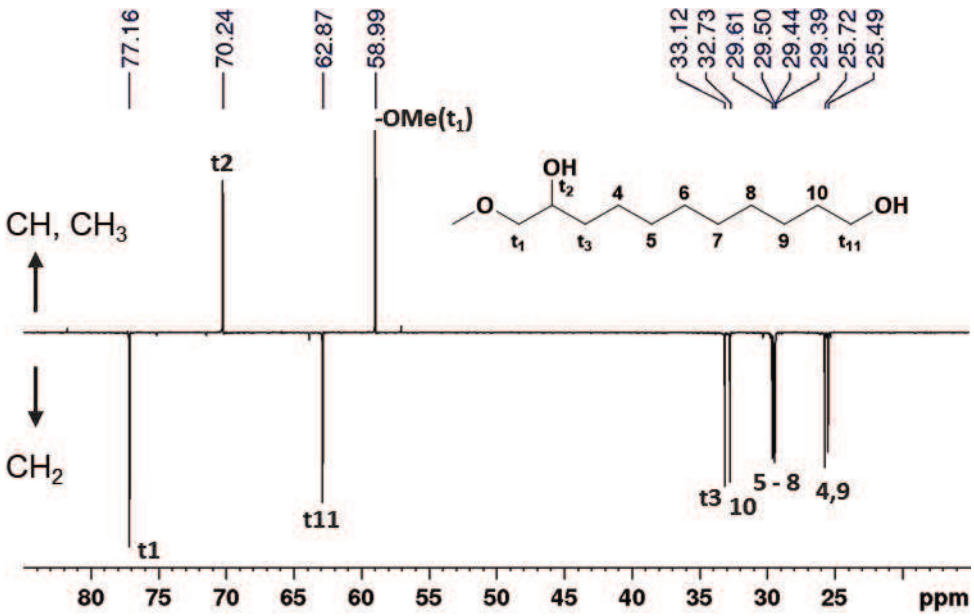

Figure SI.II-55. DEPT-135 spectrum of T_m.

7.3.2.2. Dendritic unit model molecule (D_m) – 1,2,11-trimethoxyundecane

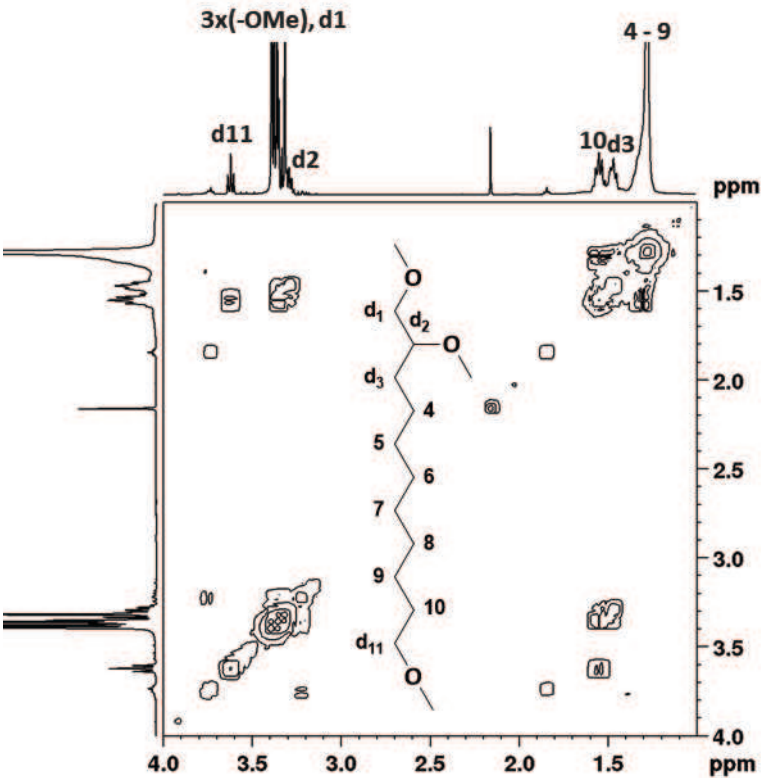

Figure SI.II-56. COSY spectrum of D_m.

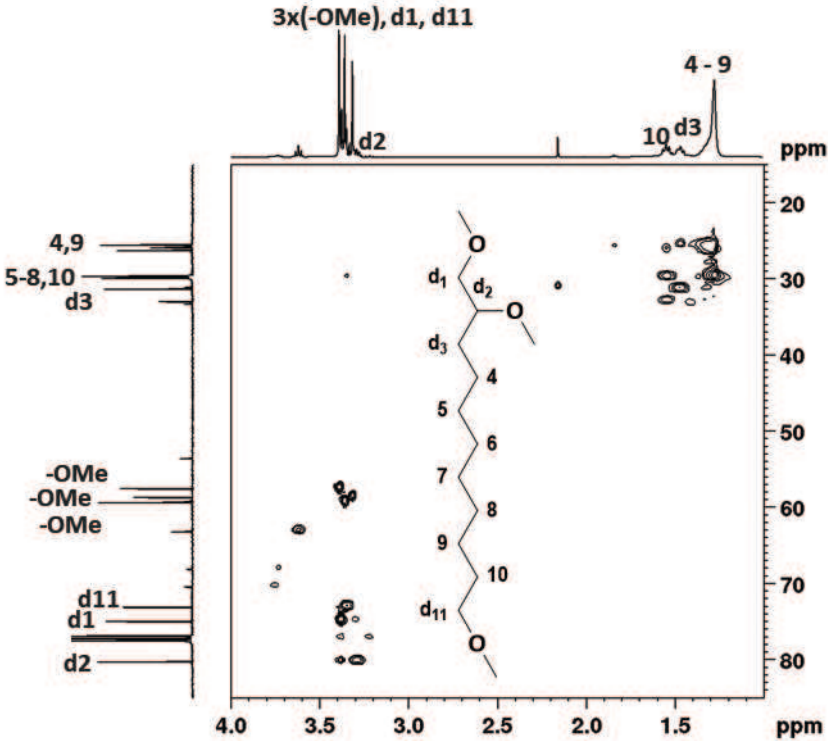

Figure SI.II-57. HSQC spectrum of D_m.

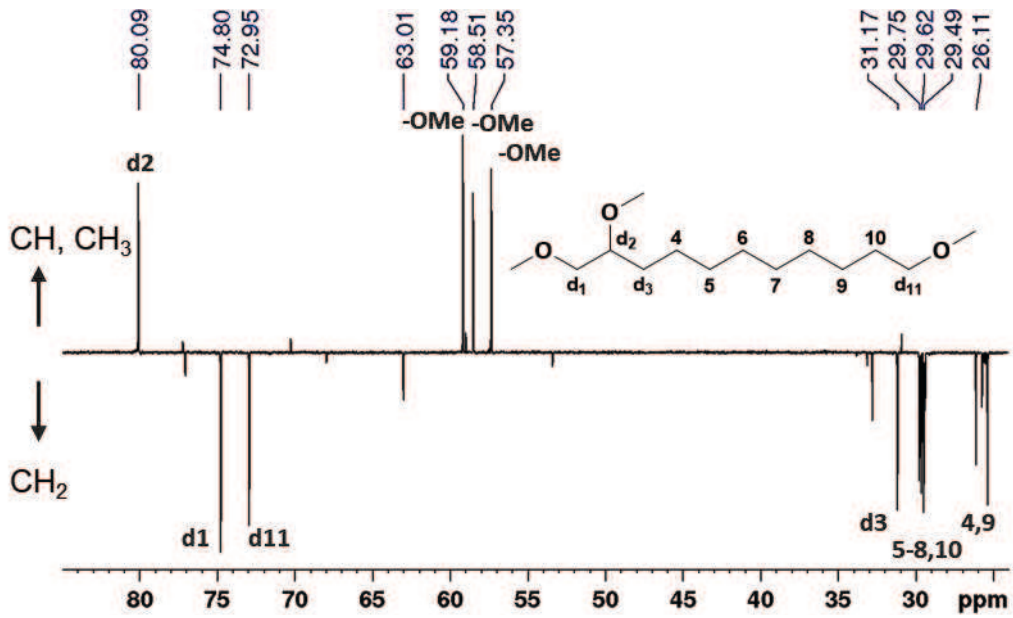

Figure SI.II-58. DEPT-135 spectrum of D_m.

7.3.2.3. Linear 1,2 model molecule ($L12_m$) – 1,11-dimethoxyundecan-2-ol

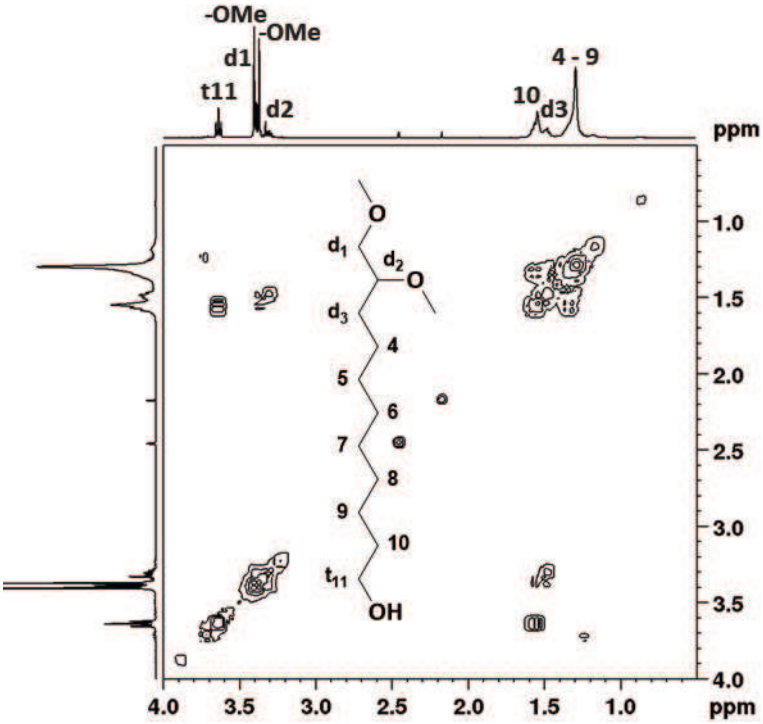

Figure SI.II-59. COSY spectrum of $L12_m$.

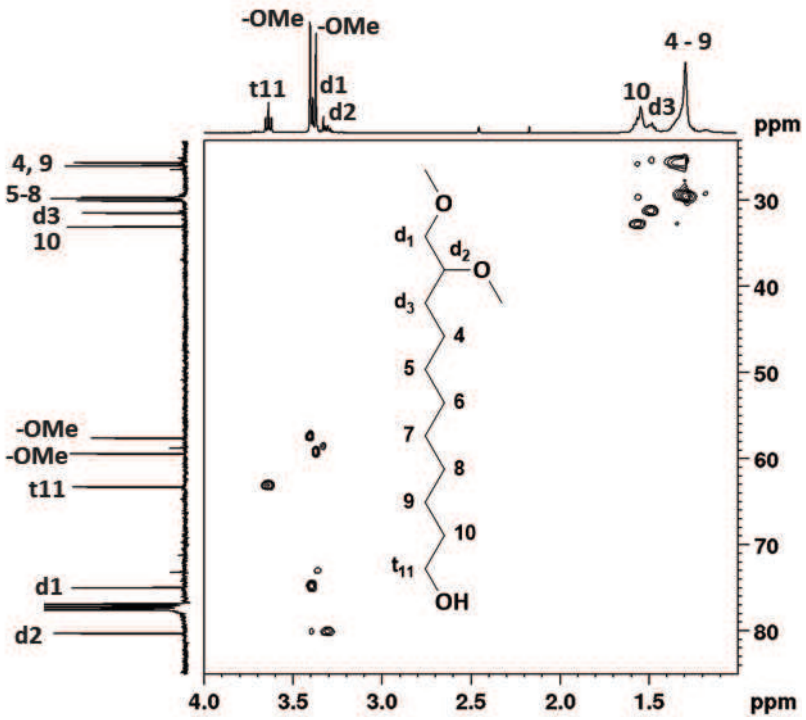

Figure SI.II-60. HSQC spectrum of L12$_m$.

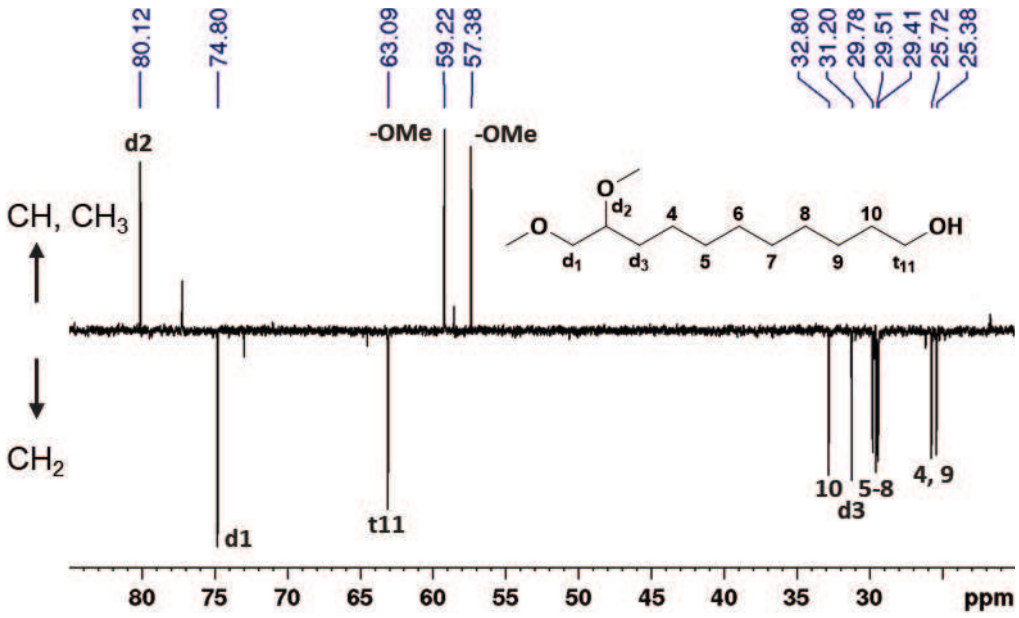

Figure SI.II.61. DEPT-135 spectrum of L12$_m$.

7.3.2.4. Linear 1,11 model molecule ($L111_m$) – 10,11-dimethoxyundecan-1-ol

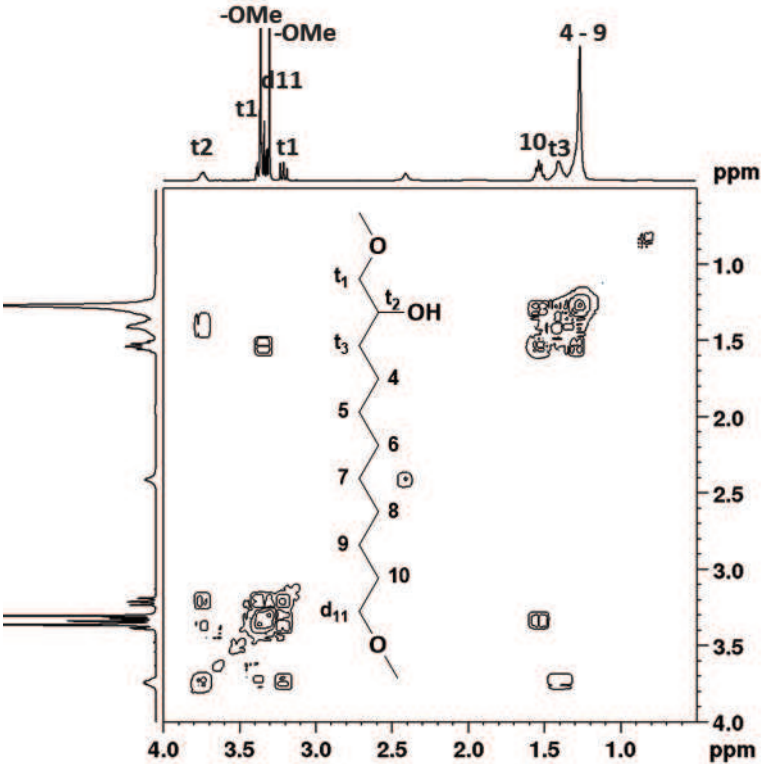

Figure SI.II-62. COSY spectrum of $L111_m$.

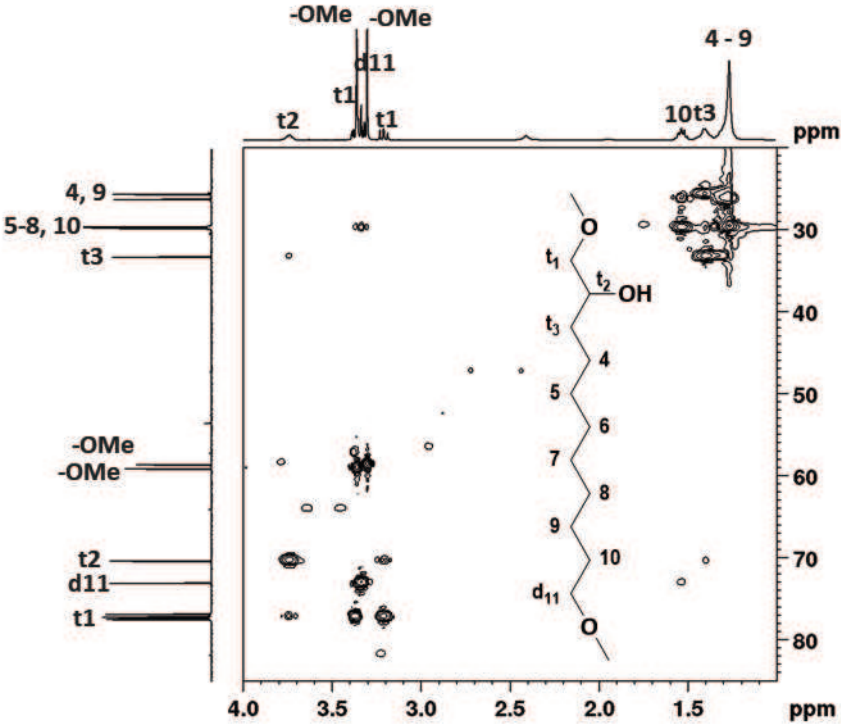

Figure SI.II-63. HSQC spectrum of $L111_m$.

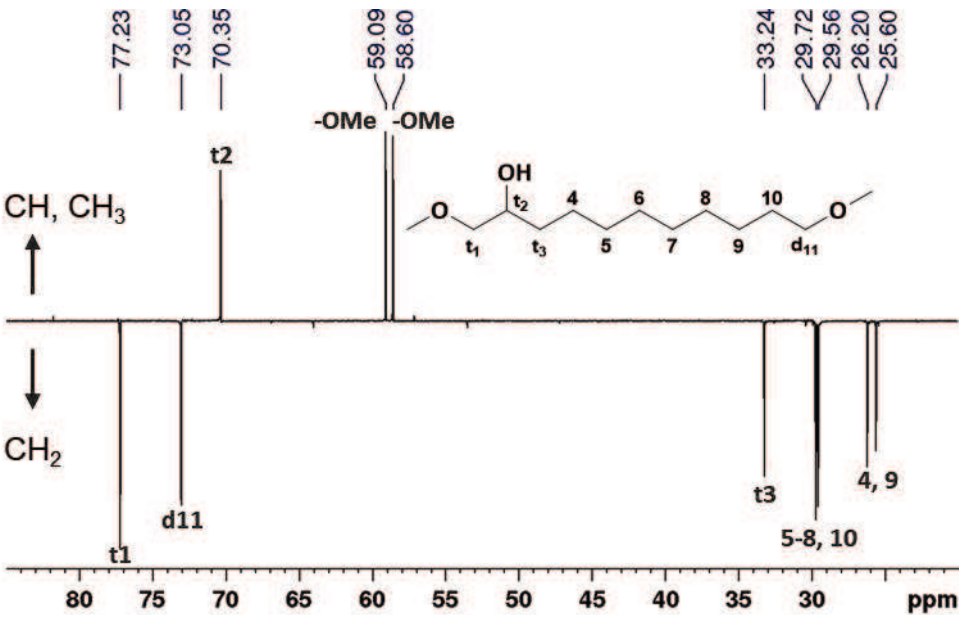

Figure SI.II-64. DEPT-135 spectrum of $L111_m$.

7.3.3. *Hb*PG obtained by ROMBP of glycidol

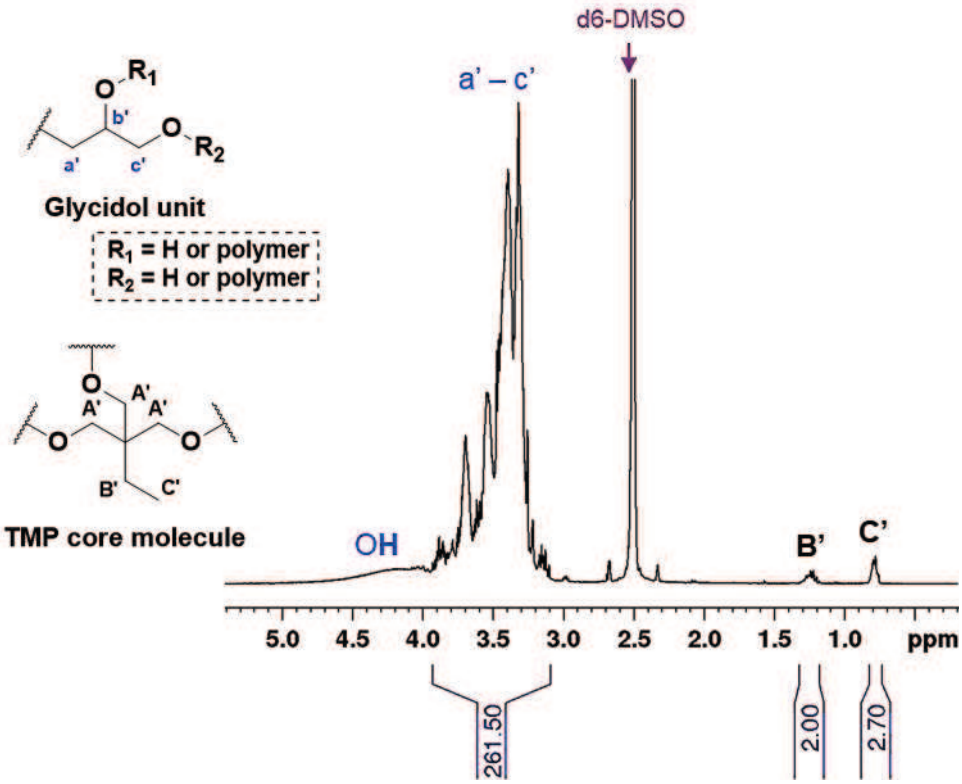

Figure SI.II-65. ^{1}H NMR (DMSO-d_6) of *hb*PG obtained by ROMBP of glycidol in bulk, at M/TMP = 50 and at TMP deprotonation = 10 %.

CHAPTER III

Functionalization and properties of hyperbranched polyesters

Keywords: Hyperbranched polyester, functionalization, succinic anhydride, unimolecular micelles, pH-sensitive, acryloyl chloride, copolymerization, 3D networks.

TABLE OF CONTENTS

1. INTRODUCTION 167

2. DERIVATIZATION OF HYPERBRANCHED POLYESTER POLYOLS WITH SUCCINIC ANHYDRIDE 170

2.1. Functionalization with succinic anhydride 171

2.2. Properties of hyperbranched polyester polysuccinate's 176

2.3. Conclusion 185

3. DERIVATIZATION OF HYPERBRANCHED POLYESTER POLYOLS WITH ACRYLOYL CHLORIDE 187

3.1. Functionalization with acryloyl chloride 190

3.2. Hyperbranched polyester polyacrylates as curing agents for the production of cross-linked PMMA's 195

3.3. Copolymerization of hyperbranched polyester polyacrylate with styrene 206

3.4. Conclusion 210

4. CONCLUSION AND OUTLOOKS 212

5. REFERENCES 213

6. EXPERIMENTAL AND SUPPORTING INFORMATION 218

6.1. Chemicals 218

6.2. Protocols 218

6.3. Appendices 222

1. Introduction

In the previous HyperBioPol project developed between the Cramail and the Taton's teams at the LCPO, and funded by the SAS PIVERT, a set of hyperbranched polyesters (*hb*PEsters) was designed from bio-based AB_n-type monomers ($n \geq 2$). These were synthesized in high scale by selective functionalization of fatty acid methyl esters (FAMEs).[1–3] In particular, synthesis of methyl 9,10-dihydroxystearate (M2HS) was achieved in high scale by hydrolysis of epoxidized high oleic sunflower oil. Polycondensation of M2HS into hyperbranched polyester polyols (*hb*PEster-OH), referred to as M2HS-*hb*PEster, was studied in details.[4] This polymer synthesis could be scaled up from gram (LCPO) to kilogram (ITERG; **Figure III-1**) and the physico-chemical properties of M2HS-*hb*PEster were also assessed, with the aim of valorising the potential of these compounds in a set of applications.

As has been extensively studied in the literature, derivatization of hyperbranched polymers, including post-functionalization of their backbone and/or their terminal chain units, is a classical means to tune their overall properties.[5,6] For instance, their solubility, crystallinity as well as their intrinsic reactivity can be adjusted in order to meet specific applications.[6–8,9] This is particularly true as far as chain end modification is concerned, due to the large number of these terminal units, *i.e.* at the periphery of globular-shaped hyperbranched structures.[10–14]

In this part of the FunHyBioPol project, we further exploited the presence of the numerous hydroxyl-end groups present in M2HS-*hb*PEsters, in order to broaden the potential applications of this bio-based polymer platform (**Figure III-2**). The derivatization of M2HS-*hb*PEsters with succinic anhydride in the one hand, and with acryloyl chloride on the other hand, was thus undertaken so as to produce water-soluble *hb*PEster-$COOH_x$ and reactive acrylate-terminated *hb*PEster-A_x, respectively. The first part of this chapter is dedicated to the functionalization procedure and to the structural characterization of the as-obtained functionalized *hb*PEsters using various techniques, including ^{1}H NMR spectroscopy, SEC and DSC analyses. In the second part, specific properties and potential applications of these modified M2HS-*hb*PEsters were investigated. More particularly, the behaviour of compounds consisting of carboxy-end groups, denoted as *hb*PEster-$COOH_x$, was examined in ethanol and in alkaline water solution, allowing us to determine their hydrodynamic and gyration radii (R_H and R_g) by X-ray scattering (SAXS/WAXS), diffusion light scattering (DLS) and viscosity measurements. These analyses were carried out in collaboration with the group of Prof. Laurence Ramos in particular with

Dr. Salvatore Constanzo, working as a postdoctoral fellow at L2C in Montpellier. In addition, acrylate-terminated derivatives, denoted as *hb*PEster-A_x, were further copolymerized with methyl methacrylate *via* free-radical copolymerization in view of creating 3D copolymeric networks with improved properties. The structure and the thermo-mechanical properties of these materials were thus evaluated.

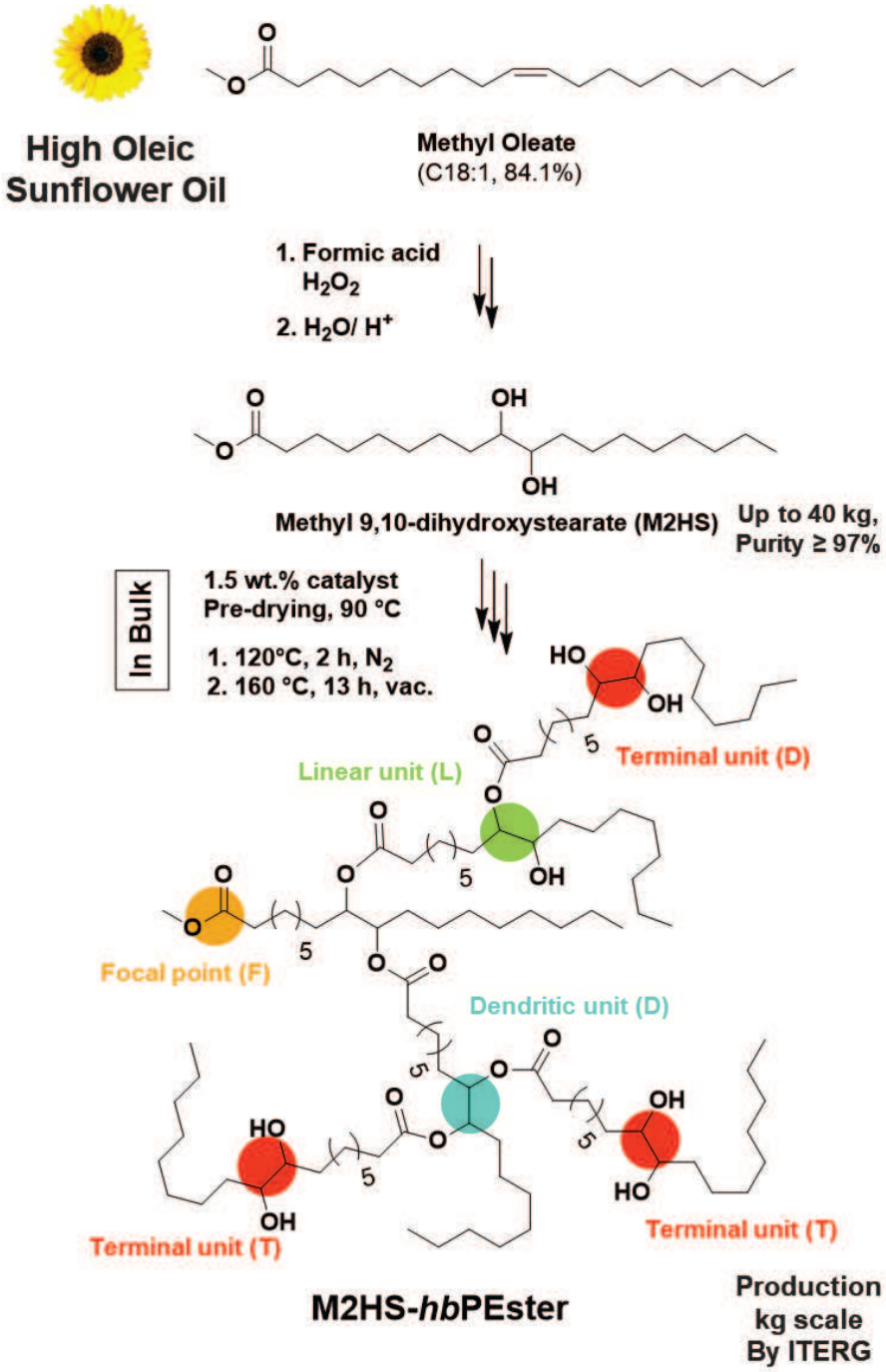

Figure III-1. From high oleic sunflower oil to M2HS-*hb*PEsters.[1–3]

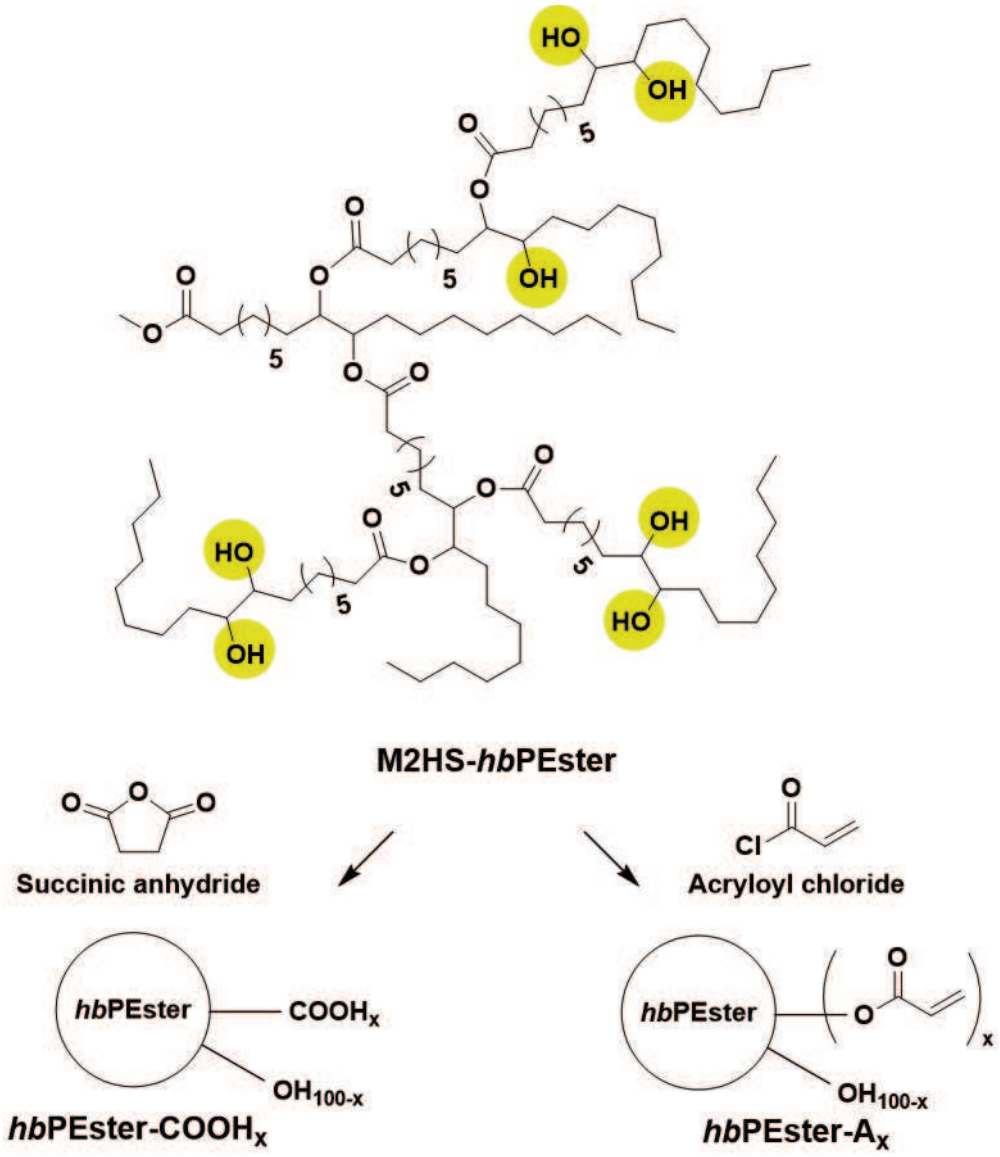

Figure III-2. Functionalization of M2HS-*hb*PEsters with succinic anhydride and acryloyl chloride.

2. Derivatization of hyperbranched polyester polyols with succinic anhydride

Stimuli-responsive hyperbranched polymers have drawn an increasing attention in the last decades; this specific topic has recently been reviewed.[15–17] Conformational changes of polymers using stimuli like light, pH, temperature or pressure is expected to modify the properties, e.g. the solubility, of hyperbranched polymers. Compounds displaying a pH-sensitiveness are particularly relevant for controlling the encapsulation and the release of drugs,[18] dyes or active molecules in general.[16,19] They may also serve as nanoreactors, [20] for instance for catalysis purpose, or as phase-transfer agents, stabilizers,[20] light-emitting nanocapsules[21] or as optical properties modifiers. Similarly to linear polymers, pH-responsive hyperbranched polymers can be divided in two categories, including pH-degradable[22] and ionisable hyperbranched polymers. Polymers showing a pH-degradable capability are often constituted of ketal or ester moieties that can irreversibly cleave under certain pH conditions; they are mainly used for drug release purposes.[22,23] As for hyperbranched polyelectrolytes, they are composed of ionisable moieties that can be protonated and deprotonated reversibly, *i.e.* in repeated cycles, depending on the pH of the solution. Creation and neutralization of charges modifies the electrostatic interactions between the polymer segments, leading to a variation of the conformational structures of these macromolecules.[19,24] As a matter of fact, the solubility and/or the coil size of the nanostructure can be varied. While some hyperbranched polymers already contain ionisable moieties into their backbone, e.g. hyperbranched polyethyleneimines[25] and hyperbranched poly(amino acid)s, non-ionisable hyperbranched polymers have to be post-functionalized to bring, for instance, carboxylic acid, phosphoric acid or amine functions, yielding hyperbranched polyelectrolytes. Surface modification of the hyperbranched polymers is particularly convenient as the reactive functional groups are mainly located at the terminal units, *i.e.* at the periphery of the globular structure.

The post-functionalization of hyperbranched polyols with anhydrides represents a convenient method to produce hyperbranched polyacids, made of COOH units. The latter functions may be further exploited as reactive sites,[26] grafting points[27–29] or as ionisable moieties.[30–34]

In this project, we derivatized *hb*PEster-OH by esterification with succinic anhydride to impart them amphiphilic properties. The so-formed *Hb*PEster-$COOH_x$ containing different amounts of acidic moieties (x) were prepared by varying the esterification reaction time. The kinetics of

reaction as well as the chemical structure and the thermo-mechanical properties of the *hb*PEster-$COOH_x$ produced were then evaluated. Changes of the solution properties of these hyperbranched polyesters were investigated with respect to the content in hydroxyl moieties (see part 2.2). In particular, the pH-dependence of the *Hb*PEster-$COOH_x$ water-solubility was studied by light-scattering and rheological measurements.

2.1. Functionalization with succinic anhydride

Acid terminated M2HS-based hyperbranched polyesters, denoted as *hb*PEster-$COOH_x$, were synthesized by reaction of succinic anhydride with the hydroxyl end groups of the *hb*PEster-OH. The reaction was catalyzed by dimethylaminopyridine (DMAP), which is commonly used for esterification reactions.[34,35] To avoid or limit inter-esterification between hyperbranched macromolecules, a large excess of succinic anhydride (5 equivalents) was employed. The derivatization of the all hydroxyl functions of *hb*PEster-OH was achieved after 1 h of reaction. Monitoring of the reaction by ^{1}H NMR spectroscopy allowed us to follow the extent of functionalization with time. In these conditions, from 23 to 100 % of OH moieties of *hb*PEster-OH were converted.

2.1.1. Determination of the derivatization rate by ^{1}H NMR

We intended to first derivatize 100 % of the hydroxyl end groups of the *hb*PEster-OH (**Figure III-3**). Succinic anhydride can react with one secondary OH of the terminal unit (T), leading to the functionalized terminal unit T'. The remaining OH of T' can also be esterified, forming the terminal unit T''. The reaction of succinic anhydride with the secondary hydroxyl group of the linear units (L) forms the functionalized linear unit L'. T' units can eventually be viewed as pseudo-linear units, while T" and L' can be assimilated to pseudo-dendritic units (**Figure III-3**).

The esterification reaction was followed by ^{1}H NMR spectroscopy (**Figure III-4**). Peaks due to $\mathbf{a_1'}$ and $\mathbf{a_2'}$ protons of the functionalized terminal unit T' show the same chemical shifts as those of protons **b** and **c** due to the linear unit L, respectively. Similarly, signals due to proton **a"** (from T"), **b'** and **c'** (from L') have the same chemical shifts than the one of **d** protons, assigned to the dendritic unit (D).

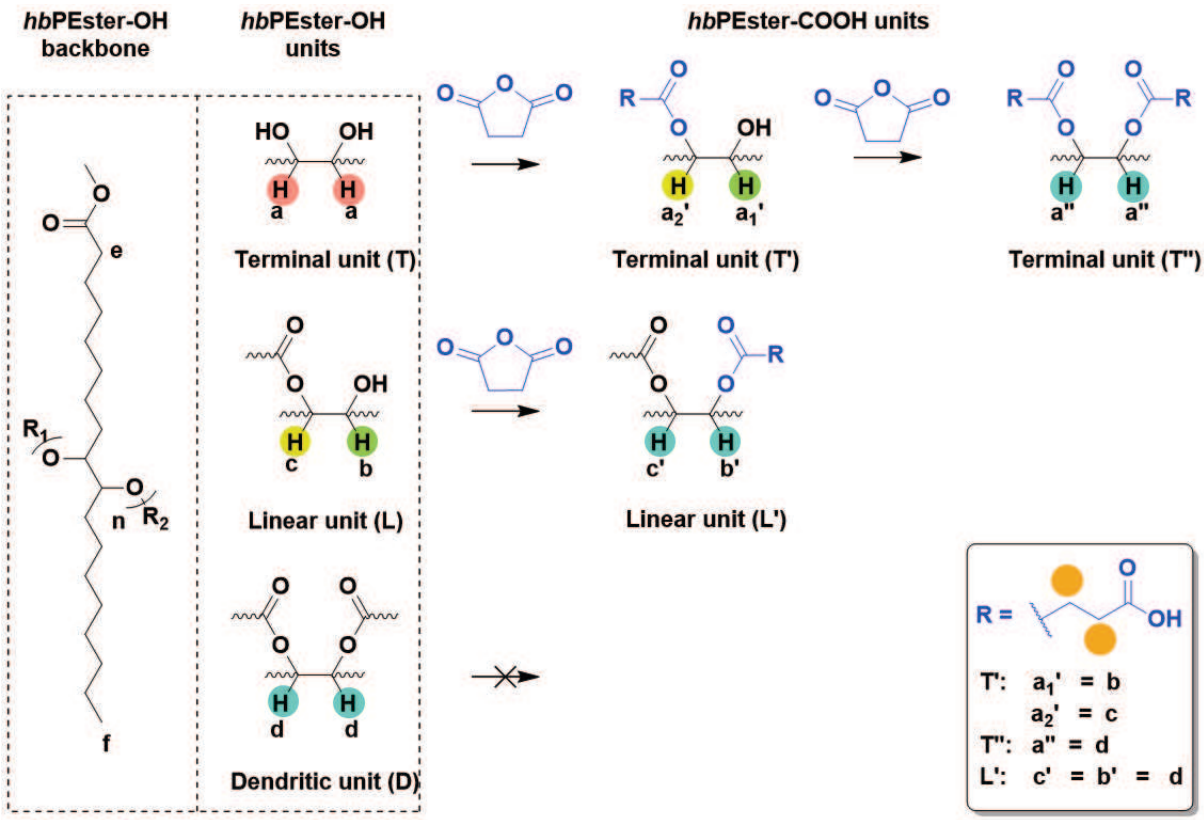

Figure III-3. Esterification reaction of M2HS-*hb*PEster-OH with succinic anhydride.

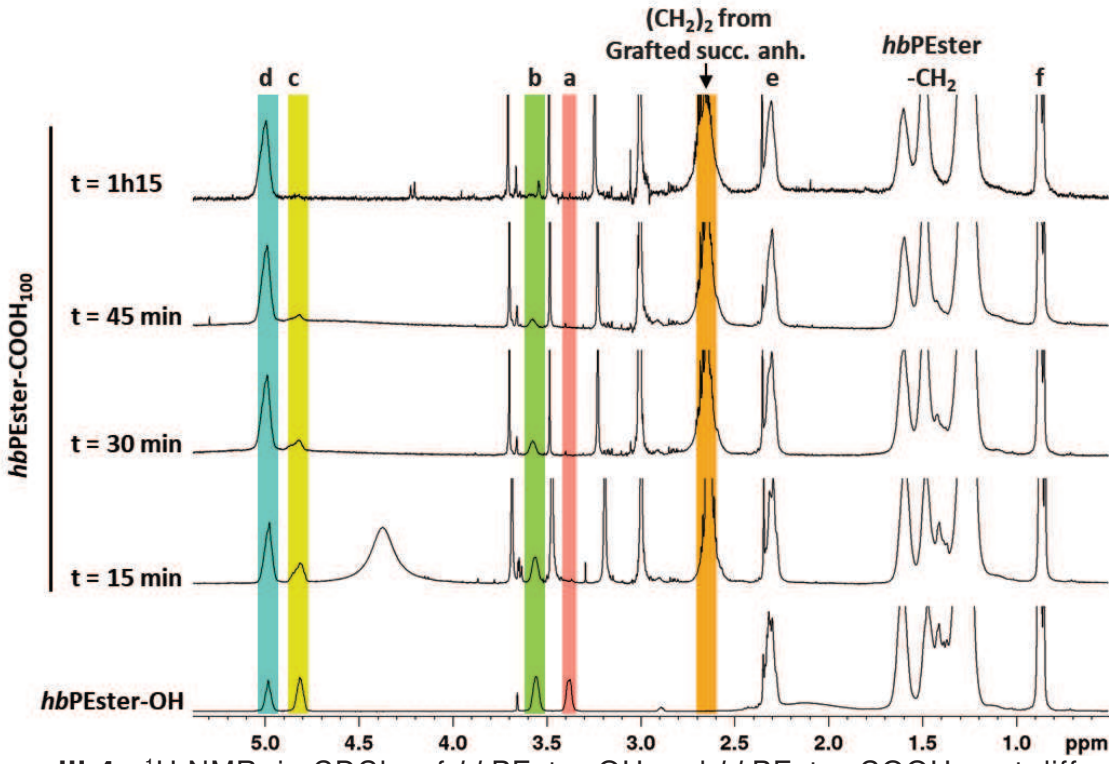

Figure III-4. ^{1}H NMR, in $CDCl_3$, of *hb*PEster-OH and *hb*PEster-$COOH_{100}$ at different reaction times.

2.1.2. Characterization of the *hb*PEster-COOH$_x$

2.1.2.1. Consumption of the different units

The integral values of the peaks corresponding to the protons **a**, **b**, **c** and **d** were used to follow the derivatization of the hydroxyl groups of *hb*PEster-OH (**Figure III-4** & **Figure III-5**). Esterification eventually took place (**Figure III-5.a**) by reaction of all terminal units (T) during the first 15 minutes, while linear units (L) and pseudo-linear units (T') were partially derivatized. After 15 minutes of reaction, the esterification of OH moieties from the pseudo-linear (T') and linear (L) units was completed. The conversion of hydroxyl groups into acidic ones could be calculated through the disappearance of the terminal, linear and pseudo-linear units, *i.e.* from the integral values of the peaks of protons **a**, **b** and **c**, using to the following equation:

$$\text{OH derivatization} = \frac{T_{consumed} + L_{consumed} + T'_{consumed}}{T_{initial} + L_{initial} + D_{initial}} \qquad \text{(Eq. III-1)}$$

Full developments leading to this equation are reported in the supporting information (Eq. SI.III-11).

The appearance of peaks at 2.65 ppm that were assigned to the CH_2 methylene groups from succinic acid moiety was also a proof of *hb*PEster-OH esterification. The blue curve in **Figure III-5.b** shows the variation of the extent of functionalization of *hb*PEster-OH with time. These data were used to determine the degree of derivatization, *x*, in the formation of *hb*PEster-COOH$_x$.

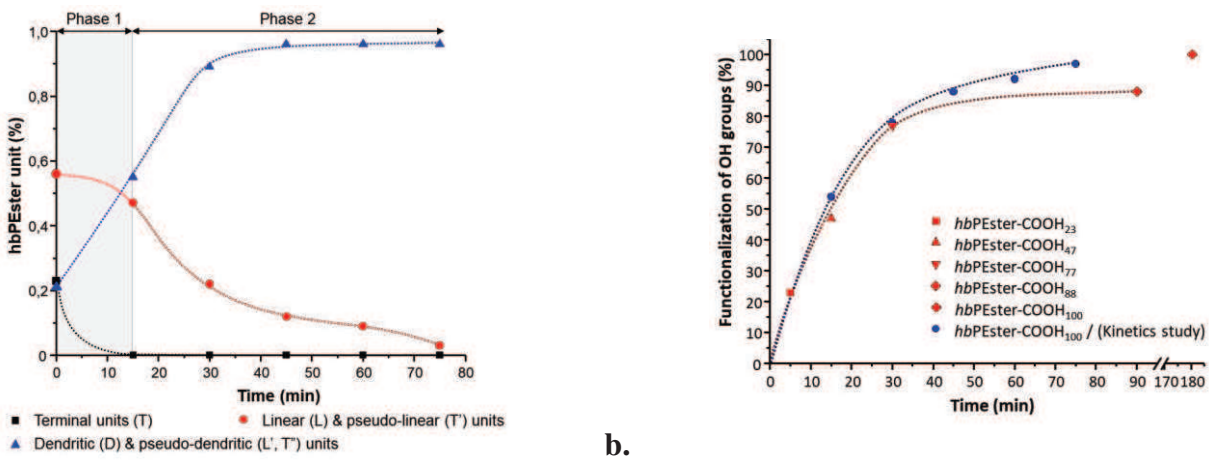

a. b.

Figure III-5. Time dependence of **a.** the amounts of *hb*PEster units and **b.** the functionalization of the hydroxyl groups of *hb*PEsters.

2.1.2.2. Molecular weight and dispersity of *hb*PEster-OH & *hb*PEster-COOH$_x$

Hyperbranched polyesters with 23, 47, 77, 88 and 100 % of derivatized OH could thus be obtained with a good control of the functionalization rate by quenching the reaction at appropriate times, by pouring the reactive mixture into acidic water solution (**Figure III-5.b.** red curve and **Table III-1**). The molecular weight of the *hb*PEster-COOH$_x$ was found to increase, from 7,300 to 13,600 g/mol, upon increasing the extent of functionalization, from 23 to 100 % (**Table III-1** and **Figure III-6**). The dispersities also varied from 3.2 to 14.1 accordingly. Such high dispersities of *hb*PEster-COOH$_{88}$ ($Đ$ = 14.1) and *hb*PEster-COOH$_{100}$ might be explained by the occurrence of inter-esterification reactions, to some extent, between hydroxyl and acidic functions, of *hb*PEster-OH and *hb*PEster-COOH$_x$ (**Figure III-7**).

Table III-1. Characterization data of *hb*PEster-OH and *hb*PEsters-COOH$_x$.

Entry	*hb*PEster	Function. (*% of OH*)	Time (*min*)	M_n [a] (*g/mol*)	$Đ$ [a]	T_g [b] (*°C*)	Yield (*%*)
1	*hb*PEster-OH	-	-	7,600	3.7	-23	-
2	*hb*PEster-COOH$_{23}$	23	5	7,300	3.2	-24	68
3	*hb*PEster-COOH$_{47}$	47	15	9,600	4.8	-21	74
4	*hb*PEster-COOH$_{77}$	77	30	10,100	4.9	-19	71
5	*hb*PEster-COOH$_{88}$	88	90	11,900	14.1	-14	85
6	*hb*PEster-COOH$_{100}$	100	180	13,600	13.8	-15	84

[a] Determined via SEC in THF using PS standard calibration [b] Obtained by DSC

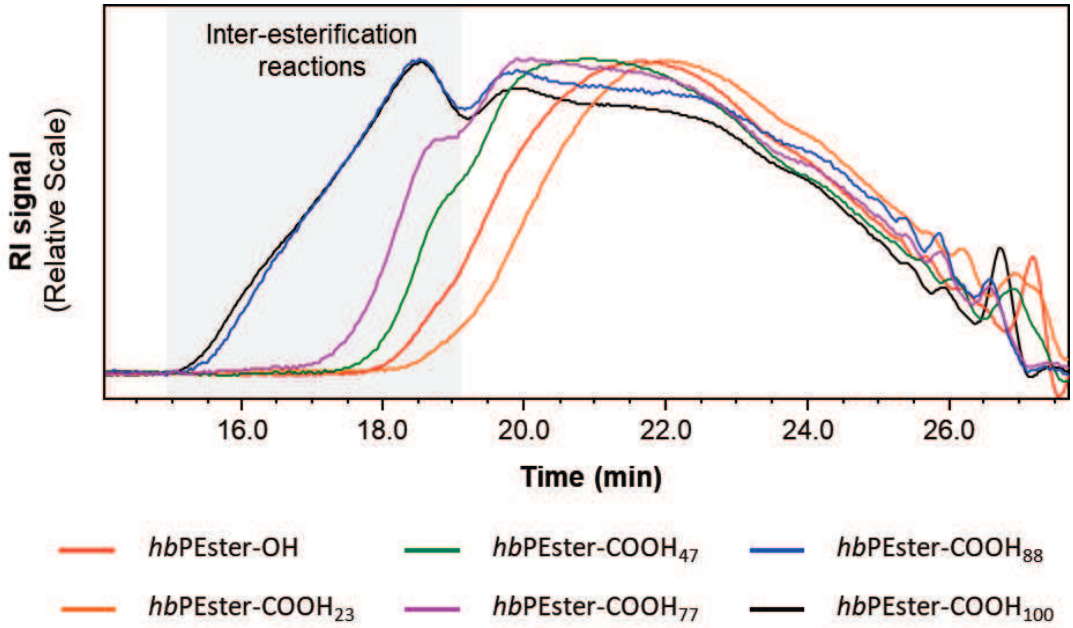

Figure III-6. SEC-RI (in THF) of *hb*PEster-OH and *hb*PEster-COOH$_x$.

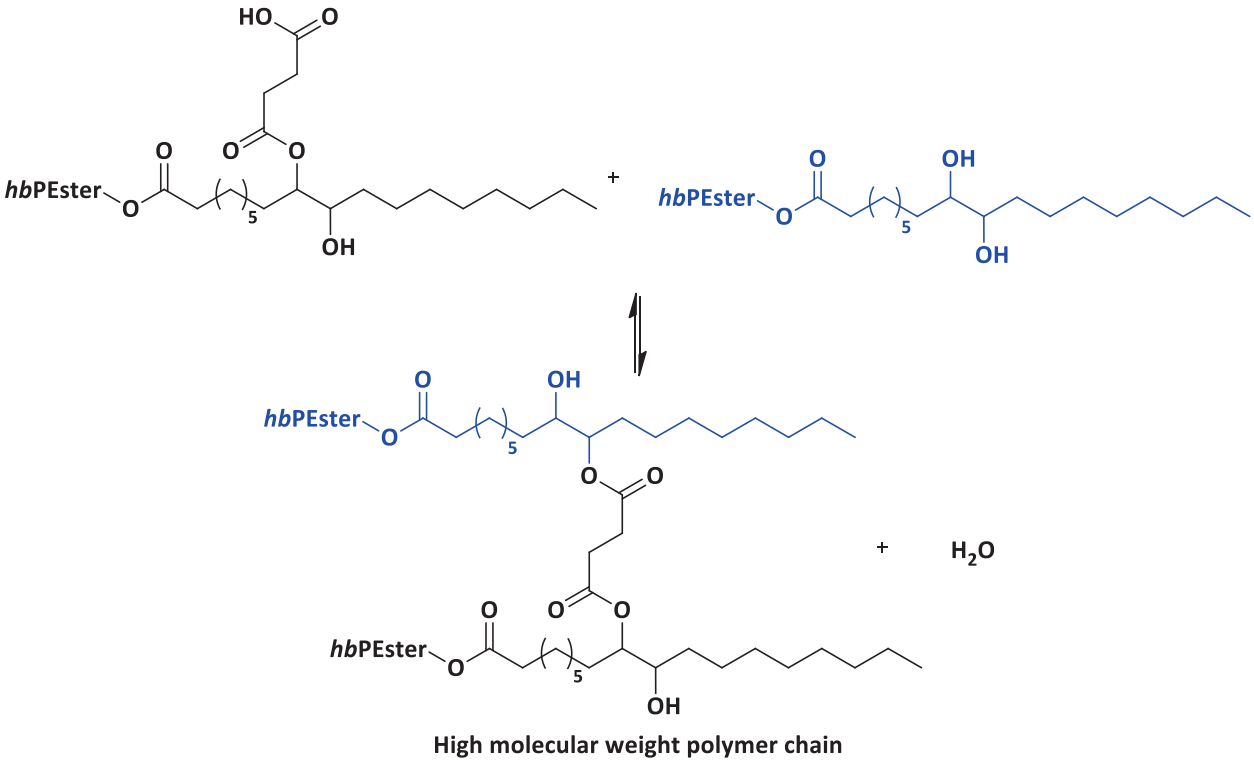

Figure III-7. Esterification of two *hb*PEster chains generating high molecular weight polymers.

2.2. Properties of hyperbranched polyester polysuccinate's

The melt and solution properties of both *hb*PEster-OH and *hb*PEster-COOH$_x$ were investigated. DSC and rheological analyses were performed for samples studied in the melt, not only to determine the T_g, but also to figure out whether these compounds are capable to chain entangle, as opposed to most hyperbranched polymers known to be brittle.[8,36] SAXS, WAXS, DLS and viscosity measurements were carried out in ethanol or in NaOH$_{aq}$ solution, to obtain the R_H and R_g values of *hb*PEster-OH and *hb*PEster-COOH$_x$. These analyses were carried out in collaboration with the group of Prof. L. Ramos, in particular with Dr. S. Constanzo.

2.2.1. Properties in the melt

As many hyperbranched polymers, *hb*PEster-OH is amorphous with a low T_g of -23 °C. This is obviously due to the long aliphatic chains constituting its backbone. Although the T_g remained unchanged for functionalization degrees of *hb*PEster-COOH$_x$ lower than 23 %, T_g slightly increased, from -23 °C (*hb*PEster-OH) to -14 °C (*hb*PEster-COOH$_{88}$), for higher contents in peripheral acidic functions in *hb*PEsters (**Table III-1**). This increase might be explained by the development of H-bondings of the acidic moieties. A master curve, representing the evolution of the storage (G') and the loss (G") modulus, as a function of the angular frequency, was then established (**Figure III-8**). These rheological analyses confirmed that both *hb*PEster-OH and *hb*PEster-COOH$_{100}$ did not entangle (G' and G" did not cross, and G" > G'). As mentioned, this is characteristic of hyperbranched polymers of low molecular weights (M_n < 100,000 g/mol).[36,37]

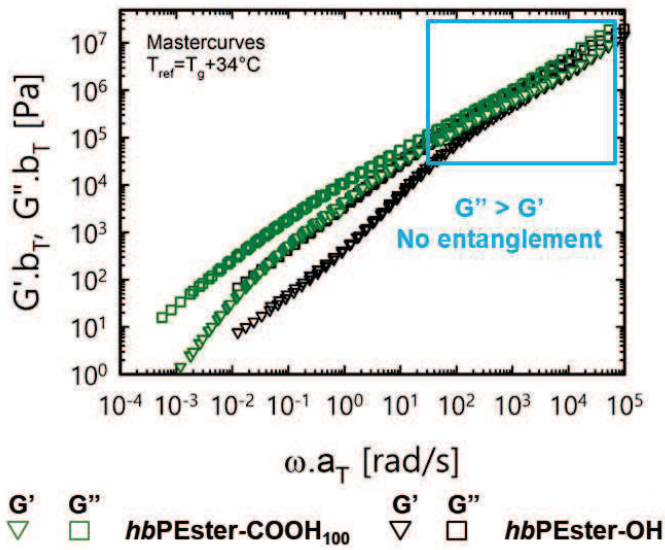

Figure III-8. G' and G" versus the angular frequency, at $T_{ref} = T_g + 34$ °C, of *hb*PEster-OH and *hb*PEster-COOH$_{100}$.

2.2.2. Solution properties in ethanol

As their parent *hb*PEster-OH compounds, *hb*PEster-COOH$_x$ were all found soluble in common organic solvents, such as DMF, THF or chloroform. Interestingly, they also proved soluble in ethanol and methanol, owing to the presence of numerous acidic functions located at the periphery. Due to its low toxicity and its ability to solubilize both the *hb*PEster-OH precursors and the *hb*PEster-COOH$_x$ derivatives, ethanol was selected to manipulate these samples for SAXS/WAXS, DLS, and viscometry analyses, in view of determining the influence of the functionalization of *hb*PEster-OH with succinic anhydride, on the gyration (R_g) hydrodynamic (R_H) radii. Results are summarized in **Table III-2**.

Table III-2. Gyration and hydrodynamic radii, calculated by SAXS/WAXS, DLS and viscometry analyses, of *hb*PEster-OH and *hb*PEster-COOH$_x$.

Entry	*hb*PEster	R_g [a] (*nm*)	$R_{H,DLS}$ [b] (*nm*)	$R_{H,IV}$ [c] (*nm*)
1	*hb*PEster-OH	4.6	6.8	3.6
2	*hb*PEster-COOH$_{23}$	5.1	No fitting function	-
3	*hb*PEster-COOH$_{47}$	15.6	85.1	-
4	*hb*PEster-COOH$_{77}$	13.0	74.9	4.1
5	*hb*PEster-COOH$_{88}$	4.9	4.7	-
6	*hb*PEster-COOH$_{100}$	13.7	Low signal	6.2

[a] Radius of gyration, calculated by SAXS/WAXS. [b] Hydrodynamic radius, calculated by DLS. [c] Hydrodynamic radius, calculated *via* intrinsic viscosity analyses.

2.2.2.1. Calculation of R_g by SAXS and WAXS

SAXS/WAXS analyses were performed on solutions of *hb*PEster-OH and *hb*PEster-COOH$_x$ samples in ethanol, at concentrations varying from 0.01 to 0.07 g/mL. SAXS/WAXS curves at 0.03 g/mL are for instance illustrated in **Figure III-9**. The R_g value was calculated from the Debye relationship (Eq. III-2)[38] and results are summarized in **Table III-2**.

$$P(q) = \frac{2}{q^4 R_g^4}\left[\exp\left(-q^2 R_g^2\right) - 1 + q^2 R_g^2\right] \qquad \text{(Eq. III-2)}$$

with q, the scattering vector and P(q), the Debye function modelling the evolution of the intensity (I) as a function of the scattering vector (q) (**Figure III-9**).

R_g was found to vary from 4.6 (*hb*PEster-OH) to 15.6 nm (*hb*PEster-COOH$_{47}$). These values are consistent with the formation of unimolecular spherical micelles yet. No correlation between the degree of functionalization and R_g was noticed (**Table III-2**). Indeed,

R_g = 4.9±0.3 nm for *hb*PEster-OH, *hb*PEster-COOH$_{23}$ and *hb*PEster-COOH$_{88}$ while R_g = 14.1±1.3 nm for *hb*PEster-COOH$_{47}$, *hb*PEster-COOH$_{77}$ and *hb*PEster-COOH$_{100}$.

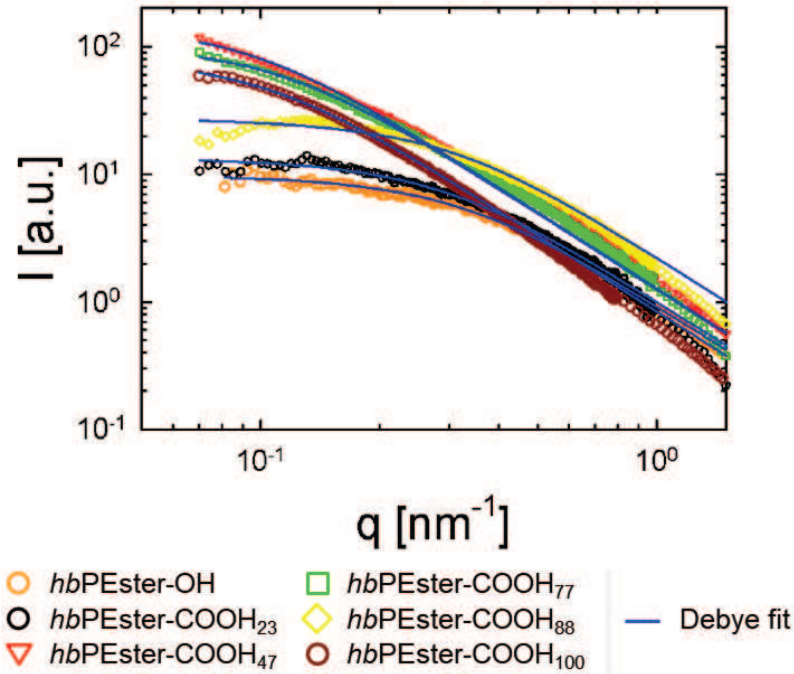

Figure III-9. SAXS/WAXS, in ethanol, of *hb*PEster-OH and *hb*PEster-COOH$_x$, at 0.03 g/mL.

2.2.2.2. Calculation of $R_{H,DLS}$ by DLS

DLS analyses were performed on solutions of *hb*PEster-OH and *hb*PEster-COOH$_x$ in ethanol, at 0.03 g/mL. The delay time dependence of the autocorrelation function, at different angles and the wave vector dependence of the delay time of *hb*PEster-COOH$_{88}$, are illustrated in **Figure III-10**, as an example. Similar curves were obtained for *hb*PEster-OH, *hb*PEster-COOH$_{23}$ hbPEster-COOH$_{47}$ and *hb*PEster-COOH$_{77}$. The signal obtained for *hb*PEster-COOH$_{100}$ was not clear enough to be studied.

$R_{H,DLS}$ of *hb*PEster-OH and *hb*PEster-COOH$_{x,x=23-88}$ were calculated according to the Stokes-Einstein equation:

$$R_H = \frac{k_B T}{6\pi\eta_s D} \qquad \text{(Eq. III-3)}$$

with k_B the Boltzmann constant, T the temperature of the system, η_s the viscosity of the solvent and D the particle's diffusion velocity. D being calculated according to (Eq. III-4) and **Figure III-10.b**.

$$Dq^2 = \frac{1}{\tau}$$

i.e. (Eq. III-4)

$$\log(\tau) = -\log(D) - 2.\log(q)$$

with q the wave factor and τ the delay time.

Values of $R_{H,DLS}$ of *hb*PEster-OH and *hb*PEster-$COOH_{88}$ were found equal to 6.8 and 4.7 nm, respectively. These correspond to dimensions usually observed for (neutral) hyperbranched polymers.[39] By comparison, *hb*PEster-$COOH_{47}$ and *hb*PEster-$COOH_{77}$ formed particles of significantly higher sizes (85.1 and 74.9 nm), which might be ascribed to the formation of aggregates of several nano-objects in solution. Yet, these aggregates could not be seen by SAXS/WAXS, explaining why R_g values measured for *hb*PEster-$COOH_{47}$ (15.6 nm) and *hb*PEster-$COOH_{77}$ (13.0 nm) were low in comparison to the corresponding $R_{H,DLS}$.

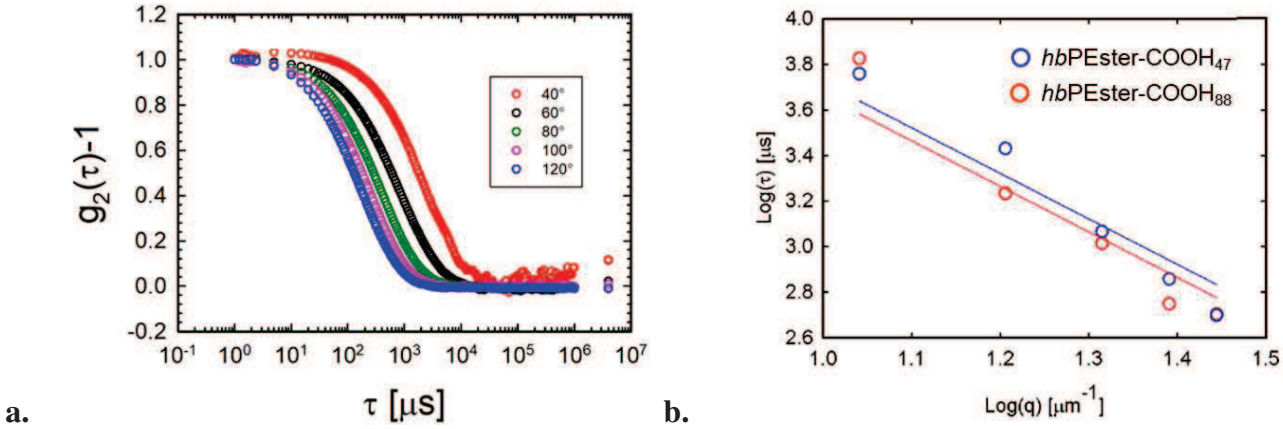

Figure III-10. DLS analyseswith **a.** the autocorrelation function versus the delay time, at different angles of *hb*PEster-$COOH_{88}$ and **b.** the delay time (log) versus the wave vector (log) of *hb*PEster-$COOH_{47}$ and *hb*PEster-$COOH_{88}$.

2.2.2.3. Calculation of $R_{H,IV}$ by intrinsic viscosity measurement

Viscosity tests were performed on solution of three representative samples, namely *hb*PEster-OH, *hb*PEster-$COOH_{77}$ and *hb*PEster-$COOH_{100}$, in ethanol at concentrations varying from 0.01 to 0.05 g/mL. Data are summarized in **Table III-2**. The curve representing the shear rate dependence of the viscosity, and the concentration dependence of the specific viscosity/concentration ratio of *hb*PEster-OH, are illustrated in **Figure III-11.a** and **Figure III-11.b**, respectively. Similar curves were obtained for *hb*PEster-$COOH_{77}$ and *hb*PEster-$COOH_{100}$.

The methodology used for calculating the intrinsic viscosity and the $R_{H,IV}$ will be exemplified for *hb*PEster-OH.

For all concentrations of *hb*PEster-OH in ethanol, the viscosity remains constant with the shear rate, which is consistent with the behaviour of a Newtonian liquid (**Figure III-11.a**). For each concentration, a specific viscosity (η_{sp}) was thus obtained:

$$\eta_{sp} = \eta - \eta_0 \qquad \text{(Eq. III-5)}$$

with η, the viscosity of the *hb*PEster solution at a concentration c, and η_0, the viscosity of pure ethanol.

The intrinsic viscosity was then calculated thanks to (Eq. III-6, *i.e.* by extrapolation of the plot illustrated in **Figure III-11.b** at c = 0 g/mL. [η] of *hb*PEster-OH was equal to 10.1 mL/g.

$$[\eta] = \lim_{c \to 0} \frac{\eta_{sp}}{c} \qquad \text{(Eq. III-6)}$$

$R_{H,IV}$ was then obtained by using the following equation:

$$R_{H,IV} = \left(\frac{3[\eta]M_w}{10\pi N}\right)^{1/3} \qquad \text{(Eq. III-7)}$$

[η] is the intrinsic viscosity and N the Avogadro number.

Values of $R_{H,IV}$ equal to 3.6 for *hb*PEster-OH, 4.1 for *hb*PEster-$COOH_{77}$ and 6.2 nm for *hb*PEster-$COOH_{100}$ were determined (**Table III-2**). These values for *hb*PEster-OH and *hb*PEster-$COOH_{100}$ correspond to unimolecular particles. By comparison, the $R_{H,IV}$ of the *hb*PEster-$COOH_{77}$ (4.1 nm) was found much lower than $R_{H,IV}$ (75.0 nm). The sensitivity of the DLS equipment to the size of bigger objects might explain these differences. Therefore, objects of 75.0 nm (DLS) probably formed by clustering unimolecular *hb*PEster-$COOH_{77}$ particles of ca. 4.1 nm (IV).

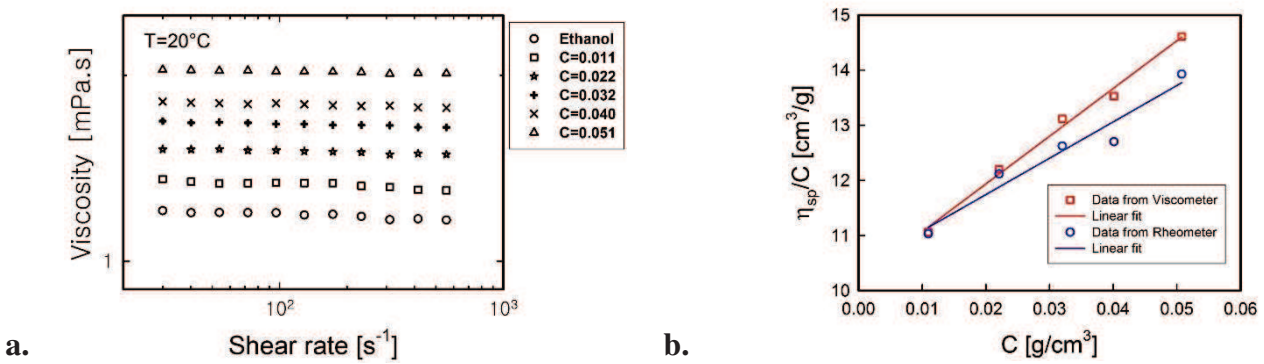

Figure III-11. Viscosity analyses of *hb*PEster-OH in ethanol with **a.** the viscosity versus the shear rate at different concentrations and **b.** the viscosity/concentration ratio versus the concentration.

2.2.3. Properties in $NaOH_{aq}$ solution

The *hb*PEster-$COOH_x$ samples were neutralized by addition of $NaOH_{aq}$, yielding hyperbranched polyester polycarboxylates, denoted as *hb*PEster-$COONa_{x/y}$, *x* corresponding to the degree of functionalization of OH, and *y* to the degree of neutralization of the COOH moieties, respectively. The influence of the degree of neutralization and the degree of functionalization on water-solubility was first studied macroscopically. SAXS/WAXS, DLS and intrinsic viscosity analyses were then performed on three *hb*PEster-$COOH_{100/y}$ samples.

2.2.3.1. Water-solubility of hbPEster-COONax/y, at macroscopic scale

Firstly, acidic moieties of *hb*PEster-$COOH_{100}$ were neutralized to completion by adding $NaOH_{aq}$, yielding *hb*PEster-$COONa_{100/100}$. Waterborne solutions of *hb*PEster-$COONa_{100/100}$ of concentrations ranging from 0 to 0.07 g/mL were prepared. Corresponding results are illustrated in **Figure III-12**. As can be seen, the water-solubility of *hb*PEster-$COONa_{100}$ was lower than 0.04 g/mL, *i.e.* less than 10% of the solubility of a PEG of 10,000 g/mol, which is equal to 0.55 g/mL.[40] Dispersion of *hb*PEster-$COONa_{100/100}$ formed above 0.04 g/mL. *Hb*PEster-$COONa_{100/y}$ were also formed by neutralizing *hb*PEster-$COOH_{100}$ at 30, 45, 60 and 75 %. Solutions were prepared at a concentration 0.03 g/mL in *hb*PEster$NA_{100/y}$. *Hb*PEster-$COONa_{100/y}$ were only found soluble for a content in carboxylate higher than 60 %.

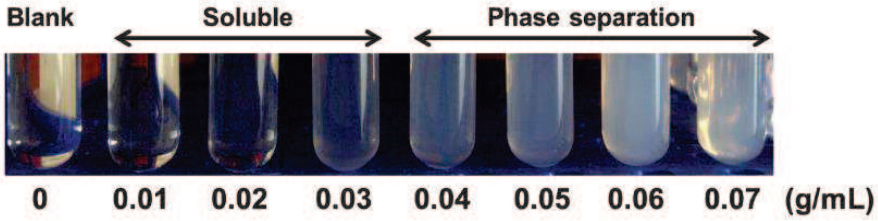

Figure III-12. *Hb*PEster-COONa$_{100/100}$ in NaOH$_{aq}$ solution, at concentration varying from 0 to 0.07 g/mL.

Acid moieties of *hb*PEster-COOH$_x$, having degree of functionalization ranging from 23 to 100 %, were also neutralized at 100 % by addition of NaOH$_{aq}$. Solutions of 0.03 g/mL of *hb*PEster-COONa$_{x/100}$ were hence prepared. The range of solutions of *hb*PEster-COOH$_{x/100}$ are illustrated in **Figure III-13**. A degree of functionalization higher than 88 % was found to be required to solubilize the *hb*PEster-COOH$_x$. Below this threshold value, indeed, a precipitate formed. After 3 months, phase separation was observed for the solutions of *hb*PEster-COOH$_{88}$ and *hb*PEster-COOH$_{100}$; full solubility was recovered after remixing.

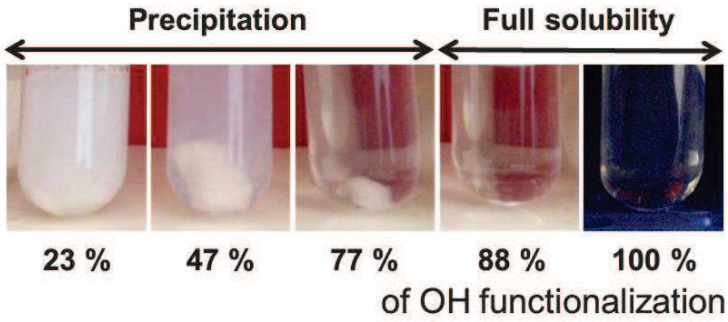

Figure III-13. *Hb*PEster-COONa$_{x/100}$ in NaOH$_{aq}$ solution, at 0.03g/mL.

2.2.3.2. Water-solubility of hbPEster-COONa$_{100/y}$

*Hb*PEster-COONa$_{100/60}$, *hb*PEster-COONa$_{100/75}$ and *hb*PEster-COONa$_{100/100}$ were analysed by DLS. In addition, *hb*PEster-COONa$_{100/100}$ was evaluated by SAXS/WAXS and viscosity tests. Results are summarized in **Table III-3.**

Table III-3. R_g, $R_{H,DLS}$ and $R_{H,IV}$ of *hb*PEster-COONa$_{100/60}$, *hb*PEster-COONa$_{100/75}$ and *hb*PEster-COONa$_{100/100}$ in water.

Entry	*hb*PEster	R_g [a] (*nm*)	$R_{H,DLS}$ [b1] (*nm*)	$R_{H,DLS}$ [b2] (*nm*)	$R_{H,IV}$ [c] (*nm*)
7	*hb*PEster-COONa$_{100/60}$	No data	14.9	9.6	No data
8	*hb*PEster-COONa$_{100/75}$	No data	11.0	7.9	No data
9	*hb*PEster-COONa$_{100/100}$	No fit	7.0	6.5	Not linear

[a] Radius of gyration, calculated by SAXS/WAXS [b1] Hydrodynamic radius, calculated by DLS using the single exponential fit [b2] using the cumulant fit [c] Hydrodynamic radius, calculated *via* intrinsic viscosity analyses

SAXS/WAXS of *hb*PEster-COONa$_{100/100}$

SAXS/WAXS analyses were performed for *hb*PEster-COONa$_{100/100}$ in solution in water at concentrations varying from 0.01 to 0.07 g/mL. Data are illustrated in **Figure III-14**. For all samples, noisy signals were observed and Debye functions thus only fitted from 0.1 to 0.3 nm^{-1} (**Figure III-12**).

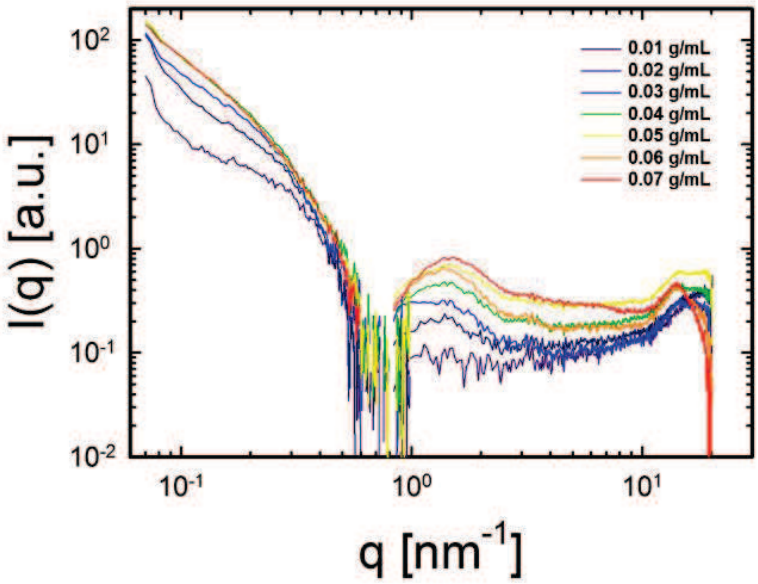

Figure III-14. SAXS/WAXS analysis of *hb*PEster-COONa$_{100/100}$.

DLS of *hb*PEster-COONa$_{100/60}$, *hb*PEster-COONa$_{100/75}$ and *hb*PEster-COONa$_{100/100}$

DLS analyses were performed on *hb*PEster-COONa$_{100/60}$, *hb*PEster-COONa$_{100/75}$ and *hb*PEster-COONa$_{100/100}$, at 0.03 g/mL (**Table III-3**). The curve illustrating the delay time as a function of the wave vector, obtained for *hb*PEster-COONa$_{100/100}$, is given in **Figure III-15**, as

an example. Similar curves were obtained for *hb*PEster-COONa$_{100/60}$ and *hb*PEster-COONa$_{100/75}$ (see **Figure SI.III-42**, in the supporting information).

Exponential and cumulant fits were used for calculating $R_{H,DLS}$ values. These were found to decrease, from 14.9 to 7.0 nm and from 9.6 to 6.5 nm, for the exponential and the cumulant fit, respectively, upon increasing the degree of neutralization from 60 to 100 %. The decrease of the particle size upon neutralization can be explained by repulsive interactions between the negative charges of the carboxylate moieties, which led to the shrinking of polymer chains.

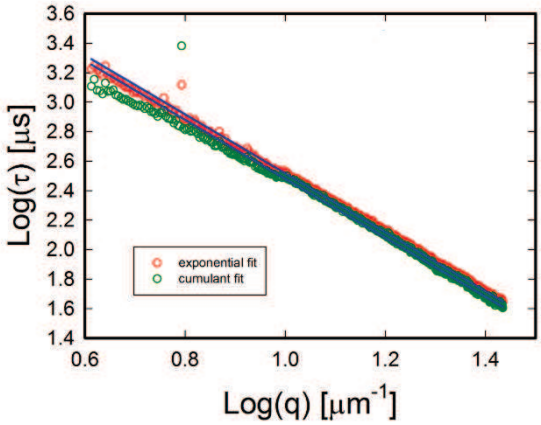

Figure III-15. DLS analysis. Delay time (log) versus the wave factor (log) of *hb*PEster-COONa$_{100/100}$.

Viscosity tests of *hb*PEster-COONa$_{100/100}$

Viscosity tests were performed on solutions of *hb*PEster-COONa$_{100/100}$ in NaOH$_{aq}$ solution at concentrations ranging from 0.01 to 0.06 g/mL. Data are summarized in **Table III-3**. The curve representing the shear dependence of the viscosity and the concentration dependence of the specific viscosity/concentration ratio are illustrated in **Figure III-16.a** and **Figure III-16.b** respectively. For concentrations ranging from 0.01 to 0.03 g/mL (soluble) and for concentrations of 0.04 and 0.05 g/mL (dispersions), the viscosity remained constant with the shear rate. In other words, these solutions and dispersions behaved as Newtonian liquids (**Figure III-12** and **Figure III-16.a**). However, at 0.06 g/mL, a drop in viscosity, from ca.1000 to ca.10 mPa.s, was noted at low shear rates (0.01 to 1 s^{-1}). Aggregates that were formed in the dispersion probably disappeared as the shear rate increased (**Figure III-16.b**).

In comparison to solutions of *hb*PEster-COOH$_{100}$ in ethanol, the curve representing the concentration dependence of the intrinsic viscosity of the solutions of *hb*PEster-COONa$_{100/100}$

in $NaOH_{aq}$ did not evolve linearly. Therefore, it was not possible to determine the $R_{H,IV}$ of *hb*PEster-$COONa_{100/100}$ in $NaOH_{aq}$.

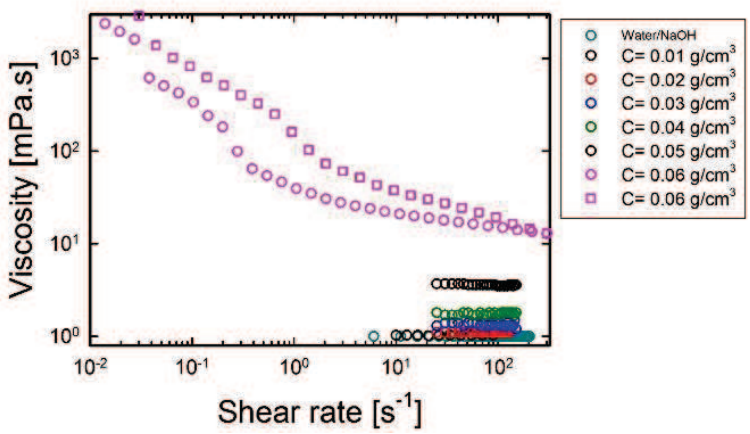

a.

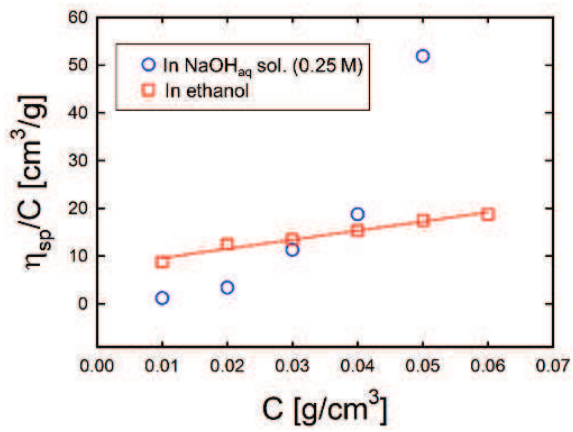

b.

Figure III-16. a. The viscosity versus the shear rate of *hb*PEster-$COONa_{100/100}$ solutions in $NaOH_{aq}$, at different concentrations and **b.** the specific viscosity/concentration ratio versus the concentration of *hb*PEster-$COOH_{100}$ (in ethanol) and of *hb*PEster-$COONa_{100/100}$ (in $NaOH_{aq}$).

2.3. Conclusion

Hyperbranched polyesters with 23, 47, 77, 88 and 100 % of derivatized OH were produced with a good control of functionalization rate by quenching the reaction after several minutes or hours. Molecular weights ranging from 7,300 to 13,600 g/mol were achieved when increasing the functionalization ratio up to 100 %. The increase of molecular weight went along with an increase of the dispersity, reaching a value as high as 14.1 for *hb*PEster-$COOH_{88}$. This was ascribed to the occurrence of esterification reactions between hydroxyl functions of *hb*PEster-OH or *hb*PEster-$COOH_x$ with the acidic functions of other *hb*PEster-$COOH_x$ (**Figure III-7**).

DSC measurements revealed that T_g slightly increased, from -23 °C for *hb*PEster-OH to -15 °C for *hb*PEster-$COOH_{100}$, when increasing the degree of functionalization. This was assigned to H-bonds generated by COOH moieties. Though, this increase in T_g was probably restricted by the increase of free volume caused by the grafted succinic acid.

Rheological analyses in the melt showed that both *hb*PEster-OH and *hb*PEster-$COOH_{100}$ were non-entangled, consistently with observations made on hyperbranched polymers of similar molecular weights (ca. 10,000 g/mol). Likely, it could be assumed that *hb*PEster-$COOH_x$ with a degree of functionalization equal to 23, 47, 77 and 88 did not entangle either.

All samples appeared to be soluble in ethanol at concentrations varying from 0.01 to 0.07 g/mL. SAXS/WAXS, DLS and intrinsic viscosity analyses indicated that unimolecular particles of *hbPEster*-OH with R_g of 4.6 nm and R_H of 5.6 ± 2.3 nm were obtained. By comparison, even though unimolecular particles might be observed for amphiphilic *hb*PEster-$COOH_x$ (R_g(*hb*PEster-$COOH_{88}$) = 4.9 nm), aggregates likely formed, as evidenced by DLS measurements. Indeed, rather high $R_{H,DLS}$ values were obtained for *hb*PEster-$COOH_{47}$ and *hb*PEster-$COOH_{77}$ (85.1 and 74.9 nm respectively), while noisy signals were acquired for *hb*PEster-$COOH_{23}$ and *hb*PEster-$COOH_{100}$.

Interestingly, *hb*PEster-$COOH_x$ samples with an extent of functionalization equal to 88 and 100 % were found soluble in water (up to 0.03 g/mL) after neutralization of 100 % of their COOH moieties. For *hb*PEster-$COOH_{100}$, 60 % of neutralization was sufficient to ensure the water solubility. In addition, DLS showed that the size of the *hb*PEster-$COOH_{100}$ particles decreased when increasing the degree of neutralization, probably due to the repulsion of negative charges.

3. Derivatization of hyperbranched polyester polyols with acryloyl chloride

The synthesis of 3D networks unsaturated polyesters (UPs) by free radical copolymerization of unsaturated polyester polyols with reactive diluents, mostly styrene and acrylic monomers is known for long.[41,42] Nowadays, more than 80 % of the cross-linkable "resins" are made utilizing unsaturated polyesters.[43] Fillers or other additives can be added to these 3D networks to reach specific properties. The latter are being used in many sectors such as building and construction, shipbuilding, pipes and vessels, automotive, paints and coatings, or electrical industry (**Figure III-17**).[43–46]

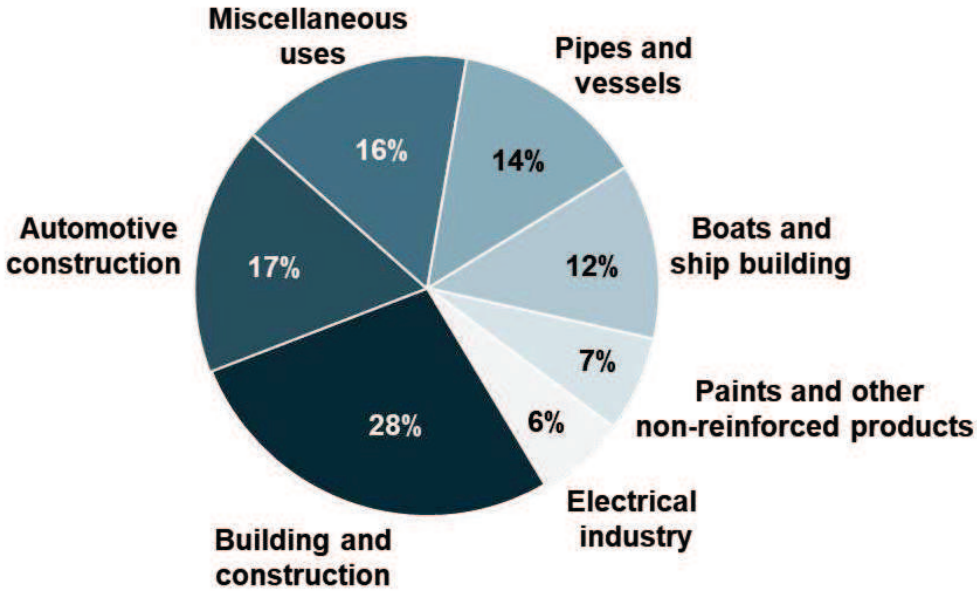

Figure III-17. Distribution of the European's consumption of unsaturated polyester resins by industry.[43]

With the aim of reducing the viscosity of the reactive mixture during the curing process, use of our hyperbranched polymers as additives to achieve cross-linkable resin formulations was here investigated. Hyperbranched polymers can indeed be added either as non-reactive additives or as curing agents.[47,48] The addition of cross-linkable hyperbranched polymers as curing agent is particularly interesting, as this enable to prevent migration of the additive into the matrix in the course of time.[26,49,50] Several unsaturated hyperbranched polyesters have been designed for this purpose.[63–65] The properties of the cured materials have been shown to mainly depend on the nature of the curing agents, *i.e.* the reactive diluent, the cross-linkable *hb*PEster or other reactive compounds. Diverse reactive diluents such as styrene, acrylic acid,[51] acrylic[51–55] or methacrylic[49,51] monomers are frequently used. Addition of epoxy di-acrylate,[55] bisphenol-A

glycidyl dimethacrylate (BisGMA),[49,51] acrylated polyurethanes[56] and acrylated poly(ethylene glycol)[52,53,57,58] has also been explored (**Figure III-18**).

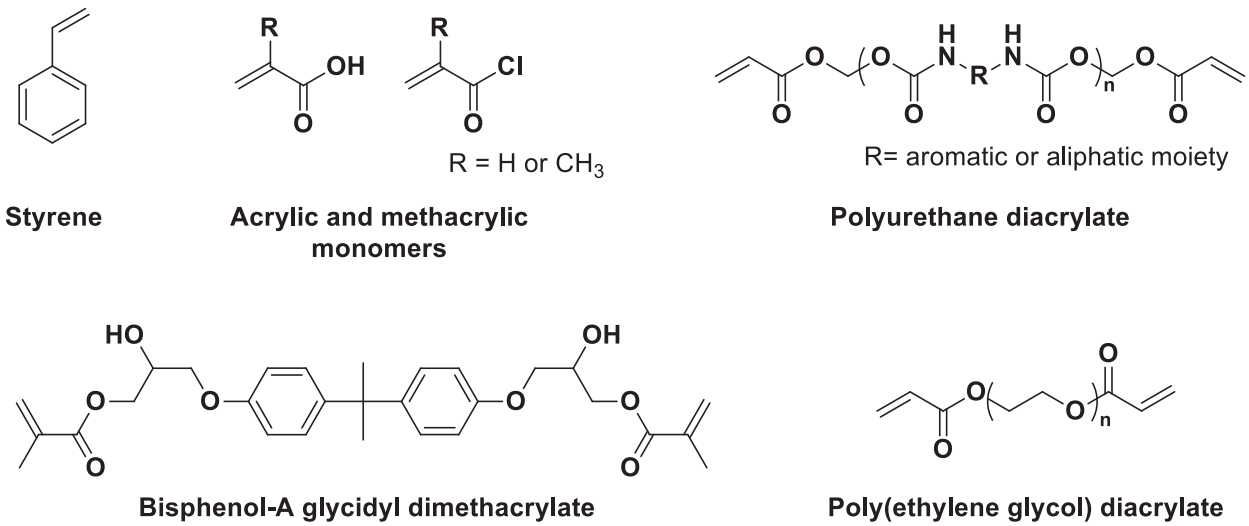

Figure III-18. Examples of reactive diluents used with cross-linkable *hb*PEsters.

Most of hyperbranched polyesters that have allowed curing the resins are derived from commercially available Boltorn™.[48–50,56–62] TMP core molecule may also be replaced with di(trimethylol propane)[52,53] or castor oil.[54] Another example of *hb*PEster has employed as curing agent was developed by Zhang *et al.*[63] The authors have polymerized an AB_2-type monomer synthesized by esterification of one TMP hydroxyl group with phthalic anhydride. In this case, the *hb*PEsters bring primary hydroxyl groups that can be derivatized into reactive polymerizable groups, via a free radical process. Esterification of OH groups has been achieved in one step using commercially available acyl chloride compounds, such as acryloyl chloride,[56,59,60] methacryloyl chloride,[49,60] or methacrylic anhydride.[49] Some anhydrides and isocyanates derivatives have also been specifically designed to be grafted onto *hb*PEsters; for instance, maleic anhydride mono-isooctyl alcohol ester (MAMIOE) was prepared by esterification of isooctyl alcohol with maleic anhydride.[63] Acrylated isocyanates have also been designed *via* the reaction of isophorone diisocyanate (IPDI) with 2-hydroxyethyl acrylate (HEA)[54,62] or acrylated polyethylene glycol.[52,53] In these latter cases, the cross-linkable moieties have been grafted to the *hb*PEsters by urethane links. The functionalization may also be performed in two steps. For instance, Lange *et al.* have acrylated the hydroxyl functions of poly(ε-caprolactone) arms that have previously been grafted onto *hb*PEsters.[60] Similarly, Wang *et al*. have synthesized *hb*PEster-PEG-acrylates.[57,58]

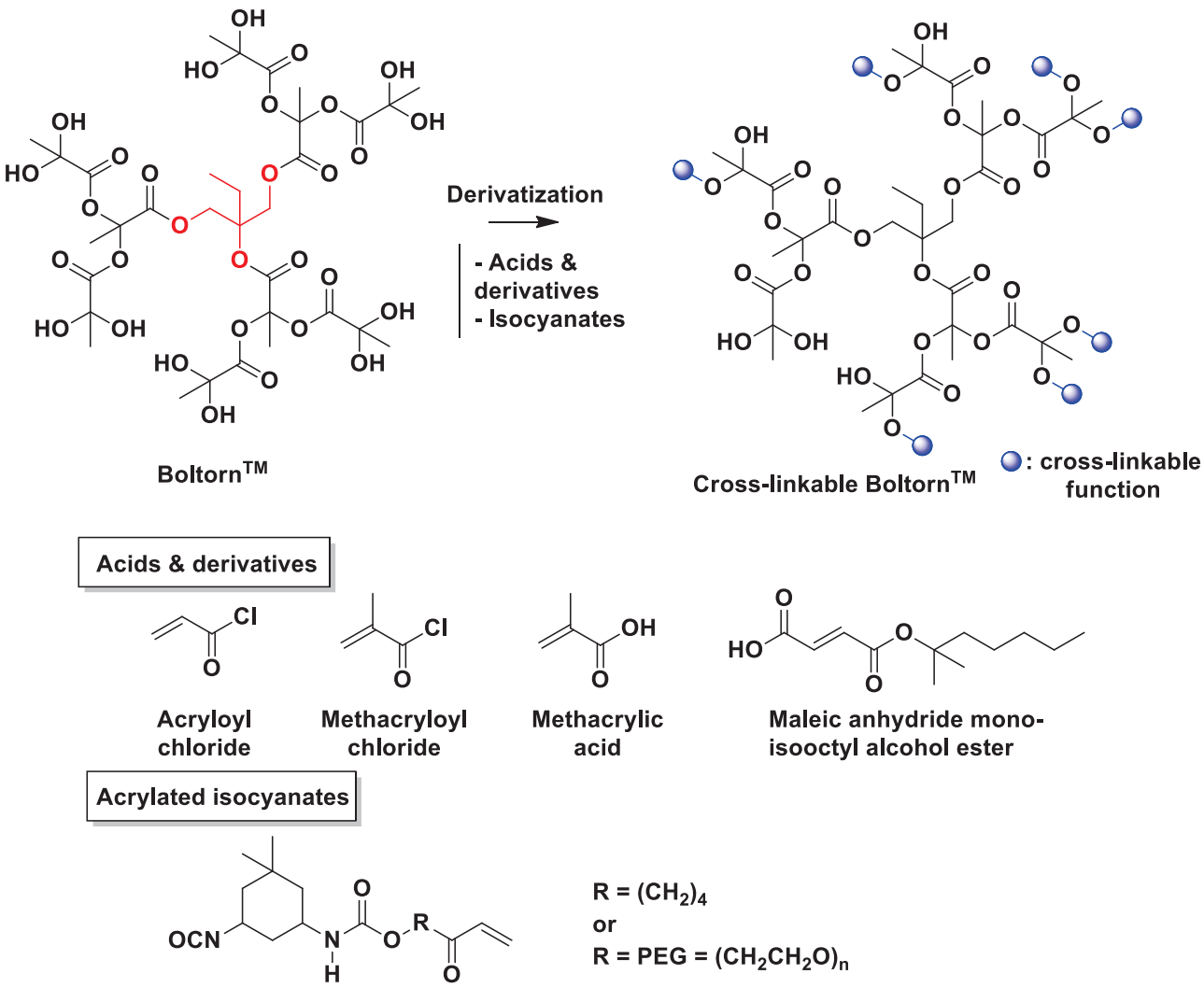

Figure III-19. Examples of derivatizations of Boltorn™ into cross-linkable hyperbranched polyester.

Addition of cross-linkable *hb*PEsters unsurprisingly modify the mechanical and thermo-mechanical properties of the final cured networks, even though it remains difficult to predict the behaviour of the final materials. For instance, increase of T_g can be observed due to reduction of chain mobility, related to the compact structure of the hyperbranched polymers and the lack of entanglement.[49,52,53,56] In contrast, the presence of long aliphatic chains within *hb*PEsters –like in our case– is expected to decrease the T_g value.[49,50,52,53,64] Similarly, while the compact structure and the cross-linking generally enhance the mechanical properties, *i.e.* to increase the tensile, compressive and flexible strengths, or pencil and shore hardness, decrease of corresponding moduli can also be observed.[49,54,56]

In this work, we derivatized the *hb*PEster-OH samples by reaction with acryloyl chloride (AC) (**Figure III-20**). Hyperbranched polyester polyacrylates with different degrees of functionalization, denoted as *hb*PEster-A_x, were thus prepared. Triethylamine was used to trap the HCl by-product, which also prevents hydrolysis of the as-formed ester bonds. Up to 94 % of the OH functions were thus derivatized after 2 h reaction. The extent of functionalization was assessed by ^{1}H NMR spectroscopy. From 21 to 94 % of OH functions were derivatized with respect to the amount of AC used. The final *hb*PEster-A_x were purified by centrifugation and analysed by SEC and DSC. *H*bPEster-A_{94} was then used as curing agent and mixed with methyl methacrylate (MMA) or styrene, with the objective at preparing re-inforced PMMA (or polystyrene, PS) networks. 2,2′-Azobis(2-methylpropionitrile) (AIBN) was used as radical source (Part 3.2).

3.1. Functionalization with acryloyl chloride

3.1.1. Determination of the functionalization ratio by ^{1}H NMR

The derivatization of the OH functions of *hb*PEster-OH by AC is detailed in **Figure III-20**. AC can react with secondary OH of the terminal unit (T), leading to the functionalized terminal unit T'. The remaining OH of T' can also be esterified, forming the terminal unit denoted as T''. Likewise, reaction of AC with the secondary hydroxyl group of the linear unit (L) generates the functionalized linear unit L'. T' can be seen as pseudo-linear units, while T" and L' can be viewed as pseudo-dendritic units.

Monitoring the esterification reaction by ^{1}H NMR spectroscopy (**Figure III-21**) showed that, despite of a similar chemical environment for protons due to T' and L units, peaks corresponding to protons $\mathbf{a_1'}$ (δ = 3.61 ppm) and $\mathbf{a_2'}$(δ = 4.92 ppm) belonging to unit T' slightly differed from those of protons **b** (δ = 3.57 ppm) and **c** (δ = 4.82 ppm) due to unit L. By comparison, protons **a"** (from T"), **b'** and **c'** (from L') have approximately the same chemical shifts than **d** proton (δ = 5.06 ppm) of the dendritic unit (D); the **d** peak was broaden and is here named **D** (δ = 4.94-5.14 ppm).

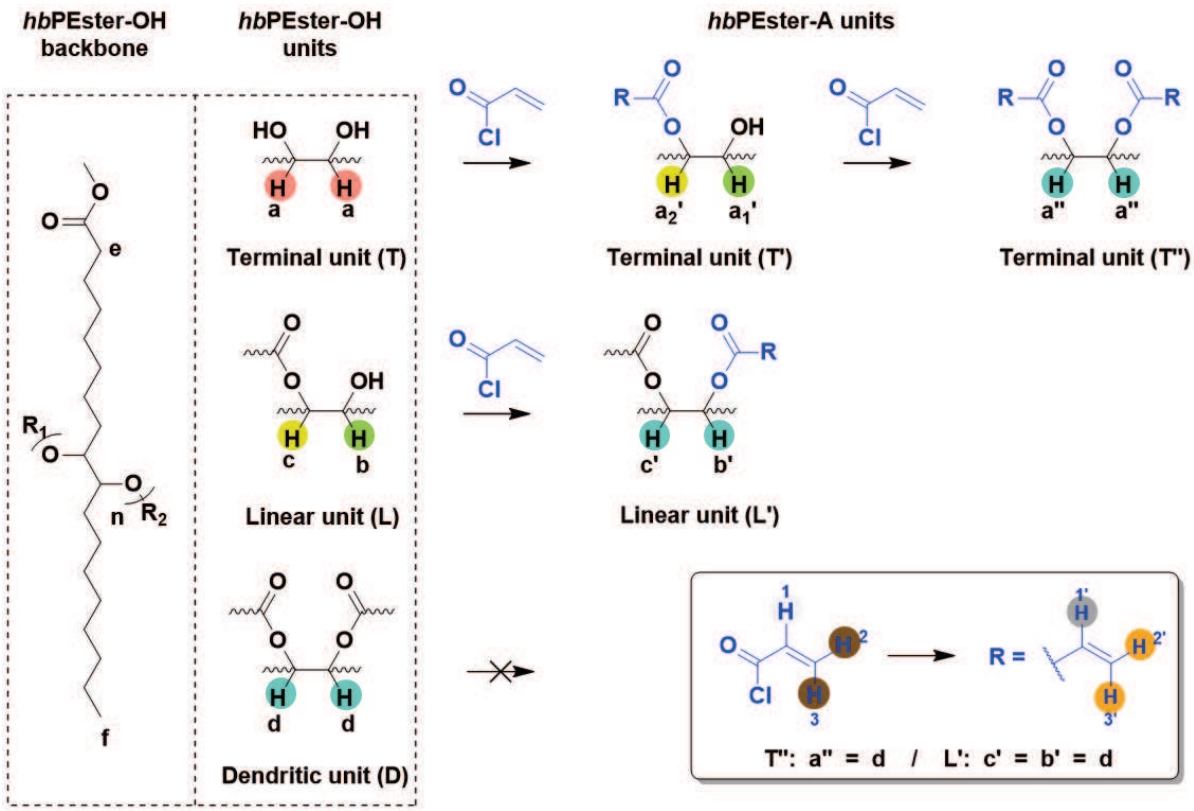

Figure III-20. Esterification of the secondary OH of *hb*PEster-OH with acryloyl chloride.

Efficient transformation of hydroxyl groups using AC was evidenced in two ways. Firstly, the peaks of protons 1, 2 and 3, from AC, shifted from 6.63, 6.34 and 6.17 ppm to 6.41, 6.12 and 5.83 ppm, respectively, after functionalization. In addition, the intensity of the peaks assigned to protons **a**, **b** and **c**, from the T and L units, decreased while the peak intensity of proton **d** increased. Similarly to the reaction of *hb*PEster-OH with succinic anhydride, the functionalization ratio was calculated according to (Eq. III-8). The complete calculations are given in the supporting information (Eq. SI.III-11).

$$\text{OH Functionalization} = \frac{2 \times (T_i - T) + (L_i - L) - T'}{2 \times T_i + L_i} \qquad \text{(Eq. III-8)}$$

For instance, according to the integral values of the ^{1}H NMR spectrum in **Figure III-21**, the integral of peak **a**, corresponding to the unit T, dramatically decreased from 0.43 to 0.02; 95 % of the terminal unit had been consumed. Similarly, the decrease of the sum of the integrals of peaks **b** and **c**, corresponding to the L units, indicated that 86 % of these units had reacted.

Finally, 96 % of T' (peaks **a₁'**and **a₂'**) generated after esterification of the hydroxyl groups from unit T, were consumed.

For instance, integral values of peaks **a**, **a₁'**, **a₂'**, **b** and **c**, observed by NMR (see **Figure III-21**), indicated that 94 % of the OH from the *hb*PEster-OH reacted with AC; the corresponding hyperbranched polymer was labelled as *hb*PEster-A_{94} (Eq. SI.III-11).

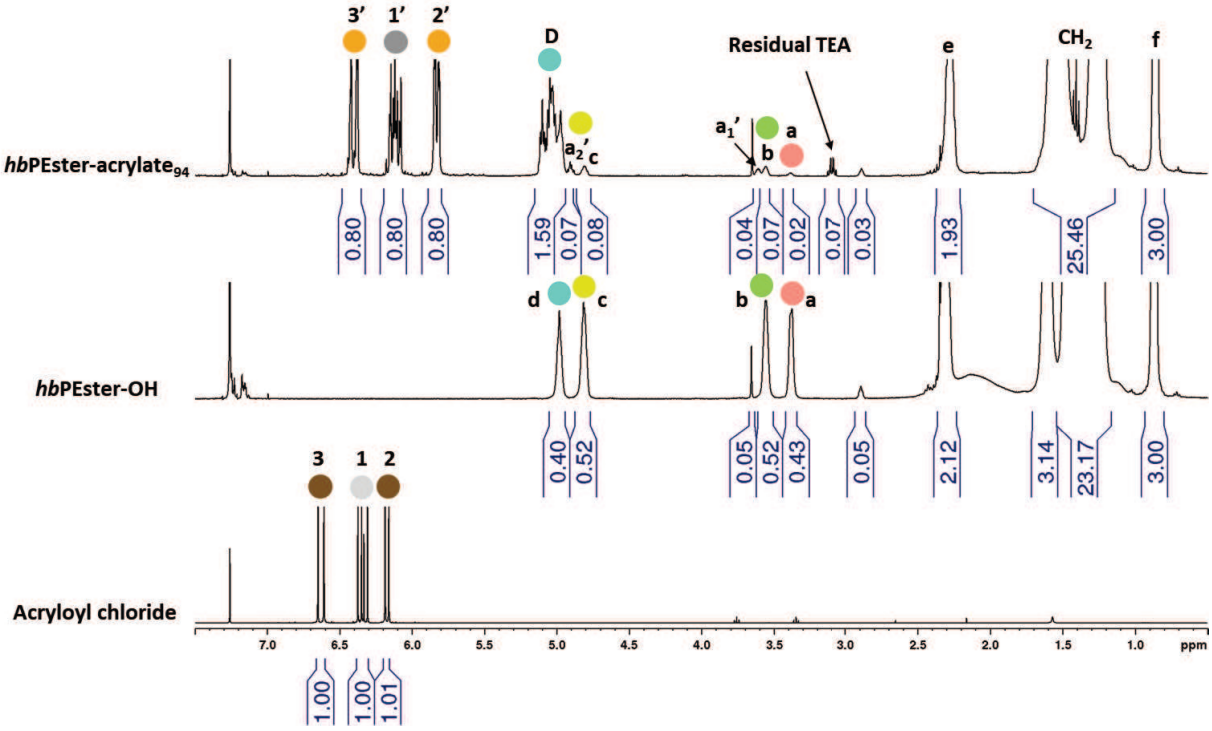

Figure III-21. ^{1}H NMR, in $CDCl_3$, of AC, *hb*PEster-OH and *hb*PEster-A_{94}.

3.1.2. Characterization of the functionalized hbPEster-Ax

3.1.2.1. Reactivity of hydroxyl chain ends

*Hb*Pester-A featuring 21, 42, 75 and 94 % of acryloyl moieties were synthesized as summarized in **Table III-4**. The OH derivatization ratio (F_{OH}) was controlled by varying the amounts of AC and triethylamine. Equimolar amounts of TEA, AC and OH groups were generally used but when targeting 100 % of functionalization, an excess of TEA (1.5 eq.) and of AC (2 eq.) was required.

Table III-4. Percentages of T, L and T' units consumed during the functionalization of *hb*PEster-OH at F_{OH} varying from 21 to 94 %.

Entry	*hb*PEster	AC/OH[a] (%)	F_{OH}[b] (%)	$T_{consumed}$ (%)	$L_{consumed}$ (%)	$T'_{consumed}$ (%)
1	*hb*PEster-OH	-	-	-	-	-
2	*hb*PEster-A_{21}	0.25	21	49	23	33
3	*hb*PEster-A_{42}	0.50	42	77	38	39
4	*hb*PEster-A_{75}	0.75	75	79	42	82
5	*hb*PEster-A_{94}	2	94	95	86	96

[a] Ratio of AC and OH from hbPEster-OH [b] Percentage of OH functionalized

Through the variation of the peaks corresponding to units T, L and T', it was possible to account for which types of units could react first. The details are summarized in **Table III-4** and illustrated in **Figure III-22**. As can be seen, peripheral T units of the *hb*PEster-OH were first engaged, generating T' units (**Figure III-22**, phases I and II). As the latter units were also located at the periphery, they reacted prior to L units (**Figure III-22**, phase III), as these are expectedly located at the core of *hb*PEster-OH, hence reacting at the last stage (**Figure III-22**, phase IV).

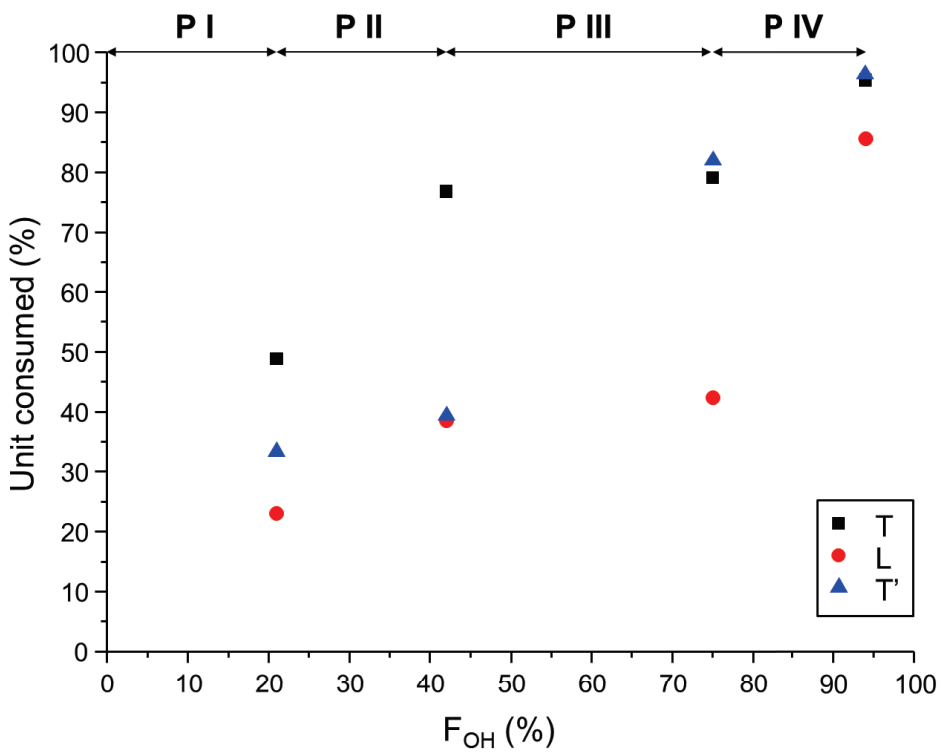

Figure III-22. F_{OH} dependence of the consumption of T, L and T' units.

3.1.2.2. Characterization of the *hb*PEster-A_x

Dimensions and thermal properties of *hb*PEster-A_x samples were determined by SEC in THF, and by DSC. The results are summarized in **Table III-5**.

Table III-5. Characterization data of *hb*PEster-OH and functional *hb*PEster-A_x.

Entry	*hb*PEster	M_n[a] (g/mol)	Đ[a]	T_g[b] (°C)	N(A)[c]	Yield (%)
1	*hb*PEster-OH	7,300	3.6	-23	0	-
2	*hb*PEster-A_{21}	8,200	4.0	-32	5	57
3	*hb*PEster-A_{42}	6,100	5.4	-37	9	52
4	*hb*PEster-A_{75}	10,600	5.6	-42	17	23
5	*hb*PEster-A_{94}	9,600	4.1	-44	21	89

[a] Determined via SEC in THF using PS standard calibration, [b] Obtained by DSC [c] Number of acrylate moieties per hbPEster-A_x

As a general trend, the molecular weight of the *hb*PEster-A_x increased, from 7300 to 10,600 g/mol, upon increasing the functionalization ratio from 21 to 94 % (**Table III-5** and **Figure III-23**). The molecular weight was hardly controlled and side reactions occurred, as demonstrated by SEC traces showing new populations between 16 and 18 min (high molecular weight region) and between 26 and 28 min (low molecular weight region). These observations are consistent with the high dispersities obtained, which ranged from 3.2 to 5.6. Transesterification reactions between several *hb*PEster entities may again explain the formation of species with high and low molecular weights, as depicted in **Figure III-24**.

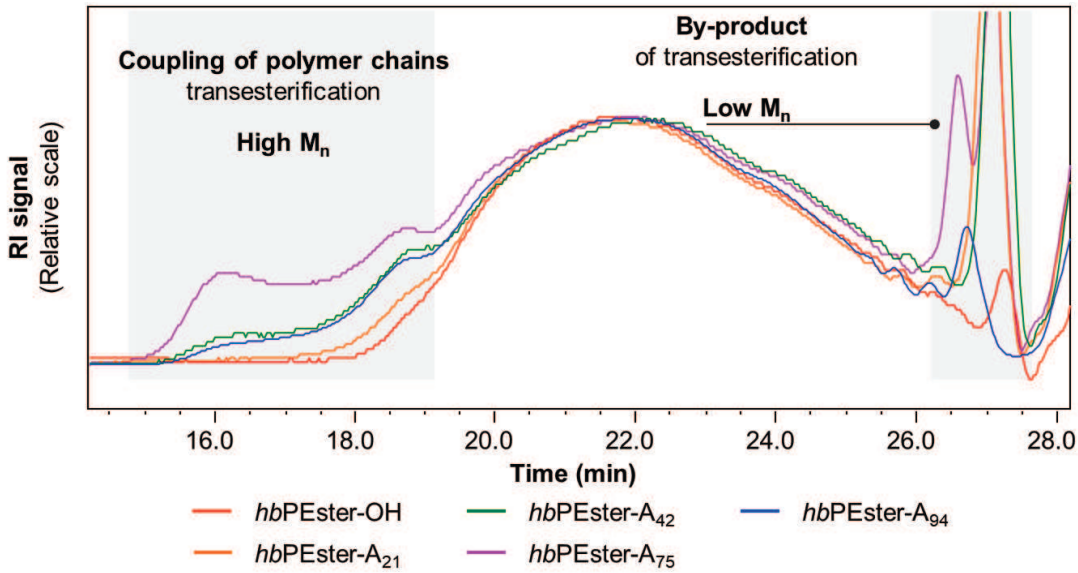

Figure III-23. SEC traces of *hb*PEster-OH and *hb*PEster-A_x.

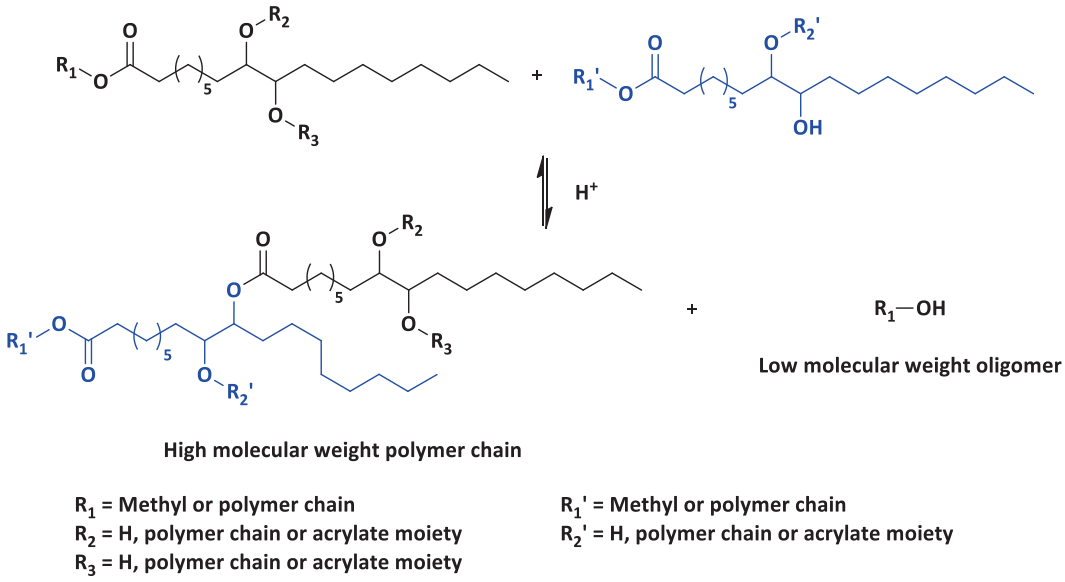

Figure III-24. Transesterification of two *hb*PEster chains generating high molecular weight polymers and low molecular weight oligomers.

As expected, the T_g value decreased when functionalizing the hydroxyl functions of *hb*PEster-OH: from -21 °C for *hb*PEster-OH to -32 °C for *hb*PEster-A_{21}. Lower T_g achieved after derivatization can be correlated to the modification of the *hb*PEster-OH shell, *i.e.* to the reaction of OH functions from the terminal units T and T'. Indeed, the T_g decreased from -32 to -42 °C for F_{OH} ranging from 21 to 75 %. For values of F_{OH} varying from 75 to 94 %, the functionalization mainly concerned OH located at the core, hence T_g remained constant ($T_g \approx$ - 43 °C).

3.2. Hyperbranched polyester polyacrylates as curing agents for the production of cross-linked PMMA's

The functionalized hyperbranched polyester *hb*PEster-A_{94} was incorporated as curing agent as a means to achieve cross-linkable formulations containing a reactive diluent and an initiator. Methyl methacrylate (MMA) was used as a co-monomer for this purpose and AIBN as a free radical initiator. The content in *hb*PEster-A_{94} was varied from 0 to 10 wt.% of the total mass of the reactive system. The methods for the sample preparation were adapted with respect to the amount of *hb*PEster-A_{94}. After curing, the resulting materials, denoted C*hb*PEster$_w$-PMMA (with *w* the mass fraction of *hb*PEster-A_{94} added into the system), were analysed by FTIR spectrometry, DSC, TGA and DMA (**Figure III-25**).

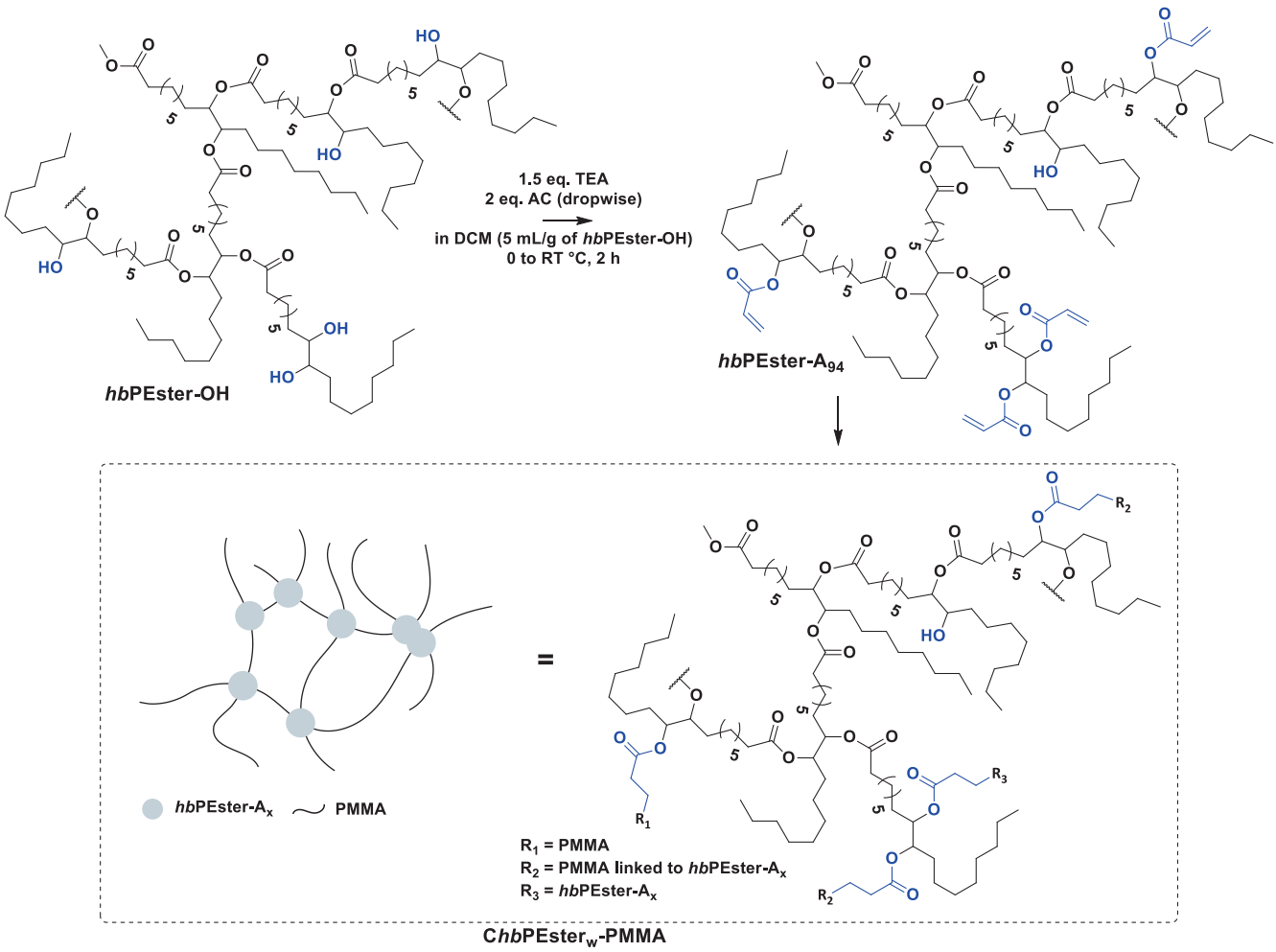

Figure III-25. Synthesis of *hb*PEster-A_{94} and formation of cross-linked C*hb*PEster$_w$-PMMA.

3.2.1. Curing of the reactive mixture and sample preparation

AIBN is an initiator which is commonly used for radical polymerization conducted between 70 and 90 °C; its 1-hour half-life temperature being equal to 82 °C.[65–67] The curing process was thus performed at 80 °C. Due to the high vapour pressure of methyl methacrylate (416 mmHg) at this temperature, precautions had to be taken to prevent the evaporation of the reactive monomer into the mould, which was not fully airtight. The curing was thus conducted in a two-step procedure (**Figure III-26**).

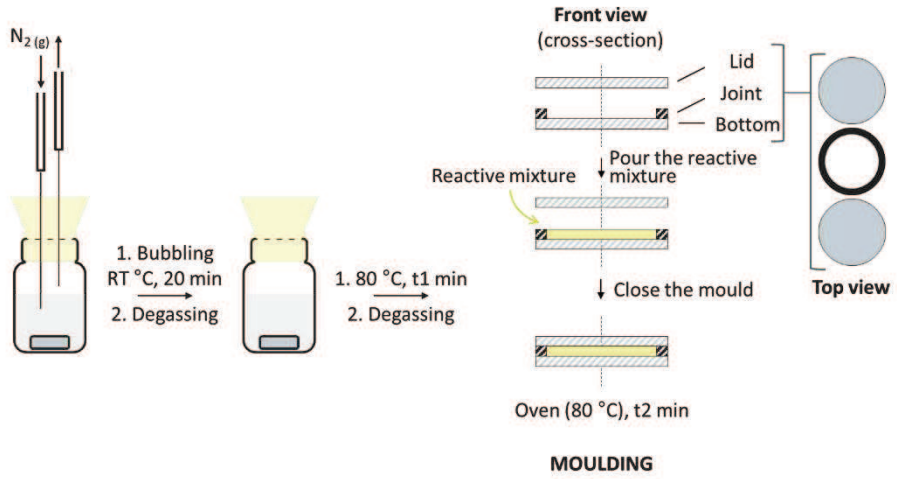

Figure III-26. Curing procedure of the MMA:*hb*PEster-A$_{94}$ systems.

Before the gel point, which was appreciated from preliminary tests performed in vials (see ESI), the curing was initiated in a "sealed" vial at 80 °C (Curing I). The reactive mixture was previously degassed in order to prevent the quenching of the free radicals by oxygen. In this way, the viscosity of the melt increased while the mixture remained fluid. The gel point was reached at different reaction times depending on the nature of the monomer and the amount of *hb*PEster-A$_{94}$ used. As a general trend, the reaction time in vial had to be reduced when increasing the concentration of curing agent in order to be able to pour the reactive mixture into the mould. For instance, the systems were cured for 17 min when incorporating 0.1 wt.% of *hb*PEster-A$_{94}$ and only 3 min when adding 10 wt.% of *hb*PEster-A$_{94}$ (**Table III-6**).

Table III-6. Composition of the curable *hb*PEster-A$_{94}$ based formulations and reaction time.

Entry	Sample	hbPEster-A$_{94}$ *(wt.%)*	t_1 *(min)*	t_2	t_3
1	PMMA	0	17	"	"
2	C*hb*PEster$_{0.1}$-PMMA	0.1	17	"	"
3	C*hb*PEster$_{1.0}$-PMMA	1	15	17 h	17 h
4	C*hb*PEster$_{5.0}$-PMMA	5	5	"	"
5	C*hb*PEster$_{10}$-PMMA	10	3	"	"

t_1, time of curing in the vial at 80 °C (curing I).
t_2, time of curing into the mould in oven at 80 °C (curing II).
t_3, time of curing into the mould in oven at 100 °C (curing III).

In a second stage, the mixture was poured into the mould, just before reaching the gel point, and cured at 80 °C for 17 h (curing stage II). However, the curing was observed not to be

complete and the samples were heated for an additional 17 h at 130 °C (curing stage III). Indeed, after curing II, the DSC analyses revealed an exothermic peak during the first ramp for all the C*hb*PEster$_w$-PMMA samples. This peak totally disappeared after the third curing (**Figure III-27).**

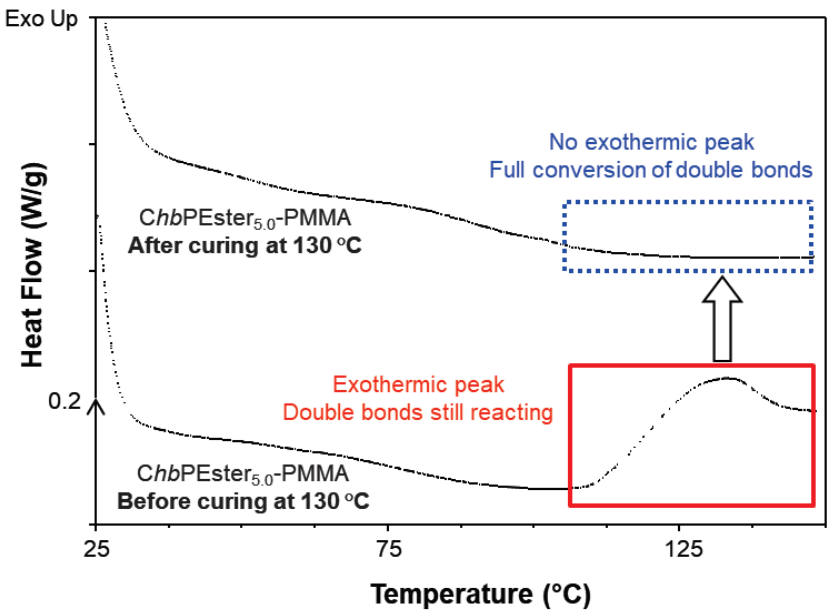

Figure III-27. DSC of C*hb*PEster$_{5.0}$-PMMA before and after the curing at 130 °C in oven.

The absence of exothermic peak on the DSC thermograms after the third stage curing indicated that no reaction of the double bond occurred after the third curing **Figure III-27**. FTIR confirmed these observations. FTIR spectra of the *hb*PEster-A$_{94}$, PMMA and C*hb*PEster$_w$-PMMA are given in **Figure III-28** and **Figure III-29**. As expected, the intensity of the peak corresponding to the C=O stretching bond ($\nu = 1723$ cm^{-1}) increased when incorporating *hb*PEster-A$_{94}$.

The curing was monitored by following the peak decrease of the C=C stretching bond ($\nu = 1637$ cm^{-1}) of the acrylate moiety (**Figure III-28** and **Figure III-29**). As shown in **Figure III-29**, a mass fraction of *hb*PEster-A$_{94}$ $\geq$ 1 wt.% was required for the double bonds to be fully reacted (disappearance of the C=C stretching band). In the case of C*hb*PEster$_{0.1}$-MMA, concentration in *hb*PEster-A$_{94}$ was too low for ensuring full conversion of acrylate moieties.

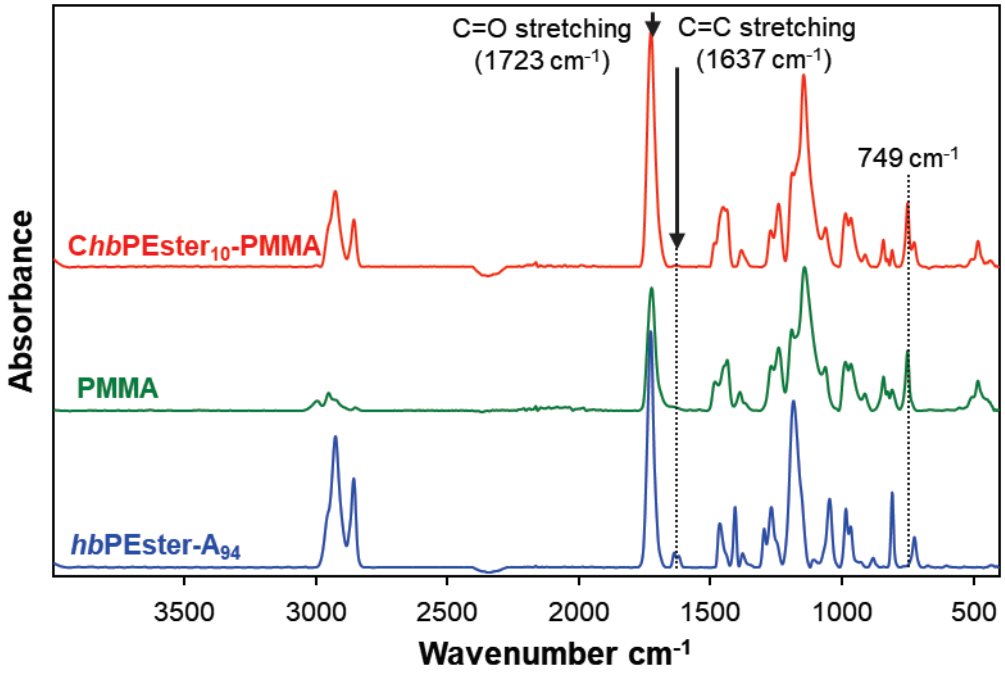

Figure III-28. FTIR spectra of *hb*PEster-A_{94}, PMMA and C*hb*PEster$_{10}$-PMMA.

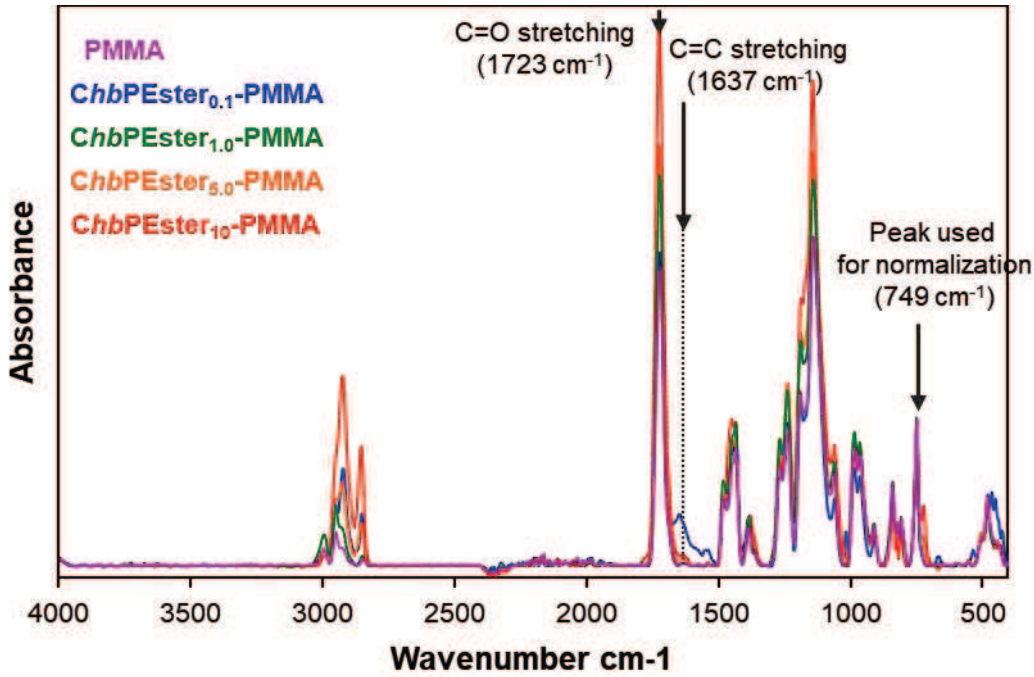

Figure III-29. FTIR spectra of PMMA and C*hb*PEster$_w$-PMMA.

3.2.2. Formation of 3D networks in the presence of *hb*PEster-A$_{94}$

Swelling tests, in THF, were then implemented on the different systems in order to determine their gel content (Eq. III-9) and swelling degree[68] (Eq. III-10). Results are summarized in **Table III-7** and illustrated in **Figure III-30**.

$$\text{Gel content} = \frac{m_{dsws}}{m_{s0}} \qquad \text{(Eq. III-9)}$$

$$\text{Swelling degree} = \frac{m_{sws} - m_{s0}}{m_{s0}} \qquad \text{(Eq. III-10)}$$

with m_{dsws} the mass of the dried swollen sample (80 °C for 24 h), m_{s0} the mass of the sample before swelling and m_{sws} the mass of the swollen sample before drying.

Table III-7. Gel contents and swelling degrees of C*hb*PEster$_w$-PMMA.

Entry	Sample	Gel content *(wt.%)*	Swelling degree *(%)*
1	PMMA	0	-
2	C*hb*PEster$_{0.1}$-PMMA	25	-
3	C*hb*PEster$_{1.0}$-PMMA	94	310
4	C*hb*PEster$_{5.0}$-PMMA	100	150
5	C*hb*PEster$_{10}$-PMMA	100	125

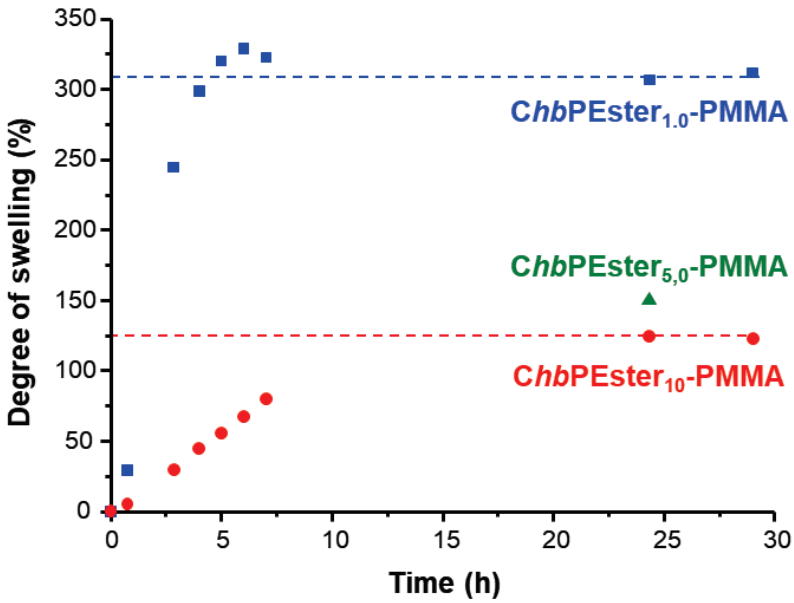

Figure III-30. Degree of swelling *versus* time, for C*hb*PEster$_w$-PMMA with w = 1, 5 and 10.

Due to the high functionality of the *hb*PEster-A_{94} (21 acrylate moieties/*hb*PEster-A_{94}), cross-linking occurred during the copolymerization of MMA and *hb*PEster-A_{94}. The incorporation of more than 1 wt.% of *hb*PEsterA_{94} was required to fully cross-link the materials (gel content ≥ 94 %, **Table III-7**). For lower mass fractions, the concentration of *hb*PEster-A_{94} was too low and only partially cross-linked materials were formed (gel content = 25 wt.%), which was consistent with the results obtained by FTIR (**Figure III-29**).

In the case of mass fractions ranging from 1 to 10 wt.%, swelling degrees of maximum 310 wt.% were obtained. As expected, the swelling degree decreased when increasing the content of *hb*PEster-A_{94} (125 wt.% for w = 10 wt.%), the networks being denser when increasing the content of curing agent (**Figure III-31**).

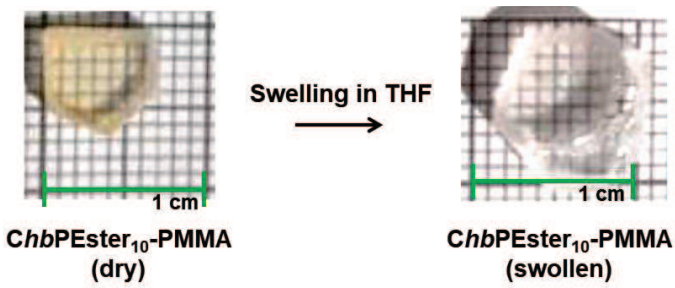

Figure III-31. Picture of C*hb*PEster$_{10}$-PMMA sample, after 30 h of swelling in THF.

3.2.3. Thermal and thermo-mechanical properties of ChbPEster$_w$-PMMA

DSC, DMA and TGA analyses were performed to determine the thermal and thermo-mechanical properties of the C*hb*PEster$_w$-PMMA. The glass transition temperatures (T_g), the storage modulus (E'), the loss modulus (E"), the 5 wt.% loss temperature and the maximum degradation temperature ($T_{d,max}$) are indicated in **Table III-8**.

Table III-8. Thermal and thermo-mechanical properties of the C*hb*PEster$_w$-PMMA.

Entry	Sample	$T_{g,1}$ [a] (°C)	$T_{g,2}$ [b] (°C)	E'(40 °C) [c] (GPa)	$T_{d5\%}$ [d] (°C)	$T_{d,max}$ [d] (°C)
1	PMMA	104	98	1,0	215	374
2	C*hb*PEster$_{0.1}$-PMMA	104	94	1,8	223	371
3	C*hb*PEster$_{1.0}$-PMMA	98	87	2,0	232	379
4	C*hb*PEster$_{5.0}$-PMMA	90	74	2,2	270	380
5	C*hb*PEster$_{10}$-PMMA	103	88	1.6	324	380

[a] T_g determined by DSC, [b] T_g measured by DMA with E" plot, [c] Storage modulus of the glassy plateau obtained by DMA at 40 °C, [d] Degradation temperatures obtained by TGA.

3.2.3.1. Glass transition temperature

As can be seen from **Table III-8**, addition of *hb*PEster-A_{94} in the PMMA matrix, at ratios ranging from 0.1 and 5 wt.%, causes the T_g of the networks' to decrease from 104 to 90 °C (DSC, **Figure III-32**). This can be explained by the fact that *hb*PEster-A_{94} additive exhibits a low T_g (-44 °C). However, for a *hb*PEster-A_{94} content of 10 wt.%, the T_g increased up to 103 °C, a value close to that of pure PMMA. This behaviour has already been reported as a consequence of the compact structure of hyperbranched polymers, which constrains the chains of the networks when the cross-linking density increases.[49,52,53,56] Similar trend was observed for T_g calculated by DMA ($T_g = T(E''_{max})$, **Figure III-33**).

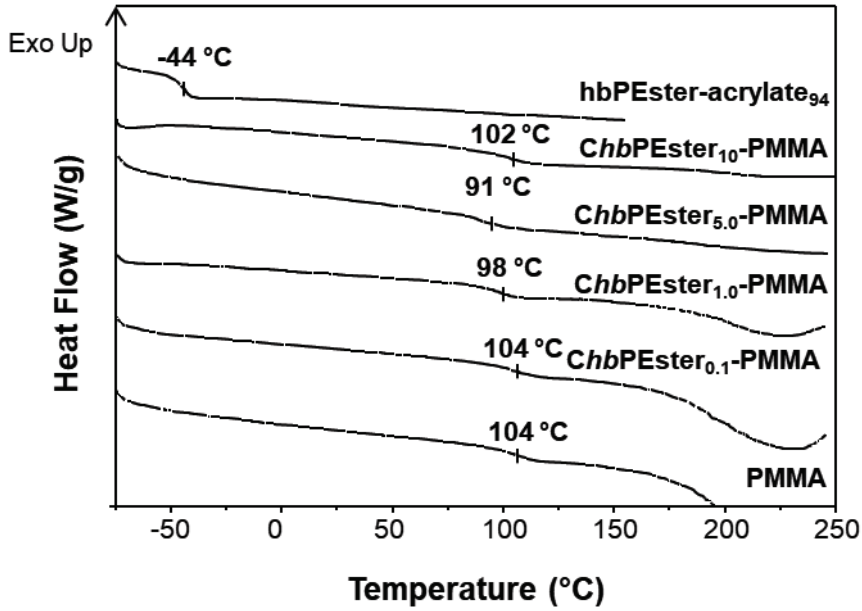

Figure III-32. DSC traces of PMMA, C*hb*PEster$_w$-PMMA and *hb*PEster-A_{94}.

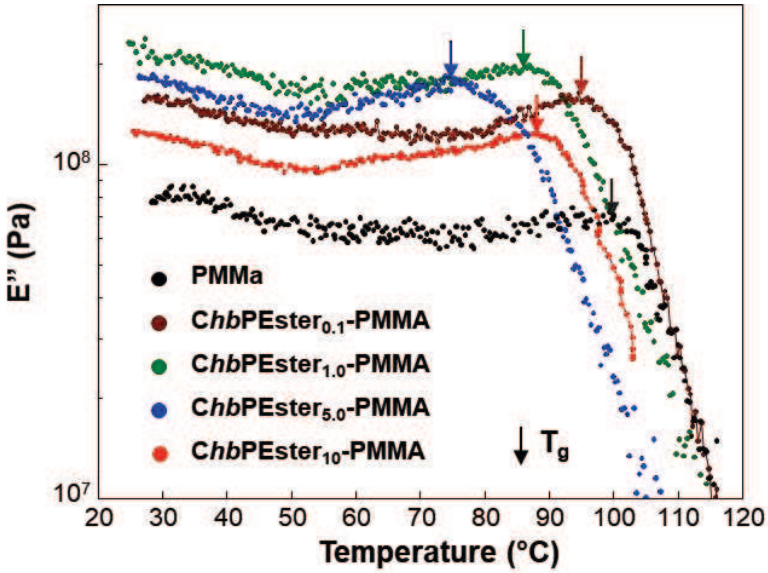

Figure III-33. Temperature versus E'' of PMMA and C*hb*PEster$_w$-PMMA, with $T_g = T(E''_{max})$.

3.2.3.2. Thermo-mechanical properties

Samples of PMMA, C*hb*PEster$_w$-PMMA, were cut in strips and analyzed by DMA (at 1 Hz, in the linear domain), using single cantilever mode. The storage moduli of the glassy state plateau were measured at 40 °C (**Figure III-34**). In addition, a frequency sweep test was performed at 150 °C (> T_g) for C*hb*PEster$_{1.0}$-PMMA, C*hb*PEster$_{5.0}$-PMMA and C*hb*PEster$_{10}$-PMMA. Data are given in **Table III-8**.

DMA experiments demonstrated that addition of *hb*PEster-A$_{94}$ led to an increase of E' at the glassy plateau, from 1 GPa (PMMA) to 2.2 GPa (C*hb*PEster$_{5.0}$-PMMA) (**Figure III-34**). This reinforcement might be ascribed to the cross-linking of the C*hb*PEster$_w$-PMMA, even though the T_g was lower than for PMMA. For instance, C*hb*PEster$_{0.1}$-PMMA having a low gel fraction (25 wt.%) have a higher storage modulus (1.8 GPa) than PMMA.

As can be seen on frequency sweep test (**Figure III-35**), G' remained almost constant with respect to ω while G" increased when increasing ω. This feature, which is characteristic of cross-linked materials, is a piece of evidence that PMMA networks were formed. Moreover, the storage modulus increased for higher contents of *hb*PEster-A$_{94}$, confirming that the *hb*PEster reinforced C*hb*PEster-PMMA networks.

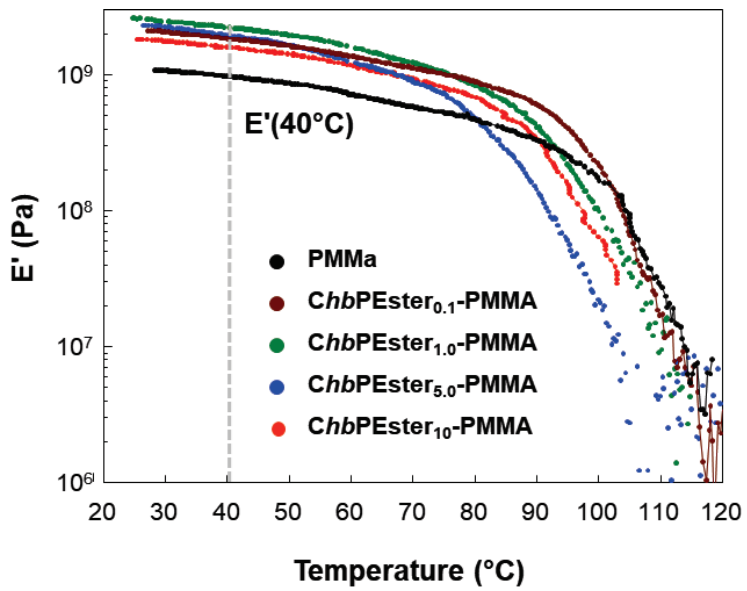

Figure III-34. DMA traces of PMMA and C*hb*PEster$_w$-PMMA.

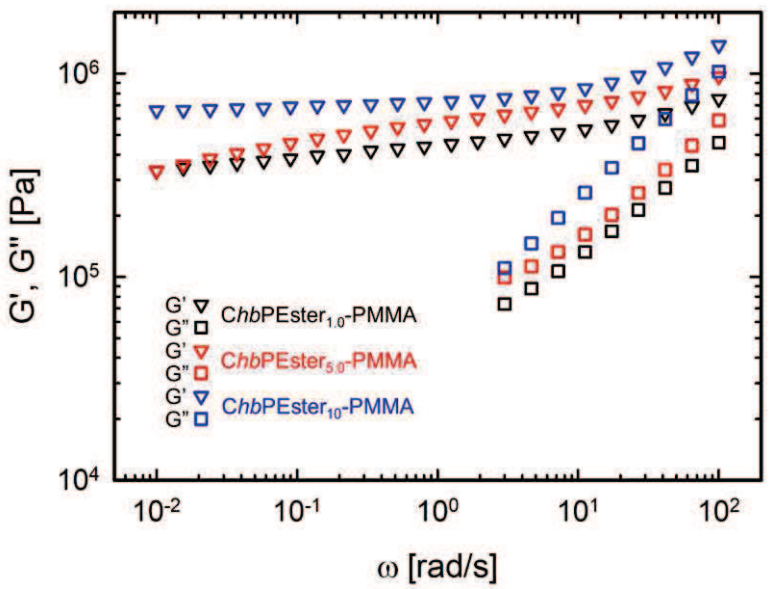

Figure III-35. G' and G" versus the angular frequency, at 150 °C, of C*hb*PEster$_{1.0}$-PMMA, C*hb*PEster$_{5.0}$-PMMA and C*hb*PEster$_{10}$-PMMA.

3.2.3.3. Thermal degradation

The thermal stability of *hb*PEster-A_{94}, PMMA and C*hb*PEster$_w$-PMMA, was determined by TGA. $T_{d5\%}$ and T_{dmax} are given in **Table III-8**. These values were compared with those obtained for *hb*PEster-A_{94} ($T_{d5\%}$ = 328 °C and T_{dmax} = 355 °C).

PMMA displayed a two-step degradation process, which is commonly observed for PMMA polymerized *via* free radical polymerization (**Figure III-36**).[69] The first weight loss, from ca. 200 to 325 °C, was ascribed to the degradation of low molecular weights PMMA formed by termination side-reactions.[70,71]

Addition of *hb*PEster-A_{94} resulted in an increase of $T_{d5\%}$ from 215 to 324 °C. It can be assumed that extent of *hb*PEster-A_{94} superior to 5 wt.% prevented termination side-reactions as the "initial" weight loss did not occur for C*hb*PEster$_{5.0}$-PMMA and C*hb*PEster$_{10}$-PMMA. To a lesser extent, T_{dmax} slightly increased from 374 °C to 380 °C when increasing the amount of *hb*PEster-A_{94} from 0 to 10 wt.%.

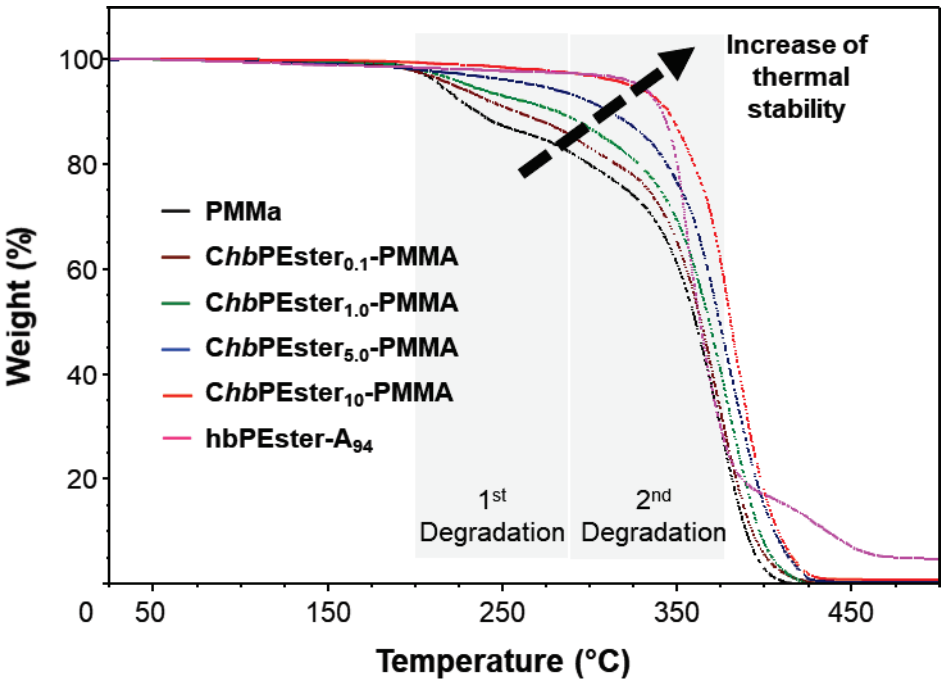

Figure III-36. TGA analyses of pure PMMA, C*hb*PEster$_w$-PMMA resins and *hb*PEster-A_{94}.

3.3. Copolymerization of hyperbranched polyester polyacrylate with styrene

3.3.1. Curing of the reactive mixture and sample preparation

Curing of *hb*PEster-A_{94}/styrene systems was performed in two steps (vial + mould), using again AIBN as initiator, similarly to the procedure uses for PMMA-based systems. As already observed, the reaction time in vial had to be reduced when increasing the concentration of *hb*PEster-A_{94}; from 160 min (0.1 wt.% of *hb*PEster-A_{94}) to 6 min (10 wt.% of *hb*PEster-A_{94}) (**Table III-9**). It can be noted that reaction times were longer for styrene than for MMA formulations; for instance, at 1 wt.% of *hb*PEster-A_{94}, increase of viscosity was observed after 55 min for styrene against 15 min for MMA. This difference was minimized when increase the amount of curing agent. Completion of the reaction was confirmed by DSC analyses, as no exothermic peak was observed during the first ramp of temperature. However, in the case of C*hb*PEster$_{10}$-PS, styrene partially evaporated during the curing in the mould.

Table III-9. Composition of the curable *hb*PEster-A_{94} based formulations and reaction time.

Entry	Sample	hbPEster-A_{94} *(wt.%)*	t_1 *(min)*	t_2	t_3
1	PS	0	160		
2	C*hb*PEster$_{0.1}$-PS	0.1	140	17 h	
3	C*hb*PEster$_{1.0}$-PS	1	55		17 h
4	C*hb*PEster$_{5.0}$-PS	5	7		
5	C*hb*PEster$_{10}$-PS	10	6	17 h*	

t_1, time of curing in the vial at 80 °C (curing I).
t_2, time of curing into the mould in oven at 80 °C (curing II).
t_3, time of curing into the mould in oven at 130 °C (curing III)
* partial evaporation of styrene.

3.3.2. FTIR spectroscopy and swelling tests

FTIR spectroscopy was performed to confirm the completion of the reaction. The same methodology as the one applied for PMMA systems was implemented for PS systems. FTIR spectra of the *hb*PEster-A_{94}, PS and C*hb*PEster$_x$-PS are given in **Figure III-37** and **Figure III-38**. The intensity of the peak corresponding to the C=C stretching bond (ν = 1637 cm^{-1}) was also followed (**Figure III-38**). Although this peak disappeared for C*hb*PEster$_{0.1}$-PS and C*hb*PEster$_{5.0}$-PS, it remained visible for C*hb*PEster$_{1.0}$-PS and C*hb*PEster$_{10}$-PS, implying that *hb*PEster-A_{94} chain ends partially reacted in the latter cases.

For 10 wt.% of *hb*PEster-A_{94}, the low intensity peak of the C=O stretching bond (ν = 1723 cm^{-1}) is particularly low, which could be ascribed to evaporation of styrene.

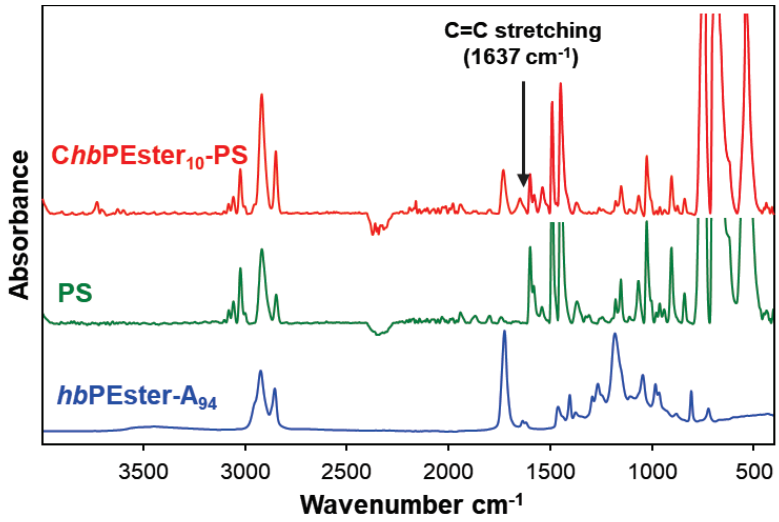

Figure III-37. FTIR spectra of *hb*PEster-A_{94}, PS and C*hb*PEster$_{10}$-PS.

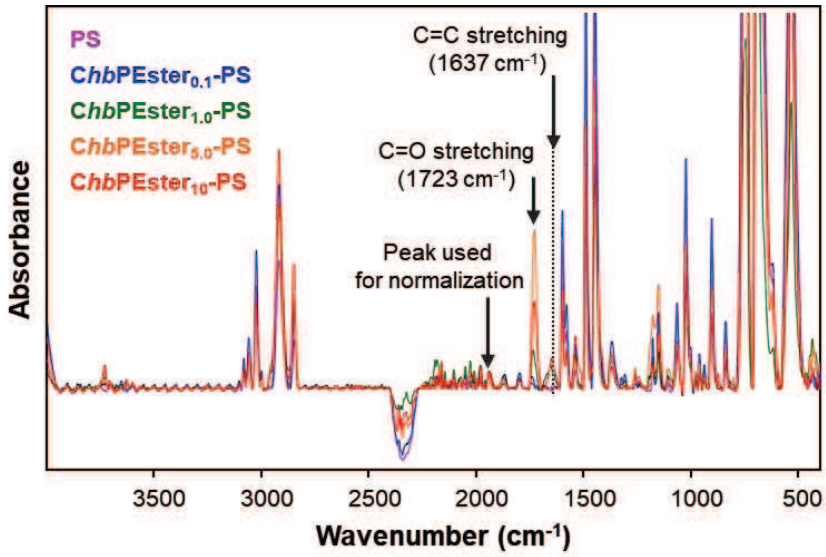

Figure III-38. FTIR spectra of PS and C*hb*PEster$_x$-PS.

Similarly to PMMA systems, no cross-linking occurred for 0.1wt.% of *hb*PEster-A_{94} and the gel content was rather limited for 1.0wt % of *hb*PEster-A_{94} (< 10 wt.%) (**Table III-10**). Gel contents close to 100 wt.% were obtained for mass fractions of *hb*PEster-A_{94} higher than 5 wt.% with swelling degrees of 290 and 160 % for C*hb*PEster$_{5.0}$-PS and C*hb*PEster$_{10}$-PS, respectively, values being in the same range to those obtained for PMMA systems.

Table III-10. Gel contents and swelling degrees of C*hb*PEster$_x$-PS.

Entry	Sample	Gel content *(wt.%)*	Swelling degree *(%)*
6	PS	0	-
7	C*hb*PEster$_{0.1}$-PS	0	-
8	C*hb*PEster$_{1.0}$-PS	< 10	-
9	C*hb*PEster$_{5.0}$-PS	100	290
10	C*hb*PEster$_{10}$-PS	96	160

3.3.3. Thermal and thermo-mechanical properties of C*hb*PEster$_w$-PS

Values of glass transition temperatures (T_g), storage modulus (E'), loss modulus (E"), 5 wt.% loss temperature and maximum degradation temperature ($T_{d,max}$) are given in **Table III-11**.

Table III-11. Thermal and thermos-mechanical of the C*hb*PEster$_w$-PS.

Entry	Sample	$T_{g,1}$ [a] *(°C)*	$T_{g,2}$ [b] *(°C)*	E'(40 °C) [c] *(GPa)*	$T_{d5\%}$ [d] *(°C)*	$T_{d,max}$ [d] *(°C)*
1	PS	101	97	1,7	369	413
2	C*hb*PEster$_{0.1}$-PS	100	98	1,9	370	413
3	C*hb*PEster$_{1.0}$-PS	102	94	1,8	379	415
4	C*hb*PEster$_{5.0}$-PS	100	94	1,5	374	414
5	C*hb*PEster$_{10}$-PS	98	97	1,4	370	414

[a] T_g determined by DSC, [b] T_g measured by DMA with E" plot, [c] Storage modulus of the glassy obtained by DMA at 40 °C, [d] Degradation temperatures obtained by TGA.

As can be seen from **Table III-11** and **Figure III-39**, no change in T_g values was observed by DSC ($T_{g,1}$ ~ 100 °C). Low decrease was observed by DMA for ($T_{g,2}$ = 94 °C) but such variation remained limited and could be attributed to experimental error.

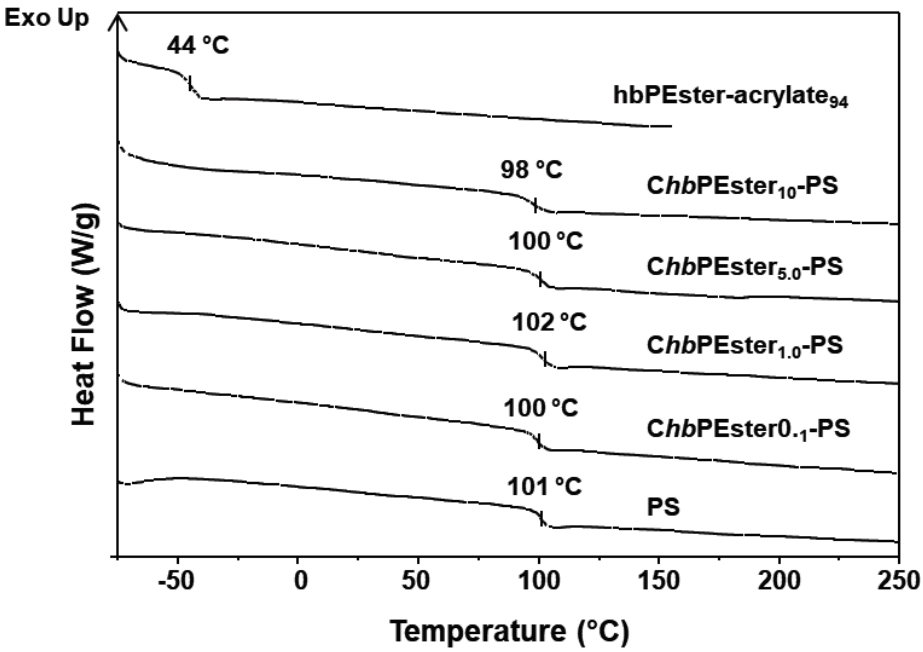

Figure III-39. DSC traces of PS, C*hb*PEster$_w$-PS and *hb*PEster-A$_{94}$.

DMA experiments demonstrated that the addition of *hb*PEster-A$_{94}$ had no effect on E' of the glassy plateau for extents of *hb*PEster-A$_{94}$ lower than 1.0 wt.%, due to the lack of cross-linking (**Figure III-40**). For more than 5.0 wt.% of *hb*PEster-A$_{94}$, the latter seems to act as a plasticizer, as E' slightly decreased from 1.7 GPa (PS) to 1.4 GPa.

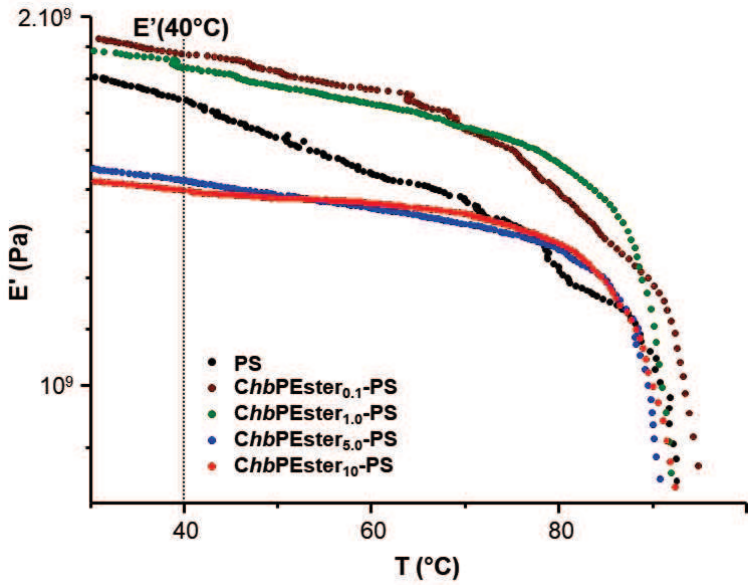

Figure III-40. DMA traces of PS and C*hb*PEster$_w$-PS.

Although the addition of *hb*PEster-A_{94} tends to enhance the thermal stability of the PMMA matrices, no influence was noted in the case of PS systems, $T_{d5\%}$ and $T_{d,max}$ remaining close to 370 °C and 413 °C, respectively, irrespective of the content of *hb*PEster-A_{94}. These results thus suggested that no copolymerization occurred between the *hb*PEster-A_{94} and the styrene.

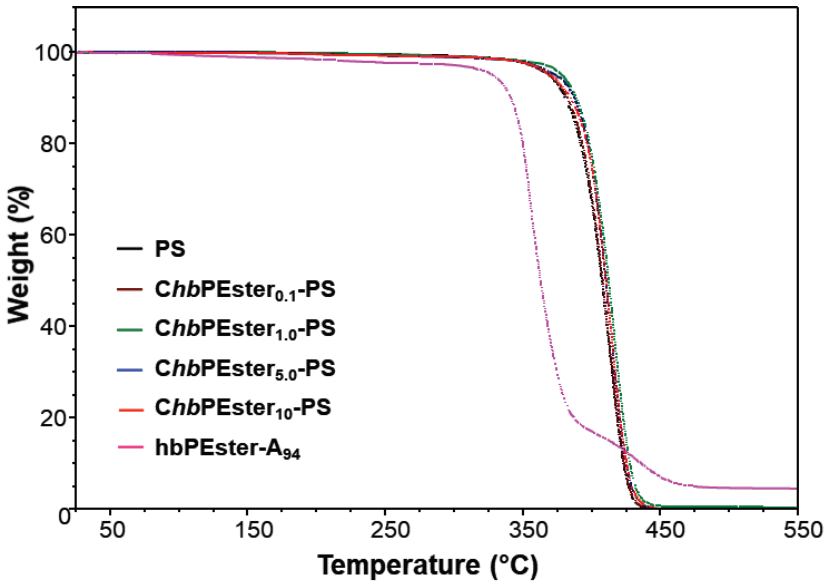

Figure III-41. TGA analyses of pure PS, C*hb*PEster$_w$-PS resins and *hb*PEster-A_{94}.

3.4. Conclusion

Bio-based M2HS-derived hyperbranched polyesters were successfully functionalized with acryloyl chloride, generating acrylate terminated hyperbranched polyesters, *hb*PEster-A_x. The extent of derivatized OH group could be varied from 21 to 94 %. Along with the derivatization step, coupling by transesterification reaction between the hyperbranched structures was speculated as attested by an increase of the polymer dispersity. The hyperbranched polyester polyacrylates could then serve as curing agents, in a similar way as regular linear unsaturated polyesters. *Hb*PEster-A_{94} was thus added to cross-linkable formulations containing a reactive diluent (MMA) and an initiator (AIBN).

PMMA-based networks were prepared by adding from 0.1 to 10 wt.% of *hb*Pester-A_{94} with respect to MMA; full cross-linking was obtained when using extent of *hb*PEster-A_{94} superior to 1 wt.%. While the glass transition temperature was reduced from 105°C to 90°C when adding 1 to 5 wt.% of *hb*PEster-A_{94}, the T_g re-increased till the T_g of native PMMA, for 10 wt.% of curing agent content; this phenomenon is explained by the compact structure of the hyperbranched polymer which constrains the chains of the networks. Thermo-mechanical

analyses confirmed that networks were formed and that *hb*PEster-A_{94} acted as a re-inforcement agent. Moreover, thermal stability was enhanced as *hb*PEster-A_{94} aimed at limiting the formation of PMMA of low molecular weights.

Similar experiments were conducted using styrene as a reactive diluent. In this case, however, full cross-linking only occurred for extents of *hb*PEster-A_{94} higher than 5.0 wt.%. Although, no significant influence on thermo-mechanical and mechanical properties was noted.

4. Conclusion and outlooks

Post-functionalization is a powerful tool for tuning the properties of hyperbranched polymers. In this work, derivatization of hyperbranched polyesters derived from plant oils, and produced at a large scale by ITERG, has been implemented. Secondary OH from M2HS-*hb*Pester can be successfully esterified, from ca. 20 to 100%, with succinic anhydride and acryloyl chloride. The derivatization of *hb*PEster-OH with succinic anhydride enables to generate amphiphilic hyperbranched polyelectrolytes having a hydrophobic core and a thin hydrophilic shell. Such compounds can be solubilized in water depending on the content of acid chain ends and on their degree of neutralization, *i.e.* of the pH. Even though it seems difficult to fully control the assembly of these specimens in solution, further tests should be performed to confirm their ability to load and release hydrophobic molecules. Their surfactant properties should be also investigated.

Acrylate-terminated hyperbranched polyesters (*hb*PEster-A) can also be synthesized by esterification of M2HS-*hb*PEster with acryloyl chloride. Copolymerization of *hb*PEster-A_{94}, used as curing agent, with methyl methacrylate or styrene leads to the formation of different networks, in which *hb*PEster act as a reinforcing agent (PMMA-based resins). Other mechanical properties such as tensile, compressive and flexible strengths, or pencil and shore hardness should be investigated in order to define appropriate applications. Due to the presence of ester bonds into the *hb*PEster-A_{94} backbone, the degradability of the samples under basic conditions could be studied. Finally, the use of other acrylates or methacrylates reactive diluents, bio-based for instance, could be investigated to extend the possible properties of the materials.

Obviously, other molecules, oligomers or polymers could be grafted to *hb*PEsters to tune their properties. For instance, derivatization with poly(ethylene glycol)s or with fatty acids of long aliphatic chains could be implemented to reinforce the solubility of these polymers in water or oils, respectively. Another objective involves the development of *hb*PEsters platform in the frame of maturation projects, with the aim of meeting specific applications. Last but not least, the synthetic pathways can be laid to other substrates, including *hb*PEthers developed in chapter II, paving the way to numerous combination of properties.

5. References

(1) Testud, B.; Grau, E.; Pintori, D.; Taton, D.; Cramail, H. New Branched Polymers, Their Preparation Process and Thereof. EU 14306642 A1, 2014.

(2) Testud, B. Vegetable Oils as a Platform for the Design of Novel Hyperbranched Polyesters, PhD Thesis, Université de Bordeaux, 2015.

(3) Testud, B.; Pintori, D.; Grau, E.; Taton, D.; Cramail, H. Hyperbranched Polyesters by Polycondensation of Fatty Acid-Based ABn-Type Monomers. *Green Chem* **2017**, *19*, 259–269.

(4) Köckritz, A.; Martin, A. Oxidation of Unsaturated Fatty Acid Derivatives and Vegetable Oils. *Eur J Lipid Sci Technol* **2008**, *110* (9), 812–824.

(5) Yates, C. R.; Hayes, W. Synthesis and Applications of Hyperbranched Polymers. *Eur Polym J* **2004**, *40* (7), 1257–1281.

(6) Gao, C.; Yan, D. Hyperbranched Polymers: From Synthesis to Applications. *Prog Polym Sci* **2004**, *29* (3), 183–275.

(7) Inoue, K. Functional Dendrimers, Hyperbranched and Star Polymers. *Prog Polym Sci* **2000**, *25* (4), 453–571.

(8) Voit, B. I.; Lederer, A. Hyperbranched and Highly Branched Polymer Architectures—Synthetic Strategies and Major Characterization Aspects. *Chem Rev* **2009**, *109* (11), 5924–5973.

(9) Yan, D.; Gao, C.; Frey, H. *Hyperbranched Polymers: Synthesis, Properties, and Applications*; John Wiley & Sons, Inc.: Hoboken, 2011.

(10) Meng, Q.; Chen, D.; Yue, L.; Fang, J.; Zhao, H.; Wang, L. Hyperbranched Polyesters with Carboxylic or Sulfonic Acid Functional Groups for Crystallization Modification of Calcium Carbonate. *Macromol Chem Phys* **2007**, *208* (5), 474–484.

(11) Malmström, E.; Johansson, M.; Hult, A. The Effect of Terminal Alkyl Chains on Hyperbranched Polyesters Based on 2,2-Bis(Hydroxymethyl)Propionic Acid. *Macromol Chem Phys* **1996**, *197* (10), 3199–3207.

(12) Ornatska, M.; Peleshanko, S.; Genson, K. L.; Rybak, B.; Bergman, K. N.; Tsukruk, V. V. Assembling of Amphiphilic Highly Branched Molecules in Supramolecular Nanofibers. *J Am Chem Soc* **2004**, *126* (31), 9675–9684.

(13) Ornatska, M.; Bergman, K. N.; Goodman, M.; Peleshanko, S.; Shevchenko, V. V.; Tsukruk, V. V. Role of Functionalized Terminal Groups in Formation of Nanofibrillar Morphology of Hyperbranched Polyesters. *Polymer (Guildf)* **2006**, *47* (24), 8137–8146.

(14) Tu, C.; Zhu, L.; Qiu, F.; Wang, D.; Su, Y.; Zhu, X.; Yan, D. Facile PEGylation of Boltorn® H40 for PH-Responsive Drug Carriers. *Polym (United Kingdom)* **2013**, *54* (8), 2020–2027.

(15) Wang, D.; Jin, Y.; Zhu, X.; Yan, D. Synthesis and Applications of Stimuli-Responsive Hyperbranched Polymers. *Prog Polym Sci* **2017**, *64* (7), 114–153.

(16) Tian, W.; Li, X.; Wang, J. Supramolecular Hyperbranched Polymers. *Chem Commun* **2017**, *53* (17), 2531–2542.

(17) Joshi, M.; Adak, B. Advances in Nanotechnology Based Functional , Smart and Intelligent Textiles : A Review. *Compr Nanosci Nanotechnology, 2nd Ed* **2018**, 1–38.

(18) Irfan, M.; Seiler, M. Encapsulation Using Hyperbranched Polymers: From Research and Technologies to Emerging Applications. *Ind Eng Chem Res* **2010**, *49* (3), 1169–1196.

(19) Zhou, Y.; Huang, W.; Liu, J.; Zhu, X.; Yan, D. Self-Assembly of Hyperbranched Polymers and Its Biomedical Applications. *Adv Mater* **2010**, *22* (41), 4567–4590.

(20) Mahdavi, H.; Sahraei, R. Synthesis and Application of Hyperbranched Polyester-Grafted Polyethylene (HBPE-g-PE) Containing Palladium Nanoparticles as Efficient Nanocatalyst.

Catal Letters **2016**, *146* (5), 977–990.

(21) Niu, S.; Yan, H.; Chen, Z.; Du, Y.; Huang, W.; Bai, L.; Lv, Q. Hydrosoluble Aliphatic Tertiary Amine-Containing Hyperbranched Polysiloxanes with Bright Blue Photoluminescence. *RSC Adv* **2016**, *6* (108), 106742–106753.

(22) Binauld, S.; Stenzel, M. H. Acid-Degradable Polymers for Drug Delivery: A Decade of Innovation. *Chem Commun* **2013**, *49* (21), 2082.

(23) Amreddy, N.; Babu, A.; Muralidharan, R.; Panneerselvam, J.; Srivastava, A.; Ahmed, R.; Mehta, M.; Munshi, A.; Ramesh, R. Recent Advances in Nanoparticle-Based Cancer Drug and Gene Delivery. *Adv Cancer Res* **2018**, *137*, 155–170.

(24) Jin, H.; Huang, W.; Zhu, X.; Zhou, Y.; Yan, D. Biocompatible or Biodegradable Hyperbranched Polymers: From Self-Assembly to Cytomimetic Applications. *Chem Soc Rev* **2012**, *41* (18), 5986.

(25) Huang, G.; Li, W.; Liu, Q.; Liu, J.; Zhang, H.; Li, R.; Li, Z.; Jing, X.; Wang, J. Efficient Removal of Uranium(VI) from Simulated Seawater with Hyperbranched Polyethylenimine (HPEI)-Functionalized Polyacrylonitrile Fibers. *New J Chem* **2018**, *42* (1), 168–176.

(26) Fei, X.; Wei, W.; Tang, Y.; Zhu, Y.; Luo, J.; Chen, M.; Liu, X. Simultaneous Enhancements in Toughness, Tensile Strength, and Thermal Properties of Epoxy-Anhydride Thermosets with a Carboxyl-Terminated Hyperbranched Polyester. *Eur Polym J* **2017**, *90* (February), 431–441.

(27) Rossi, N. A. A.; Constantinescu, I.; Kainthan, R. K.; Brooks, D. E.; Scott, M. D.; Kizhakkedathu, J. N. Red Blood Cell Membrane Grafting of Multi-Functional Hyperbranched Polyglycerols. *Biomaterials* **2010**, *31* (14), 4167–4178.

(28) Chapanian, R.; Constantinescu, I.; Brooks, D. E.; Scott, M. D.; Kizhakkedathu, J. N. Invivo Circulation, Clearance, and Biodistribution of Polyglycerol Grafted Functional Red Blood Cells. *Biomaterials* **2012**, *33* (10), 3047–3057.

(29) Pocoví-Martínez, S.; Kemmer-Jonas, U.; Pérez-Prieto, J.; Frey, H.; Stiriba, S. Supramolecular Antioxidant Assemblies of Hyperbranched Polyglycerols and Phenols. *Macromol Chem Phys* **2014**, *215* (23), 2311–2317.

(30) Volden, S.; Glomm, W. R.; Magnusson, H.; Øye, G.; Sjöblom, J. Dendrimers and Hyperbranched Polyesters as Structure-Directing Agents in the Formation of Nanoporous Silica. *J Dispers Sci Technol* **2006**, *27* (6), 893–897.

(31) Tong, J. G.; Wei, Z. Y.; Yang, H. L.; Yang, Z. Y.; Chen, Y. Study on the Phase Transition Behaviors of Thermoresponsive Hyperbranched Polyampholytes in Water. *Polym (United Kingdom)* **2016**, *84*, 107–116.

(32) Shiau, S.; Juang, T.; Chou, H.; Liang, M. Synthesis and Properties of New Water-Soluble Aliphatic Hyperbranched Poly (Amido Acids) with High PH-Dependent Photoluminescence. *Polymer (Guildf)* **2013**, *54* (2), 623–630.

(33) Sivasankarapillai, G.; Mcdonald, A. G. Synthesis and Properties of Lignin-Highly Branched Poly (Ester-Amine) Polymeric Systems. *Biomass and Bioenergy* **2010**, *35* (2), 919–931.

(34) Chaffraix, T.; Voda, A. S.; Dumée, L. F.; Magniez, K. Surface Ionic Charge Dependence on the Molecular Mobility and Self-Assembly Behavior of Ionomers Produced from Carboxylic Acid-Terminated Dendrimers. *Polym J* **2016**, *49* (2), 245–254.

(35) Stefani, S.; Kurniasih, I. N.; Sharma, S. K.; Böttcher, C.; Servin, P.; Haag, R. Triglycerol-Based Hyperbranched Polyesters with an Amphiphilic Branched Shell as Novel Biodegradable Drug Delivery Systems. *Polym Chem* **2016**, *7* (4), 887–898.

(36) Schubert, C.; Osterwinter, C.; Tonhauser, C.; Schömer, M.; Wilms, D.; Frey, H.; Friedrich, C. Can Hyperbranched Polymers Entangle? Effect of Hydrogen Bonding on Entanglement Transition and Thermorheological Properties of Hyperbranched Polyglycerol Melts.

Macromolecules **2016**, *49* (22), 8722–8737.

(37) Tonhauser, C.; Wilms, D.; Korth, Y.; Frey, H.; Friedrich, C. Entanglement Transition in Hyperbranched Polyether-Polyols. *Macromol Rapid Commun* **2010**, *31* (24), 2127–2132.

(38) Lederer, A.; Burchard, W. *Hyperbranched Polymers*; The Royal Society of Chemistry: Cambridge, UK, 2015.

(39) Calderón, M.; Quadir, M. A.; Sharma, S. K.; Haag, R. Dendritic Polyglycerols for Biomedical Applications. *Adv Mater* **2010**, *22* (2), 190–218.

(40) *The MAK-Collection for Occupational Health and Safety*; Wiley-VCH Verlag GmbH & Co. KGaA: Weinheim, Germany, 2002.

(41) Carothers, W. H. Studies on Polymerization and Ring Formation. I. An Introduction to the General Theory of Condensation Polymers. *J Am Chem Soc* **1929**, *51* (8), 2548–2559.

(42) Staudinger, H. The Formation of High Polymers of Unsaturated Substances. *Trans Faraday Soc* **1936**, *32* (32), 97.

(43) Kandelbauer, A.; Tondi, G.; Zaske, O. C.; Goodman, S. H. *Unsaturated Polyesters and Vinyl Esters*, Third Edit.; Elsevier Inc., 2013.

(44) Malik, M.; Choudhary, V.; Varma, I. K. Current Status of Unsaturated Polyester Resins. *J Macromol Sci Part C Polym Rev* **2000**, *40* (2–3), 139–165.

(45) Gonçalves, F. A. M. M.; Fonseca, A. C.; Domingos, M.; Gloria, A.; Serra, A. C.; Coelho, J. F. J. The Potential of Unsaturated Polyesters in Biomedicine and Tissue Engineering: Synthesis, Structure-Properties Relationships and Additive Manufacturing. *Prog Polym Sci* **2017**, *68*, 1–34.

(46) Miyagawa, H.; Mohanty, A. K.; Burgueño, R.; Drzal, L. T.; Misra, M. Novel Biobased Resins from Blends of Functionalized Soybean Oil and Unsaturated Polyester Resin. *J Polym Sci Part B Polym Phys* **2007**, *45* (6), 698–704.

(47) Fröhlich, J.; Kautz, H.; Thomann, R.; Frey, H.; Mülhaupt, R. Reactive Core/Shell Type Hyperbranched Blockcopolyethers as New Liquid Rubbers for Epoxy Toughening. *Polymer (Guildf)* **2004**, *45* (7), 2155–2164.

(48) Zhang, X. Modifications and Applications of Hyperbranched Aliphatic Polyesters Based on Dimethylolpropionic Acid. *Polym Int* **2011**, *60* (2), 153–166.

(49) Wan, Q.; Schricker, S. R.; Culbertson, B. M. Methacryloyl Derivitized Hyperbranched Polyester. 1. Synthesis, Characterization and Copolymerization. *J Macromol Sci Part A* **2000**, *37* (11), 1301–1315.

(50) Xu, N.; Shi, W.; Gong, M.; Feng, J. Effects of Modified Hyperbranched Polyester as a Curing Agent on the Morphology and Properties of Dynamically Cured Polypropylene/Polyurethane Blends. *J Mater Sci* **2006**, *41* (12), 3707–3713.

(51) Wan, Q.; Schricker, S. R.; Culbertson, B. M. Methacryloyl Derivitized Hyperbranched Polyester. 2. Photo-Polymerization and Properties for Dental Resin Systems. *J Macromol Sci Part A* **2000**, *37* (11), 1317–1331.

(52) Tasic, S.; Bozic, B.; Dunjic, B. Synthesis of New Hyperbranched Urethane-Acrylates and Their Evaluation in UV-Curable Coatings. *Prog Org Coatings* **2004**, *51* (4), 320–327.

(53) Dzunuzovic, E.; Tasic, S.; Bozic, B.; Babic, D.; Dunjic, B. UV-Curable Hyperbranched Urethane Acrylate Oligomers Containing Soybean Fatty Acids. *Prog Org Coatings* **2005**, *52* (2), 136–143.

(54) Wei, D.; Liao, B.; Yong, Q.; Li, T.; Wang, H.; Huang, J.; Pang, H. Castor Oil Based Hyperbranched Urethane Acrylates and Their Performance as UV-Curable Coatings. *J Macromol Sci Part A Pure Appl Chem* **2018**, *55* (5), 422–432.

(55) Mirshahi, F.; Bastani, S.; Ganjaee Sari, M. Studying the Effect of Hyperbranched Polymer Modification on the Kinetics of Curing Reactions and Physical/Mechanical Properties of UV-

Curable Coatings. *Prog Org Coatings* **2016**, *90*, 187–199.

(56) Huanyu, W.; Huiguang, K.; Wenfang, S.; Kangming, N.; Xiaofeng, S. Thermal and Mechanical Properties of UV-Cured Acrylated Hyperbranched Polyester and Its Blends with Linear Polyurethane Acrylate. *J Coatings Technol* **2003**, *75* (4), 37–40.

(57) Wang, D. K.; Rasoul, F.; Hill, D. J. T.; Hanson, G. R.; Noble, C. J.; Whittaker, A. K. The Role of Residual Cu(Ii) from Click-Chemistry in the Catalyzed Hydrolysis of Boltorn Polyester-Based Hydrogels. *Soft Matter* **2012**, *8* (2), 435–445.

(58) Wang, D. K.; Hill, D. J. T.; Rasoul, F. A.; Whittaker, A. K. Synthesis of a New Hyperbranched, Vinyl Macromonomer through the Use of Click Chemistry: Synthesis and Characterization of Copolymer Hydrogels with PEG Diacrylate. *J Polym Sci Part A Polym Chem* **2012**, *50* (6), 1143–1157.

(59) Zhang, H.; Patel, A.; Gaharwar, A. K.; Mihaila, S. M.; Iviglia, G.; Mukundan, S.; Bae, H.; Yang, H.; Khademhosseini, A. Hyperbranched Polyester Hydrogels with Controlled Drug Release and Cell Adhesion Properties. *Biomacromolecules* **2013**, *14* (5), 1299–1310.

(60) Lange, J.; Stenroos, E.; Johansson, M.; Malmström, E. Barrier Coatings for Flexible Packaging Based on Hyperbranched Resins. *Polymer (Guildf)* **2001**, *42* (17), 7403–7410.

(61) Jesberger, M.; Barner, L.; Stenzel, M. H.; Malmström, E.; Davis, T. P.; Barner-Kowollik, C. Hyperbranched Polymers as Scaffolds for Multifunctional Reversible Addition-Fragmentation Chain-Transfer Agents: A Route to Polystyrene- Core -Polyesters and Polystyrene- Block -Poly(Butyl Acrylate)- Core -Polyesters. *J Polym Sci Part A Polym Chem* **2003**, *41* (23), 3847–3861.

(62) Asif, A.; Huang, C.; Shi, W. Structure-Property Study of Waterborne, Polyurethane Acrylate Dispersions Based on Hyperbranched Aliphatic Polyester for UV-Curable Coatings. *Colloid Polym Sci* **2004**, *283* (2), 200–208.

(63) Zhang, D.; Wang, J.; Li, T.; Zhang, A.; Jia, D. Synthesis and Characterization of a Novel Low-Viscosity Unsaturated Hyperbranched Polyester Resin. *Chem Eng Technol* **2011**, *34* (1), 119–126.

(64) Maślanka, S.; Sułkowski, W. W.; Sułkowska, A. Study of Dynamics of the Cross-Linking Process of Hyperbranched Polymers. *J Therm Anal Calorim* **2010**, *102* (3), 1051–1055.

(65) Odian, G. *Principles of Polymerization*, 4th ed.; John Wiley & Sons, Inc.: Hoboken, NJ, USA, 2004.

(66) Olabisi, O.; Adewale, K. *Handbook of Thermoplastics*, 2nd ed.; CRC Press, Taylor & Francis Group: Boca Raton, 2015.

(67) Matyjaszewski, K.; Davis, T. P. *Handbook of Radical Polymerization*; Matyjaszewski, K., Davis, T. P., Eds.; John Wiley & Sons, Inc.: Hoboken, NJ, USA, 2002.

(68) Buckley, D. J.; Berger, M.; Poller, D. The Swelling of Polymer Systems in Solvents. I. Method for Obtaining Complete Swelling–time Curves. *J Polym Sci* **1962**, *56* (163), 163–174.

(69) Peterson, J. D.; Vyazovkin, S.; Wight, C. A. Kinetic Study of Stabilizing Effect of Oxygen on Thermal Degradation of Poly(Methyl Methacrylate). *J Phys Chem B* **1999**, *103* (38), 8087–8092.

(70) Grassie, N.; Vance, E. Degradation Evidence for the Nature of Chain Termination and Transfer with Benzene in the Polymerization of Methyl Methacrylate. *Trans Faraday Soc* **1953**, *49* (184), 184.

(71) Kashiwagi, T.; Inaba, A.; Brown, J. E.; Hatada, K.; Kitayama, T.; Masuda, E. Effects of Weak Linkages on the Thermal and Oxidative Degradation of Poly(Methyl Methacrylates). *Macromolecules* **1986**, *19* (8), 2160–2168.

6. Experimental and supporting information

6.1. Chemicals

All reagents and solvents were used as received, unless otherwise mentioned. Methyl 9,10-dihydroxystearate-based hyperbranched polyester (*hb*PEster-OH) was supplied by ITERG. Succinic anhydride (< 99 %), 4-(dimethylamino)pyridine (DMAP, 99 %), acryloyl chloride (> 97 %), triethylamine (99 %), methyl methacrylate (MMA, 99 %) and 2,2'-azobis(2-methylpropionitrile) (AIBN, 98 %) were purchased from Sigma Aldrich and Fisher Scientific.

*Hb*Pester-OH and succinic anhydride were dried *via* toluene heteroazeotrope. Triethylamine was dried over KOH and distilled prior to use. MMA was distilled prior to use. AIBN was precipitated from methanol and dried prior to use.

6.2. Protocols

6.2.1. Derivatization with succinic anhdyride

6.2.1.1. General procedure for the functionalization with succinic anhydride

In a Schlenk flask, under a nitrogen flow, *hb*PEster-OH[a] (2 g, 6.4 mmol of OH) and succinic anhydride[a] (3.2 g, 32 mmol) were dissolved in toluene[b] (15 mL) at 100 °C and DMAP (0.16 g, 1.3 mmol) was added to the solution under stirring. The mixture was stirred for several minutes (or hours) and was directly poured into a separating funnel containing acidified water (1M $HCl_{(aq)}$) in order to quench the reaction. The quenching time was shifted from 5 minutes to 3 hours depending on the targeted functionalization rate. Diethyl ether was added to prevent the formation of emulsions and the organic phase was washed three times with a 1M HCl aqueous solution and three times with water. Toluene and diethyl ether were removed on a rotary evaporator. The solvents were evaporated overnight under vacuum at 50 °C.

[a] Toluene was dried over Na/benzophenone and distilled under vacuum.

6.2.1.2. SAXS/WAXS analyses

The gyration radii (R_g) of the *hb*PEster-$COOH_x$ in solution were characterized by SAXS (small angle X-ray scattering) and WAXS (wide-angle X-ray scattering) experiments, which were performed with an in-house setup of the Laboratory Charles Coulomb. The scattering vector (q) was chosen to range from 10^{-1} to 10^{1} nm^{-1}.

6.2.1.3. Dynamic light scattering (DLS)

The hydrodynamic radii (R_H) of the *hb*PEster-$COOH_x$ in solution were characterized by DLS. Measurement were performed on a Brookhaven goniometer, at a wavelength $\lambda = 532$nm and for 6 different scattering angles ranging between 40 and 120°. R_H was calculated using cumulative analysis, unless otherwise mentioned.

6.2.1.4. Viscosity measurements

The viscosity of the *hb*PEster-$COOH_x$ in solution was characterized as a function of the shear rate on an Anton Paar MCR301 stress controlled rheometer at room temperature. The shear rate was varied from 2×10^{-2} to 2×10^{-2} s^{-1}.

6.2.2. Derivatization with acryloyl chloride

6.2.2.1. General procedure for the functionalization *hb*PEster-OH with acryloyl chloride – synthesis of *hb*PEster-A_{75}

In a Schlenk flask, under a nitrogen flow, *hb*PEster-OH (1.7 g, 5.3 mmol of OH) and 1 eq. of TEA (0,74 mL) were solubilized in 8.5 mL of dry DCM. The flask was connected to a trap containing a solution of KOH. 1 eq. of acryloyl chloride (0,43 mL) was added drop-wise. The overall mixture was stirred for 1h30 at room temperature. The supernatant DCM phase, containing the *hb*PEster-A_{75}, was separated from the trimethylamine salts. DCM was removed on a rotary evaporator. The *hb*PEster-A_{75} was then solubilized into toluene. The residual TEA salts precipitated and were removed after centrifugation. The solubilisation and centrifugation steps were repeated three times. Toluene was evaporated on a rotary evaporator and under vacuum at 40 °C for 48 h to yield a pale yellow viscous liquid polymer.

Note: For the synthesis of *hb*PEster-A_{94}, the full functionalization was targeted, therefore, 2 eq. of acryloyl chloride and 1.5 eq. of TEA were used in this case.

$$\text{OH Functionalization} = \frac{N(OH)_i - N(OH)}{N(OH)_i}$$

With,

$$N(OH)_i = 2 \times T_i + 1 \times L_i$$

and $$N(OH) = 2 \times T + 1 \times L1 + T'$$

$$\text{OH Functionalization} = \frac{2 \times (T_i - T) + (L_i - L) - T'}{2 \times T_i + L_i}$$

i.e. $$\text{OH Functionalization} = \frac{2 \times T_{consumed} + L_{consumed} - T'}{2 \times T_i + L_i}$$

The functionalization can thus be calculated by ^{1}H NMR:

With,

$$N(OH)_i = 2 \times \frac{I(a)_i}{2} + 1 \times \frac{I(b)_i + I(c)_i}{2}$$

and $$N(OH) = 2 \times \frac{I(a)}{2} + 1 \times \frac{I(b) + I(c)}{2} + 1 \times \frac{I(a_1') + I(a_2')}{2}$$

$$\text{OH Functionalization} = \frac{2 \times [I(a)_i - I(a)] + [I(b)_i + I(c)_i - I(b) - I(c)] - [I(a_1') + I(a_2')]}{2 \times I(a)_i + I(b)_i + I(c)_i} \quad \text{Eq. SI.III-11}$$

Eq. SI.III-11. Calculation of the percentage of functionalization of the hydroxyl groups of *hb*PEster-OH.

6.2.3. Copolymerization of *hb*PEster-A$_{94}$ with a reactive

6.2.3.1. Preparation of the reactive mixture (AIBN:MMA:*hb*PEster-A$_{94}$)

The reactive diluent, the *hb*PEster-A$_{94}$ and AIBN initiator (0.3 w%) were incorporated into a mould. The quantity of *hb*Pester-A$_{94}$ was varied from 0 to 10 w% of the total mass of the reactive mixture (2 g). The initiator and the *hb*PEster-A$_{94}$ were put under stirring for 20 min while the solution was degassed with nitrogen. The mixture was additionally degassed by three freeze-pump-thaw cycles.

6.2.3.2. Preliminary tests: curing in vial

The vial was immersed into an oil bath at 80 °C until the stirring stopped, indicating that the viscosity increased and that cross-linking probably started. Then, the mixture was cured 4 h for the PMMA-based networks and 17 h hours for the PS-based networks. The networks were cured for additional 24 h at 130 °C in an oven.

6.2.3.3. Curing in mould

The stirrer was removed and the vial was immersed into an oil bath at 80 °C for several minutes or hours, depending on the time of gelation. The reactive mixture was quickly degassed under vacuum and poured into a mould. The mould was placed in an oven at 80 °C for 17 h. The PMMA-based and PS-based resins were cured for additional 17 h at 100 °C and 130 °C respectively.

6.2.3.4. Dynamic mechanical analysis (DMA) of cured resins

On a DMA RSA 3 (TA instrument) device, the sample temperature was modulated from 25 to 120 °C, depending on the sample, and at a heating rate of 3 °C.min^{-1}. The measurements were performed in a single point bending mode on samples (strip-shaped: length = 10 mm, width = 5 mm, thickness = 1mm) , at a frequency of 1 Hz, an initial static force of 0.1 N and a strain sweep of 0.02 %.

6.2.3.5. Rheometer – G' and G" as functions of the angular frequency

On an Anton Paar MCR301 stress controlled rheometer, the sample temperature was maintained at 150 °C and angular frequencies were modulated from 10^{-2} to 10^{2} rad/s. The measurements of G' and G" were performed in the melt.

6.3. Appendices

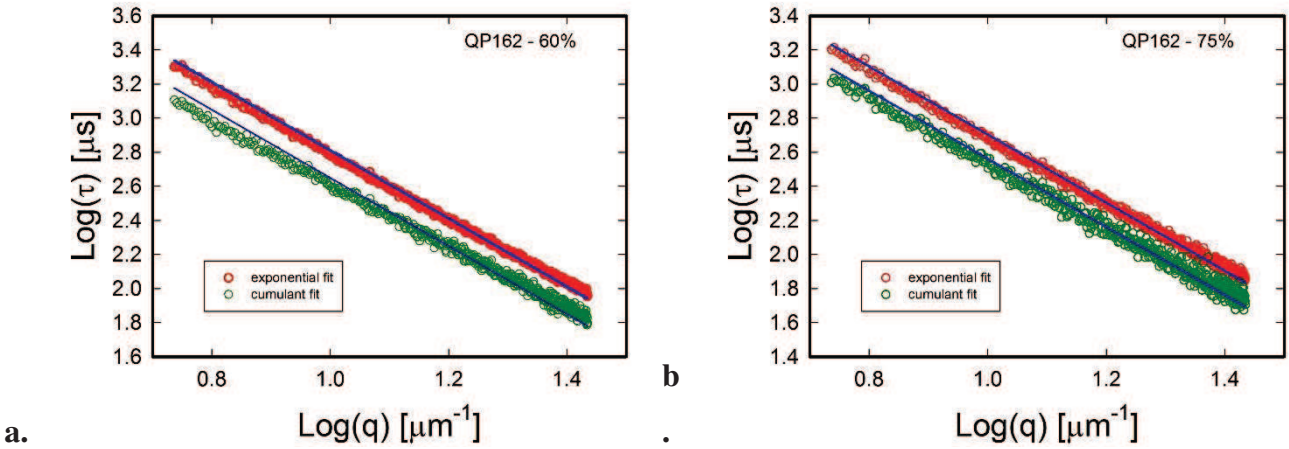

Figure SI.III-42. Dynamic light scattering measurement of *hb*PEster-$COOH_{100}$ in $NaOH_{aq}$ (0.25M) neutralized at **a.** 60 % and **b.** 75%.

GENERAL CONCLUSION & PERSPECTIVES

The aim of this thesis was to create a novel family of oleo-based hyperbranched polyethers (*hb*PEthers) and to investigate the potential of derivatized hyperbranched polyesters (*hb*PEsters) developed in the frame of the HyperBioPol (2012-2015). Vegetable oils and their derivatives are already used for the production of surfactants, lubricants, paints and coatings and are promising precursors of polymer materials. In particular, Fatty acid methyl esters (FAMEs), obtained by transesterification of vegetable oils, represent important synthons for the design of novel polymer architectures. The inherent aliphatic structure of the FAMEs, coupled with the presence of functional groups such as esters and unsaturations, enables the access to a large variety of multifunctional precursors, which have been found to be suitable for the synthesis of aliphatic *hb*PEsters and *hb*PEthers.

In the first part of FunHyBioPol project, a new bio-based α-epoxy-ω-alcohol, namely, 10,11-epoxyundecanol (EUnd) stemming from castor oil, has been synthesized and subsequently polymerized into aliphatic *hb*PEthers, denoted as *hb*PEUnd. As 10,11-epoxyundecanol (EUnd) contains both an epoxy and a primary hydroxyl group, it is regarded as a latent AB_2–*type* monomer. The best conditions suited to achieve *hb*PEUnd by ring-opening multibranching polymerization (ROMBP) was first investigated. Synthesis was achieved either in bulk or in presence of a solvent at 95 °C, the polymerization in bulk being particularly relevant from the perspective of an industrial development based on solvent-free conditions and energy saving. Several parameters, including the M/TMP ratio, the extent of TMP deprotonation or the use of solvent, were tested in order to promote the synthesis of *hb*PEUnd of high molecular weights. However, the raise of molecular weights, related to a higher M/TMP ratio, only occurred for M/TMP inferior to 50. Therefore, *hb*PEUnds of 10,000 g/mol as a maximum were achieved, which limited the possibilities of evaluating the properties of the molecular weights on the polymer properties. Unfortunately, the presence of long alkyl chains between the two hypothetical propagating alkoxides did not afford the calculation of the degree of branching of the polyethers. Yet, to the best of our knowledge, this class of aliphatic semi-crystalline hyperbranched polymers, represents one of rare examples of *hb*PEthers synthesized by ROMBP (with *hb*PG from glycidol or glycerol carbonate). In order

to create original *hb*PEthers exhibiting amphiphilic properties, random and sequential ring-opening multibranching copolymerization (ROMBcP) of EUnd with glycidol was also performed. These copolymers proved soluble in organic solvent and dispersible in water. In addition, they remained semi-crystalline despite the incorporation of glycidol, which afforded modulation of the glass transition and melting temperature, the latter being reduced from 85 to 30 °C.

The post-functionalization of the hyperbranched polymer chain ends is also a powerful tool for tuning their properties, in bulk or in solution. In the second part of this project, a method for modifying the hydroxyl groups of hyperbranched polymer polyols, *hb*PEsters, was investigated. Indeed, the derivatization of OH groups of M2HS-*hb*PEsters was undertaken in order to broaden the potential applications of these bio-based substrates. The derivatization of M2HS-*hb*PEster with succinic anhydride and acryloyl chloride has been performed in order to produce water-soluble *hb*PEster-$COOH_x$ and reactive acrylate-terminated *hb*PEster-A_x, respectively. Functionalization procedures and structural characterizations of the derivatized *hb*PEsters have been particularly studied. Derivatization has been shown to always occur in two steps; first the reaction of hydroxyl peripheral functions and then, the one of core units, all these functions being successfully derivatized. However, the functionalization step also led to inter-esterification reactions between hydroxyl and acid functions of *hb*PEsters. The specific properties and potential applications of these modified M2HS-*hb*PEster have been analysed. In particular, the behaviour of *hb*PEster-$COOH_x$ in bulk, in ethanol and in alkaline water solution (~0.03 g/mL in 0.25 $NaOH_{aq}$) was studied allowing us to determine the hydrodynamic and gyration radii (R_H and R_g) of these nano-objects, thanks to wide angle X-ray scattering (SAXS/WAXS), diffusion light scattering (DLS) and viscosity measurements. These last data could be obtained thanks to a tight collaboration with the L2C at Montpellier. Little decrease of glass transition (-23 to -15 °C) was observed after functionalization. All samples were shown to be soluble in ethanol, at concentrations varying from 0.01 to 0.07 g/mL, forming unimolecular particles of less than 6 nm for both *hbPEster*-OH and *hb*PEster-$COOH_{x,}$ even though particles of bigger sizes (75-80 nm) were observed. Neutralization of the COOH moieties of *hb*PEster-$COOH_x$ (> 60 % for *hb*PEster-$COOH_{100}$) provided them with water solubility; unimolecular particles of 11 nm were hence achieved. Acrylate-terminated *hb*PEster-A_{100} was copolymerized with reactive diluents, namely methyl methacrylate (MMA) and styrene, by free radical polymerization. For MMA, 3D-networks (100 wt.% of gel content)

were generated when using more than 1 wt.% of *hb*PEster-A_{100} curing agent. The latter acted as a thermal stabilizer ($\triangle T_{d5\%}$ = 110 °C) and a mechanical toughener. By comparison, in the case of copolymerization with styrene, full cross-linking was only achieved for extent of *hb*PEster-A_{100} superior to 5 wt.%, without significant influence on thermo-mechanical and mechanical properties.

In light of the results obtained in these chapters, several pathways can be undertaken. First, the pursuit of the work concerning the ring-opening multibranching copolymerization of EUnd with glycidol seems particularly opportune as it provides an efficient way of tuning the properties of the *hb*PEthers; moreover, other epoxides, described in literature, could be used instead (or in addition) of glycidol. Post-functionalization of the homo- and copolyethers achieved should be considered too, depending on the targeted applications. The development of a new platform of bio-based synthons, from vegetable oils or lignocellulosic resources, as precursors for the synthesis of aromatic and aliphatic *hb*PEthers, *via* cationic ring-opening polymerization for instance, is also a possibility.

Post-derivatization has also proved to be a powerful tool for tuning the solubility of the oily-based *hb*PEsters or for grafting reactive sites. Obviously, numerous molecules or polymers could be grafted to *hb*PEster, therefore, methyl methacrylate could be opportunely substitute by (or copolymerized with) other acrylates or methacrylates reactive diluents, bio-based for instance, to extend the possible properties of the materials. Last but not least, these functionalized *hb*PEsters should now be improved, in the frame of maturation projects, to meet specific applications.

MATERIALS AND METHODS

1. Nuclear Magnetic Resonance (NMR)

^{1}H and ^{13}C-NMR spectra were recorded on Bruker Avance 400 spectrometer (400.20 MHz or 400.33 MHz and 100.63 MHz for ^{1}H and ^{13}C, respectively) by using $CDCl_3$ as a solvent at room temperature, except otherwise mentioned. Two-dimensional analyses such as ^{1}H-^{1}H COSY (COrrelation SpectroscopY), ^{1}H -$_{13}C$ HSQC (Heteronuclear Single Quantum Spectroscopy) and were also performed. All DOSY (Diffusion Ordered Spectroscopy) measurements were performed at 298 K on a Bruker Avance III 400 spectrometer operating at 400.33 MHz and equipped with a 5 mm Bruker multinuclear z-gradient direct cryoprobe-head capable of producing gradients in the z direction with strength 53.5 G/cm. For each sample, 10 mg was dissolved in 0.4 ml of DMSO-d6 for internal lock and spinning was used to minimize convection effects.

2. Fourier Transformed Infra-Red-Attenuated Total Reflection (FTIR-ATR)

Infrared spectra were obtained on a Bruker-Tensor 27 spectrometer, equipped with a diamond crystal, using the attenuated total reflection mode. The spectra were acquired from 400 to 4,000 nm^{-1} using 32 scans at a resolution of 4 wavenumbers.

3. Flash chromatography

Flash chromatography was performed on a Grace Reveleris apparatus, employing silica cartridges from Grace. Cyclohexane:ethyl acetate were used as eluents. The detection was performed through ELSD and UV detectors at 254 nm and 280 nm.

4. Size Exclusion Chromatography (SEC)

4.1. In THF

Polymer molecular weights were determined by Size Exclusion Chromatography (SEC) using tetrahydrofuran (THF + lithium bromide $LiTf_2N$ 10Mm) as the eluent. Measurements in THF were performed on an Ultimate 3000 system, from Thermoscientific, equipped with a diode array detector (DAD). The system also includes a multi-angles light scattering detector (MALS), a viscometer and differential refractive index detector (dRI), from Wyatt technology. Polymers were separated on a PSS SDV Linear S gel columns (300 x 8 mm) (exclusion limits from 1,000 Da to 150,000 Da) at a flowrate of 1 mL/min. Columns temperature was held at 36 °C.

4.2. In DMF

Polymer molecular weight were determined by Size Exclusion Chromatography (SEC) using dimethylformamide (DMF + lithium bromide LiBr 1g/L) as the eluent. Measurements in DMF were performed on an Ultimate 3000 system, from Thermoscientific, equipped with a diode array detector (DAD). The system also includes a multi-angles light scattering detector (MALS) and differential refractive index detector (dRI), from Wyatt technology. Polymers were separated on two KD-803 Shodex gel columns (300 x 8 mm) (exclusion limits from 1,000 Da to 50,000 Da) at a flowrate of 0.8 mL/min. Columns temperature was held at 50°C. Polystyrene was used as the standard; dn/dc were determined using the differential refractive index detector dRI from Wyatt technology.

4.3. In chloroform

Polymer molecular weight were determined by Size Exclusion Chromatography (SEC) using chloroform (chloroform + 1 v% of triethylamine) as the eluent. Measurements in chloroform were performed on an Viscotek VE2001-GPC system, from Malvern. Polymers were separated on one column PLGel 5µm Guard (PL1110-1520), one column PLGel 5µm 100A (PL 1110-6520) and two columns Mixed C PLGel 5µm (PL1110-6500), from Agilent, at a flowrate of 0.8 mL/min. Columns temperature was held at 30°C

.

5. Differential Scanning Calorimetry (DSC)

Differential scanning calorimetry thermograms were measured using a DSC Q100 apparatus from TA instruments. For each sample, one cycle from 20 °C to 150°C at 10°C.min^{-1} followed by another from -80 to 200 °C were performed; glass transition and melting temperatures were calculated from the second heating run.

6. Thermogravimetric analysis (TGA)

Thermogravimetric analyses were performed on TGA-Q50 system from TA instruments, at a heating rate of 10 °C.min^{-1}, under nitrogen atmosphere, from room temperature to 600 °C.

7. Dynamic Mechanical Analysis (DMA)

Dynamic mechanical analyses were performed on a DMA RSA 3 from TA instruments. The sample temperature was modulated from 25 to 120 °C, depending on the sample, and at a heating rate of 3 °C.min^{-1}. The measurements were performed in a single point bending mode, at a frequency of 1 Hz, an initial static force of 0.1 N and a strain sweep of 0.02 %.

8. Rheological measurements

Rheological tests were performed on a stress-controlled rheometer Physica MCR 302 (Anton Paar, Germany) equipped with a Peltier plate and hood for temperature control. Parallel plate geometries with diameters of 8 mm and 12.5 mm were used for the tests. All measurements were carried out in air atmosphere.

Synthèse et fonctionnalisation de polymères hyper-ramifiés issus d'acides gras

Résumé : Ces travaux de thèse portent sur la valorisation de la biomasse oléagineuse, *via* la polymérisation de synthons, issus d'huiles végétales, en polymères hyper-ramifiés. Ces recherches ont conduit à la synthèse et à la purification d'un nouveau monomère biosourcé, le 10,11-epoxy undecan-1-ol (EUnd), dont la polymérisation par ouverture de cycle (ROMBP) a permis de générer des polyéthers hyper-ramifiés biosourcés. Les conditions de polymérisations ont été étudiées en laboratoire dans le but d'optimiser les rendements de synthèse mais aussi afin de contrôler la structure chimique, ainsi que leurs propriétés. La copolymérisation de l'EUnd avec le glycidol a permis d'atteindre de nouvelles propriétés, notamment en termes de solubilité. Une seconde partie fut consacrée à la fonctionnalisation de polyesters hyper-ramifiés biosourcés, développés au LCPO lors du projet HyPerBioPol. L'objectif étant de contrôler la solubilisation des composés dans différents milieux, polaires et apolaires, afin de créer des polymères pouvant être utilisés comme agents de réticulation.

Mots clés : *Huiles végétales, polymères hyper-ramifiés, polyesters, polyéthers, polycondensation, polymérisation par ouverture de cycle, fonctionnalisation*

Synthesis and functionalization of fatty acid-based hyperbranched polymers

Abstract: The aim of this thesis is to valorize oilseed biomass through the polymerization of building block, stemming from vegetable oils, into hyperbranched polymers. This research involves the synthesis and purification of a new bio-based monomer, coined as 10,11-epoxyundecanol (EUnd), which ring-opening multibranching polymerization (ROMBP) has generated bio-based hyperbranched polyethers (*hb*PEUnd). Conditions of polymerization have been studied in order to maximize yields of reaction and control both the chemical structure and the properties of *hb*PEUnd. Copolymerization of EUnd with glycidol has also been implemented, yielding hyperbranched copolyethers with varied properties (e.g. solubility). The second part of this work has been dedicated to the functionalization of bio-based hyperbranched polyesters, developed in the frame of a former project. Appropriate derivatizations have provided these modified polyesters with solubility in polar solvents and made them employable as curing agents.

Keywords: *Vegetable oils, hyperbranched polymers, polyesters, polyethers, polycondensation, ring-opening multibranching polymerization, functionalization*

Laboratoire de Chimie des Polymères Organiques
16 avenue Pey-Berland
F-33607 PESSAC